UNIVERSITEIT VAN PRETORIA
UNIVERSITY OF PRETORIA
YUNIBESITHI YA PRETORIA

Creating guidelines for the approximation of the eye and periorbital regions of South Africans using Cone Beam Computed Tomography scans

A thesis submitted to the Department of Anatomy, School of Medicine, Faculty of Health Sciences, University of Pretoria in fulfilment of the requirements for the degree of
PhD in Anatomy.

Submitted by:

Soné van der Walt

Student number: 04409604

Supervisor: Prof A.C Oettlé

Co-supervisors: Prof E.N. L' Abbé and Dr A.F. Ridel

Pretoria, 2024

© University of Pretoria

Declaration

I declare that the dissertation that I am hereby submitting to the Faculty of Health Care Sciences, University of Pretoria for the degree Doctorate in Anatomy, is my own work and that I have never submitted it to any other tertiary institution for any degree.

Name: Soné van der Walt Date: 31 May 2024

Signature: 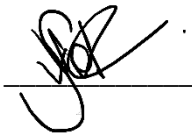

© University of Pretoria

Thesis supervisor

Prof A.C. Oettlé

Full Professor and External Supervisor

Anatomy and Histology Department, School of Medicine, Sefako Makgatho Health Sciences University, Ga-Rankuwa, Pretoria, South Africa.

Thesis co-supervisors

Prof E.N. L' Abbé

Professor

Department of Anatomy (Physical Anthropology division), Faculty of Health Sciences, University of Pretoria, Pretoria, South Africa

Dr AF Ridel

Lecturer

Department of Anatomy (Physical Anthropology division), Faculty of Health Sciences, University of Pretoria, Pretoria, South Africa

© University of Pretoria

Acknowledgements

When reflecting on my four-and-a-half-year journey, I am grateful for the numerous individuals who have supported, encouraged, and accompanied me along the way.

In particular, this project would not have been successful without the valuable input of my supervisors. Professor Ericka L' Abbé, thank you for your input, guidance and editing of the chapters and the dissertation. You always responded diligently.

Dr. Alison Ridel, I would like to thank you for your assistance in creating the templates of South African faces from my scans, automating landmarking, and generating statistical models for the prediction of the open eyes were valuable to the study. Thank you for sharing your R scripts and offering training and assistance in using it for this study.

Professor Anna Oettlé, I am grateful for the wealth of knowledge I have gained from working under your supervision, spanning not only this project but also our other endeavours together. Your guidance and mentorship have opened doors for my academic, professional and personal development. I appreciate your efforts in challenging me to step out of my comfort zone and see the positive aspects in challenging circumstances. Thank you for your motivation, inspiration, and patience throughout the years. Thank you for fighting for me and always being on my side.

I extend my gratitude to Professor Dirk Vandermeulen and Dr. Harry Matthews for their invaluable assistance in creating the MeVisLab networks necessary for conducting the data collection of the study. Your contributions were essential to the success of this project, and I could not have completed it without your expertise.

I am grateful that I could visit Dr Clément Zanolli at the University of Bordeaux. Thank you for accommodating us during our visit to your institution and assisting me with the R scripts and analysis although you weren't even a part of the project.

I would like to thank Marisca Meyer for her assistance with the repeatability tests of the manual landmarking. I appreciate your willingness to learn the MeVisLab programme just to assist me.

I am grateful for Marinda Pretorius who assisted with the creation of the line diagrams in the thesis. Thank you for making time in your busy schedule to help on short notice.

Franci, our journey of studying together since 2008 has been a remarkable one. Your friendship and support have meant the world to me. Thank you for sharing your R scripts and for assisting

© University of Pretoria

me when I did not understand the software. I feel truly blessed to have you in my life. I can't wait to see what we can achieve in the next chapter of our lives.

Suvasha, your ability to listen and offer encouragement when I felt stuck has been incredibly uplifting. Your positivity and kind words have been a source of great strength. Lané, thank you for always having my back and being part of my support structure in my personal and professional life. Daniële, I am forever grateful for the time we spend together, solving the world's problems during our drive to work. It is now my turn to motivate you to complete your PhD. Ruth, thank you for reminding me that there is a bigger picture to our current situation. Thank you for all your prayers and for keeping me accountable. I wish you the best of luck finishing your PhD.

To my mom, your unwavering support and dedication to ensure that I had the opportunity to obtain my first degree have been instrumental in my journey. Thank you for helping out with Andri and Kian and preparing meals with love so that I could work on my studies. I am deeply grateful. Oom Jan, thank you for every cup of coffee and sandwich that you made and brought to my table with a smile while I was writing my dissertation. You will never know how much it meant to me. To my dad, thank you for your motivation and interest in my research projects.

To my wonderful siblings, Heleen and Deric, thank you for being a part of my three-stranded rope. Together we can conquer the world. Thank you for your love and support, I am grateful to have you in my life.

Lastly, to my husband Peet, thank you for trying to understand when my work and studies demanded so much of my time. Thank you for believing in me and the work that I do when I felt like giving up. Thank you for being a good father to Andri and Kian, we are blessed to have you.

I could not have completed this journey without the talents and mercy that I have received from my Creator. During my PhD journey, I have learned the meaning of Philippians 4:13 "I can do all things through Him who strengthens and empowers me."

© University of Pretoria

Executive Summary

Introduction: South Africa is experiencing a rise in unidentified remains yearly, and due to poor access to healthcare and illegal immigration, standard identification methods often fail. The foundational data used to reconstruct South African faces are based on North American cadavers which result in inaccurate reconstructions. This study aimed to create guidelines for approximating the eyeball and periorbital structures for South African groups using cone-beam computed tomography (CBCT) scans.

Methods: Retrospective CBCT scans of 206 South African adults (45 black females, 52 black males, 57 white females, and 52 white males) were included in the study, of which 187 had open eyes (32 black females, 51 black males, 52 white females, and 52 white males). Three-dimensional landmarks were placed manually on the hard- and soft-tissue renderings of the face and skull as well as the outline of the eyeball in 2D using the MeVisLab © v.3.0.2 software. The 3D coordinates of these landmarks were used to calculate the linear dimensions of the orbit, eyeball, palpebral fissure, and the position of the eyeball in relation to the orbital rim. Predictive equations and predictions based on proportionality for the position of the eyeball in relation to the orbital rim, eyeball and palpebral fissure dimensions were derived from these linear dimensions. The effect of sex and population affinity on the shape of the orbit and palpebral fissure was investigated using geometric morphometric methods (GMM). The second part of the study entailed the creation and validation of prediction models based on the relationship between shape of the bony orbit and palpebral fissures using an automatic landmarking method.

Results: Sex and population affinity significantly affected the dimensions and shape of the orbit, eyeball and palpebral fissures. Black females had significantly smaller eyeballs which protruded more from the superior orbital margin than the other sex-population groups. Eyeball position, eyeball dimensions and palpebral fissure dimensions could be predicted with greater accuracy based on proportionality compared to linear regression formulae. Variations in the palpebral fissure dimensions in black South Africans were driven by shape, while it was driven by size in white South Africans. Population affinity had a greater effect on the shape of the orbital region and palpebral fissures than on the linear dimensions. The shape analysis based on the automatically placed landmarks concurred with this finding which resulted in the accurate prediction of the open eye from the underlying bony tissue with a small measurement error, especially when population affinity was added as a factor.

© University of Pretoria

Conclusion: When reconstructing South African faces, it should be noted that black South African females had significantly smaller eyeballs compared to all other groups, while the eyeball protruded more in the vertical plane in black South Africans than white South Africans. Black compared to white South Africans had a greater inner canthal distance and less upward slanting palpebral fissures. Instead of depending on normative dimensions, the palpebral fissure and eyeball position can be predicted based on the morphology of each individual without considering sex or population affinity. The open eyelids could be accurately predicted from the underlying bony tissue for the use in automatic facial approximations. These prediction results should be combined with prediction models of other facial features to create accurate, objective and less time-consuming automated facial approximations of South Africans.

Keywords: Orbital dimensions, Palpebral fissure shape, Ocular position, Prediction equations, Prediction model, Biological profiling, Facial approximation, Virtual Sculpture method, Automatic approximation

© University of Pretoria

Table of Contents

Declaration i
Acknowledgements iii
Executive Summary v
List of abbreviations xiii
1. Chapter 1: Introduction 1
1.1 Background and Rationale 1
1.2 Research problem 4
1.3 Conceptual framework 4
1.4 Aims and objectives 6
2. Chapter 2: Literature review 8
2.1 Introduction 8
2.2 Anatomy of the bony orbit, orbital and periorbital structures 8
2.2.1 Bony orbit: 8
2.2.2 Orbital and periorbital structures, including the eyelids 11
2.2.3 Eyeball 12
2.2.4 Anatomical position of the eyeball 13
2.3 Facial approximation techniques 14
2.3.1 Introduction 14
2.3.2 Traditional methods of facial approximation 14
2.3.3 Computerised 3D facial approximation methods 15
2.3.4 Approximation of the eyeball and palpebral fissure 18
2.3.5 Automatic facial approximations of the facial features 21
2.3.6 Modalities used in the creation of approximation methods 24
3. Chapter 3: Materials and Methods 26
3.1 Materials 26
3.2 Methods 27
3.2.1 Part 1: Linear distances calculated from manually placed landmarks 28
3.2.2. Part 1: Statistical analysis 36
3.2.3 Part 2: Soft-tissue prediction: Statistical analysis 41
4. Chapter 4: Results 46
4.1 Part 1: Linear measurements 46
4.1.1. Reproducibility testing 46
4.1.2. Distribution of the linear data 47
4.1.3 Asymmetry by sex-population group: 49
4.1.4 Summary statistics, univariate and multivariate analysis results 49

© University of Pretoria

4.1.5 Classification accuracy based on orbital dimensions....62
4.1.6 Prediction equations based on linear data....63
4.1.7 Comparison of data with existing literature....70
4.1.8 Shape analysis: Based on manually placed landmarks....72
4.2 Part 2: Eyelid approximation from automatic landmarks....94
4.2.1 Reproducibility testing....94
4.2.2 Multivariate normality testing....95
4.2.3 Shape analysis: Based on automatically placed landmarks....96
4.2.4 Soft-tissue prediction....97
5. Chapter 5: Discussion....100
5.1 Part 1: Guidelines based on manually placed landmarks....101
5.1.1 Variations in the linear distances....102
5.1.2 Approximation of the eyeball dimensions and position....108
5.1.3 Approximation of the palpebral fissure....109
5.1.4 Shape analysis: based on manually placed landmarks....109
5.2 Part 2: Soft tissue prediction based on automatically placed landmarks....112
5.3 Applications, limitations and future recommendations....114
6. Chapter 6: Conclusion....117
References....119
Supplementary Table 1: Comparative analysis of data with existing literature....137
Supplementary Table 2. Sexual dimorphism in linear dimensions of the orbital region....150
Supplementary Table 3. Eigenvalues and PC scores for shape analysis data on manually placed landmarks....153
Annexure A: Ethics approval from UP....156
Annexure B: Permission to collect scans from Cintocare....157
Annexure C: Ethical approval from SMU....158
Annexure D: Normality results for shape analysis....159
Annexure E: Dimensions of the orbital and periorbital regions for the use in forensic facial approximations of South Africans....163
Annexure F: Dimensions of the orbital region for biological profiling in a South African sample....173

© University of Pretoria

List of Figures

Figure 2.1. The right bony orbit with its openings 9
Figure 2.2. Anatomy of the eyelids 12
Figure 2.3. Recorded eyeball position within the orbit adapted from Dorfling and colleagues (2018) 19
Figure 2.4. Eyeball protrusion measurement adapted from Wilkinson and Mautner, 2003.... 20
Figure 2.5. Eyeball protrusion from the lateral orbital wall adapted from Stephan and Davidson 2008 20
Figure 3.1. Age distribution by sex-population group 26
Figure 3.2. Reslicing of original DICOM images. 29
Figure 3.3. Anterior view of the craniometric landmarks placed on the reconstructed cranium 32
Figure 3.4. Lateral view of the craniometric landmarks placed on the reconstructed cranium 33
Figure 3.5. Capulometric landmarks placed on the eyelids of the reconstructed face 33
Figure 3.6. 2D DICOM slice indicating the capulometric landmarks placed on the ocular rim. 34
Figure 3.7. Statistical plan for Part 1 based on manually placed landmarks 40
Figure 3.8. Statistical plan for objective 2 based on automatically projected landmarks 45
Figure 4.1 Graphical comparison between the mean dispersion results for both intra-observer and inter-observer errors of the positioning of all landmarks (mm) 46
Figure 4.2. Graphical comparison between the mean ICC results for both intra-observer and inter-observer errors 47
Figure 4.3. Proportional placement of the eyeball within the orbit from the lateral and superior orbital margins and the deepest point on the lateral orbital margin 65
Figure 4.4. Proportional dimensions of the eyeball as percentages of orbital height and width. 66
Figure 4.5. Proportional dimensions of the palpebral fissure as percentages of orbital height and width 68
Figure 4.6. Q-Q-plots of the residuals of the linear model a) hard-tissue shape against population, b) soft-tissue shape against population 73
Figure 4.7. Q-Q-plots of the residuals of the linear model a) hard-tissue shape against sex, b) soft-tissue shape against sex 74
Figure 4.8. Wire frame indicating the shape of the orbital region investigated 74
Figure 4.9. Wire frame indicating the shape of the palpebral fissure investigated 75
Figure 4.10. Scatterplot with corresponding deformation grids illustrating PC 1 against PC 2 of the complete South African sample indicating the effect of population affinity on the position of the 14 landmarks located on the orbital region 77
Figure 4.11. Scatterplot with corresponding deformation grids illustrating PC 1 against PC 2 of the complete South African sample indicating the effect of population affinity on the position of the 8 landmarks located on the palpebral fissures 78
Figure 4.12. Scatterplot with corresponding deformation grids illustrating PC 1 against PC 2 of South African males indicating the effect of population affinity on the position of the 14 landmarks located on the orbital region 80
Figure 4.13. Scatterplot with corresponding deformation grids illustrating PC 1 against PC 2 of South African males indicating the effect of population affinity on the position of the 8 landmarks located on the palpebral fissures 81

© University of Pretoria

Figure 4.14. Scatterplot with corresponding deformation grids illustrating PC 1 against PC 2 of South African females indicating the effect of population affinity on the position of the 14 landmarks located on the orbital region 83
Figure 4.15. Scatterplot with corresponding deformation grids illustrating PC 1 against PC 2 of South African females indicating the effect of population affinity on the position of the 8 landmarks located on the palpebral fissures 84
Figure 4.16. Scatterplot with corresponding deformation grids illustrating PC 1 against PC 2 of the complete sample indicating the effect of sex on the position of the 14 landmarks located on the orbital region 86
Figure 4.17. Scatterplot with corresponding deformation grids illustrating PC 1 against PC 2 of the complete sample indicating the effect of sex on the position of the 8 landmarks located on the palpebral fissures 87
Figure 4.18. Scatterplot with corresponding deformation grids illustrating PC 1 against PC 2 of white South Africans indicating the effect of sexual dimorphism on the position of the 14 craniometric landmarks 89
Figure 4.19. Scatterplot with corresponding deformation grids illustrating PC 1 against PC 2 of white South Africans indicating the effect of sexual dimorphism on the position of the 8 cephalometric landmarks 90
Figure 4.20. Scatterplot with corresponding deformation grids illustrating PC 1 against PC 2 of black South Africans indicating the effect of sexual dimorphism on the position of the 14 craniometric landmarks 92
Figure 4.21. Scatterplot with corresponding deformation grids illustrating PC 1 against PC 2 of black South Africans indicating the effect of sexual dimorphism on the position of the 8 cephalometric landmarks 93
Figure 4.22. Q-Q-plots of the residuals of the linear model a) hard-tissue shape against population, b) soft-tissue shape against population 95
Figure 4.23. Q-Q-plots of the residuals of the linear model a) hard-tissue shape against sex, b) soft-tissue shape against sex 96

© University of Pretoria

List of Tables

Table 3.1. Definitions of manually placed landmarks. 31
Table 3.2. Definition of the calculated dimensions 35
Table 4.1. Dispersion errors (mm) of landmark positioning 46
Table 4.2. Mean Intraclass Correlation coefficient test results 47
Table 4.3. Distribution of linear dimensions (p-values) as calculated from 3D landmarks 48
Table 4.4. Asymmetry specific to each sex-population group 49
Table 4.5 Summary statistics (mm) and p-values investigating the influence of asymmetry, population affinity and sexual dimorphism on orbital dimensions 51
Table 4.6 Variation in the orbital dimensions between sexes within populations and variation between populations within sex groups 52
Table 4.7 Summary statistics (in mm) and p-values investigating the influence of asymmetry, population affinity and sexual dimorphism on ocular position 54
Table 4.8 Variation in ocular position between sexes within populations and variation between population within sex groups 55
Table 4.9 Summary statistics (mm) and p-values investigating the influence of asymmetry, population affinity and sexual dimorphism on the protrusion of the eyeball. 57
Table 4.10 Variation in ocular protrusion between sexes within populations and variation between populations within sex groups 58
Table 4.11 Summary statistics (in mm) and p values testing the influence of asymmetry, population affinity and sexual dimorphism on ocular dimensions 59
Table 4.12 Variation in ocular dimensions between sexes within populations and variation between populations within sex groups 60
Table 4.13 Summary statistics (mm) and p-values investigating the influence of asymmetry, population affinity and sexual dimorphism on palpebral fissure dimensions 61
Table 4.14 Variation in palpebral fissure dimensions between sexes within populations and variation between populations within sex groups 62
Table 4.15 Classification accuracy (%) of the orbital and palpebral fissure dimensions 62
Table 4.16. Prediction equations and proportional eyeball position in relation to the superior and lateral orbital margins 64
Table 4.17. Prediction equations for the estimation of the eyeball dimensions from the orbital dimensions 67
Table 4.18. Prediction equations for the estimation of the palpebral fissure dimensions from the orbital dimensions 69
Table 4.19 Summary of significant variation in linear dimensions between South Africans and existing literature 71
Table 4.20. Dispersion errors (mm) of manual landmark placement 72
Table 4.21 Shape analysis results for craniometric landmarks. 75
Table 4.22 Shape analysis results for capulometric landmarks. 75
Table 4.23 Mean dispersion analysis of the intra- and inter-observer repeatability 94
Table 4.24 Shape analysis results for craniometric landmarks. 96
Table 4.25 Shape analysis results for cephalometric landmarks. 97
Table 4.26 Prediction errors (mm) of the predicted cephalometric landmarks according to population, sex and within sex groups, based on 187 individuals, based on trained and non-trained data. 98

© University of Pretoria

Table 4.27 Prediction errors (mm) of the predicted cephalometric landmarks according to population group and sex-population groups, based on 187 individuals, based on trained and non-trained data. 99

© University of Pretoria

List of abbreviations

2D:	Two dimensional
3D:	Three dimensional
BF:	Bayes Factor
BMI:	Body mass index
CBCT:	Cone Beam Computed Tomography
CT:	Computed Tomography
DICOM:	Digital Imaging and Communications in Medicine
FARC:	Forensic Anthropology Research Centre
FH:	Frankfort Horizontal plane
GMM:	Geometric morphometric methods
GPA:	General Procrustes Analysis
ICC:	Intra-class Correlation Coefficient
LOOCV:	Leave one out cross validation
MED:	Mean Euclidian distance
MRI:	Magnetic Resonance Imaging
MSE:	Mean Squared Error
PC:	Principal Component
PCA:	Principal Component Analysis
PLS:	Partial least squares
PLSR:	Projection onto latent structures regression
RMSE:	Root Mean Squared error
SAPS:	South African Police Service
SEE:	Standard error of the estimate
STT:	Soft tissue thicknesses
VIC:	Victim Identification Centre

© University of Pretoria

1. Chapter 1: Introduction

1.1 Background and Rationale

Developing countries, and more specifically South Africa, have more than double the number of unidentified remains yearly compared to developed countries, such as the United States, Italy and France (Reid et al., 2023). Standard identification methods, such as identification documents, DNA analysis, dental record comparisons, and fingerprints are commonly used to identify the deceased (L'Abbé et al., 2005; Dorfling et al., 2018; Beaini et al., 2021). However, these methods can only be useful to confirm an individual's identity when information regarding the person's identity is known e.g. from family members (Dorfling et al., 2018; Krüger et al., 2018). In the South African context, with the history of socio-economic disparities and migrant labour, identification may not always be possible as unclaimed remains often originate from migrants or illegal immigrants (L'Abbé et al., 2005). Another factor hindering the identification process is the recovery of incomplete remains due to scavenger activity, geological, environmental or cultural activities (L' Abbé, 2013; Small et al., 2018; Spies et al., 2018; Keyes et al., 2022).

Alternative methods, which include facial approximation, have been used to aid the Victim Identification Centre (VIC) of the South African Police Service (SAPS) in the presumptive identification of the deceased, especially in cases where skeletal remains are recovered. Facial approximation entails the construction of a face over a skull to recreate an *in vivo* face of the deceased (Stephan and Davidson, 2008; Dorfling et al., 2018; Guleria et al., 2023). Once completed, facial approximations are published in the media for the potential recognition by family members or the public to provide identification of the deceased. When constructing a face, the eyes are prioritised as they tend to play a more significant role in distinguishing individuals when compared to other facial features (Janik et al., 1978; Ellis et al., 1979; Haig, 1984; Taylor, 2000; Wilkinson, 2004; Kunjur et al., 2006; Frowd et al., 2011; Davy-Jow, 2013). The term facial approximation is also referred to as facial reconstitution (Suzuki, 1973), facial restoration (Farrar, 1977), facial sculpture (Gatliff, 1984), facial reproduction (Rhine, 1990) and facial reconstruction (Tyrrell et al., 1997). The term, "facial approximation", will be used in this project rather than "facial reconstruction", which refers to additional procedures, methods of facial surgery and the procedure of rebuilding a skull from skull fragments (Stephan, 2003).

Average soft-tissue thickness values, determined at specific bony landmarks, are commonly used in the facial approximation process (Beaini et al., 2021; Guleria et al., 2023). Reference thicknesses are determined based on a variety of methodologies and modalities and the effect of sex, ancestry, age and body mass index (BMI) have been described (Aulsebrook et al.,

© University of Pretoria

1995; Phillips and Smuts, 1996; Wilkinson, 2002; Cavanagh and Steyn, 2011; Manhein et al., 2000; Beaini et al., 2021; de Barros et al., 2021). The American and Manchester methods of facial approximation utilises soft-tissue markers, based on tissue depth measurements, to create a face on a skull (Taylor, 2000). These soft-tissue markers have been acquired by taking direct measurements on cadavers, using ultrasonic echolocation, CT and MRI (Aulsebrook et al., 1995; Phillips and Smuts, 1996; Wilkinson, 2003; Stephan and Davidson, 2008; Galdames et al., 2008; Stephan et al., 2009; Cavanagh and Steyn, 2011; Byers, 2016). Some modalities have been criticised as the subject is positioned in the supine position during scanning, causing gravity to create tissue depth measurements which are not comparable in the upright position. Using cadaveric material has an additional disadvantage in that the measurements are often influenced by soft-tissue distortion or desiccation, while the embalming medium is also likely to affect soft-tissue preservation (Wilkinson, 2004; Munn and Stephan, 2018).

Aulsebrook and colleagues (1995) pointed out that by using linear soft-tissue depth measurements to reconstruct a face, only the areas surrounding the pegs are accurate. The areas between pegs and the detail of the facial features, e.g. the eyes, are filled and modified by the artist, resulting in a subjective rather than objective facial approximation (Aulsebrook et al., 1995). On the assessment of the validity of facial approximation methods, Aulsebrook concluded that future research should focus on the quantification of facial features and that it be supported by mathematics, three-dimensional (3D) geometry and topology so that they can be compared statistically rather than subjectively (Aulsebrook et al., 1995).

A further concern is that guidelines for soft-tissue depths as well as other variables vary between and among population groups, making the broad application of guidelines for one population inaccurate for another (Cavanagh and Steyn, 2011). Substantial variation in soft-tissue depths around the periorbital region and eyeball position have been shown to vary among populations in South Africa (Dorfling et al., 2018). However, the study sample was small, measurements performed were limited and were taken on cadavers and computer tomography (CT) scans, which are affected by gravity effects and soft-tissue distortion (Dorfling et al., 2018). Studies have indicated that gravity affects the position of the eyeball within the orbit (Haslwanter et al., 1992; Harris et al., 1993; Cabungcal et al., 2001; Pierrot-Deseilligny, 2009). Substantial variation has also been noted concerning the height and width of the palpebral fissure between the sexes and among populations (Kunjur et al., 2006; Song et al., 2007; Rhee et al., 2012). These findings further highlight the necessity for developing population-specific guidelines for the position of the eyeball among South African groups (Ridel et al., 2018).

© University of Pretoria

The SAPS currently uses the “Virtual sculpture” method, performed using the Freeform Modelling Plus™ software. This software is based on the Manchester method of facial approximation, which incorporates facial muscles, soft-tissue landmarks and skull robusticity. Facial features can also be imported from a database and then scaled and positioned according to the bony landmarks of the skull. Soft-tissue markers are then imported to create the skin layer on top of the muscle layer to complete the face. The facial features are then manually changed with the aid of the haptic device in the hope that the final product will resemble the characteristics of a South African face.

The database currently in use in the Virtual Sculpting method is based on soft-tissue thicknesses of North American cadavers. Soft-tissue thicknesses are population-specific making facial approximations based on a North American database often inadequate for accurately depicting a South African person (Ridel et al., 2020b). The predicament faced by the SAPS is that the manual landmarking and fine-tuning of facial features are subjective and the reference databases are also not based on variation among South African groups. The results of inaccurate data are poor correlations between the facial soft-tissue features and the bony framework of the skull (Ridel et al., 2020b).

The Forensic Anthropology Research Centre (FARC) at the University of Pretoria is currently engaged in active research aimed at aiding the VIC of the SAPS in creating biological profiles (sex, population affinity, age and stature) of deceased children and adults to produce more accurate facial approximations (Krüger et al., 2018; Ridel et al., 2018; 2020b; Shakoane et al., 2021). Biological anthropologists have found considerable variation in facial features and underlying bony tissue among self-identified South African population groups, namely black, white and coloured South Africans. For example, the bony landmarks of the nasal aperture, such as nasal widths, nasal height, nasal bone projection, mid-facial dimensions, and menton shape differ in size and shape between black and white South Africans (Ridel et al., 2018; Braun et al. 2023). Furthermore, positive correlations have been found between the hard tissue and soft tissue structures of the human face, such that knowledge of the size and shape of a bony element, such as the menton, nasal aperture, or external acoustic meatus, can be used to predict the outlying soft tissue (Ridel et al., 2020; Erasmus et al., 2023; Braun et al., 2023). In this study, the dimensions and shape of the bony orbit and eyeball are examined, adding knowledge around variation in hard and soft tissue features so that practitioners can construct more accurate facial approximations of unknown persons in South Africa.

Promising results have been obtained in recent years by studies aiming to predict the soft tissue structure and the facial features, based on their relationship with the underlying bony tissue, using geometric morphometric methods for the nose, mouth, chin and ear

© University of Pretoria

(Vandermeulen et al., 2006; Claes, 2007; Tilotta et al., 2010; Schlager, 2013a; Guyomarc'h et al., 2014; Ridel et al., 2020a). These studies aimed to create an automated facial approximation method, which will be time efficient, objective, repeatable and would be able to create multiple facial representations based on a single skull (Vandermeulen et al., 2006; Claes, 2007). Unfortunately, most of the studies have been performed using computer tomography (CT) scans, which are taken in the supine position calling the results into question, while the landmarks were placed manually, resulting in higher observer error values (Tilotta et al., 2010; Schlager, 2013a; Guyomarc'h et al., 2014). Ridel and colleagues (2020b) provided successful statistical prediction of the soft-tissue structure of the nose from the underlying bony tissue of South Africans using cone beam computer tomography (CBCT) scans. As the open eyelids have never been predicted from the underlying bony tissue, this study aims to produce statistical models to predict the open eye of black and white South Africans from the underlying bony tissue.

1.2 Research problem

The approximation of the eyes and periorbital structures is prioritised in the facial approximation process as it is more likely than any other facial feature to lead to the recognition of a familiar face (Janik et al., 1978; Ellis et al., 1979; Haig, 1984; Taylor, 2000; Wilkinson and Mautner, 2003; Wilkinson, 2004; Kunjur et al., 2006; Frowd et al., 2011; Davy-Jow, 2013). At present facial approximation prediction equations regarding the eyeball and periorbital structures, including the palpebral fissure, are either unavailable or are limited in the South African context (Dorfling et al., 2018). Accuracy and repeatability of existing guidelines may be affected by the manual collection of landmarks, the use of data acquired from individuals in the supine position, or data based on the size and shape of structures from other populations (Wilkinson, 2004; Schlager, 2013a; Guyomarc'h et al., 2014; Munn and Stephan, 2018).

1.3 Conceptual framework

The purpose of this study is to use data from CBCT scans, negating the effect of gravity in the supine position, to improve the approximation of the eye and periorbital structures in facial approximations in South Africa. This study was divided into two parts to develop guidelines for performing computerised and automatic facial approximations. In part 1, absolute distances were calculated to determine the normative dimensions of the orbit, eyeball and palpebral fissure. Based on these linear distances, prediction methods were proposed to predict the position of the eye within the bony orbit as well as the eyeball and palpebral fissure dimensions based on proportionality of the orbital height and breadth and by linear regression for use in the virtual sculpting method, currently used by the SAPS. In part 2, an automatic landmarking method, based on well-defined, craniometric (hard-tissue) and cephalometric (soft-tissue)

© University of Pretoria

landmarks (Stephan et al., 2008; Guyomarc'h et al., 2014; Caple and Stephan, 2016) was used to objectively evaluate the shape of the bony orbit and palpebral fissure using CBCT scans of South African groups. Based on the interrelationship between the shape of the orbital rim and the palpebral fissure, statistical models were created to predict the open eyes from the underlying bony tissue for the use in automatic facial approximations.

© University of Pretoria

1.4 Aims and objectives

The study aims to create guidelines for approximating the eye and periorbital structures of South African groups using CBCT scans. The first objective was to establish the mean size of the eyeball, orbit and palpebral fissure for each sex-population group as well as the position of the eyeball within the bony orbit, which is useful in the placement of the eyeball in the orbit during the facial approximation process. Univariate analysis (ANOVA and Tukey's Pairwise tests for parametric or Kruskal-Wallis and Mann-Witney tests for non-parametric data) was conducted to determine the effect of asymmetry, sex and population affinity on these normative values. The linear dimensions were used to define the interrelationship between the position of the eyeball and orbital dimensions; eyeball- and orbital dimensions as well as the palpebral fissure and orbital dimensions which were converted to percentages (proportionality). Furthermore, linear regressions were used to create prediction equations for the use in approximation of the eyeball and palpebral fissures. The manually placed landmarks were used to determine the shape of the orbital region and the palpebral fissure. The classification accuracy for each sex-population group based on the shape and size of the orbital region was determined.

The second objective was to assess shape variation between South African sex-population groups based on automatically projected landmarks and to find the statistical interrelationship between the soft-tissue structure of the eyelids and the hard-tissue structure of the orbit to predict the soft-tissue structure of the eyelids from the underlying orbit for use in an automated facial approximation.

The specific objectives in the study include:

Part 1:

1. Calculate absolute distances from the manual placement of landmarks on the 3D or 2D surface of the palpebral fissure, bony orbit and eyeball to determine the dimensions of the bony orbit and palpebral fissure, respectively.
2. Determine the position of the eyeball within the bony orbit (outer margins of the eyeball to the orbital rim) and the protrusion of the eyeball from the bony orbit (oculus anterus to the orbital rim).
3. Determine the effect of asymmetry, sex and population affinity on the absolute distances describing the size of the orbit, eyeball, eyelids and position of the eyeball in the orbit.
4. Propose the position of the eyeball, eyeball dimensions and palpebral fissure dimensions based on proportionality, while predictive equations are proposed using linear regressions.

© University of Pretoria

5. Determine the shape of the orbit and palpebral fissure based on the manually placed landmarks on the 3D surfaces.
6. Determine the classification accuracy for each sex-population group using a discriminant function analysis (DFA) using the size and shape of the orbit.

Part 2:

1. Extract soft- and hard-tissue surfaces for each individual from the CBCT scans.
2. Create average South African soft- and hard-tissue templates based on a non-rigid surface registration process.
3. Anatomical templating by the automatic landmark projection onto each individual's extracted soft- and hard-tissue surface.
4. Determine shape variation between sex-population groups based on the automatically projected landmarks.
5. Create statistical models based on the relationship between the orbital rim and the palpebral fissure using a Projection onto Latent Structures Regression (PLSR) algorithm.
6. Validate the predicted models using cross-validation testing with the calculation of the Mean Squared Error (MSE) using leave-one-out cross-validation (LOOCV).

© University of Pretoria

2. Chapter 2: Literature review

2.1 Introduction

The soft-tissue structure of the face and facial features are influenced by age, population affinity, sexual dimorphism and positional changes (Phillips and Smuts, 1996; Wilkinson, 2002; Cavanagh and Steyn, 2011; Manhein et al., 2000; Avelar et al., 2017; Beaini et al., 2021; de Barros et al., 2021) as has also been demonstrated in South African samples (Ridel et al., 2018; Shakoane et al., 2021; Braun et al., 2023; Erasmus et al., 2023). As facial approximations are based on the relationship between the soft-tissue structure of the face and the underlying bony tissue (Schlager, 2013a), variations in the anatomy of the skull and facial features among South African groups should be described and considered in the creation of accurate facial approximations.

Investigations in the South African context of the dimensions and shape of the orbit, eyeball and palpebral fissure are limited. This study aims to provide normative values of the size, shape and position of the orbit, eyeball and palpebral fissures for South Africans, to uncover variations between sex and population groups and to derive prediction equations or models for accurate facial approximations.

In this literature review a thorough description of the anatomy of the bony orbit, orbital and periorbital structures is given and the facial approximation methods are discussed. Current guidelines used to approximate the eyeball within the orbit and the guidelines used to reconstruct the palpebral fissures are summarised and critiqued. As these guidelines are based on data derived using various modalities, an overview is given on 3D imaging with their advantages and disadvantages for their use in facial approximation research.

2.2 Anatomy of the bony orbit, orbital and periorbital structures

2.2.1 Bony orbit:

The bony orbit houses the eyeball as well as the extraocular muscles, fat, nerves and vessels (Standring, 2015). The bony orbit consists of (see *Figure 2.1*) the lesser wing of the sphenoid, orbital plate of the ethmoid, lacrimal bone, orbital plate of the frontal bone, orbital plate of the maxilla, greater wing of the sphenoid, zygomatic bones and a very small contribution by the orbital process of the palatine bone (Standring, 2015).

The orbit resembles a quadrangular pyramidal space, which has a roof, floor and a medial and lateral wall. The apex of the pyramid is directed posteromedially towards the optic canal and

© University of Pretoria

the base is directed anterolaterally towards the orbital margins. As the orbit develops around the eyeball, it protrudes outwards to accommodate the lacrimal gland. The widest part is thus not at the orbital margin, but approximately 15 mm behind it (Wolff, 1977). The bony orbit contains the optic canal, superior and inferior orbital fissures that connect the orbit to the cranial cavity, pterygopalatine and infratemporal fossae (Wolff, 1977; Moore et al., 2013; Standring, 2015).

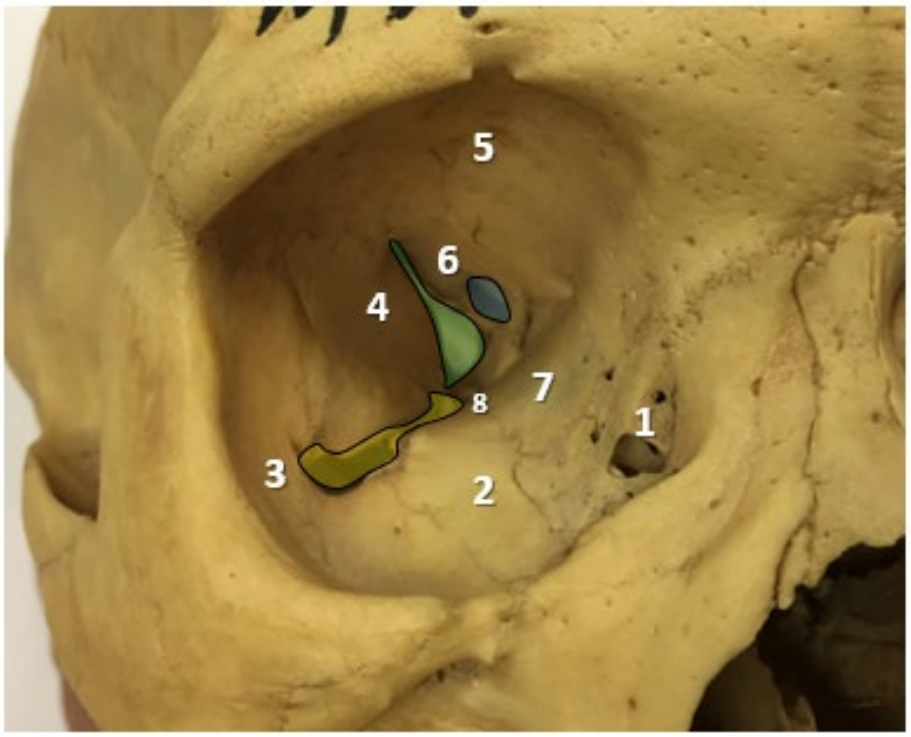

1. Lacrimal bone
2. Maxilla
3. Zygomatic bone
4. Greater wing of the sphenoid
5. Frontal bone
6. Lesser wing of the sphenoid
7. Ethmoid bone
8. Palatine bone

Blue: Optic canal

Green: Superior orbital fissure

Yellow: Inferior orbital fissure

Figure 2.1. The right bony orbit with its openings

The orbital margin has a quadrilateral shape with rounded edges and the lacrimal fossa that lies within the orbital margin. It is formed by the frontal, zygomatic and maxillary bones. Each side of the quadrilateral orbital margin is approximately 40 mm, but the width of the orbital margin is frequently greater than the height. The orbital index (= height of the orbit x100 / width of the orbit) is the relation between the height and the width of the orbit and may differ among geographically distinct groups (Wolff, 1977).

The orbital margin changes in size and shape with advancing age. At birth, the orbital margin is sharp to protect the eyeball during the birthing process. Further changes in the shape and size of the orbit depend on facial development and the development of the paranasal sinuses. At the age of seven, the orbital margin tends to be trapezoidal with less sharp margins

© University of Pretoria

compared to infants and clearly defined superomedial and inferolateral angles (Wolff, 1977). In adulthood up to senescence, shape and size changes are mostly attributed to the absorption of bone. Elderly skulls may present with holes in the orbital roof, placing the periorbital structures in direct contact with the dura mater. The lateral orbital wall often shows signs of absorption, which is less commonly seen in the medial wall or floor. The orbital fissures, in particular the inferior orbital fissure, are expanded by absorption of its margins (Wolff, 1977). Avelar and co-workers (2017) reported an initial increase in the size of the rounded orbital margin while maintaining its shape but with advancing age, most prominent in skulls >50 years of age, the orbital margins became more rectangular and thus increasing the orbital size (Avelar et al., 2017).

Limited sex differences can be observed in the skull up to puberty, but thereafter secondary sexual characteristics change the size and shape of the skull. Adult males present with a well-pronounced supraorbital rim, whereas the supraorbital rim is subtle and sharper in females (İşcan and Steyn, 2013; Avelar et al., 2017). Krüger and colleagues (2015) reported significant differences in the supraorbital margins between sexes, as well as a significant difference in the supraorbital margin between black and white South African females (Krüger et al., 2015). The more pronounced supraorbital rims may be due to the larger frontal sinuses reported in males, producing distinct superciliary ridges with a less vertical forehead (Özer et al., 2016). Studies investigating the shape and size variation in the orbital margins between sexes have concluded that sex influences the size and shape of the orbits, as males commonly present with wider, rectangular orbits and a deeper lateral orbital margin, while females present with shallow, round orbital margins (Bigoni et al., 2010; Gonzalez et al., 2011; Franklin et al., 2012; Milella et al., 2021; Toniva et al., 2022; Ajanovic et al., 2023).

Population affinity also affects the shape and size of the orbital rim. Asian orbits tend to exhibit rounded orbital contours, while Europeans present with square, more inclined orbital rims and Africans with shorter wider orbital rims (Xing et al., 2013). Rubin and deLeon (2017) concluded that the greatest population variation was noted in the curves of the medial and lateral orbital walls when the shape of the orbit was compared between white, black and Asian samples.

Asymmetry in the orbital dimensions has been reported in the literature, although its presence varies between studies. Asymmetry was noted in the orbital breadth of a French sample (Guyomarc'h et al., 2012), while asymmetry in the orbital height was recorded in a Turkish female sample (Özer et al., 2016). No significant difference was noted between the left and right orbital dimensions in a Chinese and Egyptian sample (Ji et al., 2010; Attia et al., 2018).

© University of Pretoria

2.2.2 Orbital and periorbital structures, including the eyelids

The orbital and periorbital structures include the eyeballs, muscles surrounding the eyeballs, connective tissue and fat between the eyeball and bony orbit as well as the eyelids, eyelashes and eyebrows surrounding the eyeball externally (Naini, 2011).

An intricate network of connective tissue can be found within the orbit, which forms the support structure of the eyeball. The connective tissue network also groups the orbital fat and restrains ocular rotations. Some of these connective tissue structures have clinical and anatomical importance, including the orbital septa, fascial sheath of the eye and suspensory ligament of the eyeball. The orbit also houses seven extraocular muscles, of which one elevates the superior eyelid (levator palpebrae superioris) and six move the eyeballs (four recti muscles and two oblique muscles) (Standring, 2015).

The eyelids or palpebrae are two thin movable anterior structures that protect the eye when closed (Naini, 2011; Standring, 2015). The position of the eyelids depends on the muscle tone in the levator palpebrae superioris and orbicularis oculi muscles as well as the degree of protrusion of the eyeball (Standring, 2015).

The superior eyelid extends to the eyebrow above and the inferior eyelid smooths into the cheek at the nasojugal and malar sulci. These folds intensify with advancing age as the skin is tied to the underlying periosteum. The superior eyelid is the more mobile and overlays the cornea in a forward gaze, while the inferior eyelid lies just inferior to the cornea in a forward gaze. The eyelids encircle the elliptical palpebral fissure between their boundaries and meet at the medial and lateral canthi. The anatomy of the eyelids is indicated in *Figure 2.2*. In European groups, the medial canthus is often situated approximately 2 mm lower than the lateral canthus. The inclination of the palpebral fissure is recorded as 2°± 2° in males and 4°± 2° in females, which may increase in those of Asian ancestry (Farkas, 1994; Naini, 2011).

Clinical observations noted substantial variation in the size and shape of the periorbital regions between sexes and populations (Kunjur et al., 2006; Song et al., 2007; Rhee et al., 2012). Kunjur and colleagues (2006) quantified the relationship of the eyebrow to the eyelids and the palpebral fissure in males and females of groups defined in the research as White, Indian and Chinese. White males had a significantly narrower palpebral fissure when compared to their Indian counterparts. The axis of the palpebral fissure indicated that the lateral canthus was situated significantly higher in white females when compared to Indian females. Males and females from the Chinese group presented with significantly wider inner canthal distances when compared to both the White and Indian groups (Kunjur et al., 2006). As variations have been reported between males and females and among population groups, it is necessary to

© University of Pretoria

assess if similar variations are present between white and black South Africans. Differences in the height and width of the palpebral fissures were noted between sexes (Song et al., 2007); females had greater palpebral fissure heights whereas males had greater palpebral fissure widths. However, this variation has not been observed in other groups (Song et al., 2007). Asymmetry was also noted with the left side presenting with a taller palpebral fissure height than the right side in both males and females.

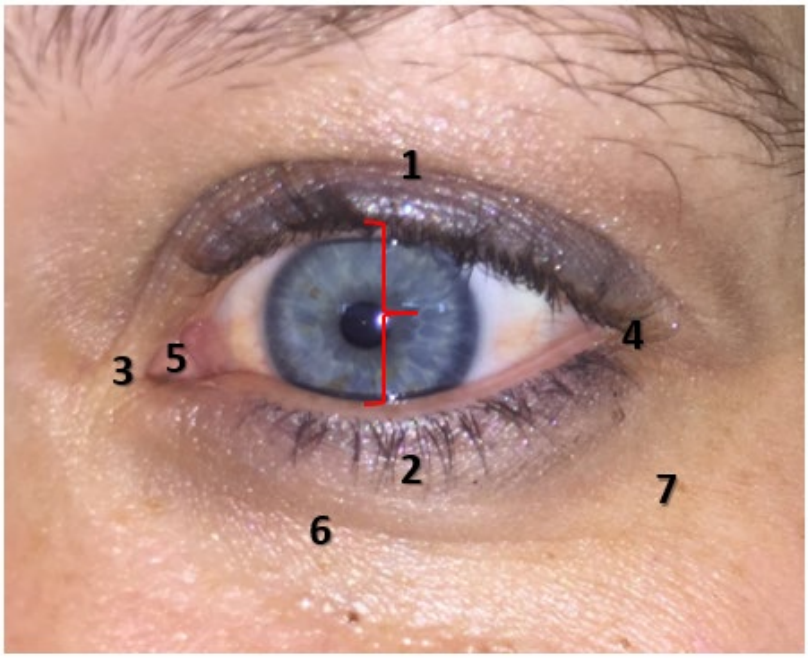

1. Superior eyelid
2. Inferior eyelid
3. Medial canthus
4. Lateral canthus
5. Lacrimal caruncle
6. Nasojugal sulcus
7. Malar sulcus

Red bracket: palpebral fissure

Figure 2.2. Anatomy of the eyelids

2.2.3 Eyeball

The eyeball is covered by three distinct layers, the corneoscleral envelope, which forms the tough, inelastic outer layer has two parts, the cornea, the transparent anterior sixth and the sclera and the white opaque posterior five sixths. The uvea forms the middle layer and is highly vascularised comprising the choroid, ciliary body and the iris. The retina forms the internal photosensitive layer which contains photoreceptors and neurons involved with the initial processing of visual stimuli (Moore et al., 2013; Standring, 2015).

The eyeball is not a spherical structure but consists rather of two fused spheres, the cornea is the smaller sphere with a radius of 7.8 mm when compared to the sclera with a radius of 12 mm. The junction of the cornea and sclera is marked by the external scleral sulcus, known as the limbus.

The reference textbooks and published literature describe the size of the eyeball as 23.4 - 25 mm in diameter from anterior to posterior (sagittal/axial length) and 23 - 25 mm from side to side (transverse). The vertical diameter has been described as 23.5 - 25 mm (Wolff, 1977;

© University of Pretoria

Wilkinson et al., 2012; Moore et al., 2013; Bekerman et al., 2014; Standring, 2015). The axial length of the eyeball is more variable than the vertical and transverse diameters.

The literature reviewed is not in agreement regarding the variation between eyeball sizes among the sexes. Wolff (1977) found male eyeballs to be somewhat larger than female eyeballs (Wolff, 1977). Bekerman and co-workers (2014) found no statistically significant difference in the size of the eyeball between the different sexes, populations or age groups. They found the right eyeball to be slightly smaller than the left, but the difference was not significant (Bekerman et al., 2014).

2.2.4 Anatomical position of the eyeball

The eyeball is found superolaterally within the anterior orbit. It occupies only one-fifth of the orbital cavity. When a line is drawn from the superior to inferior orbital margins the cornea will barely touch this line in forward gaze. When a line is drawn from the lateral to medial orbital margins, approximately one-third of the globe would project anterior to it. The eyeball is shielded within the lateral orbits. The interpupillary distance is 58-60 mm, with the distance between the medial canthi approximately half of this distance. Certain dysmorphic cranial disorders may distort these distances e.g. hypertelorism increases the interpupillary distance while Waardenberg's syndrome increases the inner canthal distance (Wesoly, 2017; Liu et al., 2020).

Exophthalmometry is valuable in determining globe positioning in the anterior-posterior plane in living individuals as it gauges eyeball protrusion while seated with gravitational effects acting inferiorly. A Hertel or the Luedde exophthalmometer measures the projection of the eyeball from the deepest point on the lateral orbital margin to the most anterior point of the cornea (Stephan, 2002). To measure eyeball protrusion using one of these devices, the exophthalmometer is placed firmly against the lateral orbital margin and the projection of the cornea can thus be read off the scale (Davanger, 1969; Stephan, 2002). Studies have indicated that globe projection is significantly greater in males when compared to females (de Juan et al., 1980; Dunsky, 1992). Significant differences in globe projection between black and white Americans have also been reported (Brown and Douglas, 1975; de Juan et al., 1980; Bogren et al., 1986; Barretto and Mathog, 1999). Barretto and Mathog (1999) noted a significant difference in globe projection between males and females of both black American and white American groups. These observations correspond to the findings of Dunsky (1992) who also found a statistically significant projection between black American males and females, with males having a greater mean projection when compared to females within the same population group (Dunsky, 1992).

© University of Pretoria

2.3 Facial approximation techniques

2.3.1 Introduction

Facial approximation is the construction of a face over a skull to recreate an *in vivo* face of a deceased person (Stephan and Davidson, 2008; Dorfling et al., 2018; Guleria et al., 2023). This process is based on the presumed morphological relationship between the underlying bone and the soft-tissue of the face (Schlager, 2013a). Welcker (1884) and His (1895) were the first scientists to use skeletal remains to produce facial approximations (Welcker, 1884; His, 1895).

2.3.2 Traditional methods of facial approximation

Three categories of facial approximation techniques exist, including 1) two-dimensional (2D) facial approximation and craniofacial superimposition (Ubelaker et al., 1992; Taylor, 2000; Ubelaker, 2015; Stephan et al., 2019; Guleria et al., 2023), 2) three-dimensional (3D) manual facial approximation (Snow et al., 1970; Gerasimov, 1971; Praig and Neave, 1997; Vanezis and Vanezis, 2000; Guleria et al., 2023) and 3) 3D computer-based facial approximation (Vanezis and Vanezis, 2000; Wilkinson 2003; 2010). For a 2D facial approximation, an image of a face is created two-dimensionally by drawing or by superimposing a photograph onto the skull under investigation (Taylor, 2000). Three-dimensional (3D) manual facial approximation is the recreation of a face onto a skull using clay (Snow et al., 1970; Gerasimov, 1971; Praig and Neave, 1997; Wilkinson, 2004, 2010). There are three main methods of 3D manual facial approximation techniques: anatomical or Russian, anthropometric or American, and combination or Manchester (Verzé, 2009; Guleria et al., 2023).

The anatomical or Russian method was created by Mikhail Gerasimov in 1971. This method is divided into two phases (Verzé, 2009). In the first phase, the soft-tissue elements (e.g. facial muscles and fat), are modelled onto a target skull based on the robusticity of the muscle attachment sites. In the second phase, the final modelling, a thin layer is modelled onto the facial soft-tissue structures (Gerasimov, 1971; Verzé, 2009; Gupta et al., 2015; Guleria et al., 2023). The second phase introduces bias, as it relies on the subjective opinion of the artist to recreate the facial features based on the underlying bony tissue (Verzé, 2009). This method was further criticized by Gupta and colleagues (2015) as it is time consuming and requires in depth Anatomical knowledge (Gupta et al., 2015).

When using the anthropometric or American method, the first step in the facial approximation process is to place pegs, representing the average soft-tissue thicknesses (STT), on the surface of the skull at specific anatomical landmarks (Taylor, 2000; Verzé, 2009). The pegs may be attached via the planar or the imported peg method (Mires et al., 2003; Wilkinson et

© University of Pretoria

al., 2006). These pegs may differ in number and thickness depending on sex, age and population. The soft-tissue is recreated by filling in the spaces between the pegs with modelling clay (Taylor, 2000). With this method, the practitioner does not consider the underlying anatomical structures as they do with the Russian method (Snow et al., 1970). Another disadvantage of relying on STT values only, is that only the areas related to the pegs will be recreated accurately, while the areas between the pegs would rely on artistic skill (Aulsebrook et al., 1995). As the American and Russian methods requires great experience and skills, these methods are not currently used (Gupta et al., 2015; Guleria et al., 2023).

Facial soft-tissue thicknesses have been recorded for various geographical locations, as well as some South African groups, including black South African females and South Africans of mixed racial origin (Aulsebrook et al., 1995; Phillips et al., 1996; Cavanagh and Steyn, 2011). In the Manchester method, Richard Neave combined both anatomical and anthropometric methods (Praig and Neave, 1997; Verzé, 2009; Gupta et al., 2015; Guleria et al., 2023). With the combined method the artistic subjectivity, which takes place between pegs, is significantly reduced because the face is reconstructed according to anatomical principles (Praig and Neave, 1997; Guleria et al., 2023). In the manual Manchester method, the facial muscles are placed as they span across their origin and attachment to the skull surface. Other relevant facial structures are modelled onto the face (e.g. the parotid gland). Secondly, facial features such as the eyeballs and eyelids are placed and modelled according to published data (Stephan, 2002; Wilkinson and Mautner, 2003; Gupta et al., 2015). After the muscle layer has been placed, the Manchester method requires a skin layer, which can be established using tissue depth markers as guides (Taylor, 2000; Wilkinson and Rynn, 2012). The skin layer can be placed with the additional method (placing balls of clay varying in size in the areas that need to be filled and then smoothed out) or the offset method (placing clay strips of approximately 4 mm between STT markers to fill in the spaces between the placed facial muscles and structures (Wilkinson and Rynn, 2012). Lastly, textures are added to create a realistic reconstruction.

2.3.3 Computerised 3D facial approximation methods

In an attempt to develop a method that is less subjective, more time-efficient and which produces multiple variations of a face, computer-based programmes have been used for creating facial approximations (Turner et al., 2006; Gupta et al., 2015). Two computer-based approaches exist, the “Virtual sculpture” method and the automated method (Wilkinson, 2005; Turner et al., 2005; Claes et al., 2006; Wilkinson et al., 2006; Claes et al., 2010; Wilkinson and Rynn, 2012; Lee et al., 2012). In 2003 Wilkinson introduced the computerised “Virtual sculpture” method which aims to imitate and expand on the 3D manual Manchester method

© University of Pretoria

(Wilkinson, 2003). This computer method combines facial anatomy, facial expression, anthropometry, anthropology as well as the relationship between the hard- and soft-tissues of the face (Wilkinson, 2004). The “Virtual sculpture” method operates using the FreeForm Modelling Plus™ software with haptic feedback (Phantom Desktop™ haptic Device) which allows physical contact between the computer and the user via the Haptic device (Wilkinson, 2003).

During a facial approximation using the computerised Manchester method, pre-modelled muscles are imported from a database to reconstruct the anatomical structures of the face (Wilkinson et al., 2006). As the facial muscles have reliable attachments and morphology, each muscle is individually employed and altered relative to the size and proportions of the skull (Wilkinson, 2003; Wilkinson et al., 2006; Lee et al., 2012). Each muscle can be deformed and changed individually to fit the robusticity of the skull. To create the facial shape and profile, it is important to import and deform all the craniofacial muscles as well as other important anatomical structures, such as the parotid gland and superior temporal vessels (Wilkinson and Rynn, 2012; Lee et al., 2012). Certain facial features can be imported from a database and then scaled and positioned according to the bony landmarks of the skull (Wilkinson et al., 2006). To create the skin layer, soft-tissue depth markers can be imported to complete the face and by using the haptic device, the areas around the markers and facial features can be modified and smoothed out (Wilkinson and Rynn, 2012). By using the programme tools, for instance, the “tug” tool, age-related changes can be modelled for a more realistic reconstruction (Wilkinson, 2003).

The “Virtual Sculpture” method, performed by Freeform Modelling Plus™ software, is the method of choice for the South African Police Service (SAPS), to approximate the face following the estimation of the biological profile (Ridel et al., 2020b). The skull of the unidentified individual is scanned using a Metrascan 210 which is imported into the Freeform Plus modelling software (Wilkinson et al., 2006; Ridel et al., 2020b). The soft-tissue depth markers are placed onto the imported skull at predefined bony landmarks using a 3D stylus. Currently, the soft-tissue depth markers placed to create the skin layer, are from a North American database derived from cadaver based studies (Ridel et al., 2020b). The areas surrounding the soft-tissue depth markers, especially surrounding the facial features, are then manually changed to create a face that supposedly resembles the unidentified individual thus resulting in less accurate and more subjective approximations (Ridel et al., 2020b).

The influence of sex, population affinity, age and BMI on the STT values of the face have been thoroughly investigated and variations have been noted and described in the literature (Aulsebrook et al., 1995; Phillips and Smuts, 1996; Wilkinson, 2002; Cavanagh and Steyn,

© University of Pretoria

2011; Manhein et al., 2000; Beaini et al., 2021; de Barros et al., 2021). Creating a facial approximation based on STT values obtained from another sex or population group will result in an inaccurate reconstruction which should be taken into consideration when performing a facial approximation (Phillips and Smuts, 1996; Ridel et al., 2020b).

Another factor that has also been investigated is the effect of gravitational forces on the soft-tissue structure of the face. The majority of published research describing the STT values of the periorbital region and the positioning of the eyeball within the orbit has been performed on cadavers, CT or MRI scans (Aulsebrook et al., 1995; Phillips and Smuts, 1996; Wilkinson et al., 2003; Galdames et al., 2008; Stephan et al., 2008; Stephan et al., 2009; Cavanagh and Steyn, 2011, Dorfling et al., 2018). In 2004, Wilkinson criticised these methods stating that gravity may influence measurements taken on participants or patients in the supine position (Wilkinson, 2004).

Contradicting results have been published as some authors found gravity to affect the soft-tissue structure of the face, while others reported little variation in STT values between the supine and prone positions (de Greef et al., 2006; See et al., 2008; Baillie et al., 2015; Stephan and Preisler, 2018). Common variations in STT values due to positional changes and the effect of gravity are commonly described in the lateral facial landmarks (Wilkinson 2002; de Greef et al., 2006; See et al., 2008; Munn and Stephan, 2018). There has been limited research on the impact of gravity on the positioning of the eyeball in the bony orbit and the periorbital structures in humans. Research on cats and rhesus monkeys has shown displacement of the eyeball in both supine and prone positions (Haslwanter et al., 1992; Harris et al., 1993; Cabungcal et al., 2001). Pierrot-Deseilligny concluded that gravity plays a role in the vertical position of the eyeball in humans based on results obtained from positional changes of the head (Pierrot-Deseilligny, 2009). Apart from the effect of gravity on the eyeball, the periorbital structures are also influenced by gravity. In a more recent study, Munn and Stephan re-evaluated the effect of gravity on STT values by using high-resolution dimensional imaging stereo-photographs of 62 subjects in the supine and prone positions. They found a significant difference in the STT values lateral and inferior to the orbit as the soft-tissue retracted laterally during the supine position (Munn and Stephan, 2018). However, the gravitational effect on the position of the eyeball in the orbit has not been quantified. Developing guidelines for the approximation of a South African face using CBCT images will negate the possible effects of gravity in the supine position and desiccation, and could address some of the current objections about this computer-based facial approximation method.

© University of Pretoria

2.3.4 Approximation of the eyeball and palpebral fissure

When the eyeball is positioned in the bony orbit during a facial approximation, globe positioning takes place in three planes: the superior-inferior plane, medial-lateral plane and the anterio-posterior plane. During the approximation of the eyeball, pre-existing eyeballs with a standard diameter of 25 mm are positioned within the orbits (Wilkinson et al., 2006; Lee et al., 2012; Gupta et al., 2015). In the late 1980's, the position of the eyeball in the mediolateral and supero-inferior planes was achieved by placing the eyeball centrally within the orbit (Gatliff, 1984; Krogman and İşcan, 1986; Gatliff and Taylor, 2001; Taylor and Craig, 2005). Yet other researchers have found that the eyeball is closer to the superior and lateral orbital margins, rather than centrally placed (Goldnamer, 1923; Whitnall, 1932; Wolff, 1977; Dorfling et al., 2018) (*Figure 2.3*). The eyeball is currently placed in the centre of the orbit and then adjusted manually (Krogman and İşcan, 1986; Lee et al., 2012; Wilkinson and Rynn; 2013).

Stephan and Davidson aimed to clarify the contradicting data in 2008, by dissecting four Australian cadavers (2 males, 2 females). Various measurements were taken in order to describe the exact position of the canthi and the eyeball, respectively. Their results showed that the lateral canthus was 4.5 mm from the lateral orbital margin and the medial canthus was 4.8 mm from the medial orbital margin. The position of the eyeball was 5.1 mm from the superior orbital margin, 7.8 mm from the inferior orbital margin, 7.0 mm from the medial orbital margin and 4.0 mm from the lateral orbital margin (Stephan and Davidson, 2008). In 2009, Stephan repeated the same study but increased the sample size to 9 cadavers to test the results found in 2008. The results demonstrated the same trend: the eyeball is more supero-laterally positioned (Stephan et al., 2009).

Dorfling and co-workers (2018) determined the position of the eyeball in the orbit using cadavers from a South African sample and found a similar supero-lateral location of the eyeball within the orbit. The authors described the position of the eyeball as 3.4 mm from the superior orbital margin, 6.1 mm from the inferior orbital margin, 8.3 mm from the medial orbital margin and 4.2 mm from the lateral orbital margin (Dorfling et al., 2018). The lateral canthus is at an equal level to the malar tubercle and is somewhat higher than the medial canthus (Farkas, 1994; Stephan et al., 2008). According to Anastassov and van Damme (1996), the lateral canthus moves downwards, lower than the medial canthus with the advancement of age (Anastassov and van Damme, 1996).

© University of Pretoria

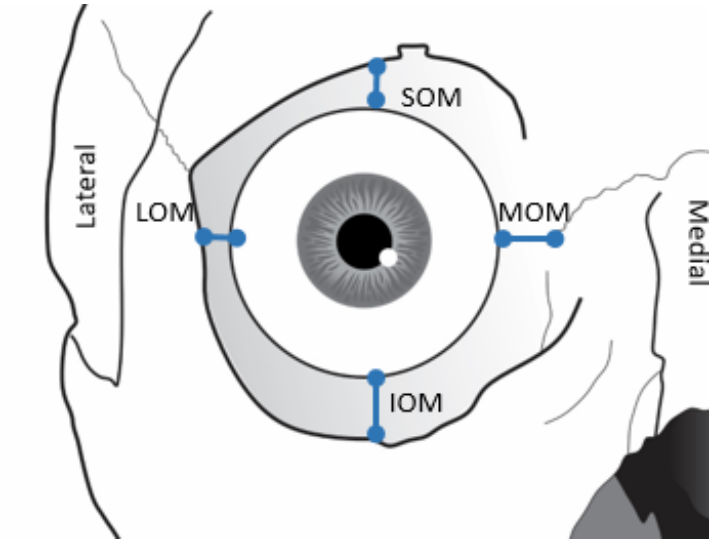

Figure 2.3. Recorded eyeball position within the orbit adapted from Dorfling and colleagues (2018)

To place the eyeball in the anterior-posterior plane, the cornea can be located at the junction of a line drawn from the superior orbital margin to the inferior orbital margin and the other line intersecting the orbit between the above-mentioned landmarks. Gatliff and Snow, (1979) confirmed the above theory and stated that the cornea would touch a line drawn from the superior to the inferior orbital margins (Gatliff and Snow, 1979). However, more recent research, performed on MRI from 39 patients, indicated that the eyeball projects 3.80 ± 2.48 mm from a line connecting the midpoints of the supra- and infraorbital margins (Wilkinson and Mautner, 2003) (*Figure 2.4*). Another cadaveric study described that the eyeball projects 15.90 ± 2.60 mm from the deepest point on the lateral orbital margin (Stephan et al., 2008; Stephan et al., 2009) (*Figure 2.5*). Currently, the eyeball is positioned in the orbit at a depth at which the iris should touch a tangent taken from the mid superior orbital margin to the mid inferior orbital margin (Stephan, 2002; Wilkinson and Mautner, 2003; Lee et al., 2012; Gupta et al., 2015).

© University of Pretoria

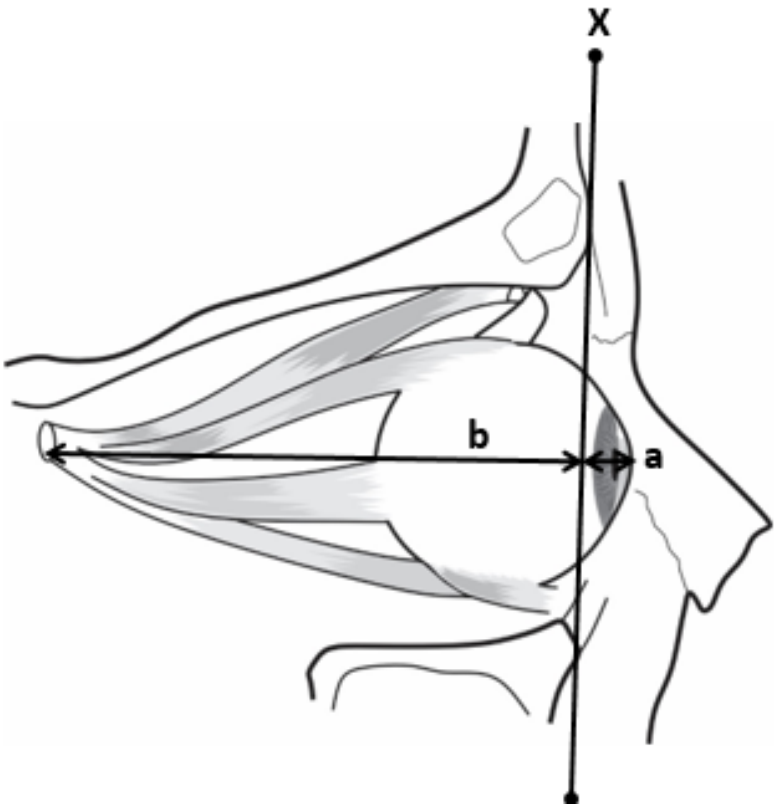

X: Line tangential to mid-SOM and mid-IOM

a: Eyeball protrusion

b: Orbital depth

Figure 2.4. Eyeball protrusion measurement adapted from Wilkinson and Mautner, 2003

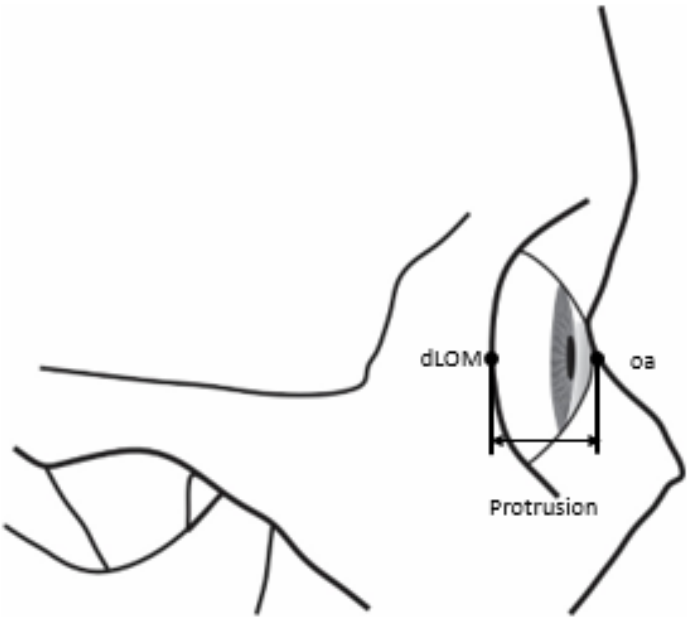

oa: oculus anterius

dLOM: deepest point on the lateral orbital margin

Figure 2.5. Eyeball protrusion from the lateral orbital wall adapted from Stephan and Davidson 2008

© University of Pretoria

Two common methods exist to reconstruct the eyelids. The first is referred to as the extrusion method (Mires et al., 2003; Mahoney and Rynn, 2011). During this process, the eyelids are constructed by extruding an offset piece the thickness of the eyelid from the surface of the eyeball. The offset piece is aligned to the attachments of the eyelids at the medial and lateral canthi. The eyeball surface is extruded backwards, creating upper and lower lids based on the eyeball radius (standard eyeballs are placed with a diameter of 25 mm). The palpebral fissure is created by aligning the lateral and medial canthi to their attachments. Individual lids can be isolated and adjusted to their attachments onto the lacrimal crest and malar tubercle, respectively. Majority of the eyelid should adhere to the shape of the eyeball, and the superior eyelid should overhang the inferior eyelid at the lateral aspect.

The alternative method used for the reconstruction of the eyelids is the addition method (Wilkinson et al., 2006; Wilkinson and Rynn, 2012). This method utilises a pre-made orbicularis oculi muscle sculpted for a 25 mm diameter eyeball. The imported orbicularis oculi muscle is positioned in such a way that the palpebral part is in contact with the superior and inferior eyelids. While initially positioned for a perfect fit, adjustments are necessary to accommodate for hard-tissue variation in the orbital region. The orbital part of the orbicularis oculi muscle is also repositioned to accurately meet surrounding bones, without affecting the palpebral part that remains in contact with the eyeball. Finally, the soft tissue between the upper and lower orbital margins is sculpted towards the eyelids, considering variation in eyelid patterns influenced by orbital shape and subcutaneous fat distribution.

2.3.5 Automatic facial approximations of the facial features

The use of computer-aided facial approximations has increased, as these methods are fast and efficient and it reduces the subjectivity of the practitioner (Guleria et al., 2023). Following the digitisation of the skull of the unknown individual, a face is selected from a database according to the sex, population affinity and age of the individual which fits onto the skull like a mask. The soft-tissue is adjusted according to the applicable STT values. Unfortunately, the facial features remain challenging to reconstruct using this technique (Guleria et al., 2023). Currently, most facial approximations based on automated methods create faces with closed eyes. Open eyes can then be selected from a database which fit the dimensions of the closed eyes in order to produce a facial approximation with open eyes (Vanezis et al., 2000; Gupta et al., 2015; Guleria et al., 2023).

During the past two decades, forensic scientists have attempted to create automated computer-assisted methods to approximate the facial features from the underlying bone based on a variety of different methods and with wide ranges of uncertainty. In 2005, Turner and colleagues introduced a reality enhancement facial approximation (RE/FACE) software to

© University of Pretoria

create automated facial approximations from CT scans of Americans (Turner et al., 2005). An algorithm was used to warp surfaces based on crest lines and curves, followed by a two-step Iterative Closest Point (ICP) registration process. Further deformations were conducted using thin-plate splines. For this method, no anatomical landmarks were identified or placed, and no measurement errors were reported.

Vandermeulen and colleagues (2006) introduced a fully automated 3D computerised facial approximation method in 2006 using Geometric morphometric (GMM) techniques based on 20 CT scans. GMM is a useful tool to observe the shape and size of a biological structure. GMM is based on the Cartesian coordinates of landmarks which allow for a useful visual representation of statistical results as actual shapes or deformations. In this method, the geometry of the landmark configuration is preserved by a set of 3D landmark coordinates (Rohlf and Marcus, 1993; Bookstein, 1996, 1997; Zollikofer and Ponce de León, 2002; Adams et al., 2004; Zelditch et al., 2004, Slice, 2007; Mitteroecker, 2009). In the study conducted by Vandermeulen and colleagues (2006), a template skull (average face) was created considering all the features of the 20 imported facial CT scans. Newly imported skulls were then warped to fit onto the template skull in order to create a facial approximation (Vandermeulen et al., 2006).

To improve on the technique introduced by Vandermeulen and colleagues (2006), Claes and supervisors (2007) described a semi-automated computerised robust statistical facial approximation method (Vandermelen et al., 2006; Claes, 2007). This concept builds on a statistical craniofacial model in which the relationship between soft-tissue thicknesses and facial shape was measured at 52 predefined landmarks on 400 subjects with the aid of ultrasound measuring technology (Claes, 2007). The same 52 corresponding landmarks were placed manually on the skull. In this model, an ‘elastic’ face is transformed to fit onto a target skull (Claes, 2007). In order to create a robust statistical embedded registration framework, several surface registration tasks were performed. These tasks involved the establishment of the geometrical relationship between the surface of the face and the surface of the skull (Claes, 2007). The Root-Mean-Squared-Error (RMSE) was calculated of the distances between analogous points of the original training set data and the model description to determine the accuracy of the shape (Claes, 2007). This was calculated for all facial entries. The global RMSE was reported as 1.38 mm (Claes, 2007) meaning that an average deviation of 1.38 mm was seen globally, over all reconstructions.

Another predictive method was described by Tilotta and co-workers (2010) based on 47 CT scans of a French sample. The study used an automatic patch extraction and surface estimation method based on the placement of four landmarks (nasion, rhinion, anterior nasal

© University of Pretoria

spine and nasospinale) onto the skull aiming to predict the soft-tissue structure of the nose based on the hard-tissue patch (Tilotta et al., 2010). The disadvantage of this method involved using geometrically determined rectangular regions for the patch extraction, rather than regions outlined by defined anatomical landmarks (Schlager, 2013a).

An improved approximation method was introduced by Schlager (2013a) based on GMM to predict the soft-tissue structure of the nose using Chinese and European CT scans. Fourteen craniometric and 15 capulometric anatomical landmarks were used to define the region of interest. The nasal prediction was based on the statistical interrelationship of the hard- and soft-tissue structures considering sex, age and population affinity. Using principal component regression and projection onto latent structures regressions (PLSR) models, this study predicted the soft-tissue structure of the nose with a prediction error ranging from 1.2 -1.4 mm (based on mesh-to-mesh distances), while the prediction error increased to 2.0 - 2.7 mm when population affinity (European and Chinese) was added as a factor (Schlager, 2013a). Disadvantages of this method included the use of CT scans, in which the patient is scanned in the supine position, exposing the soft-tissue structure to gravitational forces, and the manual placement of landmarks onto a large dataset, which may lead to an increased observer error.

An anthropological facial approximation in three dimensions (AFA3D) method was developed in 2014 by Guyomarc'h and colleagues. This is a comprehensive method, which integrated GMM, statistical models and in addition, took STT values into account for the prediction of facial features. This approach yielded a set of 100 cutaneous landmarks, which were then transformed into facial shapes by warping a unified template. This is the first study including the approximation of the eyes using GMM (Guyomarc'h et al., 2014). Following a PLSR, a leave-one-out re-sampling method was used to calculate the uncertainty of the approximations. The capulometric landmarks (endocanthion, exocanthion, oculus anterior and palpebrale inferior) could be predicted with an average measurement error of 2.9 mm, ranging between 2.6 – 3.1 mm across the sample of 92 CT scans of French males and females. Unfortunately, this method was also based on placing manual landmarks on surface renderings created from CT scans. The position of the palpebrale superior was not included, which would have resulted in a more accurate prediction of the open eyes (palpebral fissure).

In 2020, Ridel and associates created a method predicting the soft-tissue structure of the nose of white and black South Africans (Ridel et al., 2020). This study addressed the shortcomings of the existing literature by using CBCT and an automatic landmarking method in a similar approach as described by Schlager (2013a) and Guyomarc'h (2014). The use of CBCT scans negates the effect of gravity associated with a supine position on the soft-tissue structures of the face, while an automatic landmarking method has been proven to be more accurate and

© University of Pretoria

reliable (Ridel et al., 2020a; 2020b). The accuracy of the predictions was tested by estimating the mean squared error (MSE), while a leave-one-out cross-validation (LOOCV) method was used to assess the performance of the equation regression. The MSE was compared between the training and the predicted data. Their method proved repeatable and objective (Ridel et al., 2020b). This method should be considered to assess the prediction accuracies of the eyelids, ears and mouth of South Africans.

At present a fully automated 3D computerised facial approximation method is possible, involving the automatic placement of landmarks on a CBCT target skull and the accurate prediction of the surface of the face by using projection onto latent structures regression (PLSR) algorithms. However, greater accuracy of prediction is needed for other facial features such as the eye, and skeletal and soft-tissue variation found among South Africans.

2.3.6 Modalities used in the creation of approximation methods

2.3.6.1 Computed Tomography (CT) scans

Automatic computer-aided facial approximations aimed at predicting the facial features from the underlying bony tissue have been based on conventional CT scans. During a CT scan, a complete image volume of the scanned object taken around a single rotational axis is created from a large series of 2D X-ray images. An X-ray source is mounted on a rotatable ring, which rotates around the patient in the supine position, with an array of detectors located across from the X-ray source. During CT scanning, the X-rays pass through the patient in the supine position, while the ring rotates, and are recorded by the detectors on the opposite side. The attenuation of the radiation produces information regarding the internal features of the scanned patient (Ridel, 2018).

As patients are placed in the supine position during CT scanning, gravity effects the position of the facial features and soft-tissue thicknesses of the face in such a way that it influences the accuracy of facial approximations expected to be recognisable in an upright position (Wilkinson, 2002; de Greef, 2006; See et al., 2008; Munn and Stephan, 2018). In a study conducted by Munn and Stephan (2018), a 1 – 4 mm difference was noted in the facial soft-tissue between the upright and supine positions, resulting in facial contours changing significantly with positional changes (Munn and Stephan, 2018). Automatic computer assisted approximations predicting the soft-tissue of the face based on CT data could lead to errors or inaccurate approximations (Schlager, 2013; Guyomarch et al., 2014).

© University of Pretoria

2.3.6.2 Cone Beam Computed Tomography (CBCT) scans

Cone-beam computed tomography (CBCT) utilises a rotating gantry system equipped with an X-ray source and detector fixed on opposing ends. A divergent, cone-shaped beam of ionising radiation is directed through the region of interest (ROI) towards a flat-panel detector on the opposite side. Only a single rotational sequence is necessary to obtain enough information (typically 150 – 600 images dependant on the ROI) to reconstruct an image (Scarfe and Farman, 2008).

The main differences between conventional CT scans and CBCT scans include the flat fan shaped beam, moving in a helical manner, taking multiple images or slices of the ROI during a CT scan (Scarfe and Farman, 2008). All the slices are stacked to create a 3D representation. Each slice requires a separate scan and 2D reconstruction, resulting in an increased radiation exposure. CBCT scans however captures the information of the entire ROI in a single rotational sequence (Scarfe and Farman, 2008). Besides the lower radiation exposure of the patient during CBCT scanning, an additional advantage includes the higher spatial resolution (0.1 – 0.4 mm) compared to CT scans (0.6 – 1.5 mm) (Scarfe and Farman, 2008; Casselman et al., 2013; Guyomarc'h et al., 2014). The greatest advantage, for facial approximation studies, is that CBCT scans are taken in the upright position to evaluate the soft-tissue structure of the face in their natural position (Scarfe and Farman, 2008; Casselman et al., 2013; Ridel, 2018).

Unfortunately, all automatic computer-aided facial approximations have been based on CT scans which introduce errors due to the gravitational forces on the soft-tissue differently to the upright position needed for facial recognition. This study utilised CBCT scans, negating the effect of gravity on the orbital and periorbital tissues to produce more accurate and reproducible results.

© University of Pretoria

3. Chapter 3: Materials and Methods

3.1 Materials

Retrospective cone-beam computed tomography (CBCT) scans of 206 South African adults (45 black females, 52 black males, 57 white females, 52 white males) were used in this study. Patients were grouped according to the metadata of each patient embedded in the CBCT scans. The average age of the complete sample was 40.9 years. The average age of the white South African sample was 42.6 years, with females slightly older (44.3 years) than males (40.8 years). The average age of the black South African sample was younger, with an average age of 39.0 years. Black South African females were older (42.0 years) compared to their male counterparts (36.4 years) (*Figure 3.1*).

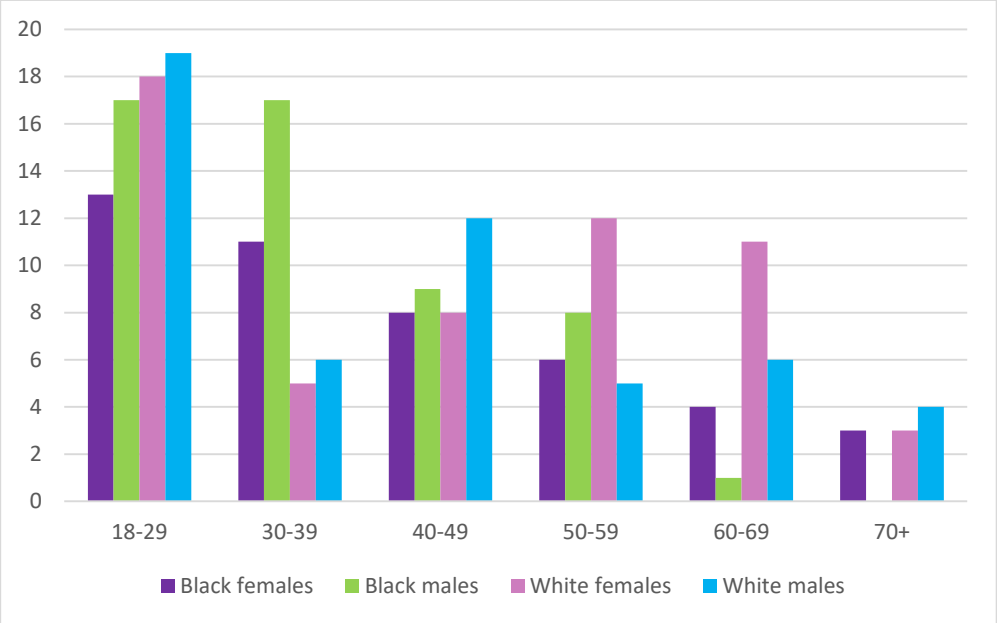

Figure 3.1. Age distribution by sex-population group

Ethical approval was obtained from the Human Research Ethics Committee (HREC) of the Faculty of Health Sciences, University of Pretoria (323/2020) (Annexure A). The CBCT scans were collected from the Oral and Dental Hospital, University of Pretoria; Oral Health Centre, Sefako Makgatho Health Sciences University; and from a private institution (Permission to collect scans: Annexure B; Ethical clearance from the Sefako Makgatho University Ethics Committee: Annexure C). All patients with pathological and/or traumatic effects or facial deformities of the midface were excluded from the study. Preference was given to patients with open eyes, however, due to the limited availability of scans meeting all inclusion criteria for black South African females, scans with closed eyes were also included for this group. Importantly, closed-eye scans allowed for the assessment of bony orbit dimensions, eyeball dimensions, and eyeball position within the

© University of Pretoria

orbit no differently to those with closed eyes. For the prediction of soft-tissue from underlying hard-tissue 187 of the selected 206 CBCT scans were of patients with open eyes (32 black females, 51 black males, 52 white females, and 52 white males).

At the time of scanning, patients were seated in an upright position, with a relaxed facial expression. A Planmeca ProMax CBCT 3D scanner with the following specifications: 90kV, 8mA, 11.2 mA, voxel size of 0.4 mm^3, and a maximum field of view of 230 (diameter) mm by 260 (height) mm were used at the Oral and Dental hospital, University of Pretoria and the Private institution in Pretoria, while a Newtom VGi CBCT 3D scanner with the same specifications and maximum field of view were used at the Oral Health Care Centre, Sefako Makgatho Health Sciences University. As parameters varied between patients, the field of view and parameters might have varied between patients.

The CBCT scans were obtained in a DICOM (Digital Imaging and Communications in Medicine) format to be imported into MeVisLab © v.3.0.2 software (Medical image processing and visualization), an open-source computer software programme (available from https://www.mevislab.de/). The MeVisLab software is used for medical image processing and visualisation. The software programme, MeVisLab includes complex modules for segmentation, registration, volumetric and qualitative functional and morphological analysis and permits the development of clinical application prototypes and the testing of new algorithms.

3.2 Methods

The study had two objectives for evaluating the 2D and 3D data. The first objective involved the manual placement of preselected landmarks onto the two-dimensional (2D) DICOM slices and three-dimensional (3D) segmented surfaces. As the eyeball does not exhibit a density dissimilar from other facial soft tissue structures, it cannot be isolated and reconstructed as a 3D model. As a reconstructed 3D surface is a prerequisite for automatic landmarking, manual landmarking is required for placing landmarks on the eyeball. Absolute distances were calculated to determine the normative dimensions of the eyeball, orbit, and palpebral fissure specific to the South African population. The position of the eyeball within the orbit was determined based on landmarks selected from the literature to ensure comparability (Stephan and Davidson, 2009; Guyomarc'h et al., 2012; Guyomarc'h et al., 2014). The manually placed landmarks were used to determine the normative shape of the orbital region and palpebral fissure for each sex-population group.

The second objective involved automatic landmarking (Ridel et al., 2020b) to develop statistical models for the prediction of the open eyelids from the underlying bony tissue for the use in automated craniofacial reconstructions.

© University of Pretoria

3.2.1 Part 1: Linear distances calculated from manually placed landmarks

Due to the spherical shape of the eyeball and the identification of landmarks on the eyeball's outermost margins, the original DICOM files were resliced orthogonally to the Frankfort Horizontal plane (FH) (Moore et al., 2013) to prevent orientation bias.

The rotate and reslice module in MeVisLab was created to reslice the DICOM files according to the FH plane. To identify the left and right porion and orbitale respectively for the FH plane (*Figure 3.2*a), a hard-tissue surface was generated by the segmentation process. In order to calculate the dimensions of the eyeball, DICOM images were segmented into soft-tissue (face) and hard-tissue (skull) surfaces, after which the DICOM images were repositioned according to the FH plane, resliced according to this plane, and then landmarks were identified and applied manually.

The segmentation process renders a soft-tissue surface or a hard-tissue surface image by finding the threshold values between the segmented components according to the "Half Maximum Height" (HMH) quantitative iterative thresholding method (Spoor et al., 1993). The segmentation process identifies the best limit between substances of different densities (between the soft tissue of the face and the skull in this case) without any intervention by the user. To determine the best limit between different densities to classify a certain region, a label for each pixel of the image is assigned. Global thresholds are set when adequate contrast is achieved between these different regions, so that the data can be separated by their grey levels. The areas corresponding to the segmentation are created and can then be viewed. Threshold values for hard-tissue typically vary between 1450 – 1550 and for soft-tissue between 450 – 550.

Following the segmentation process, 3D-triangular surface meshes were constructed. A 3D hull, that represents a solid object, was formed by triangular meshes that consist of an infinite number of connected triangles. Orthogonal frontal and sagittal planes were created automatically as planes perpendicular to the FH, using the porions and orbitale to establish the horizontal plane in the module. *Fig 3.2* (b – d) indicates the resliced 2D DICOM images, with the eyeballs located on the same plane after all head rotation was eliminated from the original DICOM images.

© University of Pretoria

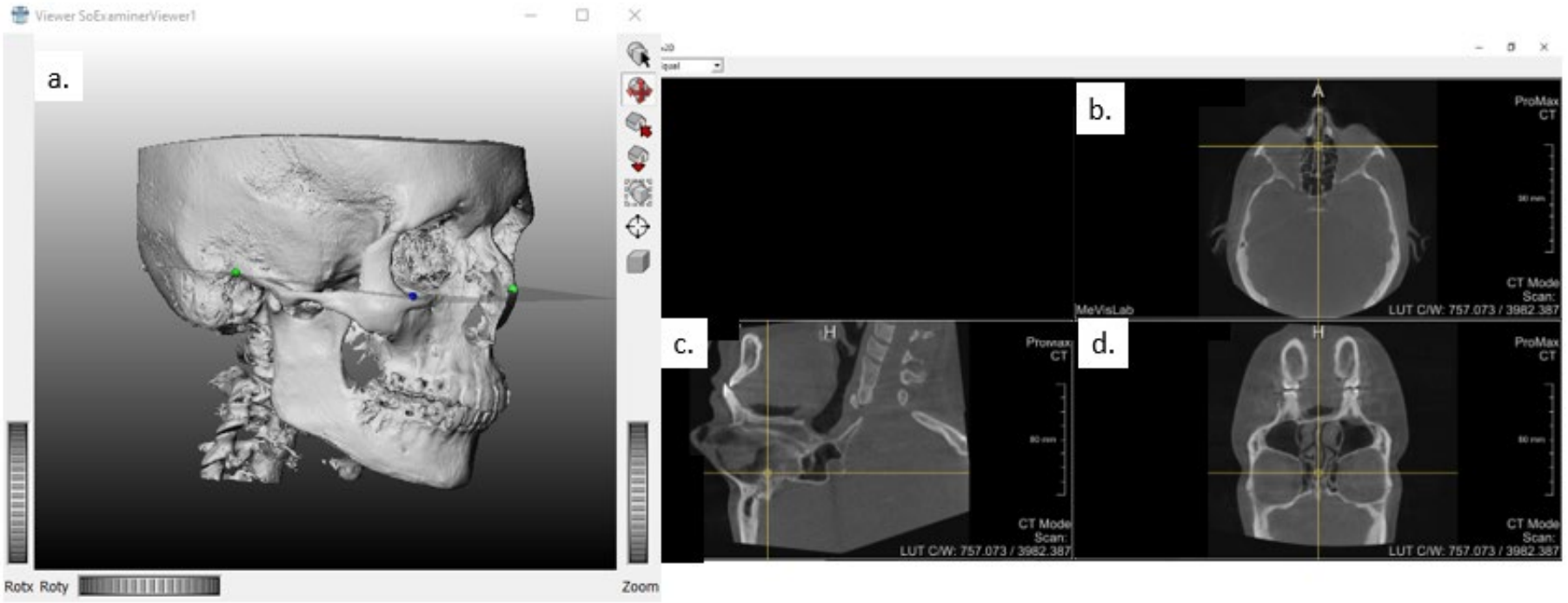

Figure 3.2. Reslicing of original DICOM images

a) Landmarks indicating the position of the FH plane. Newly created 2D slices denoting the eyes in the same planes with no rotation of the head b) axial plane, c) sagittal plane and d) coronal plane.

© University of Pretoria

After the scan preparation was completed, seven bilateral craniometric landmarks and 10 bilateral capulometric landmarks, in addition to those used to create the FH, were selected as guided by published literature indicated in the footnote of *Table 3.1* (*Figure 3.3* – *Figure 3.6*). The 3D coordinates of each landmark were used to calculate distances for determining orbital height and breadth, the position of the eyeball in relation to the orbital margin, globe projection, and the dimensions of the eyeball and palpebral fissure (Table 3.2). Franklin and colleagues (2005) noted that linear measurements derived from traditional anthropometric measuring techniques, are comparable with linear measurements derived from three-dimensional landmark coordinates and can be successfully used in traditional linear dimension studies (Franklin et al., 2005).

The position of the eyeball relative to the orbital margin was determined in two different ways to 1) maximize its comparison with the literature and 2) its usability for facial approximations. The position of the equator of the eyeball in relation to the orbital margin was used to measure the depth of the placement of the eyeball within the orbit, in contrast, the position of the oculus anterius in relation to the orbital margin was used to define the protrusion of the eyeball.

© University of Pretoria

Table 3.1. Definitions of manually placed landmarks.

	Landmark	Abbrv.	Definition
Craniometric			
	Nasion	n	The junction of the internasal suture with the nasofrontal suture
	Porion	po	The highest point on the superior margin of the external acoustic meatus
	Supraconchion	sk	The superior-most point on the supra-orbital margin (excluding the supraorbital notch where present)
	Orbitale	or	Inferior-most point on the infra-orbital margin
	Dacryon	d	The junction of the sutures between the frontal, maxillary and lacrimal bones
	Ectoconchion	ek	The most lateral point of the orbital rim following a line bisecting the orbit from the dacryon
	Frontomolare orbitale	fmo	Most anterior point of the zygofrontal suture on the orbital rim
	The deepest point on lateral orbital margin	dLOM	Deepest point along the lateral orbital margin
	Zygion	zy	The most lateral extent of the lateral surface of the zygomatic arch
Capulometric: Eyeball			
	Oculus anterius	oa	Most anterior point of the eyeball
	Oculus posterius	op	Most posterior point of the eyeball
	Oculus mediale	om	Most medial point of the eyeball
	Oculus laterale	ol	Most lateral point of the eyeball
	Oculus superius	os	Most superior point of the eyeball
	Oculus inferius	oi	Most inferior point of the eyeball
Capulometric: Eyelids			
	Endocanthion	en’	The most medial point of the palpebral fissure, at the inner commissure of the eyeball
	Exocanthion	ex’	Most lateral point of the palpebral fissure, at the outer commissure of the eyeball
	Palpebrale superius	ps’	The central point on the margin of the upper eyelid
	Palpebrale inferius	pi’	The central point of the margin of the inferior eyelid

From Stephan and Davidson, 2008; Guyomarc’h et al., 2012 and Guyomarc'h et al., 2014

© University of Pretoria

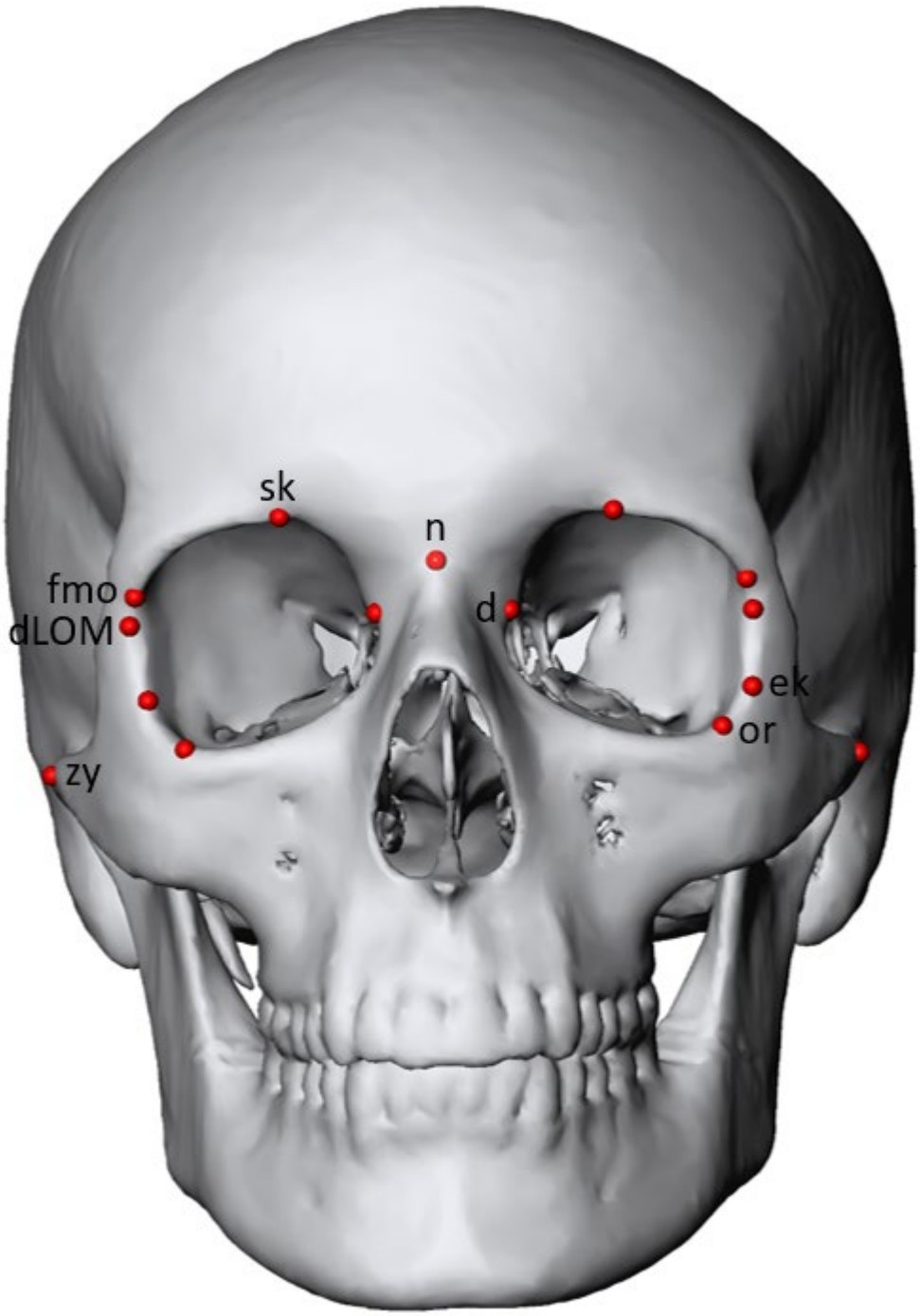

Figure 3.3. Anterior view of the craniometric landmarks placed on the reconstructed cranium

© University of Pretoria

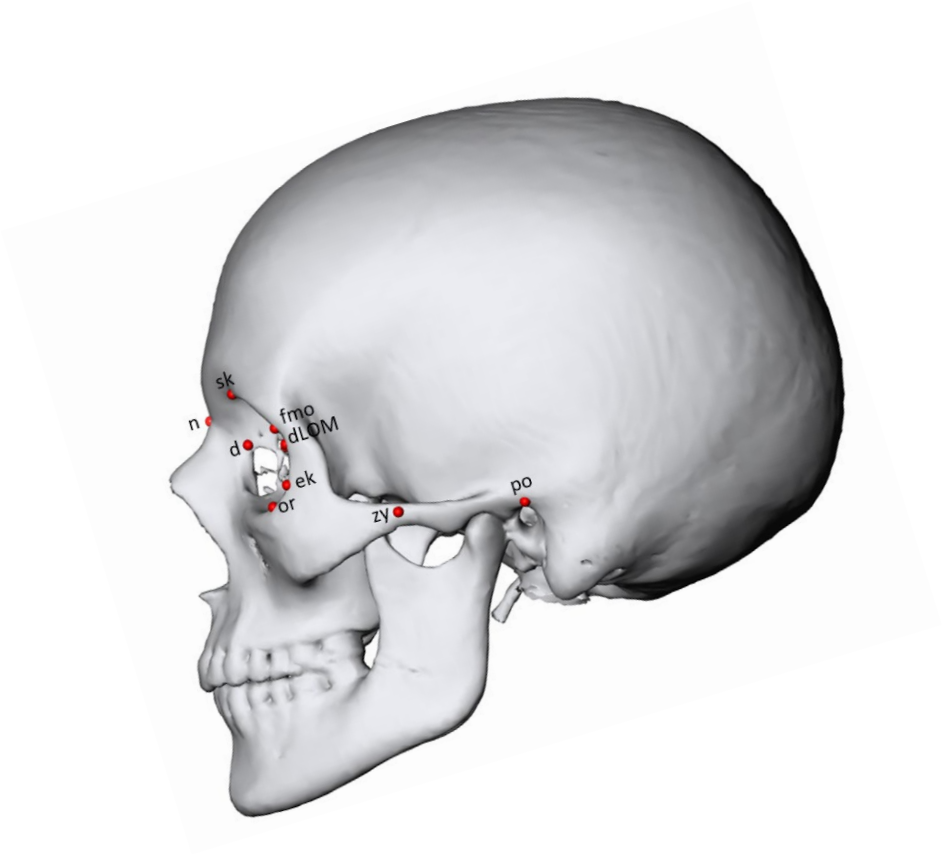

Figure 3.4. Lateral view of the craniometric landmarks placed on the reconstructed cranium

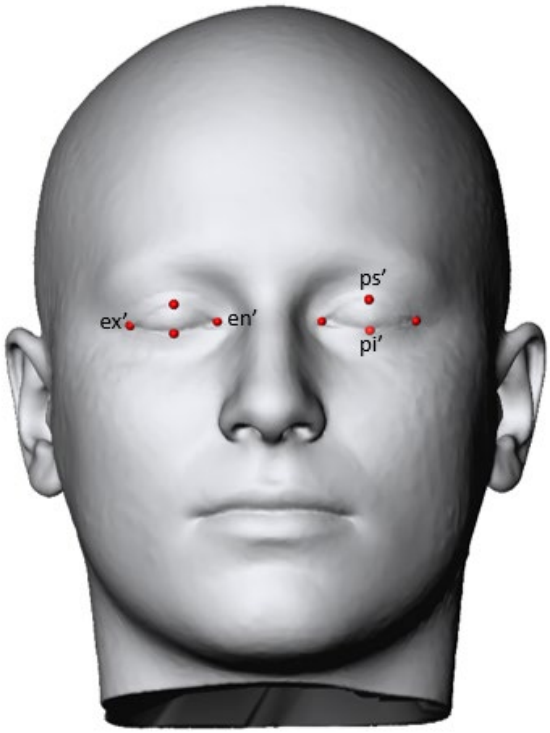

Figure 3.5. Capulometric landmarks placed on the eyelids of the reconstructed face

© University of Pretoria

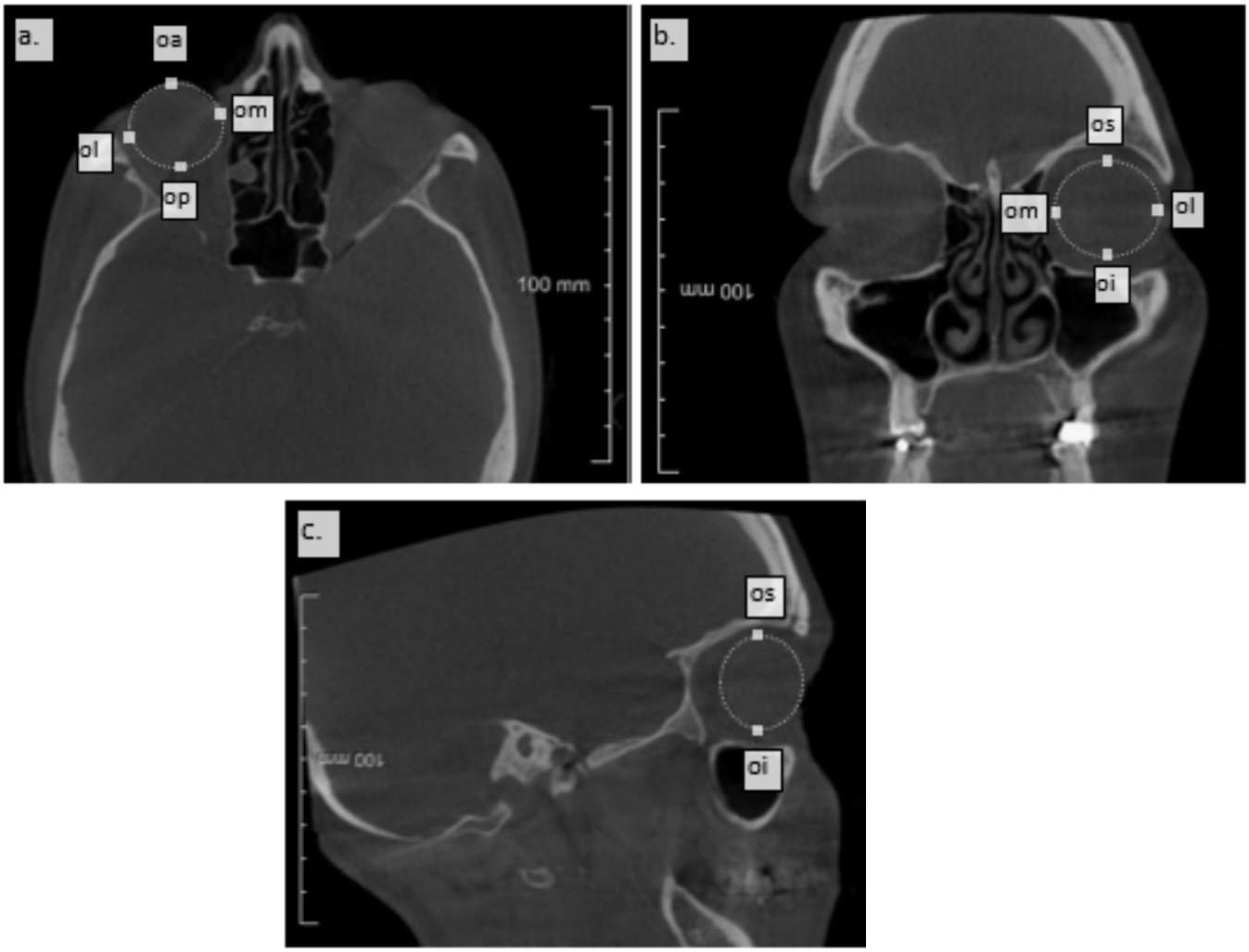

Figure 3.6. 2D DICOM slice indicating the capulometric landmarks placed on the ocular rim. a) axial view; b) coronal view; c) sagittal view

© University of Pretoria

Table 3.2. Definition of the calculated dimensions

Measurement	Abbr.	Definition:
Orbital dimensions		
Orbital height	sk - or	Distance between the supraconchion and the orbitale
Orbital breadth (1)	d - ek	Distance between the dacryon and ectoconchion
Orbital breadth (2)	d-dLOM	Distance between the dacryon and the deepest point on the lateral orbital margin
Interorbital distance	d - d	Distance between the daryons of both sides
Bizygomatic breadth	zy - zy	Distance between the zygions, indicating the width of the face
Orbital index		(Orbital height / Orbital breadth) * 100
Palpebral fissure dimensions		
Palpebral fissure height	ps' – pi'	Distance between the palpebrale superius and - inferius
Palpebral fissure width	en' – ex'	Distance between the endocanthion and exocanthion
Eyeball dimensions		
Ocular height	os- oi	Distance between the oculus superius and oculus inferius
Ocular breadth	ol - om	Distance between the oculus laterale and oculus mediale
Ocular length (Axial length)	oa - op	Distance between the oculus anterius and oculus posterius
Eyeball position		
Superior orbital margin (SOM) – Oculus superius	sk - os	Distance between the supraconchion and the oculus superius
Inferior orbital margin (IOM) – Oculus inferius	or – oi	Distance between the orbitale and the oculus inferius
Medial orbital margin (MOM) – Oculus mediale	d – om	Distance between the dacryon and oculus mediale
Lateral orbital margin (LOM) – Oculus laterale	ek – ol	Distance between ectoconchion and oculus laterale
Deepest point of the LOM – Oculus laterale	dLOM - ol	Distance from the deepest point on the lateral orbital margin to the oculus laterale
Eyeball protrusion		
Superior orbital margin (SOM) – Oculus anterius	sk – oa	Distance between the supraconchion and the oculus anterius
Inferior orbital margin (IOM) – Oculus anterius	or – oa	Distance between the orbitale and the oculus anterius
Medial orbital margin (MOM) – Oculus anterius	d – oa	Distance between the dacryon and oculus anterius
Lateral orbital margin (LOM) – Oculus anterius	ek - oa	Distance between ectoconchion and oculus anterius
Deepest point from the lateral orbital margin – Oculus anterius	dLOM - oa	Protruded distance between the deepest point on the lateral orbital margin to the oculus anterius

© University of Pretoria

3.2.2. Part 1: Statistical analysis

A flow diagram of the statistical analysis plan for the first objective of this study is found in Figure 3.7. All statistics concerning the first part of the study were conducted using the PAST 4 (Hammer et al., 2021) programme, while all shape analysis and predictions based on shape were conducted using the R-studio software, version 1.0.44-®2009.

3.2.2.1 Calculation of linear dimensions

Following the manual placement of the described landmarks, the 3D coordinates (x, y, z) for each landmark were exported in an XML format and imported into an Excel spreadsheet. The data was imported into PAST in order to calculate inter-landmark distances (*Table 3.2*).

3.2.2.2 Reproducibility testing

In order to determine the reproducibility of the manually placed landmarks and the repeatability of the calculation of the linear distances, 20 scans were randomly selected representing each sex-population group. The primary investigator (intra-observer) placed landmarks on the scans, while an independent researcher, not involved in the study (inter-observer), placed landmarks on the same 20 scans.

The independent researcher received two training sessions on the programme from the as well as a clear and figure and detailed table with the definitions of each landmark. Although the independent researcher was not familiar with the programme, she holds relevant qualifications in Human Anatomy. The same MeVisLab network, used for the data collection, was shared with the independent researcher with a recording of the process to aid in the placement of landmarks.

The reproducibility of the landmark placement was assessed by measuring landmark dispersion, allowing for comparison of the reproducibility of landmarks to previous studies (Guyomarc'h et al., 2012; 2014). Dispersion measures the average distance between a landmark's mean placement and all subsequent placements of that landmark. By using the dispersion Δ_{ij} for each landmark *i* and individual *j* the precision of the (intra-observer and inter-observer) landmark placement can be calculated. Dispersion is defined as the Mean Euclidean Distance (MED) of the sample landmark *p ijk* to the mean *p ij of* the (x, y, z)-coordinates of landmark *i* over all observations *k* (inter, intra, resp.) for subject *j*:

$$\Delta_{ij} = \sum_{k=1}^{K} \frac{\|p_{ijk} - \underline{p}_{ij}\|}{K}, with\ \underline{p}_{ij} = \sum_{k=1}^{K} \frac{p_{ijk}}{K}$$

© University of Pretoria

Variation of dispersion between the intra and inter-observers was reported as distances in mm with a standard deviation (*Table 3.1*).

An Intraclass Correlation Coefficient test (Two-way random effects, absolute agreement, single rater/measurement: ICC) 2,1) was performed to determine the repeatability of the linear distances (*Table 3.2*). Interpretation of the ICC results was based on the description by Koo and Li (2016).

3.2.2.3 Distribution of linear data

The distribution (normality) of the linear data calculated from the manually placed landmarks, was determined by performing a Shapiro-Wilk test (Hernandez, 2021). Statistical tests to determine variations between groups (sexes, population groups and sex-population groups) were selected based on the Shapiro-Wilk test results.

3.2.2.4 Summary statistics, univariate and multivariate analysis of the linear data

Summary statistics (mean, standard deviation and range) were conducted to determine the normative orbital, ocular and palpebral fissure dimensions as well as the normative eyeball position. To determine the effect of asymmetry (left vs right), sex and population affinity on the data, an ANOVA test was conducted on the parametric data, and a Kruskal-Wallis test was conducted on the non-parametric data. Variance among the four sex-population groups was determined using a Tukey's pairwise test for parametric data and a Mann-Whitney pairwise test for non-parametric data. The level of significance was set as $\alpha=0.05$.

3.3.1.5 Discriminant function analysis based on the dimensions and shape of the orbit

Facial approximation of an unidentified individual is based on a biological profile, which includes sex and population affinity. As cranial features are considered to be useful in the estimation of sex-population groups (Rosas and Bastir, 2002; Kimmerle et al., 2008; Green and Curnoe, 2009; İşcan and Steyn, 2013), the orbital dimensions and shape considered in this study were subjected to discriminant function analyses to determine its classification accuracy for estimating sex and population affinity.

3.2.2.6 Predictive equations based on the linear data

The position of the eyeball as well as the dimensions of the eyeball and palpebral fissure dimensions were proposed. To investigate a potential correlation between orbital morphology and eyeball position, the distance from the eyeball to the superior (supraconchion) and lateral (deepest point on the lateral orbital margin) orbital rim were expressed as percentages of orbital breadth (OB) and height (OH), respectively. The eyeball height and palpebral fissure

© University of Pretoria

height was expressed as percentages of OH, while the eyeball width and palpebral fissure width was expressed as percentages of OB. These results are described as position by proportionality.

In addition, bivariate linear regression was performed on one independent (or predictor) and one dependent (predicted) variable based on the description of Guyomarc'h and colleagues (2012) to propose prediction equations (Guyomarc'h et al., 2012). A linear regression is by definition a relation that is a function. From these correlations, the correlation coefficient (r) or strength (level of correlation) and direction of the correlation as well as the coefficient of determination (R squared) were reported to comment on the precision of the model, while the regressions are important to derive mathematical models as in this case the predictive equations produced

3.2.2.7 Comparison of linear data with existing literature

To compare the sample sizes, means and variations in the dimensions of the orbit, eye, palpebral fissure and the position of the eye in the orbit with the available literature, comparative analysis was performed using two-sample t-tests (*BSDA* package in R) and a Bayes Factor calculation (*BayesFactor* package in R) (Morey et al., 2015; Arnholt and Evans, 2017). In our statistical analysis, the Bayes Factor (BF) quantifies the ratio of evidence favouring the alternative hypothesis, which suggests a difference between population means, compared to the evidence favouring the null hypothesis. The results of the BF were interpreted as follow: Values ranging between -0.5 to 0.5 indicate weak evidence of population variation. Values between 0.5 to 1, indicate a substantial variation, 1 to 1.5 indicates a strong variation and 1.5 to 2 indicate a very strong variation between populations. Values greater than 2 indicate a decisive variation. Negative values in the same ranges reflect similar strengths, but concur with the null hypothesis.

3.2.2.8. Shape analysis of the orbit and palpebral fissure, based on manually placed landmarks

Reproducibility of the landmarks used for the shape analysis was determined as described at 3.3.1.2 in the preceding text. To test the normality of the manual landmark data distribution, multivariate normality testing was performed by interpreting quantile-quantile (Q-Q) plots (Scrucca, 2000), created by using the hard- and soft-tissue PC scores. Q-Q plots assume that variables are distributed according to the distribution tested. The closer the plotted values are to the diagonal line, the greater the probability of a multivariate normality distribution (Schlager, 2013b). All results were verified using non-parametric testing. Results were considered reliable when both tests provided similar outcomes.

© University of Pretoria

A Generalised Procrustes Analysis (GPA) (Goodall, 1991; Dryden and Mardia, 2016) was performed on the Cartesian coordinates of the manual landmarks placed on the hard- and soft tissue surfaces (Kendall, 1984; Klingenberg and McIntyre, 1998; Slice, 2001; Klingenberg et al., 2001). The raw data was used as these raw landmark coordinates comprise information on the position and orientation as well as the shape and size of the landmark configurations. Unfortunately, it also contains “nuisance parameters” like the orientation on position of each landmark. A GPA was used to separate the shape from the “nuisance parameters” by translating and rotating all configurations until the summed squared distances between the landmarks and the corresponding sample average is a minimum (Gower, 1975; Rohlf and Slice, 1990; Mitteroecker, 2009). The created landmark configurations are known as Procrustes shape coordinates after the landmarks have been superimposed, scaled and rotated and only contain information regarding the shape of the configurations.

Following the GPA analysis, data reduction was achieved by Principal Component Analysis (PCA) to quantify the different shapes observed. PCA reduces the dimensions of a data set by creating independent principal component (PC) scores for the hard- and soft-tissue coordinates to highlight variations in shapes. Principal component scores representing 95% of the sample’s overall variance were used for statistical testing. To determine if any population-specific differences exist, the influence of sex was tested on each population separately, while sexual dimorphism was determined by testing the influence of population on each sex group.

To quantify and visualize group-specific variations in the periorbital region parametric (MANOVA) and non-parametric (50-50 MANOVA and permutation testing) tests were performed.

3.3.1.9 Discriminant function analysis based on the dimensions and shape of the orbit

Similar to the linear dimensions of the orbit, the classification accuracy for the shape of the orbit was tested as well. This gave insight to the effect of size on the variation noted between groups, as GMM remove the effect of size in order to only investigate shape variation.

© University of Pretoria

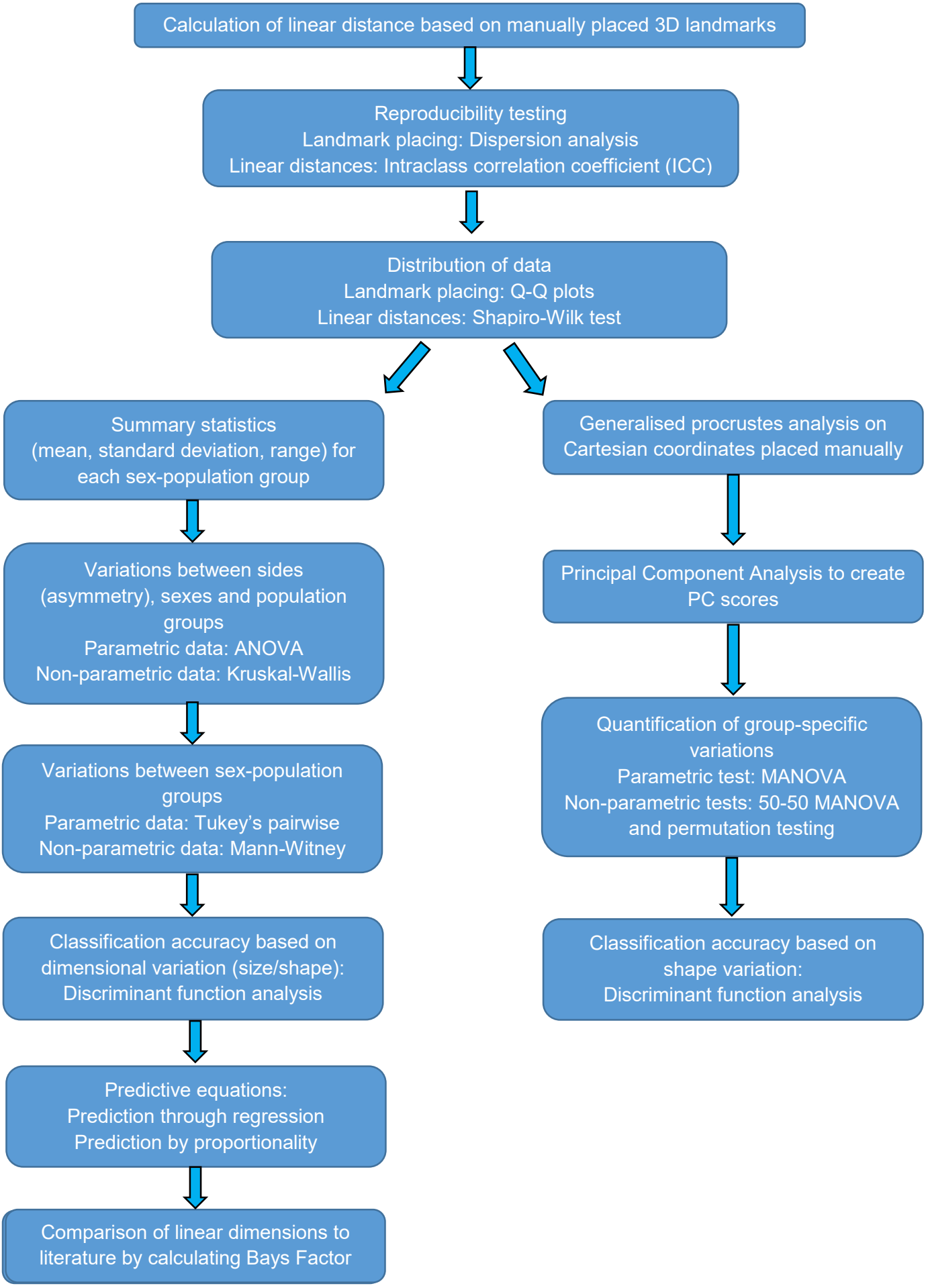

Figure 3.7. Statistical plan for Part 1 based on manually placed landmarks

© University of Pretoria

3.2.3 Part 2: Soft-tissue prediction: Statistical analysis

A flow diagram of the statistical analysis plan for the second objective of this study is found in Figure 3.8.

3.4.2.1. Anatomical templating

A total of 187 CBCT scans were included (32 black females, 51 black males, 52 white females, and 52 white males). All scans of patients with closed eyes (mostly black South African Females) were excluded from objective 2.

Similarly, to Part 1, CBCT images in DICOM format were imported into the MeVisLab © v. 2.7.1 software programme for segmentation and 3D surface mesh generation. Once 3D soft- and hard-tissue surface meshes were created, a surface mesh initialisation procedure was performed. For the initialisation process, a set of landmarks was placed manually, refer to *Table 3.1*, on the floating reference template (created by a large French sample) (Ridel et al., 2020) and the target (segmented skulls from the South African population generated in this study) surfaces to interactively translate and rotate the surfaces and to bring them into a uniform coordinate system. The accuracy of the initialisation process determines the non-rigid surface registration results. During the non-rigid-surface registration process, the geometrical relationship between surfaces was created so that reference hard- and soft-tissue templates could be produced. An average South African face was created and average skulls were created for white and black South Africans, respectively, and containing dense sets of landmarks (Ridel et al., 2020).

Lastly, selected landmarks (*Table 3.1*) were indicated once on the reference templates. The landmarks placed on the created warped surface were associated with corresponding 3D points on the reference template. Thus, information encoded in the 3D surface depiction was extracted and made comparable. During the anatomical templating process, the reference template representing the average South African face, was warped non-rigidly by making use of the MeVisLab © 3.0.2 software to fit the corresponding surface (target surface) of all subjects in the study. The warping procedure was performed iteratively with a ridged alignment, followed by a gradual more flexible registration of landmarks. Finally, by the automatic landmarking procedure, every landmark of the template was projected onto all the target surfaces of the subjects, establishing a dense point-based anatomical correspondence between all subjects. To perform statistical analysis, landmark coordinates were recorded within a common coordinate system (Ridel et al., 2020).

© University of Pretoria

3.4.2.1 Landmarks

The same seven bilateral craniometric and four bilateral capulometric landmarks, used in part 1 of the study (*Table 3.1*), were paced once on the template skulls and face and projected onto the aligned surfaces of each sex-population group. The 3D coordinates of the landmarks of each patient were captured in XML format for further statistical analysis.

3.4.2.2 Shape analysis of the orbit and palpebral fissure based on predicted (automatic) landmarks

Geometric morphometrics (GMM) was used to assess and quantify the differences in shape attributed to known factors (sex and population affinity) and covariates on the hard- and soft-tissue shapes to build statistical models for the estimation of the shape of the palpebral fissure.

The R-studio software, version 1.0.44-®2009-2016 for Microsoft Windows, was used to determine the shape and shape variations of the orbit and palpebral fissures as well as the prediction of the soft tissue based on the underlying bony tissue.

The reproducibility of the landmark placement was tested by performing a dispersion analysis as described in part 1. The templates were landmarked by the primary investigator (intra-observer) and independently by the co-supervisor (inter-observer). These landmarks were projected onto 20 randomly selected scans. The Mean Euclidean Distance (MED) and Standard Deviation (SD) were reported for each landmark for both the intra- and inter-observer error. A MED of 2 mm or below is deemed acceptable (Ridel et al., 2018).

Similar to the shape analysis performed on the manually placed landmarks, a GPA was performed on the 3D coordinates of the landmarks projected onto the hard- and soft-tissue surfaces. A PCA followed to reduce the data and to identify the areas where the most variation between sexes and populations were present.

Multivariate normality of the projected (automatic) landmark data was assessed using quantile-quantile (Q-Q) plots (Scrucca, 2000) constructed from the principal component (PC) scores of hard and soft tissues. Non-parametric tests were employed for verification. Consistency between the results of the parametric and non-parametric tests ensured the reliability of the normality assessment.

The prediction of the soft-tissue structure from the underlying bone is dependent on their inter-relationship, shape analysis of the orbit and palpebral fissures were conducted again, but based on the projected (automatic) landmark data. GMM were used to quantify and visualise the covariance between the hard-and soft tissue structures of the bony orbit and the palpebral

© University of Pretoria

fissures. The covariates; population variation and sexual dimorphism were performed on the complete sample. To identify any population-specific differences, the influence of sex was thereafter performed on each population separately.

A parametric (MANOVA) and two non-parametric (50-50 MANOVA and permutation testing) tests were performed to quantify and visualise the variations found in the periorbital region and the covariates. Discriminant function analysis (DFA) was applied using the R package *Morpho* through leave-one-out cross-validation (Schlager, 2013b; Schlager and Rüdell, 2015). The DFA finds linear combinations of variables that display intergroup differences, which in turn define linear discriminant functions. The linear discriminant coefficients are defined from the non-null eigenvectors of the between-group variance-covariance "scaled" by the within-group variance-covariance. A DFA test can be used to determine how likely an unknown/test sample belongs to a specific group taking into account the variability between groups.

A multiple analysis of variance (MANOVA) was used to test whether or not the independent grouping variable simultaneously explained a statistically significant amount of variance in the dependent variable. For this study, MANOVA was applied using the R-package *geomorph* (Adams et al., 2020). A non-parametric, modified version of MANOVA, designed for many potentially correlated response variables, 50-50 MANOVA, was applied using the R-package *ffmanova* (Langsrud, 2002; Langsrud et al., 2007; Langsrud and Mevik, 2012). Permutation testing, based on resampling, was applied using the R-package *Morpho* (Schlager, 2013b). Permutation testing computes the sampling distribution for each variable (e.g. sexual dimorphism).

A two blocks partial least squares (PLS) analysis, a valuable tool to predict trends in a dataset, was used to evaluate the covariation between the hard- and soft-tissue of the periorbital region and its dependence on sex and population affinity (Rohlf and Corti, 2000; Schlager, 2013a).

3.4.2.3 Statistical modelling for statistical prediction of the soft tissue surface of the open eye and periorbital region

A Partial Least Squares Regression (PLSR) algorithm was employed to extract predictive information for soft-tissue shape. This method identifies linear combinations of predictor variables (hard-tissue shape and additional factors) that maximally covary with the response variable (soft-tissue shape) (Wold et al., 2001; Martens and Naes, 2002; Abdi, 2010). PLSR constructs a multivariate linear model by relating two data matrices, X (predictors) and Y (response). PLSR is similar to PCR, but a single PLSR model can be built for multiple Y (response) variables. By using PLSR a high level of prediction can be achieved because of its ability to analyse data with colinear, noisy or even incomplete variables (Wold et al., 2001).

© University of Pretoria

The accuracy of the periorbital soft-tissue predictions made from the hard-tissue surface was assessed in terms of metric deviations. Accuracy testing is an essential step to allow comparison of the results to published studies. The validation of the prediction models was performed using cross-validation testing. Cross-validation testing addresses overfitting and under fitting of data, which lead to poor predictions. The mean squared error (MSE) was calculated using the leave-one-out-cross-validation (LOOCV) method, and compared between the training data and the predicted data (RMSE) (Mevik and Cederkvist, 2004). The impact of population affinity and sex were evaluated by adding them to the models as predictors and comparing the results of the MSE (training data) and RMSE (predicted data). The mean Euclidean distance (MED) was calculated over all landmarks and all subjects.

© University of Pretoria

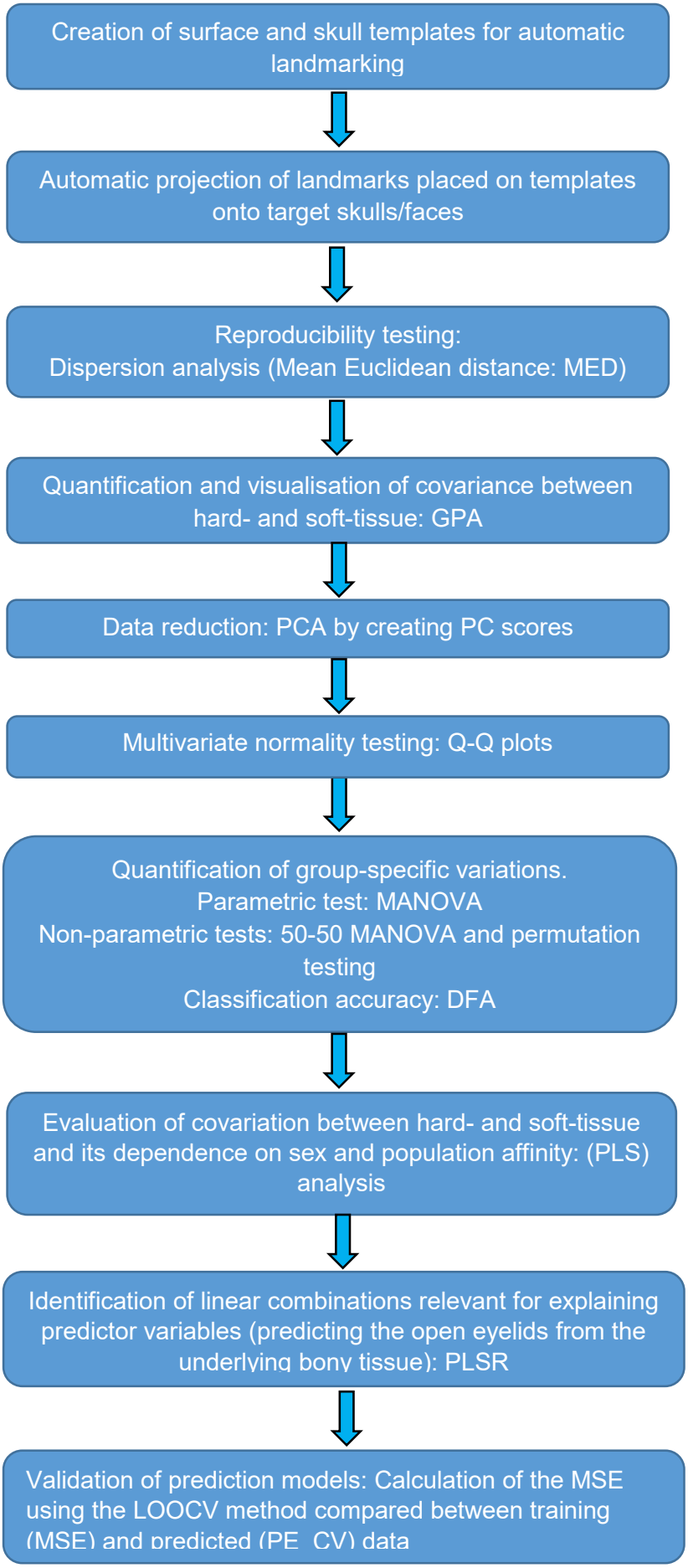

Figure 3.8. Statistical plan for objective 2 based on automatically projected landmarks

© University of Pretoria

4. Chapter 4: Results

4.1 Part 1: Linear measurements

4.1.1. Reproducibility testing

The dispersion analysis indicated lower mean values for landmark positioning by the intra-observer (mean: 0.72 mm) as compared to the inter-observer (mean: 1.13 mm) (*Table 4.1*). A visualisation of the dispersion errors per landmark as obtained by the intra- and inter-observers can be noted in *Figure 4.1*. Although the dispersion analysis results differed between observers, the curves followed a similar pattern. The mean dispersion of all landmarks placed by both observers fell within the acceptable range (below 2 mm), except for the position of dacryon by the inter-observer which were above this range (Ridel et al., 2021).

Positioning of landmarks on the eyeball were prone to observer error for both inter- and intra-observers testing, and the placement of the exocanthion had a greater mean Euclidian distance (MED) compared to the endocanthion. The placement of the frontomolare-orbitale and endocanthion were most reliable by both inter and intra-observers (*Figure 4.1*).

Table 4.1. Dispersion errors (mm) of landmark positioning.

	Intra-observer error		Inter-observer error	
	Mean	SD	Mean	SD
Landmarks	0.72	0.46	1.13	0.65

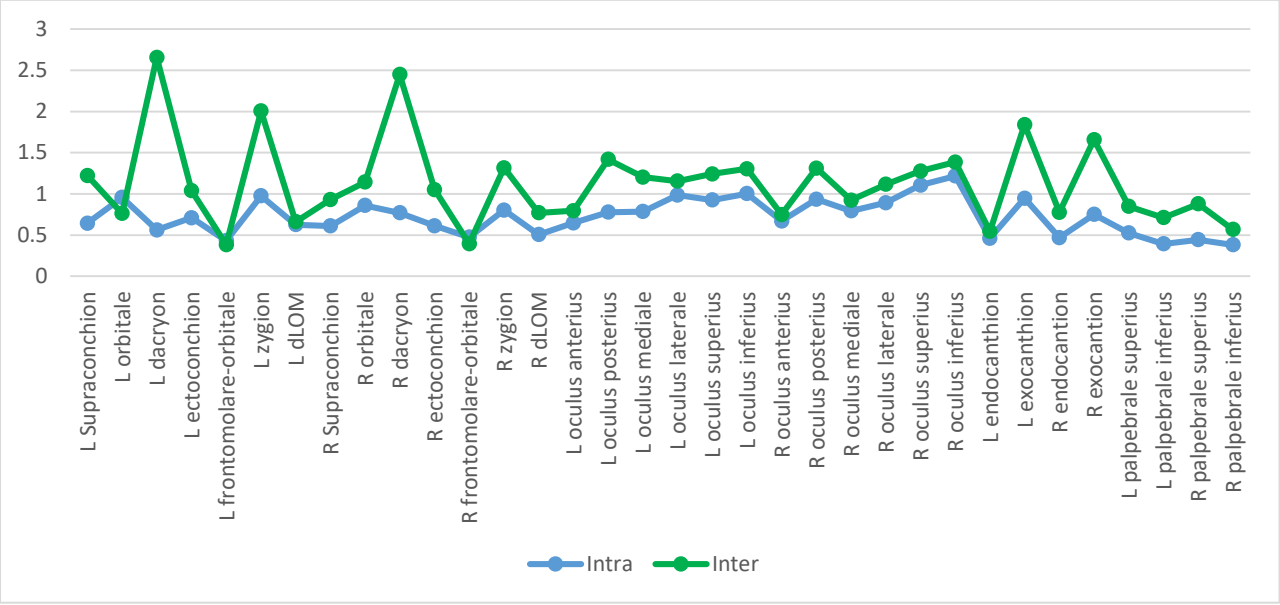

Figure 4.1 Graphical comparison between the mean dispersion results for both intra-observer and inter-observer errors of the positioning of all landmarks (mm)

© University of Pretoria

The Intraclass correlation coefficient (ICC) indicated greater repeatability of measurements by the intra-observer (mean: 0.76) compared to the independent inter-observer (mean: 0.62), although agreement followed a similar trend (*Table 4.2*). Concerning the intra-observer ICC results, excellent repeatability (ICC > 0.9) was noted for the right orbital height, orbital breadth, interorbital distance and bizygomatic breadth as well as the position of the oculus anterius (most projecting point on the cornea) in relation to the lateral, medial and superior orbital margins. Good agreement (ICC between 0.75 and 0.9) was noted for right orbital height, right palpebral fissure height, and the position of the equator of the eyeball in relation to the superior and medial orbital margins. The position of the equator of the eyeball to the inferior and lateral orbital margins and palpebral fissure width displayed moderate, ICC 0.5 – 0.75, agreement, as well as the axial length of the eyeballs. ICC values below 0.5 were noted for the ocular height and breadth (*Figure 4.2*).

Table 4.2. Mean Intraclass Correlation coefficient test results

	Intra-observer error		Inter-observer error	
	Mean	SD	Mean	SD
Landmarks	0.76	0.25	0.62	0.28

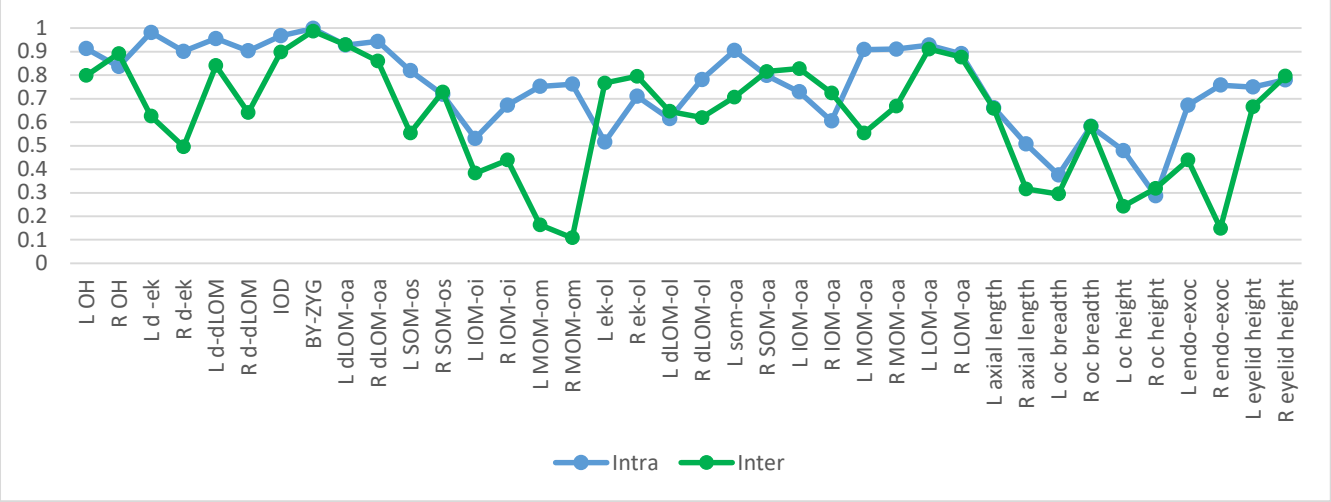

Figure 4.2. Graphical comparison between the mean ICC results for both intra-observer and inter-observer errors

4.1.2. Distribution of the linear data

Majority of the calculated linear dimensions were normally distributed, while certain linear dimensions were not normally distributed in specific sex-population groups. All non-parametric data are indicated in bold (*Table 4.3.)* and non-parametric tests were utilised to test variance between those groups.

© University of Pretoria

Table 4.3. Distribution of linear dimensions (p-values) as calculated from 3D landmarks

Measurement	Entire sample	Sex	Black South Africans	White South Africans	Black females	Black males	White females	White males
Orbital height (L)	0.56	0.46	0.11	0.83	0.91	0.48	0.24	0.48
Orbital height (R)	0.83	0.38	0.07	0.91	0.43	0.16	0.80	0.65
Orbital breadth (L)	0.08	0.18	0.30	**0.05**	0.23	0.15	0.09	0.20
Orbital breadth (R)	0.68	0.28	0.35	0.21	**0.02**	0.35	0.48	**0.01**
Orbital breadth (dLOM-d)	0.77	0.61	0.59	0.93	0.43	0.81	0.73	0.13
Orbital breadth (dLOM-d))	0.33	0.37	0.31	0.28	0.26	0.14	0.71	0.24
Interorbital distance	0.11	0.40	0.28	0.86	0.27	0.42	0.97	0.59
Bizygomatic breadth	0.19	0.05	0.58	0.32	0.15	0.47	0.27	0.49
Eyeball projection (L)	0.54	0.56	0.49	0.73	0.26	0.96	0.46	0.31
Eyeball projection (R)	0.13	0.34	**0.05**	0.46	0.12	0.67	0.61	**0.01**
SOM to os (L)	0.67	0.93	0.59	0.20	0.93	0.13	0.61	0.95
SOM to os (R)	**0.00**	**0.01**	0.25	**0.00**	0.29	0.13	**0.00**	0.62
IOM to oi (L)	0.68	0.95	0.64	0.47	0.45	0.27	0.33	0.79
IOM to oi (R)	0.46	0.74	0.51	0.68	0.29	0.71	0.55	**0.04**
MOM to om (L)	0.93	0.71	0.41	0.24	0.32	0.51	0.24	0.50
MOM to om (R)	**0.03**	0.36	0.12	0.62	**0.03**	0.83	0.97	0.16
LOM to ol (L)	0.51	0.63	0.35	0.81	0.64	0.68	0.88	0.56
LOM to ol (R)	0.93	0.96	0.38	0.60	0.71	0.30	0.97	0.56
LOM (ek) to ol (L)	0.29	0.37	0.25	0.26	0.82	0.89	0.07	0.10
LOM (ek) to ol (R)	**0.03**	0.54	**0.01**	**0.04**	0.43	**0.05**	0.56	0.41
Eyeball width (L)	0.47	0.38	0.52	0.66	0.08	0.82	0.62	0.56
Eyeball width (R)	0.33	0.15	0.86	0.74	0.23	0.16	0.63	0.69
Eyeball height (L)	0.32	0.66	0.61	0.46	0.06	0.55	0.22	0.27
Eyeball height (R)	0.50	0.73	0.18	0.47	0.50	0.59	0.65	0.12
Anterior-posterior diameter (L)	0.36	0.38	0.79	0.39	0.96	0.77	0.19	0.87
Anterior-posterior diameter (R)	**0.01**	**0.01**	0.25	0.14	**0.01**	0.65	0.08	0.13
Width of palpebral fissure (L)	0.29	0.45	**0.01**	0.62	0.35	0.45	0.66	0.44
Width of palpebral fissure (R)	0.22	0.12	0.67	0.21	0.68	0.97	**0.04**	0.10
Height of palbebral fissure (L)	**0.00**	**0.00**	**0.03**	**0.00**	0.07	0.22	**0.05**	0.18
Height of palbebral fissure (R)	**0.00**	**0.01**	**0.01**	**0.00**	0.97	0.09	**0.01**	0.15
SOM-oa (L)	0.68	0.23	0.88	0.84	0.23	0.36	0.75	0.69
SOM-oa (R)	0.88	0.98	0.63	0.06	0.77	0.19	0.94	0.93
IOM-oa (L)	0.12	0.97	0.11	0.32	0.26	0.50	0.95	**0.03**
IOM-oa (R)	0.37	0.44	0.67	0.08	0.61	0.78	0.26	0.12
MOM-oa (L)	0.84	0.51	0.62	0.12	0.35	0.21	0.35	0.07
MOM-oa (R)	**0.02**	**0.00**	0.84	**0.02**	0.50	0.71	**0.01**	0.44
LOM-oa (L)	0.47	0.52	0.31	0.18	0.25	0.61	0.36	0.08
LOM-oa (R)	0.85	0.91	0.12	0.88	0.40	0.28	0.47	0.67

All non-parametric data are indicated in bold

© University of Pretoria

4.1.3 Asymmetry by sex-population group:

Some asymmetry was noted in this sample (*Table 4.4*). White South African males presented with the greatest asymmetry compared to other South African groups. In white males, a statistically significant difference in the orbital breadth between sides (p = 0.00) was observed, with the orbital breadth on the left being wider or larger (43.49 mm) than the right (42.02 mm). Asymmetry was also noted in the distance between the lateral orbital margin (LOM) and the oculus laterale (p = 0.04), with the eyeball located closer to the ectoconchion on the left (12.77 mm opposed to 13.40 mm). A statistically significant difference was similarly noted in the measurement between the left LOM and the oculus anterius (p = 0.01) with the LOM located closer to the oculus anterius on the left (24.84 mm opposed to 25.85 mm). Often, the ocular and orbital dimensions were greater on the left compared to the right, however, a significantly (p = 0.01) wider palpebral fissure was noted on the right in white South African males (28.22 mm opposed to 27.16 mm).

Asymmetry was noted in black South African females in the distance from the medial orbital margin (MOM) and the oculus mediale (p = 0.01). The right eyeball was positioned closer to the MOM compared to the left (11.73 mm as opposed to 10.75 mm). A statistically significant difference was observed in the measurement from the lateral orbital margin (ectoconchion) to the oculus laterale (p = 0.00) in white South African females. The eyeball was located closer to the LOM on the left compared to the right (10.46 mm as opposed to 11.89 mm). No asymmetry was noted between any measurements for black South African males.

As differences were observed, statistical analyses were performed on each side separately.

Table 4.4. Asymmetry specific to each sex-population group

Parameter	South African black females	South African white females	South African black males	South African white males
Orbital breadth (ek-d)	0.93	0.70	0.51	**0.04**
MOM to oculus mediale	**0.01**	0.39	0.73	0.08
Ectoconchion to oculus laterale	0.71	**0.00**	0.74	**0.04**
LOM to oculus anterius	0.63	0.12	0.14	**0.01**
Palpebral fissure width	0.45	0.39	0.43	**0.01**

Significant p values (p ≤ 0.05) are indicated in bold.

4.1.4 Summary statistics, univariate and multivariate analysis results

4.1.4.1 Orbital dimensions

Orbital breadth was greater than orbital height, suggesting on average, a more rectangular-shaped orbit in general in South Africans (*Table 4.5*).

© University of Pretoria

White South Africans have larger orbital heights (p = 0.02 (L); p = 0.01 (R)) when compared to black South Africans. No statistically significant difference was noted in the orbital breadth or the orbital index between these two population groups (*Table 4.5*).

Black South Africans had a wider interorbital distance when compared to white South Africans (p = 0.00). Although statistically significant differences were observed in the interorbital distance between groups, no population differences were recorded concerning bizygomatic breadth. Thus, the facial breadth does not vary between population groups, but the orbits are located further apart in black South Africans.

South African females had significantly smaller orbital dimensions (p = 0.00), interorbital distances as well as bizygomatic breadths (p = 0.00) compared to their male counterparts (*Table 4.5*).

© University of Pretoria

Table 4.5 Summary statistics (mm) and p-values investigating the influence of asymmetry, population affinity and sexual dimorphism on orbital dimensions

		Sex-population groups						
Measurement	Side	South African black females n=45	South African white females n=57	South African black males n=52	South African white males n=52	Asymmetry (p)	Population (p)	Sex (p)
Orbital height	L	**35.73** *2.98* (29.44 - 42.22)	**37.39** *2.27* (30.52 - 43.60)	**37.64** *2.33* (33.63 -45.06)	**38.15** *2.27* (33.18 - 42.78)	0.72	**0.02**	**0.00**
	R	**35.91** *2.94* (28.74 - 40.23)	**37.76** *2.15* (33.31 - 42.14)	**37.60** *2.76* (32.34 - 43.93)	**38.10** *2.52* (33.34 - 43.35)		**0.01**	**0.00**
Orbital breadth (d-ek)	L	**40.10** *2.79* (35.73 - 46.30)	**40.58** *1.45* (37.63 - 44.60)	**42.30** 1.83 (39.10 - 45.77)	**42.74** *1.51* (39.41 - 45.83)	0.37	0.77	**0.00**
	R	**40.14** *2.63* (35.55 - 45.32)	**40.70** *1.81* (38.02 - 44.46)	**42.55** *2.02* (38.10 - 46.28)	**43.49** *2.10* (40.03 - 48.98)		0.39	**0.00**
Orbital breadth (d-LOM)	L	**38.67** *2.72* (32.78 – 43.99)	**39.69** *1.63* (36.55 – 44.03**)**	**40.74** *2.25* (35.35 – 46.10)	**42.02** *1.74* (38.65 – 45.71)	0.34	**0.02**	**0.01**
	R	**39.19** *2.51* (35.29 – 44.89)	**39.96** *1.92* (36.46 – 44.48)	**41.10** *2.18* (36.75 – 46.47**)**	**42.34** *20.3* (38.31 – 46.54)		0.50	**0.00**
Orbital index: OH/OB (d-ek)	L	**89.17** *±5.09* *(81.82-103.14)*	**92.23** *± 6.12* *(75.74 – 108.52)*	**89.04** *± 5.12* *(80.12 – 106.38)*	**89.30** *± 4.89* *(77.34 – 98.69)*	0.59	**0.01**	**0.02**
	R	**89.53** *± 5.80* *(75.84 – 102.51)*	**92.88** *± 5.50* *(78.14 – 106.34)*	**88.40** *± 5.75* *(77.06 – 102.25)*	**87.72** *± 5.88* *(74.36 – 100.59)*		0.08	**0.00**
Orbital index: OH/OB (d-dLOM)	L	**92.46** *±5.46* *(84.65 – 112.95)*	**94.29** *± 5.77* *(80.81 – 107.05)*	**92.49** *± 4.99* *(82.66 – 104.52)*	**90.81** *± 4.48* *(78.82 – 100.13)*	0.29	0.08	**0.00**
	R	**91.68** *± 5.84* *(78.99 – 104.72)*	**97.58** *± 5.29* *(80.97 – 106.76)*	**91.54** *± 6.11* *(80.42 – 110.84)*	**90.02** *± 4.83* *(78.11 – 101.37)*		0.32	**0.00**
Interorbital distance	-	**21.65** *± 2.68* (16.98 - 29.22)	**19.09** *± 2.35* (14.45 - 24.43)	**22.62** *± 2.80* (15.83 - 29.22)	**20.11** *± 2.34* (15.82 - 25.28)	-	**0.00**	**0.00**
Bizygomatic breadth	-	**121.80** *± 7.87* (105.29 - 136.65)	**123.03** *± 4.97* (113.41 - 135.81)	**132.19** *± 7.21* (112.37 - 154.04)	**131.35** *± 4.33* (122.51 - 140.73)	-	0.73	**0.00**

Bold values: mean; Italic values: standard deviation, brackets: minimum and maximum values. Significant p values ($p \leq 0.05$) are indicated in bold.

© University of Pretoria

From the average dimensions noted for each sex-population group in *Table 4.5*, sexual dimorphism in the face is more prominent in white than black South Africans. The effect of sex and population affinity within subgroups was further investigated (*Table 4.6*).

Although sexual dimorphism affected all dimensions when males and females from both population groups were analysed together, it is worth noting that variation in the orbital height is only observed in the black South African sample as white South African females had a squarer shaped orbit, while the interorbital distance does not vary between sexes within the populations.

The effect of population affinity is more profound within sex groups than in the population as a whole (*Table 4.6*). White South African females often have similar orbital dimensions to black South African males. Orbital height varies between South African females only, with white South African females presenting with larger orbital heights than black South African females. Orbital breadth varies between South African males only, with wider orbital breadths noted in white South African males than black South African males. White South African females presented with the largest orbital indexes compared to black South African females and white South African males.

Table 4.6 Variation in the orbital dimensions between sexes within populations and variation between populations within sex groups

		Sexual dimorphism within populations		Population variation within sex groups	
Measurement	Side	Black South Africans n=97	White South Africans n=109	SA females n=102	SA males n=104
Orbital height	L	**0.00**	0.40	**0.00**	0.26
	R	**0.01**	0.69	**0.01**	0.75
Orbital breadth (d-ek)	L	**0.00**	**0.00**	0.36	0.23
	R	**0.00**	**0.00**	0.33	**0.04**
Orbital breadth (d-dLOM)	L	**0.00**	**0.00**	0.07	**0.01**
	R	**0.00**	**0.00**	0.26	**0.02**
Orbital index: OH/OB (d-ek)	L	0.89	**0.02**	**0.02**	0.63
	R	0.27	**0.00**	**0.02**	0.36
Orbital index: OH/OB (d-dLOM)	L	0.28	**0.00**	**0.02**	0.36
	R	0.99	**0.00**	**0.05**	0.50
Interorbital distance	-	0.21	0.17	**0.00**	**0.00**
Bizygomatic breadth	-	**0.00**	**0.00**	0.75	0.90

Significant p values ($p \leq 0.05$) are indicated in bold.

© University of Pretoria

4.1.4.2 Location of the eyeball in the orbit:

The position of the eyeball relative to the orbital rim was determined in two different ways to maximise 1) its comparison with the literature and 2) its usability for facial approximations. The position of the equator of the eyeball can be used to measure the depth of the placement of the eyeball within the orbit. In contrast, the position of the oculus anterius in relation to the orbital rim is used to define the protrusion of the eyeball.

4.1.4.2.1 Ocular placement: Equator in relation to the orbital rim

The equator of the eyeball is located within the orbit and is not linearly in line with the orbital rim. In general, the equator of the eyeball was located deeper in relation to the superior orbital rim, compared to the inferior orbital rim, while the eyeball was located closer to the lateral orbital margin specifically in relation to the deepest point on the lateral orbital rim (dLOM) compared to the medial orbital margin (MOM) (*Table 4.7*).

Asymmetry was also noted in the position of the eyeball in the horizontal plane, as the eyeballs were generally located closer to the MOM on the right, while it was located closer to the LOM (ectoconchion) on the left.

In general, the eyeball was located deeper in the bony orbit in white South Africans when compared to black South African females. The eyeballs were located further from the superior, inferior and medial orbital margins in white South Africans than black South Africans. Less variation was noted in the position of the equator in relation to the dLOM than the ectoconchion between population groups.

The equator of the eyeball in South African males was located deeper in the bony orbit when compared to their female counterparts. These differences were significant in relation to the position of the equator to the superior orbital margin, medial orbital margin and the ectoconchion on the left lateral orbital margin (*Table 4.7*).

© University of Pretoria

Table 4.7 Summary statistics (in mm) and p-values investigating the influence of asymmetry, population affinity and sexual dimorphism on ocular position

		Sex-Population groups						
Measurement (mm)	Side	South African black females (n=45)	South African white females (n=55)	South African black males (n=49)	South African white males (n=48)	Asymmetry (p)	Population (p)	Sex (p)
SOM-os	L	**9.40**	**10.64**	**11.98**	**11.78**	0.21	**0.00**	0.22
		1.96	*1.84*	*1.68*	*2.26*			
		(6.24 – 13.76)	(6.06 – 14.35)	(7.59 – 16.08)	(6.80 – 17.30)			
	R	**9.53**	**11.20**	**12.28**	**12.28**		**0.00**	**0.05**
		1.40	*2.17*	*1.76*	*2.20*			
		(7.36 – 14.03)	(8.04 – 17.32)	(8.12 – 17.31)	(7.58 – 18.73)			
IOM-oi	L	**8.99**	**9.04**	**10.38**	**9.60**	0.64	**0.00**	0.11
		1.80	*2.22*	*1.83*	*1.30*			
		(5.30 – 11.89)	(4.85 – 14.63)	*(5.44 – 14.68)*	(6.66 – 12.61)			
	R	**8.93**	**9.23**	**10.12**	**9.38**		**0.01**	0.30
		2.18	*20.3*	*1.50*	*1.76*			
		(4.93 – 13.58)	(5.06 – 15.41)	(7.02 – 13.45)	(5.29 – 12.98)			
MOM-om	L	**11.57**	**11.97**	**11.81**	**13.13**	**0.02**	**0.00**	**0.00**
		1.45	*1.61*	*1.45*	*1.42*			
		(8.74 – 14.57)	(7.99 – 14.76)	(9.30 – 15.45)	(10.32 – 16.44)			
	R	**10.70**	**12.08**	**11.81**	**12.67**		**0.01**	**0.00**
		1.29	*1.75*	*1.45*	*1.67*			
		(8.04 – 14.61)	(80.2 – 15.69)	(8.68 – 14.72)	(9.37 – 15.64)			
LOM (ek)-ol	L	**11.84**	**10.86**	**10.44**	**12.74**	**0.00**	0.48	**0.01**
		1.85	*1.34*	*1.55*	*1.62*			
		(7.42 – 15.43)	(7.82 – 13.59)	(7.32 – 14.08)	(8.88 – 16.59)			
	R	**12.01**	**10.94**	**11.80**	**13.31**		**0.00**	0.40
		1.63	*1.67*	*1.80*	*1.35*			
		(9.29 – 15.43)	(7.64 – 14.91)	(6.68 – 16.12)	(10.67 – 16.31)			
LOM (dLOM)-ol	L	**9.39**	**9.17**	**8.29**	**9.30**	0.59	0.06	0.10
		1.96	*1.81*	*1.68*	*1.98*			
		(5.92 – 14.70)	(5.44 – 13.37)	(4.70 – 12.34)	(5.60 – 13.89)			
	R	**9.45**	**9.07**	**8.23**	**9.65**		0.14	**0.02**
		11.69	*1.84*	*1.50*	*1.49*			
		(5.09 – 13.94)	(5.99 – 13.46)	(4.99 – 11.37)	(6.38 – 12.30)			

Bold values: mean; Italic values: standard deviation, brackets: minimum and maximum values. Significant p values ($p \leq 0.05$) are indicated in bold.

© University of Pretoria

The sex and population-specific variations in the dimensions of the orbit directly influence the position of the eyeball in the orbit. The effect of sex and population affinity was investigated within subgroups to identify variations specific for each group.

These specific variations are noted in *Table 4.8*. The position of the eyeball was less variable in males compared to females. The eyeball of black South African males was located significantly closer to the left MOM (dacryon) and both LOM (ectoconchion) when compared to white South African males. This was expected as South African males have similar ocular dimensions, but white South African males presented with significantly larger orbital breadths.

The eyeball of black South African females was located significantly closer to all orbital margins (p=0.00) compared to white South African females, except the lateral orbital margin, measured from the ectoconchion and deepest point on the lateral orbital margin as well as the left MOM.

Variation in the position of the equator of the eyeballs in relation to the MOM was side-specific, but can be explained by the asymmetry noted in the MOM-om measurement.

Table 4.8 Variation in ocular position between sexes within populations and variation between population within sex groups

		Sexual dimorphism within populations		Population variation within sex groups	
Measurement (mm)	Side	Black South Africans n=94	White South Africans n=103	SA females n=100	SA males n=97
SOM-os	L	**0.01**	0.93	**0.00**	0.07
	R	**0.00**	0.99	**0.00**	0.16
IOM-oi	L	0.99	0.07	**0.00**	0.67
	R	0.89	0.12	**0.01**	0.98
MOM-om	L	0.89	**0.00**	0.98	**0.00**
	R	**0.00**	**0.01**	**0.05**	0.37
LOM (ek) - ol	L	**0.01**	**0.00**	**0.00**	**0.00**
	R	**0.01**	**0.00**	0.93	**0.00**
LOM (dLOM) - ol	L	0.45	**0.00**	0.64	0.63
	R	0.99	**0.00**	**0.02**	0.71

Significant p values ($p \leq 0.05$) are indicated in bold.

4.1.4.2.2 Ocular protrusion: Oculus anterius in relation to the orbital rim

Asymmetry was noted in the protrusion of the oculus anterius, measured from the ectoconchion (*Table 4.9*) in all sex-population groups.

Although black South Africans presented with more protruding eyeballs than white South Africans, few statistically significant differences were observed in the protrusion between the two South African groups. Significant variation was noted between populations with regard to

© University of Pretoria

the position of the eyeball in relation to the SOM and LOM (ectoconchion), although the variation seems to be sex specific.

Little variation was observed in the position of the eyeball between the sexes, although a significant difference was noted with regard to the protrusion of the eyeball from the LOM measured from the dLOM as well as the ek. The values were greater in females compared to males (*Table 4.9*).

© University of Pretoria

Table 4.9 Summary statistics (mm) and p-values investigating the influence of asymmetry, population affinity and sexual dimorphism on the protrusion of the eyeball.

		Sex-population groups						
Measurement (mm)	Side	South African black females (n=45)	South African white females (n=55)	South African black males (n=49)	South African white males (n=48)	Asymmetry (p)	Population (p)	Sex (p)
Protrusion (dLOM – oa)	L	**24.02** *2.26* (19.15 – 28.34)	**23.59** *1.61* (20.55 – 27.92)	**24.60** *1.91* (20.55 – 27.92)	**25.16** *1.81* (20.44 – 28.10)	0.08	0.99	**0.00**
	R	**24.17** *1.91* (20.18 – 29.62)	**22.89** *1.97* (20.35 – 28.93)	**24.31** *1.89* (20.35 – 28.93)	**24.31** *1.89* (20.35 – 28.93)		0.07	**0.00**
SOM-oa	L	**21.31** *2.74* (15.71 – 26.43)	**19.59** *2.06* (114.55 – 24.73)	**20.84** *2.04* (16.46 – 26.61)	**19.65** *1.85* (15.87 – 23.62)	0.94	**0.00**	0.73
	R	**20.95** *2.51* (14.84 – 25.13)	**19.58** *2.15* (13.98 – 24.45)	**21.00** *2.12* (16.25 – 26.64)	**19.60** *2.05* (14.09 – 23.32)		**0.00**	0.73
IOM-oa	L	**20.51** *2.90* (15.26 – 26.70)	**20.13** *1.80* (15.96 –23.79)	**19.70** *1.99* (15.88 – 25.08)	**20.42** *1.75* (17.05 – 24.80)	0.07	0.77	0.28
	R	**19.76** *2.59* (14.73 – 24.80)	**20.08** *2.10* (16.01 – 24.45)	**19.00** *1.96* (14.56 – 23.69)	**19.92** *2.01* (15.86 – 25.26)		**0.04**	0.12
MOM-oa	L	**23.35** *2.47* (18.63 – 27.85)	**22.81** *1.67* (19.12 – 26.95)	**23.20** *1.97* (16.59 – 26.65)	**24.33** *1.71* (21.53 – 28.33)	0.27	0.39	**0.01**
	R	**24.70** *3.93* (19.03 – 35.31)	**22.57** *2.02* (18.61 – 26.92)	**22.89** *1.90* (17.71 – 27.30)	**23.66** *1.94* (19.68 – 29.08)		0.31	0.50
LOM (ek)-oa	L	**23.79** *1.53* (20.19 – 26.54)	**22.81** *2.25* (17.78 – 29.35)	**24.14** *1.77* *(20.13 – 27.56)*	**23.50** *1.63* (19.13 – 27.03)	**0.00**	**0.00**	**0.03**
	R	**25.25** *3.71* (18.40 – 33.88)	**23.45** *2.84* (19.58 – 27.19)	**24.72** *2.08* (19.72 – 30.31)	**24.70** *1.69* (21.18 – 28.75)		**0.03**	**0.02**

Bold values: mean; Italic values: standard deviation, brackets: minimum and maximum values. Significant p values ($p \leq 0.05$) are indicated in bold.

© University of Pretoria

The eyeball protruded further from the dLOM in black South African females compared to their male counterparts, although it was not significant, while significantly greater protrusion values were noted in white South African males, when compared to their female counterparts (*Table 4.10*). Population variation was also more profound in females, with black South African females presenting with greater protrusion values compared to white South African females.

Table 4.10 Variation in ocular protrusion between sexes within populations and variation between populations within sex groups

		Sexual dimorphism within populations		Population variation within sex groups	
Measurement (mm)	Side	Black South Africans n=94	White South Africans n=103	SA females n=100	SA males n=97
Protrusion: (dLOM – oa)	L	0.46	**0.00**	0.67	0.47
	R	0.99	**0.00**	**0.01**	0.81
SOM-oa	L	0.72	0.99	**0.00**	**0.00**
	R	0.99	0.99	**0.01**	**0.00**
IOM-oa	L	0.26	0.99	0.81	0.61
	R	0.33	0.98	0.88	0.16
MOM-oa	L	0.73	**0.00**	0.52	**0.00**
	R	0.08	0.14	**0.00**	0.45
LOM (ek)-oa	L	0.79	0.24	**0.04**	0.31
	R	0.99	**0.05**	**0.02**	0.99

Significant p values ($p \leq 0.05$) are indicated in bold.

4.1.4.3 Ocular dimensions:

No asymmetry was noted in the ocular dimensions of this South African sample.

Ocular dimensions were always greater in length in the white South African sample when compared to black South Africans. Statistically significant variation was observed in the axial length of both eyeballs, left ocular breadth and right ocular height (*Table 4.11*).

Ocular dimensions were consistently greater in South African males when compared to their female counterparts (*Table 4.11*); however, significant differences in sexual dimorphism for these dimensions was only present in black South Africans (*Table 4.12*).

© University of Pretoria

Table 4.11 Summary statistics (in mm) and p values testing the influence of asymmetry, population affinity and sexual dimorphism on ocular dimensions

		Sex-population groups						
Measurement (mm)	Side	South African black females (n=45)	South African white females (n=57)	South African black males (n=52)	South African white males (n=52)	Asymmetry (p)	Population (p)	Sex (p)
Ocular breadth (OB)	L	**22.44** *1.60* (19.79 – 26.43)	**23.34** *1.47* (20.59 – 26.92)	**23.23** *1.20* (20.65 – 26.08)	**23.55** *1.39* (20.00 – 26.99)	0.34	**0.02**	**0.01**
	R	**22.78** *1.54* (20.02 – 26.70)	**23.61** *1.47* (20.72 – 26.47)	**23.14** *1.38* (20.10 – 25.85)	**23.62** *1.49* (21.29 – 27.31)		0.50	**0.00**
Ocular height (OH)	L	**23.77** *1.44* (19.98 – 26.40)	**24.60** *1.86* (20.80 – 28.40)	**23.88** *1.43* (20.80 – 27.20)	**25.23** *1.55* (22.40 – 28.80)	0.51	0.18	**0.00**
	R	**23.89** *1.66* (20.80 – 27.85)	**23.92** *1.97* (18.40 – 28.00)	**23.93** *1.40* (20.80 – 26.80)	**25.30** *1.47* (22.40 – 28.40)		**0.01**	**0.00**
Axial/ocular length (OL)	L	**21.98** *1.23* (18.28 – 25.10)	**23.14** *1.30* (20.29 – 25.85)	**23.50** *1.22* (20.54 – 26.31)	**23.27** *1.17* (20.82 – 25.68)	0.69	**0.00**	**0.04**
	R	**22.16** *1.36* (19.22 – 24.80)	**23.39** *1.04* (20.90 – 25.85)	**23.27** *1.28* (20.12 – 26.87)	**23.32** *1.05* (21.26 – 25.46)		**0.01**	**0.00**

Bold values: mean; Italic values: standard deviation, brackets: minimum and maximum values. Significant p values ($p \leq 0.05$) are indicated in bold.

© University of Pretoria

Further examination and analysis of the ocular dimensions within sex and population groups indicated that all ocular dimensions vary significantly between black South African males and females, with black males presenting with larger eyeball compared to their female counterparts. No statistically significant difference was noted in ocular dimensions between sexes in the white South African sample (*Table 4.12*). Black South African females had significantly shorter axial lengths for both eyeballs when compared to white South African females. No statistically significant difference was found between the South African males.

Table 4.12 Variation in ocular dimensions between sexes within populations and variation between populations within sex groups

		Sexual dimorphism within populations		Population variation within sex groups	
Measurement (mm)	Side	Black South Africans n=97	White South Africans n=109	SA females n=102	SA males n=103
Ocular breadth/width (OB)	L	**0.01**	0.64	**0.03**	0.88
	R	**0.01**	0.33	0.07	0.73
Ocular height (OH)	L	**0.05**	0.64	**0.03**	0.87
	R	0.99	0.33	0.07	0.99
Axial length / ocular length (OL)	L	**0.00**	0.76	**0.00**	0.95
	R	**0.00**	0.67	**0.00**	0.99

Significant p values ($p \leq 0.05$) are indicated in bold.

4.1.4.4 Palpebral fissure dimensions :

The only asymmetry noted in the palpebral fissure dimensions in this South African sample, was noted in the orbital height.

Black South Africans presented with greater palpebral fissure heights and widths, which was only significant on the left (*Table 4.13*).

South African females presented with narrower palpebral fissure widths when compared to white South African males (p= 0.00), while no significant difference was noted in the height of the palpebral fissure between the sexes (*Table 4.13*).

© University of Pretoria

Table 4.13 Summary statistics (mm) and p-values investigating the influence of asymmetry, population affinity and sexual dimorphism on palpebral fissure dimensions

		Sex-Population groups						
Measurement	Side	South African black females (n=45)	South African white females (n=57)	South African black males (n=52)	South African white males (n=52)	Asymmetry (p)	Population (p)	Sex (p)
Palpebral fissure width	L	**26.87** *± 3.43* (20.31 - 33.88)	**25.90** *± 1.62* (23.07 - 29.88)	**28.22** *± 2.10* (23.89 - 33.90)	**27.16** *± 2.14* (20.44 - 31.25)	0.18	**0.00**	**0.00**
	R	**26.89** *± 3.58* (18.65 - 35.32) n=33	**26.18** *± 1.75* (22.49 - 30.06) n=57	**27.86** *± 2.45* (22.87 - 36.64) n=52	**28.22** *± 2.11* (22.11 - 32.03) n=52		0.24	**0.00**
Palpebral fissure height	L	**9.27** *± 1.61* (6.42 - 13.67)	**8.86** *± 1.23* (6.54 - 11.96)	**9.72** *± 1.88* (6.21 - 13.51)	**8.95** *± 1.15* (6.91 - 12.67)	0.45	**0.01**	0.19
	R	**8.99** *± 1.33* (6.81 - 12.47)	**8.88** *± 1.10* (6.97 - 12.00)	**9.54** *± 1.80* (5.42 - 13.70)	**8.83** *± 1.21* (5.87 - 11.29)		0.12	0.18

Bold values: mean; Italic values: standard deviation, brackets: minimum and maximum values. Significant p values ($p \leq 0.05$) are indicated in bold.

© University of Pretoria

The effect of sex on the palpebral fissure dimensions within populations yielded similar results as in the entire South African sample. South African males always presented with greater palpebral fissure widths compared to South African females, regardless of population affinity (*Table 4.14*).

Table 4.14 Variation in palpebral fissure dimensions between sexes within populations and variation between populations within sex groups

		Sexual dimorphism within populations		Population variation within sex groups	
Measurement (mm)	Side	Black South Africans n=97	White South Africans n=109	SA females n=102	SA males n=103
Palpebral fissure width	L	**0.02**	**0.03**	0.17	0.08
	R	**0.01**	**0.00**	0.48	0.37
Palpebral fissure height	L	0.85	0.68	0.14	0.57
	R	0.56	0.99	0.34	0.78

Significant p values ($p \leq 0.05$) are indicated in bold.

4.1.5 Classification accuracy based on orbital dimensions

The discriminatory ability of the orbital dimensions was determined based on a discriminant function analysis (DFA) (*Table 4.15*). A greater difference was noted between sexes over populations. Sex can be estimated with a higher accuracy compared to the estimation of population affinity. Therefore, if sex of the person is known, the classification accuracy for population increases, especially in South African females.

Table 4.15 Classification accuracy (%) of the orbital and palpebral fissure dimensions

	Orbital dimensions
Population	75.25
Pop*males	77.32
Pop*females	84.40
Sex	80.10
Sex*white	78.43
Sex*black	73.08

© University of Pretoria

4.1.6 Prediction equations based on linear data

The prediction of the position of the eyeball and palpebral fissure dimensions in relation to the orbital rim was determined by predicting the protrusion as a percentage of the orbital height and/or breadth and secondly, prediction equations were proposed through linear regression.

In order to establish an association between orbital morphology and eyeball position, the absolute distances of the eyeball to the superior and lateral (for anterior projection) orbital margins were expressed as percentages of orbital breadth (OB) and -height (OH), respectively (*Table 4.16*; *Figure 4.3*). In this study, orbital height varied significantly between white and black South Africans, as well as between sexes, while ocular breadth was sexually dimorphic but not population specific. As the projection of the eyeball from the dLOM was sexually dimorphic and the distance from the superior orbital margin (supraconchion) to the oculus anterius was influenced by population affinity, these two measurements were selected as the primary predictors of eyeball projection. All predictions were restricted to one side - the left side - to exclude effects of asymmetry.

Based on the entire sample, the supero-inferior position of the eyeball (measured from the supraconchion) averaged 54.77 % of the OH (SD: 2.70 mm; SEE: 0.19 mm), while the mediolateral position (measured from the deepest point on the lateral orbital margin) averaged 65.57 % of the OH (SD: 2.49 mm; SEE: 0.18 mm). The anteroposterior position of the eyeball averaged 58.84 % of the OB (SD: 2.07; SEE: 0.15). Sex and population specific predictions, based on proportionality, did not improve the standard error of the estimate (SEE), instead, an increase in the SEE was observed and a decrease was noted in the standard deviation (SD) in the white South African and male South African groups. The greatest SEE was noted in black South African females (*Table 4.16*).

Secondly, the correlations between orbital height and breadth versus eyeball positioning (relative to the oculus anterius) were evaluated. Bivariate regression was performed on one independent (or predictor) and one dependent (predicted) variable. The dependent variables are indicated in Table 4.16. The lateral orbital margin served as the predictor for mediolateral and anteroposterior positioning, while the superior orbital margin predicted supero-inferior positioning. The SEE were greater for the linear regression prediction equations compared to the prediction by proportionality. Similar to the predictions by proportionality, SEE values were greater in individual sex-population groups compared to the SEE observed in the entire sample (2.05 – 2.58 mm vs. 3.61 – 6.94 mm). The coefficient of determination (R^2) however indicated poor correlation between the hard tissue (independent/predictor) and the position of the eyeball (dependent/predicted variable) which influences the accuracy (greater SEE values noted) of the prediction equations (*Table 4.16*).

© University of Pretoria

Table 4.16. Prediction equations and proportional eyeball position in relation to the superior and lateral orbital margins

Eyeball position	Prediction through linear regression					Prediction by proportionality		
	Equations	r	R^2	p-value	SEE (mm)	Percentage	SD (mm)	SEE (mm)
Entire sample								
Supero-inferior	0.024*OH + 19.415	0.03	0.00	0.71	2.39	54.78 % of OH from sk	2.70	0.19
Mediolateral	0.094*OH + 20.831	0.12	0.02	0.09	2.05	65.58 % of OH from dlom	2.49	0.18
Anteroposterior	0.255*OB + 13.761	0.28	0.08	**0.05**	2.58	58.84 % of OB from dlom	2.07	0.15
White South Africans								
Supero-inferior	0.116*OH + 15.244	0.13	0.02	0.18	3.25	52.23 % of OH from sk	2.17	0.21
Mediolateral	0.160*OH + 18.293	0.19	0.04	0.05	3.07	64.75 % of OH from dlom	2.16	0.21
Anteroposterior	0.457*OB + 5.326	0.45	0.20	**0.00**	3.75	57.61 % of OB from dlom	1.77	0.13
Black South Africans								
Supero-inferior	0.045*OH + 19.394	0.05	0.00	0.61	3.27	57.56 % of OH from sk	2.83	0.29
Mediolateral	0.053*OH + 22.390	0.07	0.01	0.50	2.86	66.48 % of OH from dlom	2.77	0.29
Anteroposterior	0.137*OB + 18.683	0.16	0.03	0.12	3.57	59.17 % of OB from dlom	2.43	0.25
South African females								
Supero-inferior	0.034*OH + 19.103	0.04	0.00	0.71	3.43	55.93 % of OH from sk	2.97	0.30
Mediolateral	-0.075*OH + 26.549	-0.11	0.01	0.29	2.62	65.39 % of OH from dlom	2.87	0.29
Anteroposterior	-0.021*OB + 24.640	-0.04	0.00	0.82	3.66	59.15 % of OB from dlom	2.36	0.24
South African males								
Supero-inferior	0.028*OH + 19.206	0.03	0.00	0.77	3.57	53.39 % of OH from sk	2.29	0.23
Mediolateral	0.226*OH + 16.309	0.27	0.07	**0.01**	3.18	65.77 % of OH from dlom	2.00	0.20
Anteroposterior	0.548*OB + 1.564	0.46	0.21	**0.00**	4.63	58.52 % of OB from dlom	1.68	0.17
Black South African females								
Supero-inferior	0.164*OH + 15.462	0.18	0.03	0.24	4.95	59.93 % of OH from sk	3.00	0.45
Mediolateral	-0.132*OH + 28.735	-0.17	0.03	0.25	4.09	67.78 % of OH from dlom	3.32	0.50
Anteroposterior	-0.061*OB + 26.479	0.01	0.08	0.62	4.96	60.23 % of OB from dlom	2.93	0.44
White South African females								
Supero-inferior	0.103*OH + 15.754	0.11	0.01	0.41	4.60	52.66 % of OH from sk	2.33	0.31
Mediolateral	0.047*OH + 21.847	0.07	0.00	0.63	3.61	63.43 % of OH from dlom	2.17	0.29
Anteroposterior	0.140*OB + 17.902	0.16	0.02	0.36	6.15	58.27 % of OB from dlom	1.69	0.23

© University of Pretoria

Table 4.16 *Prediction equations and proportional eyeball position in relation to the superior and lateral orbital margins* continues

Black South African males								
Supero-inferior	-0.032*OH + 22.060	-0.04	0.00	0.80	4.92	55.39 % of OH from sk	2.38	0.34
Mediolateral	0.251*OH + 15.131	0.30	0.09	**0.04**	4.41	65.29 % of OH from dlom	1.99	0.28
Anteroposterior	0.563*OB + 0.804	0.48	0.23	**0.00**	6.42	58.12 % of OB from dlom	1.74	0.25
White South African males								
Supero-inferior	0.136*OH + 14.480	0.16	0.03	0.28	4.78	51.75 % of OH from sk	1.98	0.29
Mediolateral	0.181*OH + 18.255	0.22	0.05	0.14	4.61	66.26 % of OH from dlom	2.02	0.29
Anteroposterior	0.500*OB + 3.841	0.41	0.17	**0.00**	6.94	58.85 % of OB from dlom	1.66	0.24
Significant p values (p ≤ 0.05) indicated in bold.								

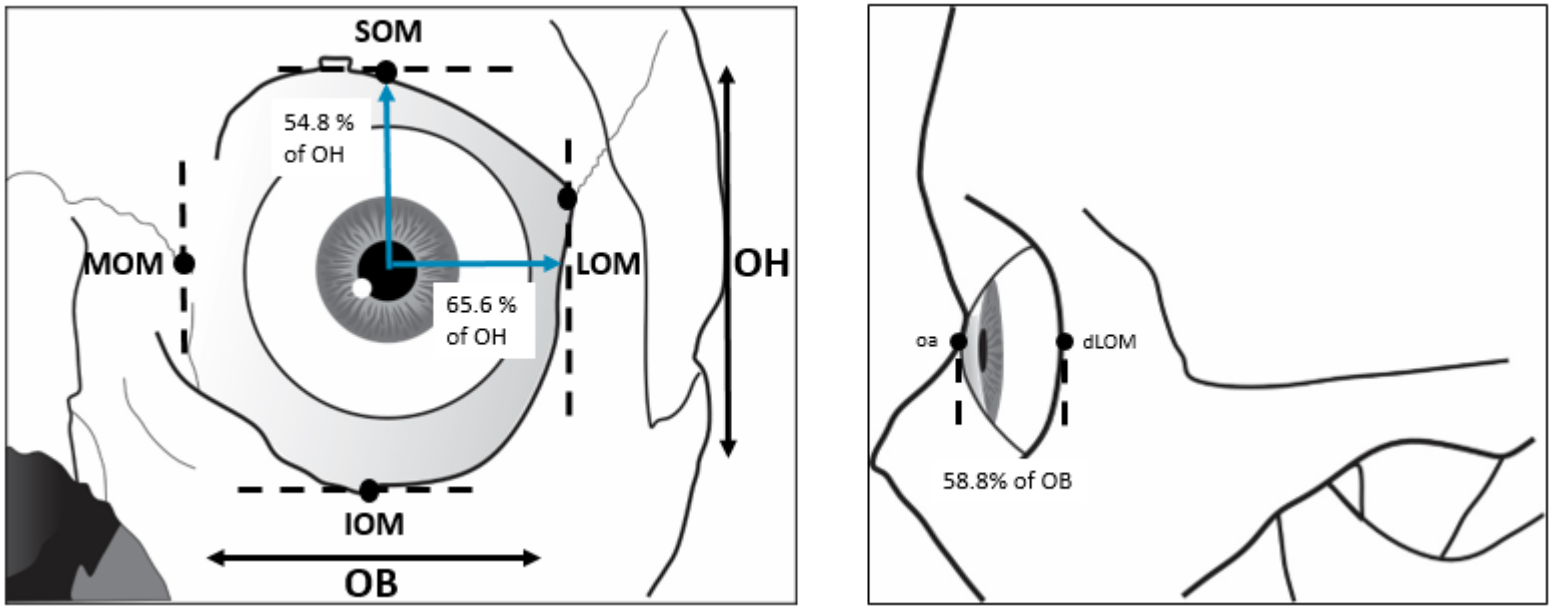

Figure 4.3. Proportional placement of the eyeball within the orbit from the lateral and superior orbital margins and the deepest point on the lateral orbital margin

© University of Pretoria

Eyeball dimensions were similarly predicted from the orbital dimensions. The orbital breadth was used as predictor for eyeball width, while orbital height was used as predictor for eyeball height. Although significant p-values were noted for the correlation between the hard- and soft-tissue dimensions of the orbital region, low correlation values (R^2) was obtained, while the SEE for the entire sample ranged between 0.75 – 2.09 mm.

The eyeball dimensions can be predicted with lower SEE values based on its proportionality with the orbital dimensions. The eyeball width averaged 56.04 % of the OB (SD: 1.68; SEE: 0.12), while the eyeball height averaged 65.70 % of the OH (SD: 2.10 mm; SEE: 0.01 mm) (*Figure 4.4*) . The SD decreased with known sex and population affinity in females and in black South Africans, although it did not improve the standard error of the estimate (SEE) (*Table 4.17*).

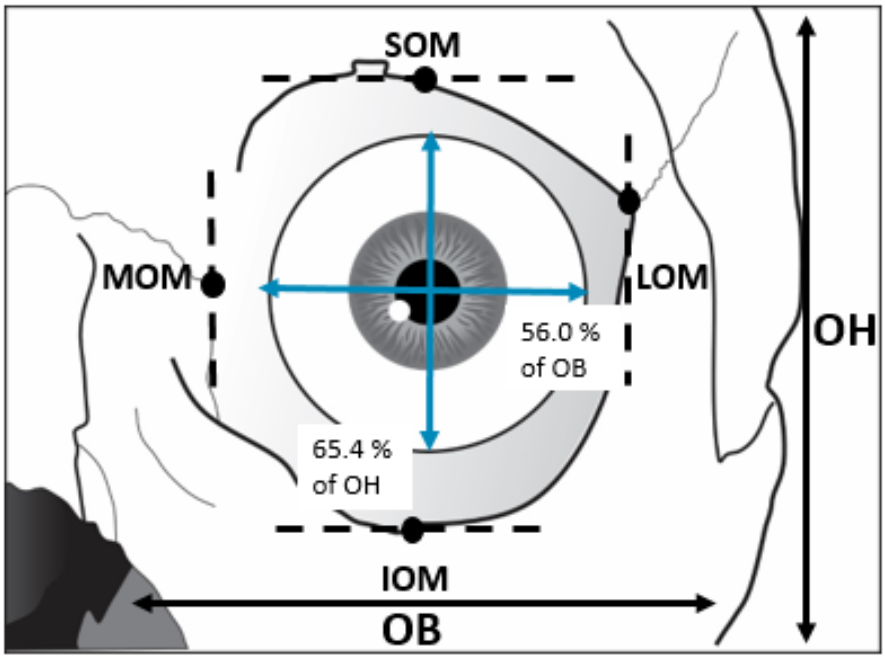

Figure 4.4. Proportional dimensions of the eyeball as percentages of orbital height and width

© University of Pretoria

Table 4.17. Prediction equations for the estimation of the eyeball dimensions from the orbital dimensions

	Prediction through linear regression					Prediction by proportionality		
Eyeball diameter	Equations	r	R^2	p-value	SEE (mm)	Percentage	SD (mm)	SEE (mm)
Entire sample								
Eyeball width	y = 0.235*OB + 13.456	0.32	0.10	**0.00**	2.09	56.04 % OB	1.68	0.12
Eyeball height	y = 0.172*OH + 17.988	0.25	0.06	**0.01**	1.75	65.70 % OH	2.10	0.01
White South Africans								
Eyeball width	y = 0.016*OB + 22.685	0.02	0.00	0.83	3.18	56.31 % OB	1.73	0.17
Eyeball height	y = 0.048*OH + 22.663	0.07	0.00	0.51	2.77	65.24 % OH	2.18	0.21
Black South Africans								
Eyeball width	y = 0.356*OB + 8.292	0.50	0.25	**0.00**	2.69	55.74 % OB	1.63	0.17
Eyeball height	y = 0.253*OH + 14.948	0.39	0.15	**0.00**	2.28	66.20 % OH	2.01	0.21
South African females								
Eyeball width	y = 0.307*OB + 10.547	0.40	0.16	**0.00**	2.85	56.59 % OB	1.59	0.16
Eyeball height	y = 0.131*OH + 19.042	0.24	0.06	**0.02**	1.94	65.44 % OH	2.03	0.20
South African males								
Eyeball width	y = -0.011*OB + 23.997	-0.01	0.00	0.92	4.18	55.472 % OB	1.75	0.18
Eyeball height	y = 0.118*OH +20.460	0.14	0.02	0.16	3.17	265.96 % OH	2.16	0.22
Black South African females								
Eyeball width	y = 0.369*OB + 7.523	0.58	0.33	**0.00**	3.20	55.70 % OB	1.52	0.23
Eyeball height	y = 0.263*OH + 14.379	0.52	0.27	**0.00**	2.28	66.81 % OH	1.73	0.26
White South African females								
Eyeball width	y = 0.034*OB + 21.822	0.04	0.00	0.80	5.30	57.32 % OB	1.60	0.22
Eyeball height	y = -0.041*OH + 25.454	-0.07	0.00	0.64	3.24	64.33 % OH	2.21	0.30
Black South African males								
Eyeball width	y = 0.125*OB + 18.280	0.13	0.00	0.75	3.36	55.78 % OB	1.79	0.26
Eyeball height	y = 0.156*OH + 18.812	0.18	0.01	0.53	5.29	65.64 % OH	2.25	0.32
White South African males								
Eyeball width	y = -0.171*OB + 30.870	-0.18	0.03	0.22	5.87	55.16 % OB	1.76	0.25
Eyeball height	y = 0.061*OH + 22.836	0.10	0.01	0.59	4.30	66.28 % OH	2.08	0.30

Significant p values ($p \leq 0.05$) indicated in bold

© University of Pretoria

The dimensions of the palpebral fissure were predicted from the orbital dimensions (*Table 4.17*) in order to approximate the open eye. A stronger correlation was noted between the palpebral fissure width and orbital breadth compared to palpebral fissure height and ocular height. Black South Africans and black South African females presented with the strongest correlation between the dimensions of the orbit and palpebral fissures, although it did not improve the SEE. The results of the proposed prediction equations to determine the dimensions of the palpebral fissure had the lowest SEE for the sample as a whole, while the SEE increased when sex and population affinity were added as factors.

Based on the entire sample, palpebral fissure width averaged 65.35 % of the OB (SD: 2.14 mm; SEE: 0.15 mm), while the palpebral fissure height averaged 24.65 % of the OH (SD: 1.53 mm; SEE 0.11 mm) (*Figure 4.5*). The dimensions of the palpebral fissure could be predicted based on proportionality with a smaller error (0.15 mm vs. 2.90 mm and 0.11 mm vs. 1.55 mm) compared to the prediction equations (linear regressions), especially when the samples were combined and should be considered as the method of choice for the positioning of the eyeball within the bony orbit (*Table 4.18*).

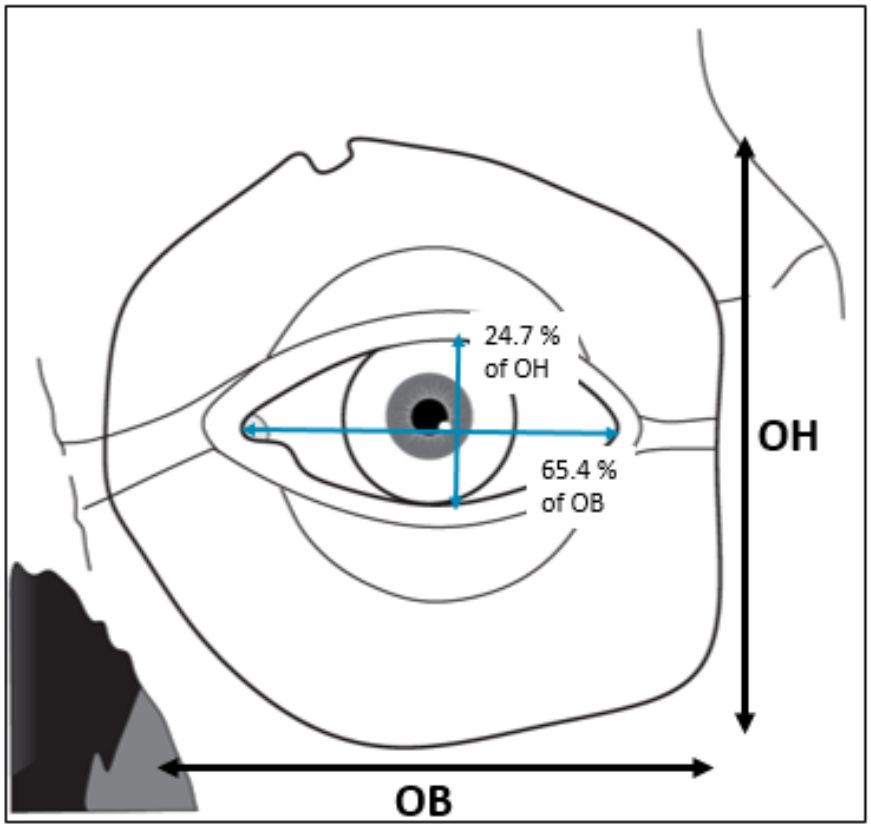

Figure 4.5. Proportional dimensions of the palpebral fissure as percentages of orbital height and width

© University of Pretoria

Table 4.18. Prediction equations for the estimation of the palpebral fissure dimensions from the orbital dimensions

	Prediction through linear regression					Prediction by proportionality		
Palpebral fissure dimensions	Equations	r	R^2	p-value	SEE (mm)	Percentage	SD (mm)	SEE (mm)
Entire sample								
Palpebral fissure width	y = 0.561*OB + 3.831	0.50	0.25	**0.00**	2.90	65.35 % OB	2.14	0.15
Palpebral fissure height	y = 0.101*OH + 5.391	0.18	0.03	**0.02**	1.55	24.65 % OH	1.53	0.11
White South Africans								
Palpebral fissure width	y = 0.393*OB + 10.207	0.38	0.14	**0.00**	3.97	63.93 % OB	1.80	0.18
Palpebral fissure height	y = 0.182*OH + 2.017	0.35	0.13	**0.00**	1.81	23.57 % OH	1.084	0.11
Black South Africans								
Palpebral fissure width	y = 0.696*OB – 1.093	0.61	0.37	**0.00**	3.91	66.91 % OB	2.29	0.24
Palpebral fissure height	y = 0.087*OH + 6.322	0.15	0.02	0.19	2.44	26.01 % OH	1.81	0.20
South African females								
Palpebral fissure width	y = 0.641*OB + 0.476	0.53	0.28	**0.00**	4.21	65.32 % OB	2.20	0.22
Palpebral fissure height	y = 0.093*OH + 5.594	0.19	0.04	0.07	1.86	24.68 % OH	1.44	0.15
South African males								
Palpebral fissure width	y = 0.311*OB + 14.564	0.24	0.06	**0.02**	5.53	65.38 % OB	2.07	0.21
Palpebral fissure height	y = 0.088*OH + 5.988	0.12	0.02	0.23	2.77	24.65 % OH	1.62	0.16
Black South African females								
Palpebral fissure width	y = 0.816*OB – 5.833	0.66	0.44	**0.00**	5.65	66.96 % OB	2.60	0.39
Palpebral fissure height	y = 0.105*OH – 5.492	0.30	0.09	0.19	2.75	26.41 % OH	1.62	0.28
White South African females								
Palpebral fissure width	y = 0.230*OB + 16.577	0.21	0.04	0.13	6.01	63.99 % OB	1.63	0.22
Palpebral fissure height	y = 0.125*OH + 4.146	0.24	0.06	0.07	2.57	23.65 % OH	1.16	0.16
Black South African males								
Palpebral fissure width	y = 0.426*OB + 10.233	0.34	0.12	**0.02**	7.22	66.86 % OB	2.00	0.29
Palpebral fissure height	y = 0.036*OH + 11.060	-0.04	0.00	0.76	4.49	25.75 % OH	1.97	0.28
White South African males								
Palpebral fissure width	y = 0.297*OB + 14.606	0.22	0.05	0.13	8.15	63.87 % OB	2.00	0.29
Palpebral fissure height	y = 0.256*OH – 0.806	0.48	0.23	**0.00**	2.60	23.48 % OH	0.99	0.14

Significant p values ($p \leq 0.05$) indicated in bold

© University of Pretoria

4.1.7 Comparison of data with existing literature

In order to aid the comparison with the published literature, specifically concerning population variation, the Bayes Factor (BF) were calculated for each dimension. Supplementary Table 1 presents a comprehensive summary of the comparison of existing literature with the findings of this study according to each sex-population group, along with the BF and their interpretation. *Table 4.19* summarises the results of supplementary table 1, which indicates that more than two-thirds of the linear dimensions of South Africans vary significantly compared to other population groups.

South African females presented with a similar number of agreements with studies on African and non-African groups, while black South African males presented with a greater number of agreements as compared to white South African males and females. The comparisons and effects of the variations are discussed in detail in Chapter 5.

© University of Pretoria

Table 4.19 Summary of significant variation in linear dimensions between South Africans and existing literature

Linear distance / dimension	n = 23		n = 72		Total
	African groups with similar dimensions	African groups with different dimensions	Non-Africans with similar dimensions	Non-Africans with different dimensions	
Black SA Females					
Left orbital height	1	2	4	4	11
Left orbital breadth	1	2	0	8	11
Left orbital index	0	2	0	1	3
Interorbital distance	0	2	2	2	6
Bizygomatic breadth	2	1	0	7	10
Left ocular height	0	1	0	1	2
Left ocular breadth	0	1	0	2	3
Left ocular/axial length	0	1	1	3	5
Left eye protrusion from dLOM	1	0	0	5	6
Left eye protrusion from IOM	1	0	1	1	3
Left eye protrusion from MOM	1	0	0	2	3
Left eye protrusion from SOM	0	1	1	1	3
Left palpebral fissure height	0	1	0	11	12
Left palpebral fissure width	1	1	6	9	17
White SA Females					
Left orbital height	0	3	2	6	11
Left orbital breadth	2	1	0	8	11
Left orbital index	0	2	0	1	3
Interorbital distance	0	2	0	4	6
Bizygomatic breadth	2	1	0	7	10
Bizygomatic breadth	2	1	0	7	10
Left ocular height	0	1	0	1	2
Left ocular breadth	0	1	0	2	3
Left ocular/axial length	0	1	2	2	5
Left eye protrusion from dLOM	1	0	0	5	6
Left eye protrusion from IOM	1	0	1	1	3
Left eye protrusion from MOM	1	0	1	1	3
Left eye protrusion from SOM	0	1	0	2	3
Left palpebral fissure height	0	1	5	6	12
Left palpebral fissure width	1	1	2	13	17
Black SA Males					
Left orbital height	2	1	3	5	11
Left orbital breadth	2	1	1	7	11
Left orbital index	1	1	0	1	3
Interorbital distance	0	2	2	2	6
Bizygomatic breadth	2	1	1	6	10
Left ocular height	0	1	0	1	2
Left ocular breadth	1	0	0	2	3

© University of Pretoria

Table 4.19 continues

Linear distance / dimension	African groups with similar dimensions	African groups with different dimensions	Non-Africans with similar dimensions	Non-Africans with different dimensions	Total
Left ocular/axial length	1	0	2	2	5
Left eye protrusion from dLOM	1	0	0	5	6
Left eye protrusion from IOM	0	1	1	1	3
Left eye protrusion from MOM	1	0	0	2	3
Left eye protrusion from SOM	0	1	1	1	3
Left palpebral fissure height	1	0	2	9	12
Left palpebral fissure width	0	2	4	11	17
White SA Males					
Left orbital height	1	2	3	5	11
Left orbital breadth	2	1	0	8	11
Left orbital index	1	1	0	1	3
Interorbital distance	0	2	0	4	6
Bizygomatic breadth	2	1	1	6	10
Left ocular height	0	1	0	1	2
Left ocular breadth	1	0	0	2	3
Left ocular/axial length	1	0	2	2	5
Left eye protrusion from dLOM	1	0	0	5	6
Left eye protrusion from IOM	0	1	1	1	3
Left eye protrusion from MOM	0	1	0	2	3
Left eye protrusion from SOM	0	1	0	2	3
Left palpebral fissure height	1	0	2	9	12
Left palpebral fissure width	0	2	3	12	17

4.1.8 Shape analysis: Based on manually placed landmarks

4.1.8.1 Reproducibility testing

In order to determine variation in the shape of the orbits and palpebral fissures, and to ensure that it is comparable with the results of the linear dimensions calculated for each sex-population group, the shape analysis was conducted using the same landmarks placed in part 1. With special focus on the craniometric and capulometric landmarks only (*Table 4.20*) the capulometric landmarks were placed with higher accuracy than the craniometric landmarks. The dispersion error of both observers fell within an acceptable range (Ridel et al., 2018).

Table 4.20. Dispersion errors (mm) of manual landmark placement

	Intra-observer error		Inter-observer error	
	Mean	SD	Mean	SD
Craniometric landmarks	0.68	0.51	1.20	0.78
Capulometric landmarks	0.55	0.37	0.98	0.62

© University of Pretoria

4.1.8.2 Multivariate normality testing

Multivariate normality testing was conducted by visually assessing the distribution of Q-Q plots (Scrucca, 2000). The graph illustrates the actual values of squared Mahalanobis distances (circles) plotted against those of an ideal multivariate normal distribution (solid line). A closer alignment with the diagonal line suggests a stronger adherence to the multivariate normal distribution. A MANOVA (parametric data) 50-50 MANOVA and permutation test (non-parametric) were conducted on all data to assess significance without relying on the assumption of normality from visually analysing the Q-Q plots.

Figure 4.6 presents a Q-Q plot comparing Mahalanobis distances expected in normally distributed data with those computed from this sample. Some deviation from the norm was noted in the orbital shape, while the palpebral fissure shape followed a normal distribution. The effect of population within sex groups was also investigated. The distribution of these data sets can be observed in Annexure D.

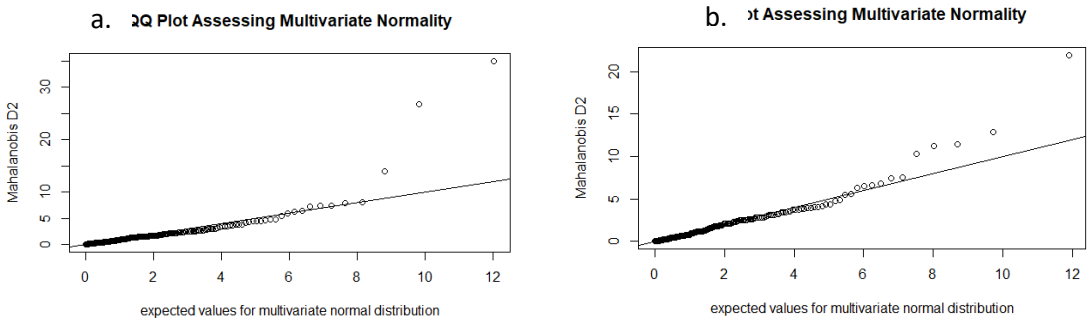

Figure 4.6. Q-Q-plots of the residuals of the linear model a) hard-tissue shape against population, b) soft-tissue shape against population

Concerning the effect of sexual dimorphism on the shape of the orbit and palpebral fissure, the Q-Q plots of Mahalanobis distances expected in perfectly normal distributed data versus those calculated from the sample, indicated three outliers in the hard-tissue components, while the soft-tissue components followed a normal distribution with slight variation from the norm (Figure 4.7). The effect of sexual dimorphism within population groups was also investigated. The distribution of these data sets can be observed in Annexure D.

© University of Pretoria

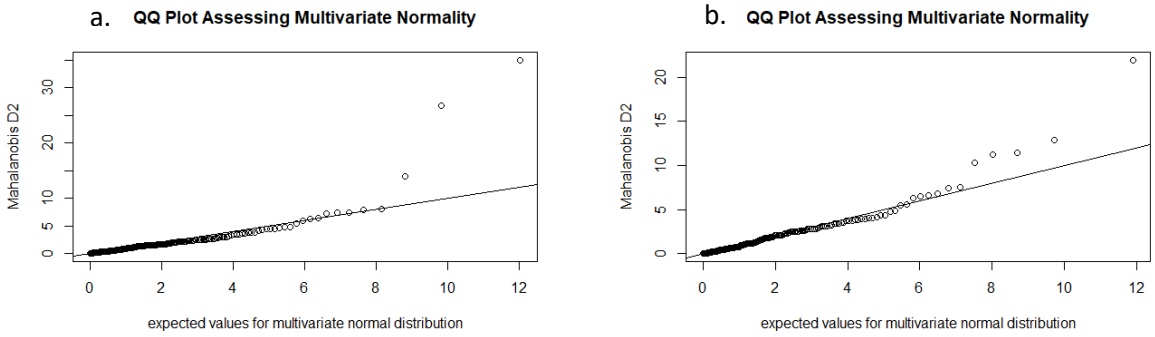

Figure 4.7. Q-Q-plots of the residuals of the linear model a) hard-tissue shape against sex, b) soft-tissue shape against sex

4.1.8.3 Shape analysis: variation between groups and classification accuracies

In the following section, the effect of population affinity and sex was determined on the shape of the orbital region (*Figure 4.8* and *Table 4.21*) and palpebral fissures (*Figure 4.9* and *Table 4.22*) respectively. The effect of these variables was tested in the entire sample, as well as in each sex-population group. Parametric and non-parametric testing was applied to accommodate the data that was not normally distributed. Supplementary Table 3 contains all the Eigenvalues and Principal Scores for each analysis conducted.

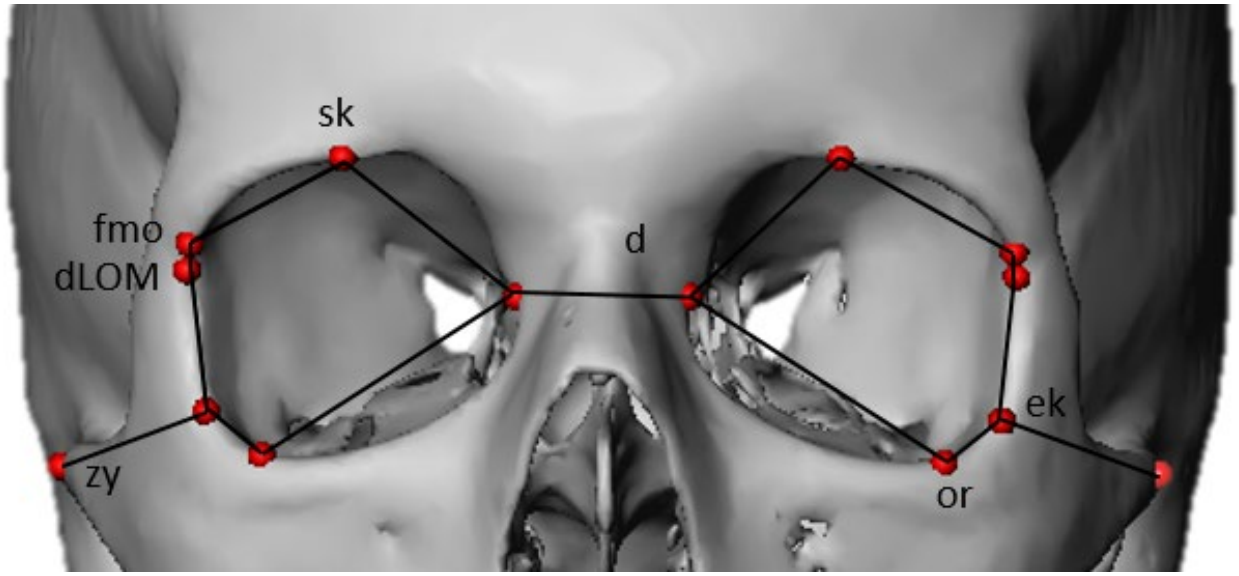

Figure 4.8. Wire frame indicating the shape of the orbital region investigated

© University of Pretoria

Table 4.21 Shape analysis results for craniometric landmarks.

	MANOVA	50-50 MANOVA	PERMUTATION	DFA
Population affinity	**0.00**	**0.00**	**0.00**	81.07
Pop*males	**0.00**	**0.00**	**0.00**	84.62
Pop*females	**0.00**	**0.00**	**0.00**	85.29
Sex	0.12	0.15	0.47	54.85
Sex*white	**0.00**	**0.00**	**0.00**	84.40
Sex*black	0.15	0.22	**0.02**	61.86

Significant p values (p ≤ 0.05) are indicated in bold.

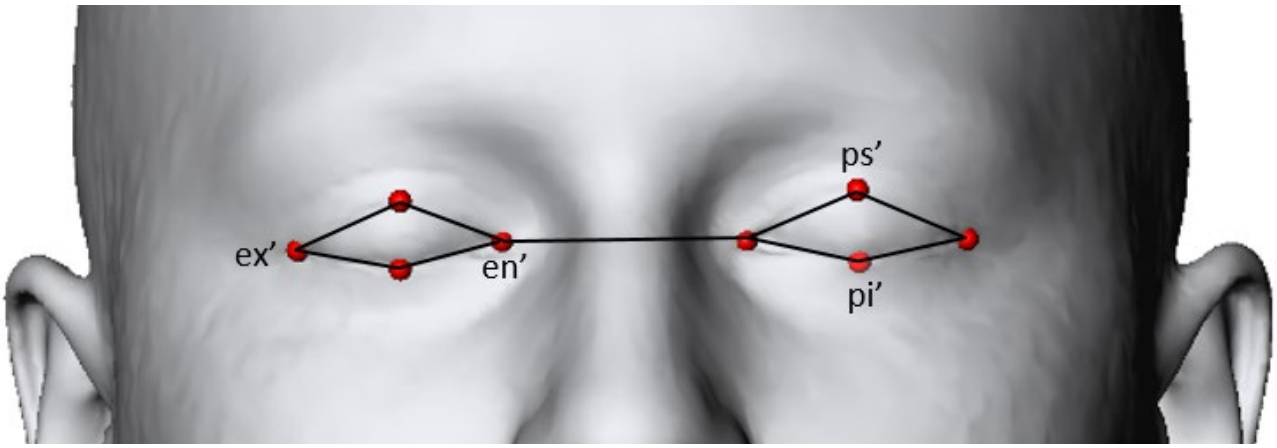

Figure 4.9. Wire frame indicating the shape of the palpebral fissure investigated

Table 4.22 Shape analysis results for capulometric landmarks.

	MANOVA	50-50 MANOVA	PERMUTATION	DFA
Population affinity	**0.03**	**0.04**	0.07	62.18
Pop*males	0.14	0.15	0.15	60.58
Pop*females	**0.02**	**0.04**	0.08	66.29
Sex	**0.01**	**0.01**	0.29	60.10
Sex*white	0.09	0.11	0.48	58.33
Sex*black	**0.03**	**0.04**	**0.02**	63.53

Significant p values (p ≤ 0.05) are indicated in bold.

Population affinity significantly influenced the shape of the orbits (*Table 4.21*) and palpebral fissures (*Table 4.22*) of the complete sample regardless of the statistical tests employed (MANOVA, 50-50 MANOVA and permutation testing). Principal component (PC) 1 accounted for 20.56 % of orbital shape variation, while PC 2 accounted for 13.93 % (*Figure 4.10*). The maximum shape deformation of PC 1 reflects the extreme of the black South African population who displayed a more projecting orbitale and a wider distance between the zygions when compared to the minimum shape. With regard to the palpebral fissure shape deformation, PC 1 accounted for 27.40 % of the variation and PC 2, 13.93 %, although greater overlap of the population groups was noted for the soft-tissue shape indicating less variation between population groups (*Figure 4.11*).

© University of Pretoria

Classification accuracy for population affinity based on orbital shape was high (81.07 %) and increased to 84.62 % and 85.29 % in males and females, respectively with known sex (*Table 4.21*). Classification accuracy for population affinity is much lower based on the shape of the palpebral fissure (62.17 %) compared to the orbital shape. As a significant difference exists in the shape of the palpebral fissure of South African females, classification accuracy increases to 66.29 % in this group if sex is known (*Table 4.22*).

© University of Pretoria

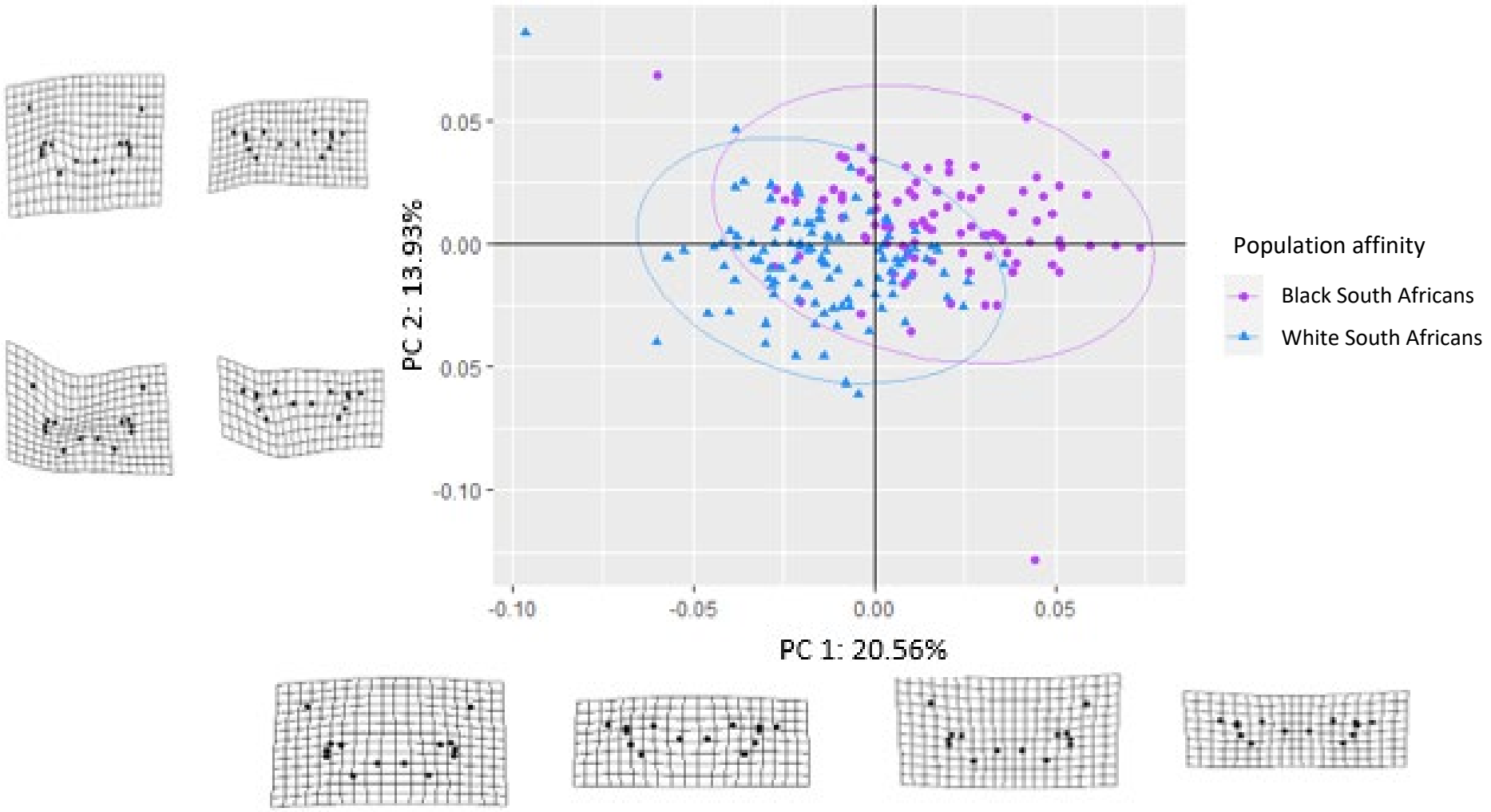

Figure 4.10. Scatterplot with corresponding deformation grids illustrating PC 1 against PC 2 of the complete South African sample indicating the effect of population affinity on the position of the 14 landmarks located on the orbital region

© University of Pretoria

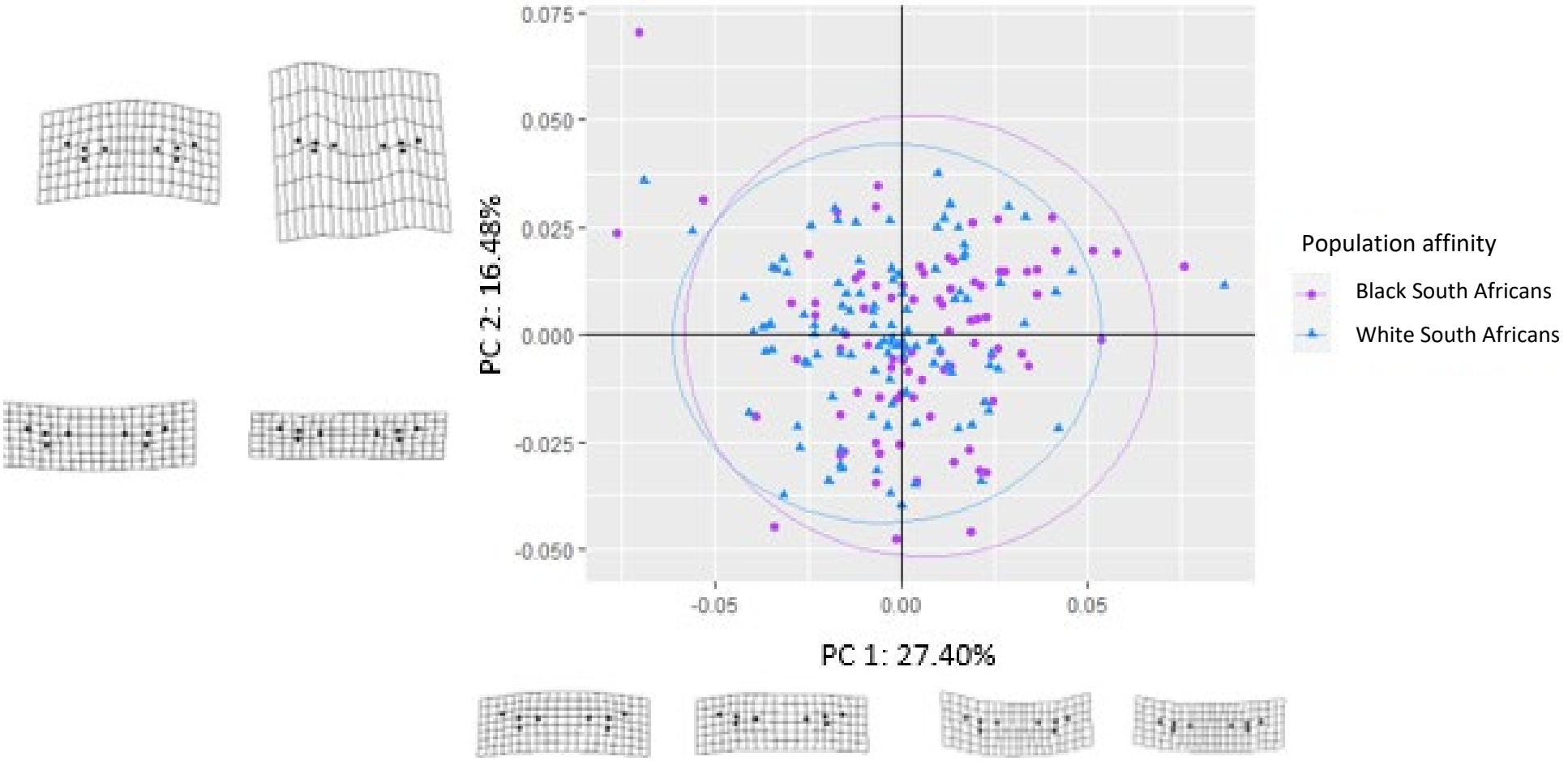

Figure 4.11. Scatterplot with corresponding deformation grids illustrating PC 1 against PC 2 of the complete South African sample indicating the effect of population affinity on the position of the 8 landmarks located on the palpebral fissures

© University of Pretoria

*Population*males*

Population had a significant influence on the shape of the orbital region of South African males based on parametric and non-parametric tests. A distinct shape variation in the orbital region between white and black South African males was noted as depicted in *Figure 4.12*. Principal component 1 was responsible for 23.23 % of variation and PC 2, 13.79%. With more positively loaded PC scores observed in white South African males, this group exhibited a smaller interorbital distance and greater protrusion at the supraconchion. The DFA was 84.62 % (*Table 4.21*).

With regard to the shape of the palpebral fissure, no significant difference was noted between South African male groups and a lower DFA of 60.58 % was obtained (*Table 4.22*). PC 1(30.73 %) versus PC 2 (17.13 %) is illustrated in *Figure 4.13*. Shape variations were noted where the endocanthion was located more superficial while the exocanthion moves posterolateraly in black South African males. A wider spread along the PC 2 axis in the shape of the palpebral fissure was observed in black South African males. A greater inner canthal distance is noted in this group, which corresponds with the hard-tissue results which indicated a wider interorbital distance in black South Africans.

© University of Pretoria

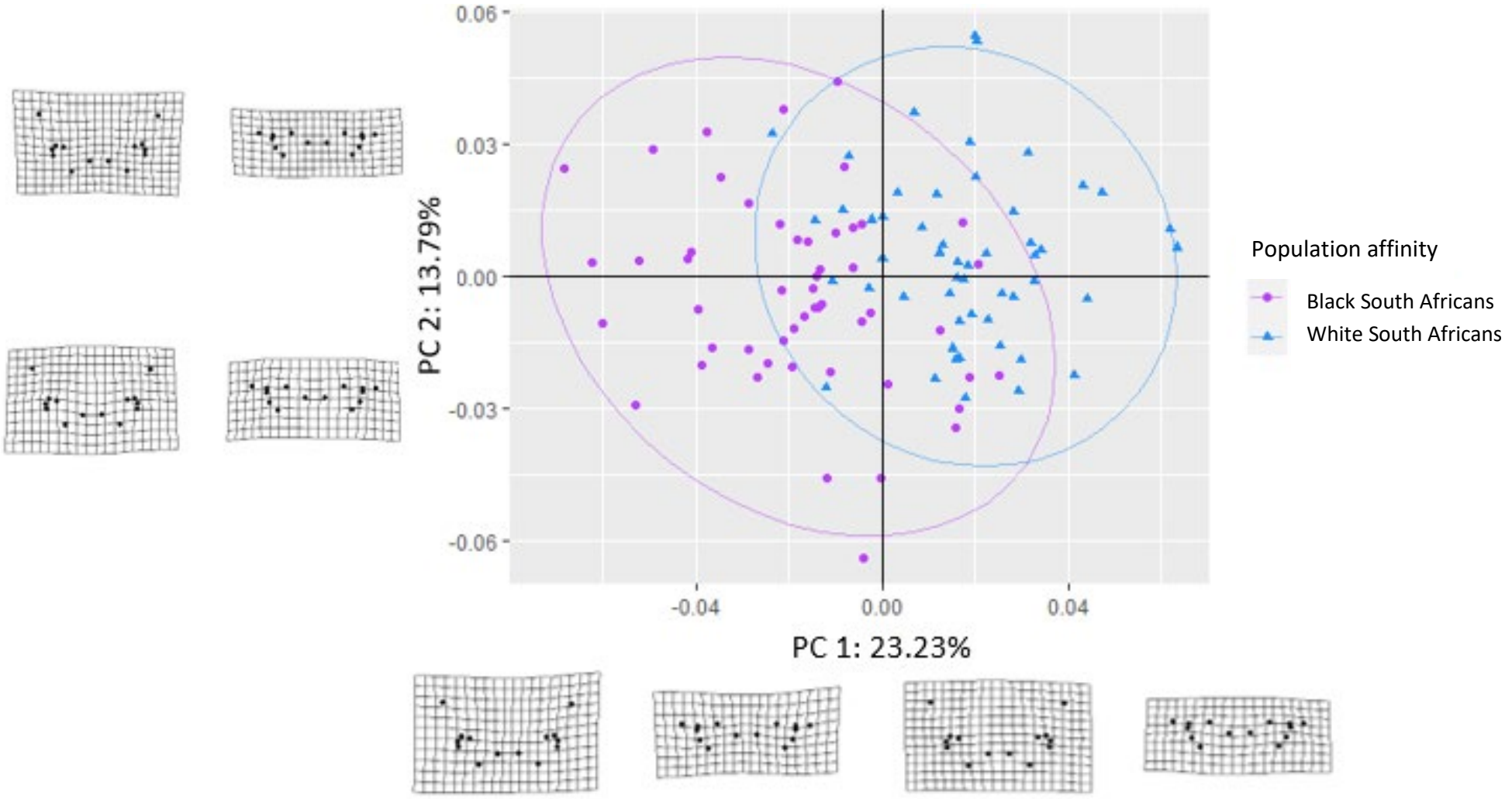

Figure 4.12. Scatterplot with corresponding deformation grids illustrating PC 1 against PC 2 of South African males indicating the effect of population affinity on the position of the 14 landmarks located on the orbital region

© University of Pretoria

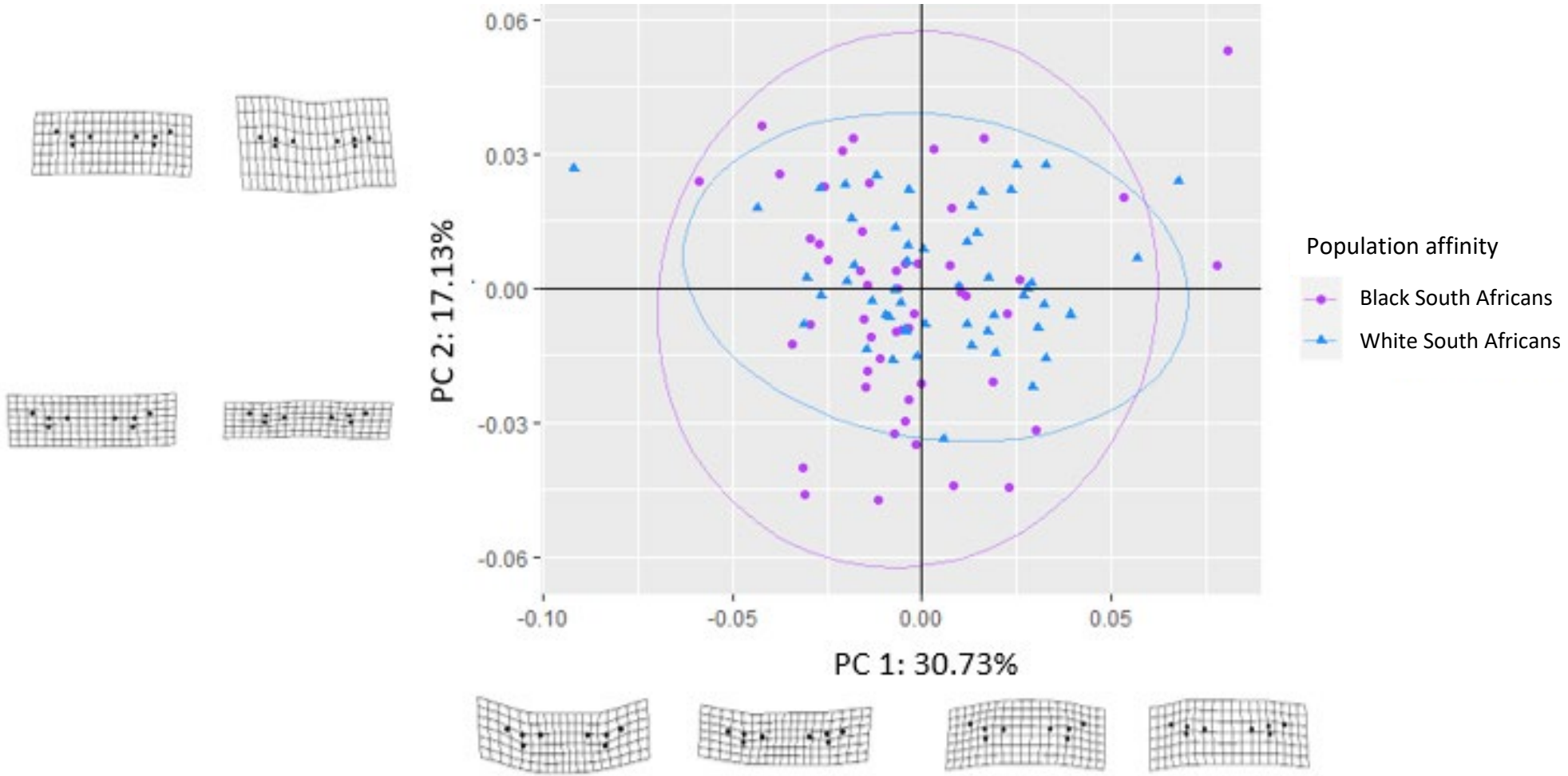

Figure 4.13. Scatterplot with corresponding deformation grids illustrating PC 1 against PC 2 of South African males indicating the effect of population affinity on the position of the 8 landmarks located on the palpebral fissures

© University of Pretoria

*Population*Females*

A statistically significant variation in the shape of the orbital region was noted between white and black South African females based on parametric and non-parametric tests. Classification accuracy based on orbital shape was 85.29 %, which increased from 81.07 % for the complete sample (*Table 4.21*). *Figure 4.14* illustrates the shape differences observed between South African females. As black South African females leaned towards a more positive PC 1 (responsible for 23.23 % of variation), the largest shape variation noted was a smaller orbital height and a more medial position of the supraconchion in this group.

The shape of the palpebral fissure also varied significantly between the South African female groups, with a DFA of 66.29 % (*Table 4.22*) and a greater overlap in the PC 1 (27.01 %) and PC 2 (17.18 %) graph (*Figure 4.15*). The most significant variation in palpebral fissure shape, as shown in *Figure 4.15*, was observed among black South African females compared to white South African females. Black South African females had smaller palpebral fissures, whereas white South African females exhibited a more superiolaterally slanted palpebral fissure.

© University of Pretoria

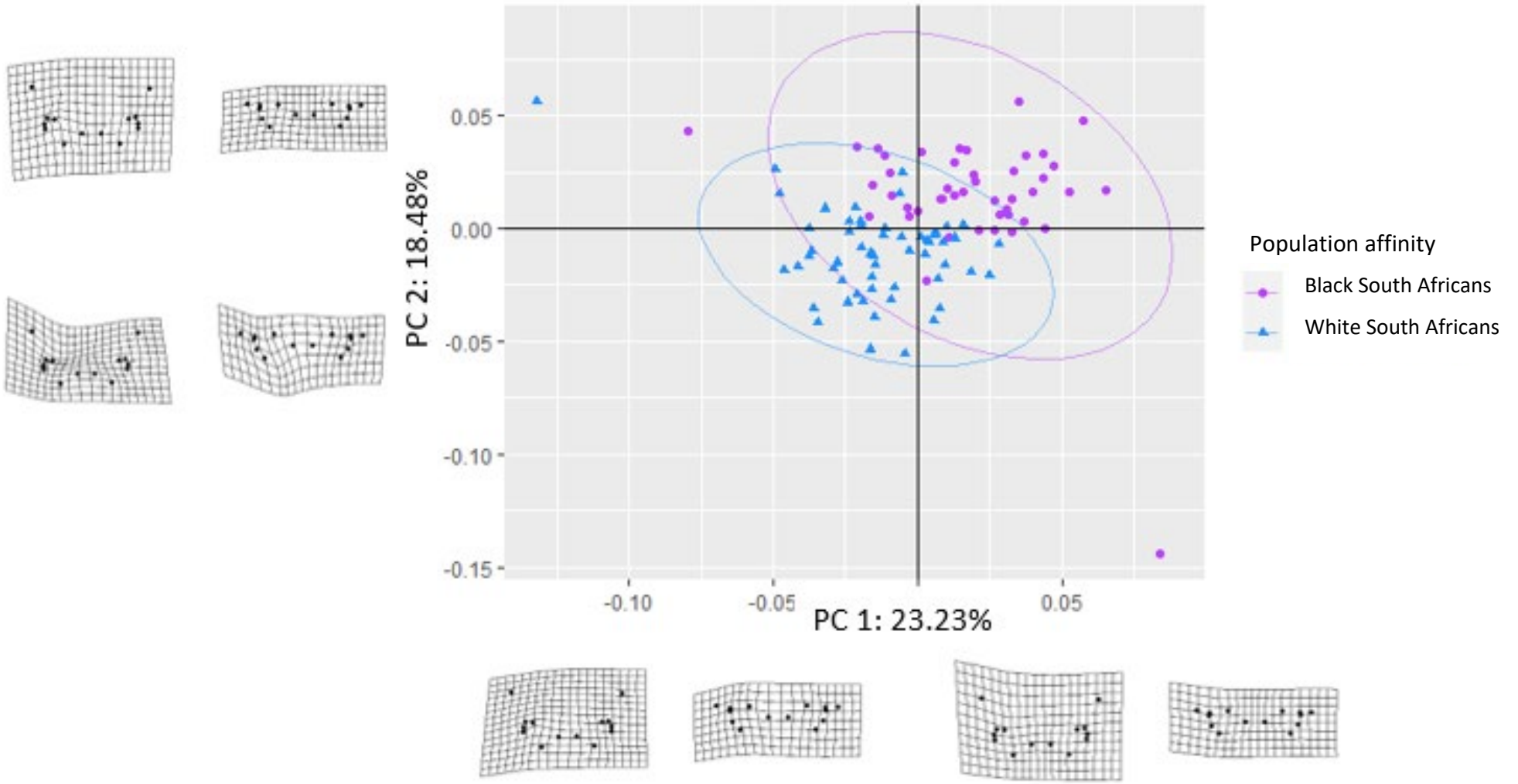

Figure 4.14. Scatterplot with corresponding deformation grids illustrating PC 1 against PC 2 of South African females indicating the effect of population affinity on the position of the 14 landmarks located on the orbital region

© University of Pretoria

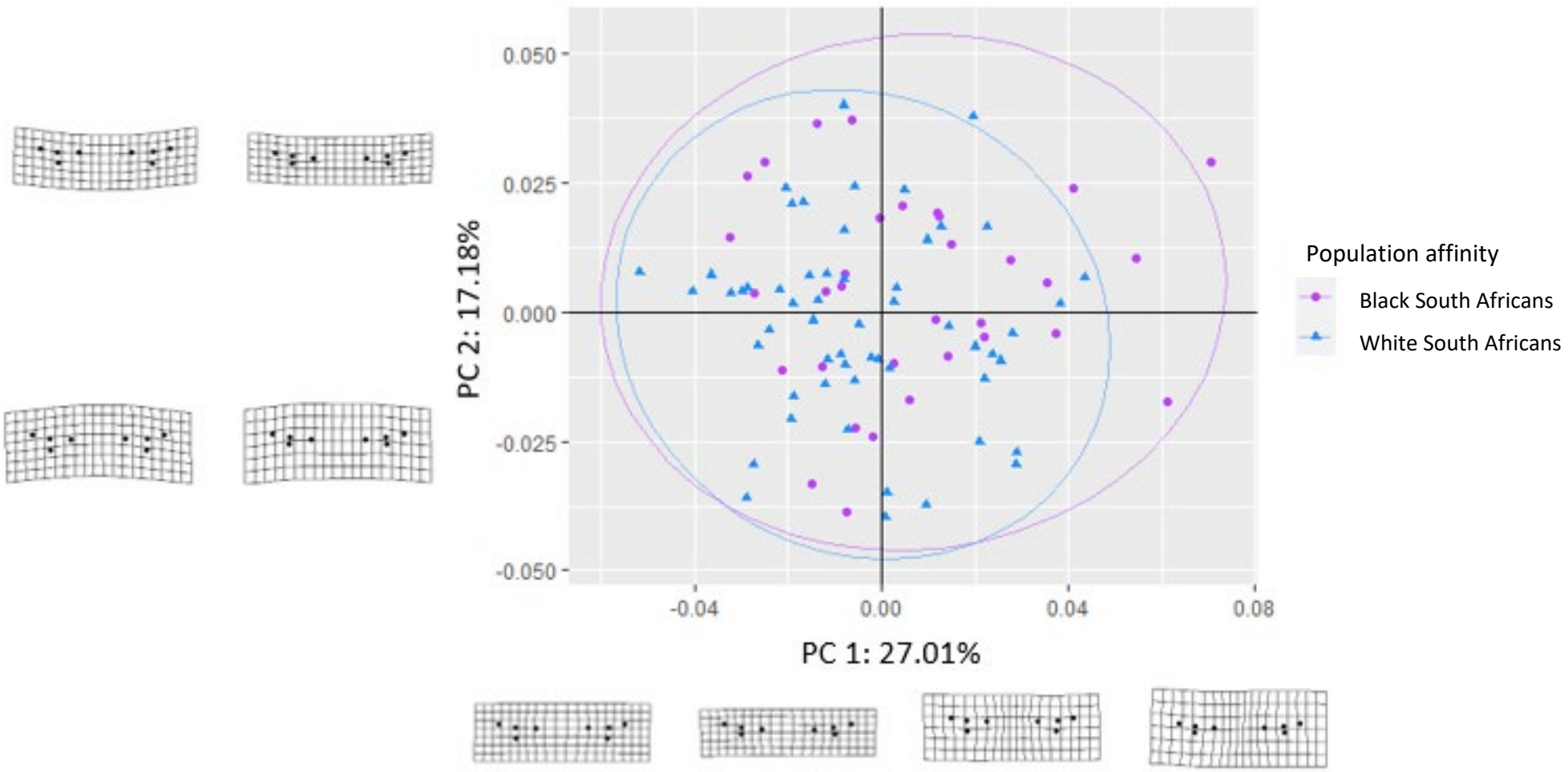

Figure 4.15. Scatterplot with corresponding deformation grids illustrating PC 1 against PC 2 of South African females indicating the effect of population affinity on the position of the 8 landmarks located on the palpebral fissures

© University of Pretoria

Sexual dimorphism

Sex did not have a significant influence on the shape of the bony orbit of the complete sample. Classification accuracy for sex based on orbital shape was much lower (54.85 %) compared to population affinity (*Table 4.21*). Shape deformations are presented in *Figure 4.16*, with PC 1 responsible for 20.56 % of variation and PC 2, for 13.93 %. Greater variation was noted in the South African female sample across PC 1 and PC 2. The maximum shape shows an increase in the distance between the zygions as well as an increase in orbital breadth.

Sexual dimorphism in the shape of the palpebral fissure was observed across the entire sample, with a classification accuracy of 60.10 % (*Table 4.22*). *Figure 4.17* illustrates the minimum and maximum shape variations of the palpebral fissure. Principal Component 1 (PC 1) explained 27.40 % of the variation between sexes, and Principal Component 2 (PC 2) explained 16.48 %. Males showed greater variation along PC 1, which primarily reflects differences in the width of the palpebral fissure.

© University of Pretoria

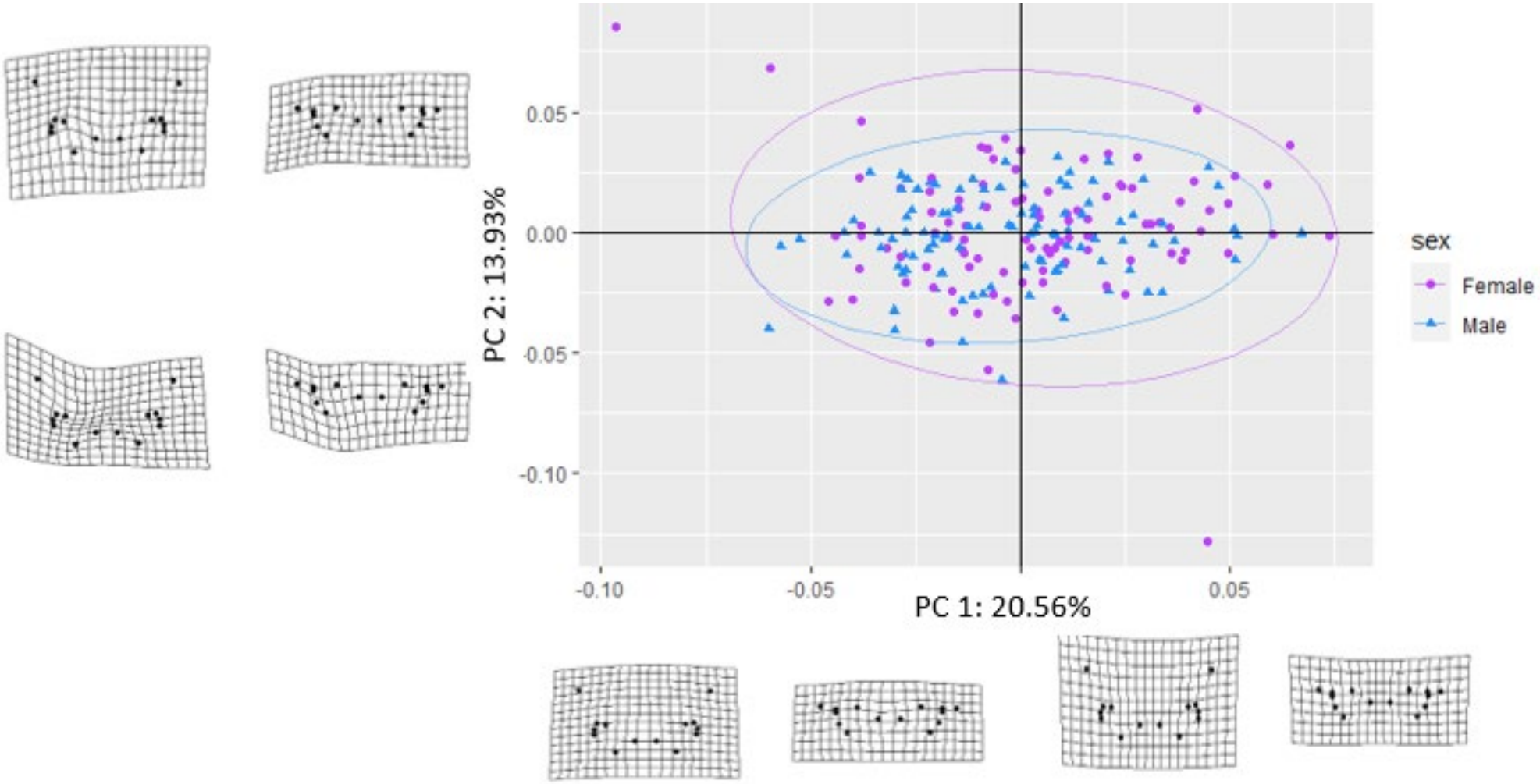

Figure 4.16. Scatterplot with corresponding deformation grids illustrating PC 1 against PC 2 of the complete sample indicating the effect of sex on the position of the 14 landmarks located on the orbital region

© University of Pretoria

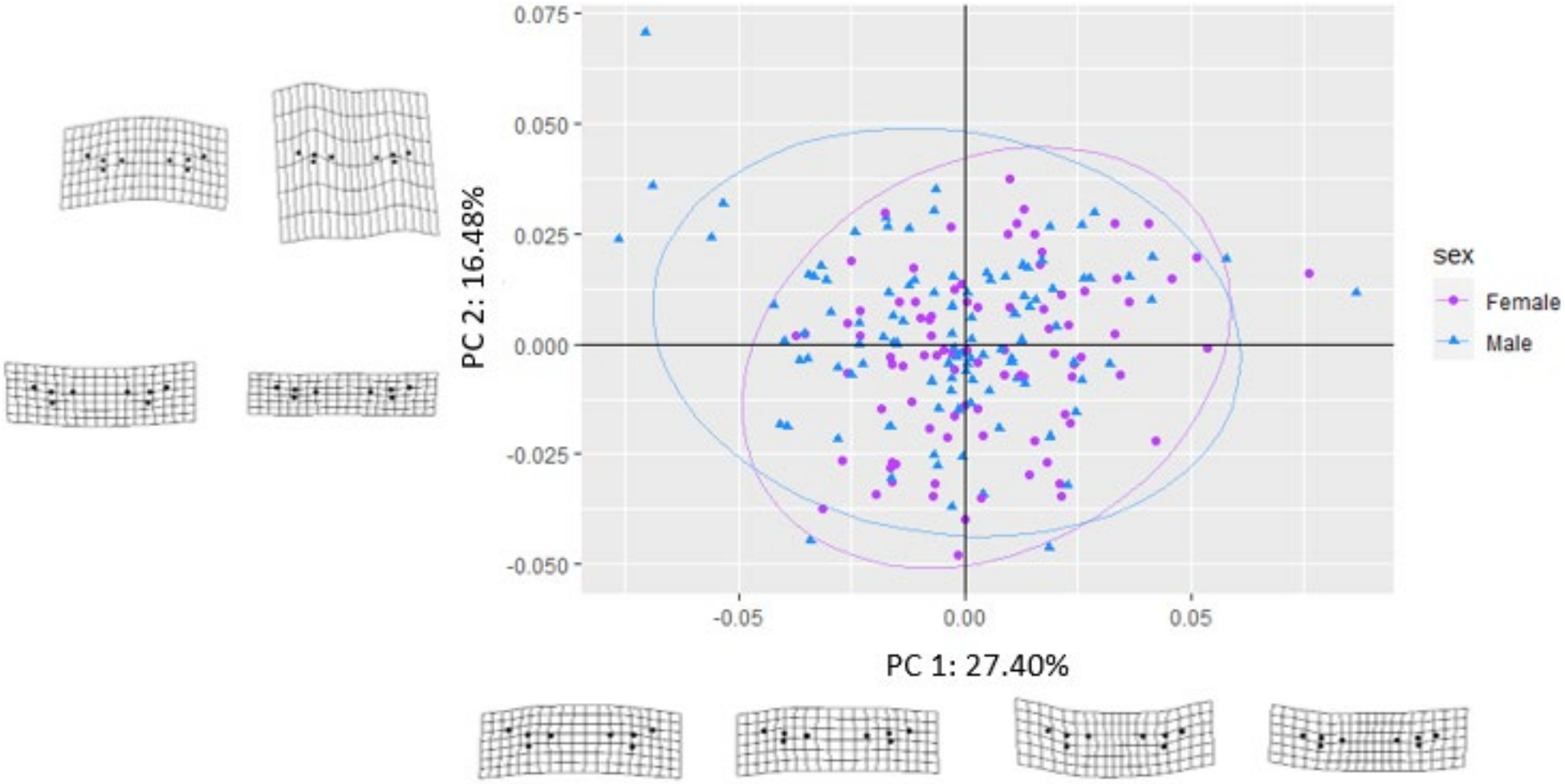

Figure 4.17. Scatterplot with corresponding deformation grids illustrating PC 1 against PC 2 of the complete sample indicating the effect of sex on the position of the 8 landmarks located on the palpebral fissures

© University of Pretoria

*Sex*White South African*

Sex significantly influences the shape of the orbit in white South Africans. When population affinity is known, the classification accuracy for sex increases significantly to 84.40 % (*Table 4.21*). Principal Component 1 (PC 1) explains 19.45 % of the variation, and Principal Component 2 (PC 2) explains 14.28 %, showing a slight overlap between sexes. Females exhibit greater variation along PC 1 and have a more positively loaded PC 2, whereas males display a neutral PC 1 and a more negatively loaded PC 2 (*Figure 4.18*). The most notable variation between the maximum and minimum shapes of the orbital region occurs in the lateral movement of the zygions, leading to a wider facial breadth. Additionally, the supraconchion and orbitale diverge, increasing the orbital height in white South African females.

Sex did not influence the shape of the palpebral fissure in white South Africans as the PC graph (*Figure 4.19*) illustrates overlap and little variation in the palpebral fissure shape of white South Africans. A DFA of 58.33 % (*Table 4.22*) was achieved for this group. The slight differences noted in the shape of the palpebral fissure included a slightly narrower palpebral fissure observed in white females and a more obtuse lateral angle at the exocanthion as this landmark is located more posterolateral in white South African males.

© University of Pretoria

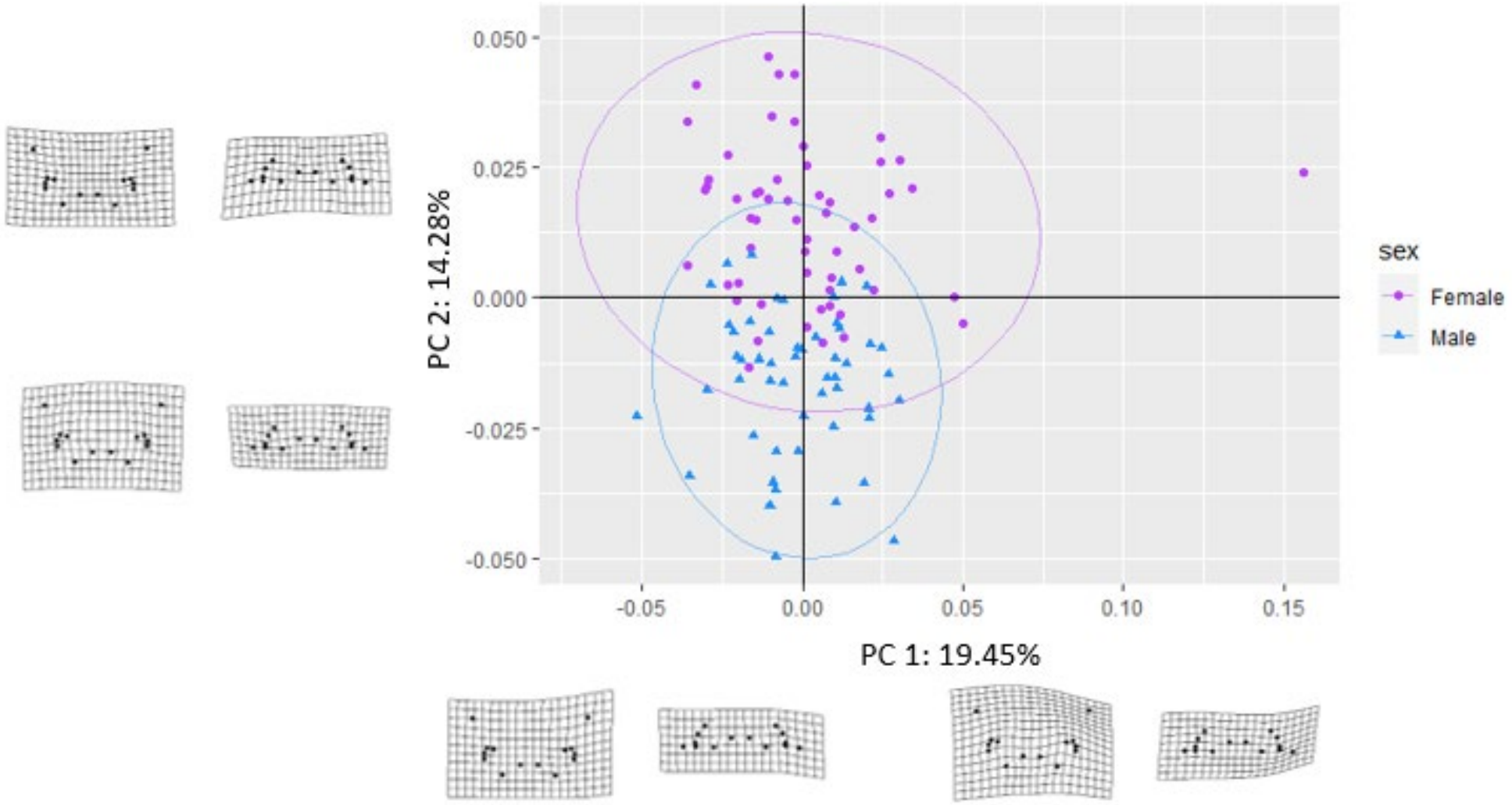

Figure 4.18. Scatterplot with corresponding deformation grids illustrating PC 1 against PC 2 of white South Africans indicating the effect of sexual dimorphism on the position of the 14 craniometric landmarks

© University of Pretoria

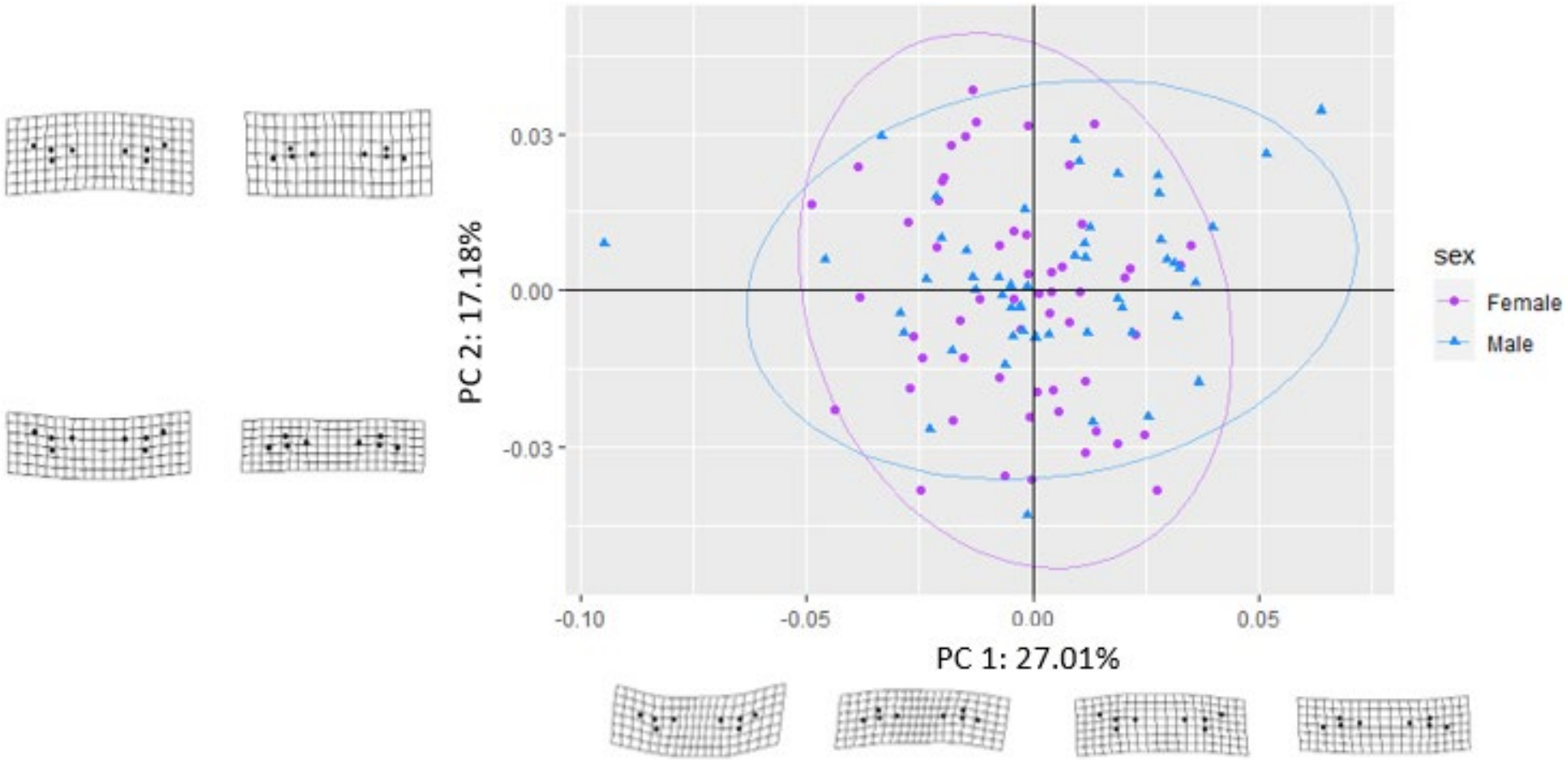

Figure 4.19. Scatterplot with corresponding deformation grids illustrating PC 1 against PC 2 of white South Africans indicating the effect of sexual dimorphism on the position of the 8 cephalometric landmarks

© University of Pretoria

*Sex*Black South African*

When testing the effect of sex on the orbital shape in black South Africans, the MANOVA and 50-50 MANOVA tests indicated no statistical significance (*Table 4.21*). The classification accuracy for sex within the black South African sample was 61.86 %. *Figure 4.20* shows the shape deformations for the minimum and maximum PC scores, with PC 1 accounting for 19.69% of the variation and PC 2 for 16.29 %. Black South African females exhibited greater shape variation in the orbital region compared to males. Sex influenced the depth of the curve along the lateral orbital margin and the orbital height.

Variation of palpebral fissure shape was statistically significant between the sexes in black South Africans (*Table 4.22*) with a DFA of 63.53 %. PC 1 accounted for 27.28 % of variation and PC 2 for 18.33 % (*Figure 4.21*). The sample was more widely spread across PC 1 and PC 2 was noted in the black male sample indicating greater shape variation in this group. The shape deformations indicate that the most significant variation between sexes within the black South African population is in the slant of the palpebral fissure. In females, the exocanthion is positioned more superiorly, while males tend to have a wider palpebral fissure.

© University of Pretoria

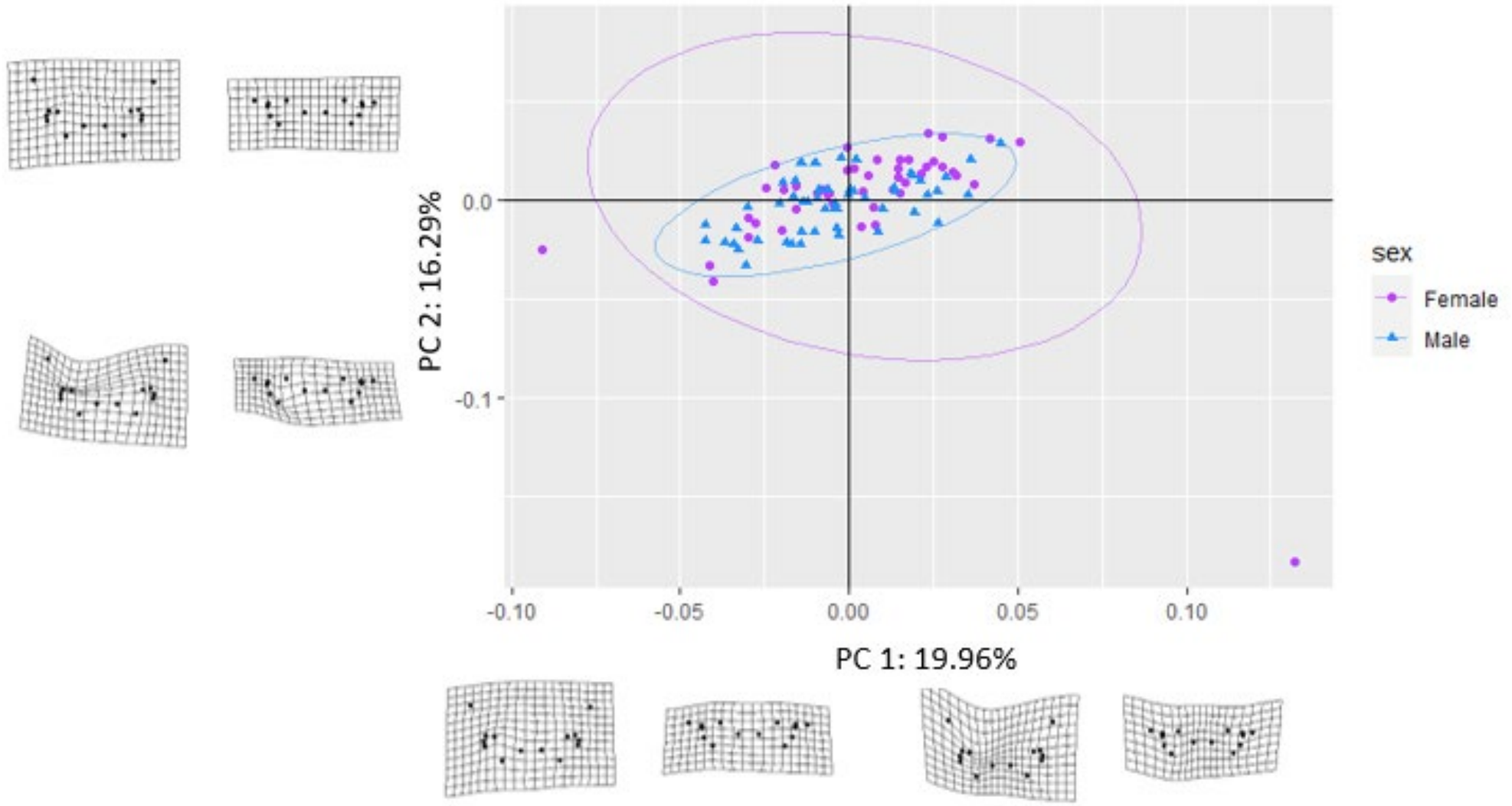

Figure 4.20. Scatterplot with corresponding deformation grids illustrating PC 1 against PC 2 of black South Africans indicating the effect of sexual dimorphism on the position of the 14 craniometric landmarks

© University of Pretoria

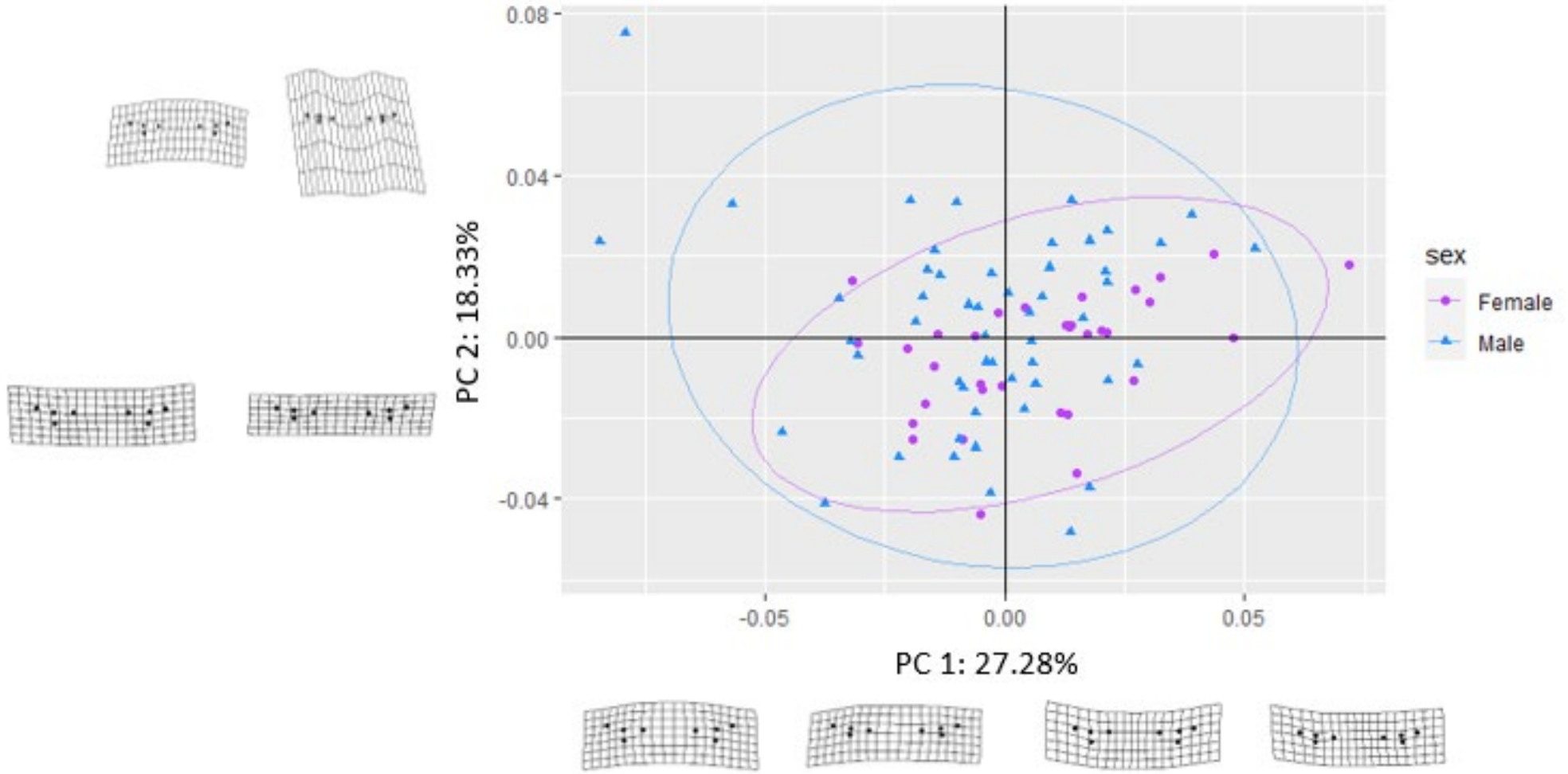

Figure 4.21. Scatterplot with corresponding deformation grids illustrating PC 1 against PC 2 of black South Africans indicating the effect of sexual dimorphism on the position of the 8 cephalometric landmarks

© University of Pretoria

4.2 Part 2: Eyelid approximation from automatic landmarks

In order to predict the soft tissue shape of the palpebral fissure from the underlying bony tissue, variance in the shape of the orbital region and palpebral fissure was determined based on automatically projected landmarks.

4.2.1 Reproducibility testing

A mean dispersion analysis was performed on the data to determine the average reproducibility of the craniometric and cephalometric landmark placement (*Table 4.23*). The landmarks with the highest accuracy by both observers include the supraconchion, dacryon, zygion and seven of the eight landmarks placed on the palpebral fissures. The landmarks with the highest mean dispersion were the orbitale, ectoconchion, left frontomolare-orbitale, left deepest point on the lateral orbital margin and left palpebrale inferius. Although these landmarks presented with greater dispersion values, it was still consistently below 1.50 mm. The only landmark with a dispersion value above 2 mm was the left frontomolare-orbitale, placed by the inter-observer. Average dispersion error for all soft and hard-tissue landmarks for both observers were below 1.10 mm (*Table 4.23*).

Table 4.23 Mean dispersion analysis of the intra- and inter-observer repeatability

			Intra-observer	Inter-observer
Craniometric	Landmark	Abbrv.	Observer error (mm)	
	Supraconchion	sk	L: 0.51	L: 0.77
			R: 0.56	R:0.44
	Orbitale	or	L: 0.85	L: 2.27
			R: 1.12	R: 1.44
	Dacryon	d	L: 0.47	L: 1.05
			R: 0.61	R: 0.54
	Ectoconchion	ek	L: 0.81	L: 1.29
			R: 1.29	R: 1.60
	Frontomolare orbitale	fmo	L: 0.44	L: 2.240
			R: 0.69	R: 0.43
	The deepest point on lateral orbital margin	dLOM	L: 0.73	L: 1.27
			R: 0.49	R: 0.76
	Zygion	zy	L: 0.51	L: 0.77
			R: 0.56	R:0.44
Mean observer error			0.69 ± 0.25	1.09 ± 0.60
Capulometric				
	Endocanthion	en’	L: 0.79	L: 0.42
			R: 0.66	R: 0.66
	Exocanthion	ex’	L: 0.42	L: 0.16
			R: 0.53	R: 0.58
	Palpebrale superius	ps’	L: 0.66	L: 0.32
			R: 0.68	R: 0.33
	Palpebrale inferius	pi’	L: 1.38	L: 0.40
			R: 0.24	R: 0.48
Mean observer error			0.67 ± 0.31	0.42 ± 0.15

© University of Pretoria

4.2.2 Multivariate normality testing

Q-Q plots (Scrucca, 2000) were used to visually assess the distribution of the data according to population groups, sex groups and sex-population groups. The graph illustrates the actual values of squared Mahalanobis distances (circles) plotted against those of an ideal multivariate normal distribution (solid line). The closer the Mahalanobis distances are to the diagonal line, the more normal the distribution of the data is.

Concerning population variation, *Figure 4.22* presents a Q-Q plot comparing Mahalanobis distances expected in ideally normally distributed data with those computed from this sample. The hard-tissue data followed the diagonal line, with slight deviation at the tail end. The soft-tissue data were right or positively skewed. The effect of sexual dimorphism within population groups was also investigated. The distribution of these data sets can be observed in Annexure D.

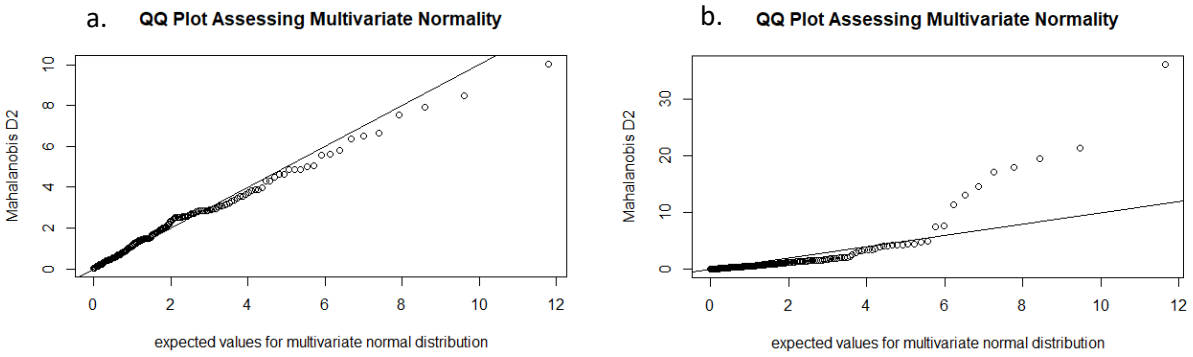

Figure 4.22. Q-Q-plots of the residuals of the linear model a) hard-tissue shape against population, b) soft-tissue shape against population

The effect of sex on the shape of the orbit and palpebral fissures based on the automatic landmarking procedure was also investigated. Concerning the effect of sexual dimorphism on the shape of the orbit and palpebral fissure, the Q-Q plots of Mahalanobis distances expected in perfectly normal distributed data versus those calculated from the sample, indicated a slight right deviation in the tail end of the hard-tissue components, while the soft-tissue components followed a normal distribution with a positive deviation from the norm in the tail end (*Figure 4.23*). The effect of population affinity within sex groups was also investigated. The distribution of these data sets can be observed in Annexure D.

© University of Pretoria

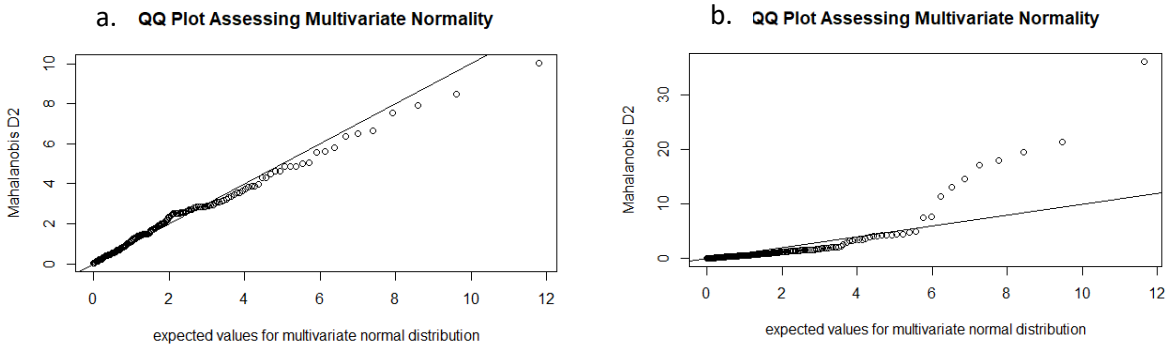

Figure 4.23. Q-Q-plots of the residuals of the linear model a) hard-tissue shape against sex, b) soft-tissue shape against sex

Due to some configurations indicating a slight to moderate deviation from the norm, parametric and non-parametric tests were applied to test the significance of the variation between groups.

4.2.3 Shape analysis: Based on automatically placed landmarks

The shape of the orbital region is significantly influenced by population affinity and presented with a classification accuracy of 92.94 % (*Table 4.24*). PC 1 accounted for 27.88 % of the variance while PC 2 accounted for 17.78 %. However, sex did not significantly influence the shape of the orbital rim and had a classification accuracy of 54.34 %. With known sex, classification accuracy for population affinity increased to 94.60 % in males and 96.39 % in females, respectively. A better separation was noted in the PC graphs with known sex. When the influence of sex was investigated with known population, classification accuracy decreased in white South Africans. Although PC 1 and PC 2 accounted for 44.28 % of variation between sexes in the white South African sample, a great overlap was noted. On the other hand, classification accuracy increased for sex with known population affinity in black South Africans (*Table 4.24*).

Table 4.24 Shape analysis results for craniometric landmarks.

	MANOVA	50-50 MANOVA	PERMUTATION	DFA
Population affinity	**0.00**	**0.00**	**0.00**	92.94
Pop*males	**0.00**	**0.00**	**0.00**	94.06
Pop*females	**0.00**	**0.00**	**0.00**	96.39
Sex	0.44	0.34	0.55	54.34
Sex*white	0.91	0.90	0.78	48.54
Sex*black	0.33	0.33	0.33	59.26

Significant p values ($p \leq 0.05$) are indicated in bold.

Population affinity and sexual dimorphism did not significantly influence the shape of the palpebral fissures when South Africans were considered as a single group (Table 4.25). However, a significant difference in palpebral fissure shape was found between population

© University of Pretoria

groups within specific sex groups. With known sex, the classification accuracy for population affinity increased to 66.67 % for males and 72.72 % for females (Table 4.25). The classification accuracy for population affinity was 66.67 % for South African males and 72.72 % for females. The PC graph indicated greater variation in the female group, leading to higher classification accuracy. A significant difference in palpebral fissure shape was observed only in the white South African sample, where individuals could be correctly classified by sex with 65.30 % accuracy.

Table 4.25 Shape analysis results for cephalometric landmarks.

	MANOVA	50-50 MANOVA	PERMUTATION	DFA
Population affinity	0.34	0.38	**0.01**	58.82
Pop*males	**0.03**	**0.01**	**0.01**	66.67
Pop*females	**0.05**	**0.03**	**0.00**	72.72
Sex	0.20	0.16	**0.02**	57.06
Sex*white	**0.02**	**0.02**	**0.00**	65.30
Sex*black	0.14	0.09	0.07	62.50

Significant p values ($p \leq 0.05$) are indicated in bold.

4.2.4 Soft-tissue prediction

The predictive performance of the PLSR models in predicting cephalometric landmarks for the entire sample are summarised in *Table 4.26*. The relationship with underlying craniometric landmarks resulted in prediction errors of 1.72 mm for the trained data (PE) and 1.63 mm for the untrained data (PE_cv). Surprisingly, the prediction errors for population affinity and sex based on the training data were 1.49 mm and 2.62 mm, respectively. However, during cross-validation testing, similar or slightly smaller errors were obtained. Notably, the male and female subgroups exhibited smaller prediction errors compared to the combined sex group.

© University of Pretoria

Table 4.26 Prediction errors (mm) of the predicted cephalometric landmarks according to population, sex and within sex groups, based on 187 individuals, based on trained and non-trained data.

Landmarks	Plain		Population		Sex		Sex: Female		Sex: Male	
	PE	PE_CV	PE	PE_CV	PE	PE_CV	PE	PE_CV	PE	PE_CV
Endocanthion L	1.77	1.66	1.66	1.55	2.98	2.98	2.48	2.54	2.29	2.54
Exocanthion L	1.72	1.67	1.65	1.61	2.46	2.46	2.37	2.02	2.17	2.05
Palpebrale superius L	1.74	1.63	1.78	1.70	2.74	2.74	2.45	2.30	2.23	2.11
Palpebrale inferius L	1.70	1.54	1.49	1.15	2.37	2.37	2.38	1.93	2.19	2.07
Endocanthion R	1.75	1.65	1.54	1.48	2.79	2.79	2.45	2.34	2.26	2.14
Exocanthion R	1.66	1.55	1.41	1.32	2.33	2.33	2.30	1.88	2.13	2.01
Palpebrale superius R	1.72	1.68	1.18	1.70	2.78	2.78	2.45	2.34	2.26	2.14
Palpebrale inferius R	1.71	1.63	1.17	1.06	2.48	2.48	2.44	2.04	2.26	2.13
RMSEP	1.72	1.63	1.49	1.45	2.62	2.62	2.42	2.17	2.23	2.15

Incorporating both populations as a factor, the prediction errors exhibited a wider range, varying from 2.13 to 2.45 mm for the trained data and from 2.07 to 2.33 mm for the untrained data (refer to *Table 4.27*). Notably, the exocanthion demonstrated the smallest prediction error in both white and black South African females, while the palpebrale superius exhibited the smallest prediction error in white and black South African males. Comparatively, black South Africans displayed a slightly higher prediction error (2.45 mm for trained data and 2.33 mm for non-trained data) than white South Africans (2.19 mm for trained data and 2.07 mm for non-trained data). Moreover, when sex and population affinity were combined as factors in predicting the palpebral fissure based on the underlying hard-tissue structure, black South African males showed the smallest prediction error.

© University of Pretoria

Table 4.27 Prediction errors (mm) of the predicted cephalometric landmarks according to population group and sex-population groups, based on 187 individuals, based on trained and non-trained data.

Landmarks	White South Africans		White SA females		White SA males		Black South Africans		Black SA females		Black SA males	
	PE	PE_CV	PE	PE_CV	PE	PE_CV	PE	PE_CV	PE	PE_CV	PE	PE_CV
Endocanthion L	2.27	2.14	3.76	3.64	3.45	3.64	2.54	2.42	5.89	5.74	3.43	3.31
Exocanthion L	2.15	2.02	3.54	3.42	3.79	3.42	2.40	2.28	5.46	5.21	3.25	3.13
Palpebrale superius L	2.20	2.08	3.51	3.39	3.16	3.39	2.49	2.37	5.92	5.87	3.19	3.07
Palpebrale inferius L	2.17	2.04	3.56	3.44	3.95	3.44	2.41	2.28	5.56	5.37	3.21	3.09
Endocanthion R	2.23	2.11	3.61	3.49	3.15	3.49	2.50	2.38	5.87	5.70	3.28	3.16
Exocanthion R	2.10	1.98	3.23	3.10	3.78	3.10	2.32	2.20	5.18	4.96	2.99	2.87
Palpebrale superius R	2.23	2.11	3.41	3.29	3.15	3.29	2.49	2.36	5.86	5.36	3.13	3.00
Palpebrale inferius R	2.23	2.10	3.53	3.41	3.89	3.41	2.49	2.37	5.54	5.33	3.21	3.09
RMSEP	2.19	2.07	3.52	3.40	3.49	3.40	2.45	2.33	5.68	5.44	3.21	3.09

© University of Pretoria

5. Chapter 5: Discussion

Accurate placement of the eyeballs and reconstruction of the periorbital structures are crucial in facial approximations for victim identification (Stephan and Davidson, 2008; Frowd et al., 2011; Davy-Jow, 2013). This project aimed to develop guidelines to assist in the facial approximation process of South Africans, specifically focusing on the eyeball and periorbital regions. Currently, in the absence of population-specific guidelines to approximate the orbital region of South Africans, a standard-sized eyeball with a diameter of 25 mm is used in facial approximations, and the eyelids are reconstructed using a standardised method, without considering the influence of sex and population affinity (Wilkinson, 2010; İşcan and Steyn, 2013; Gupta et al., 2015). In 3D computer-generated facial approximations, the face is typically created with closed eyes. To depict the open eye, eyeballs are selected from a database to match the dimensions of the closed eyes, resulting in a subjective approximation (Vanezis et al., 2000; Gupta et al., 2015; Guleria et al., 2023).

This study established guidelines for facial approximations by determining the normative 2D (linear) and 3D (shape) dimensions of the orbit, palpebral fissure, and eyeball. It also assessed the depth at which the eyeball is positioned within the orbit and its projection from the orbital rim. To define the interrelationships between the eyeball dimensions, eyeball position and the palpebral fissure dimensions versus the orbital dimensions as proportions, the calculated linear distances of the eye and palpebral fissure were converted to percentages of orbital height (OH) or orbital breadth (OB). In addition, correlations were performed by linear regression based on these linear dimensions to develop predictive equations for eyeball positioning as well as eyeball and palpebral fissure approximations. Despite the weak correlations found between the linear dimensions of the orbit (hard-tissues) and the orbital structures (soft-tissues), the regression models as well as the proportionality methods produced predictions that approximated the observed values without considering sex or population affinity. It is therefore anticipated, that the resulting normative values will be useful in the Virtual Sculpture method (Wilkinson, 2003), currently employed by the South African Police Service (SAPS). While the proportions and predictive equations are expected to deliver accurate results, further consideration is necessary as explored later in this chapter.

The classification accuracies for sex and population affinity of the orbital 2D (linear) and 3D (shape) dimensions were determined by discriminant function analyses. It was found that classification of the orbital region in South Africans according to sex increased greatly when population group was taken into consideration. The orbital region could be useful for biological profiling in the forensic anthropological context when considered along with other markers.

© University of Pretoria

Furthermore, this study explored the correlation between the hard- and soft-tissue shapes of the orbital region to predict the open eye from the underlying hard-tissue using statistical models, to facilitate automatic, objective facial approximations for both white and black South African males and females. However, the prediction accuracy improved when population affinity was added as factor.

5.1 Part 1: Guidelines based on manually placed landmarks

Guidelines for the approximation of the eyeball and periorbital regions based on linear and shape dimensions were derived from manually placed landmarks. Linear dimensions and shape of the cranium, specifically the orbital region, vary between population groups and sexes (Graw et al., 1999; Pretorius et al., 2006; Bigoni et al., 2010; Gonzalez et al., 2011; Franklin et al., 2012; Xing et al., 2013; Stull et al., 2014; Bejdová et al., 2018; Rubin et al., 2017; Milella et al., 2021; Toneva et al., 2022; Ajanović et al., 2023; Prevost et al., 2023). The noted sex variations are often due to size differences rather than shape variations (Abdel Fatah et al., 2014; Musilová et al., 2016; Toneva et al., 2022), while population variation more often involves the shape or the relationships between the linear dimensions reflecting shape in some way (Jagesur, 2022). On the other hand, shape variation has been noted to be influenced by size (Bejdová et al., 2018; Chovalopoulou and Bertsatos, 2018). As 3D shape data contains more information than 2D linear data, it is important to also study the variations between shapes when exploring the variations between groups. In the current study, shape variation of the orbits and palpebral fissures based on the manually placed landmarks was investigated by making use of GMM in order to comment on the effect of population affinity and sex on the variance in shape without the effect of size.

To ensure that the created guidelines will produce reliable results beyond this project, rigid reproducibility testing was performed on the manually placed 3D landmarks as well as the distances mathematically derived from them and found acceptable. Landmarks placed on the orbital rim and palpebral fissure achieved high repeatability due to their precise definition, which was reflected in the linear dimensions calculated using these landmarks. Conversely, landmarks placed on the eyeball, which are classified as type 3 landmarks (Bookstein, 1991), were more challenging. Casselman et al. (2013) noted the difficulty in the visualisation of soft-tissue on 2D CBCT slices as noted in defining the eyeball outline in this study. However, as patients with open eyeballs were used in this study, the oculus anterius could be accurately placed in the sagittal view.

© University of Pretoria

5.1.1 Variations in the linear distances

The linear dimensions utilised in formulating guidelines, (dimensions of the orbit, eyeball, and palpebral fissure, along with measurements reflecting the positioning of the eyeball within the orbit) demonstrated unique population and population-dependent sex variations. Notably, in terms of orbital dimensions, white males exhibited the largest measurements, a finding consistent with their tendency to possess larger cranial dimensions compared to other sex-population groups (L' Abbé et al., 2013; Krüger et al., 2015; Jagesur, 2022). The significantly greater interorbital distance in black South Africans was not unexpected because of the wider nasal bridge previously described in the black South African population (Ridel et al., 2018). White South African females presented with greater orbital indices (a more square-shaped orbit), due to a relatively greater orbital height as compared to the more rectangular orbit in other South African groups. Reciprocating the orbital dimensions, the ocular dimensions did not differ significantly from males, within the white population, resulting in relatively larger eyeballs when considering the generally smaller dimensions in females. The reason for the sex differences in white South Africans is unknown, but might simply be a way to ensure that optical refraction is maintained. This was not the case for black females in whom all ocular dimensions were significantly smaller than in other groups.

The differences in the normative dimensions of the orbit and eyeball between black and white South Africans leads to variation in the eyeball's position within the bony orbit. In white females, the distance from the superior orbital margin (supraconchion) to the equator of the eyeball is larger than black females, indicating that the eyeball is positioned further from the superior orbital margin. This was expected as white females presented with significantly greater orbital heights. White South African males have greater orbital breadths, and because their ocular dimensions are similar to those of black South African males, there is a larger space between the equator of the eyeball and both the lateral orbital margin (ectoconchion) and the medial orbital margin (dacryon). This spacing should be considered during facial approximations for this group.

Black South African females presented with more protruding eyeballs in the vertical and horizontal planes when compared to white South African females. Increased distances were noted from the orbital walls to the oculus anterius in this group, regardless of the significantly smaller orbital and ocular dimensions noted in black South African females. These findings support the shallower position of the eyeball in relation to the superior orbital margin as discussed before. Less variation was noted in protrusion values between South African males, although the eye protruded more from the superior orbital margin supraconchion in black South African males.

© University of Pretoria

Although the width of the palpebral fissure significantly differed between the South African populations investigated, the palpebral fissure height was not influenced by sex or population affinity. Similar observations were noted by Barretto and Mathog (1999) who found significant variation in eyeball protrusion between white and black Americans, but no variation in the palpebral fissure height. Farkas and colleagues (2007) investigated the effect of age, sex and population affinity on the dimensions of the palpebral fissure and similarly reported no significant differences between white and black Americans.

The linear distances recorded in this study were compared to the published literature based on diverse population groups. The authors acknowledge that comparisons with the literature not only involve comparisons between population groups but also entail comparison between modalities used in the various studies reviewed, while differences in scan qualities, CBCT models and settings, software used and observer factors, e.g. differences in interpretations of landmarks and experience could also have influenced the data characteristics (Gaia et al., 2013; Kosalagood et al., 2015). In numerous instances, a BF far greater than 2 was noted (decisive BF), and population variation can be assumed.

In order to quantify the variation (BF) between South Africans and the linear dimensions of published literature of other population groups, data were grouped according to orbital dimensions, ocular dimensions, protrusion of the eye and palpebral fissure dimensions (Supplementary Table 1). By determining the BF, the substantial difference noted between the orbital heights of the white and black South African females of this study was strengthened by decisive evidence (BF= 11.83) that the orbital height of this white South African female sample varied with the black South African female sample of Dayal and colleagues (2008). In general, white South African females presented with similar or more often, greater orbital dimensions when compared to other groups. Similar orbital heights are reported in a Turkish sample (Özer et al., 2016) as well as in Korean (Kim et al., 2016) females, although the BF was weak. Greater orbital heights have been reported in white South Africans compared to white American, (Weaver et al., 2010), Chinese (Ji et al., 2010), French (Guyomarc'h et al., 2012), Korean (Shin et al., 2016) and Italian (Cappella et al., 2020) females, while the orbital breadth in white South African females is greater than Turkish (Özer et al., 2016), Egyptians (Attia et al., 2018), Korean (Kim et al., 2016; Shin et al., 2016), white American (Weaver et al., 2010), Chinese (Ji et al., 2010), French (Guyomarc'h et al., 2012), Iranian (Khani et al., 2023) and Italian (Cappella et al., 2020) females.

Although the comparisons of the findings of this study to existing literature highlight the variation among population groups regarding the dimensions of the orbital region, slightly more comparable dimensions were seen in black South African females than white South African

© University of Pretoria

females. The orbital height of black South African females is similar to those reported on Egyptians (Attia et al., 2018), French (Guyomarc'h et al., 2012), Iranians (Khani et al., 2023) and Koreans (Shin et al., 2016). However, decisive BF evidence shows significant variation in the orbital height of black South African females compared to Korean (Kim et al., 2016), white American (Weaver et al., 2010) and Chinese (Ji et al., 2010) females. Greater variation was noted in the orbital breadth of black South African females (strong to decisive BF evidence), as black South African females presented with wider orbits compared to Turkish (Özer et al., 2016), Egyptian (Attia et al., 2018), Korean (Kim et al., 2016; Shin et al., 2016), white American (Weaver et al., 2010), Chinese (Ji et al., 2010), French (Guyomarc'h et al., 2012), Iranian (Khani et al., 2023) and Italian (Cappella et al., 2020) females.

Weak BF evidence indicates no difference between the population means of the orbital breadth and height of South African males. Similar comparative results were noted as the orbital height resembled Turkish (Özer et al., 2016), Korean (Kim et al., 2016) and Iranian (Khani et al., 2023) males (substantial BF). Greater orbital heights and widths were recorded in South African males compared to white American (Weaver et al., 2010), Chinese (Ji et al., 2010), French (Guyomarc'h et al., 2012), Korean (Shin et al., 2016) and Italian (Cappella et al., 2020) males.

The findings of this study showed that the interorbital distance of black South Africans is significantly greater compared to white South Africans (supported by a decisive BF), while white South Africans presented with the smallest interorbital distance compared to the existing literature. However, similar interorbital distances compared to black South Africans have been recorded in Iranians (Khani et al., 2023) and Italians (Cappella et al., 2020), while even greater interorbital distances were noted in Chinese (Ji et al., 2010), Egyptians (Attia et al., 2018) and white Americans (Weaver et al., 2010), regardless of sex.

Bizygomatic breadth does not vary significantly between black and white South Africans. When the bizygomatic breadth of South Africans is compared to the literature, Egyptians (Attia et al., 2018; Celebi et al., 2018), Italians (Celebi et al., 2018) and Mexican Americans (Celebi et al., 2017) have narrower faces while African Americans (Farkas et al., 2007), North American whites (Farkas et al., 2007) and Colombians (Celebi et al., 2017) have wider faces compared to South Africans. The variation in the bizygomatic breadth between South Africans and Iranians was sex-specific, as Iranian males have similar bizygomatic breadths compared to South African males, while Iranian females have greater bizygomatic breadths compared to South African females (Byat et al., 2018).

All ocular dimensions differ between black and white South African females (substantial to decisive BF), while only the ocular height varied significantly between South African males

© University of Pretoria

(decisive BF). Ocular heights in both male and female white South Africans were greater than reported in most other studies and were surpassed only by the Korean sample (Shin et al., 2018). On the other hand, smaller ocular breadths compared to Koreans (Shin et al., 2018) and Australians (Rana et al., 2022) were noted in South Africans.

The axial length of the eye was significantly shorter in black South African females, and the significant BF suggests that it is also significantly shorter compared to Turkish (Özer et al., 2016), European (Wilkinson and Mautner, 2003), Australian (Rana et al., 2022) and Korean (Shin et al., 2018) females. Comparable axial lengths were noted between white South Africans and black South African males, Turkish (Özer et al., 2016) and Europeans (Wilkinson and Mautner, 2003), while Australians (Rana et al., 2022) and Koreans (Shin et al., 2018) have elongated eyeballs.

Due to the lower repeatability of the ocular position of the equator in relation to the orbital rim, and the lack of comparative literature, the protrusion of the eyeball from the orbital margin will be discussed. South Africans have very little variation in the ocular protrusion from the lateral orbital margin. Although black South African females presented with greater protrusion values of the eye in relation to the lateral orbital rim when compared to white South African females, the variation was not significant (BF reports weak evidence of no difference). South Africans however have the greatest ocular protrusion values from the lateral orbital wall, regardless of sex or population affinity, compared to the existing literature (Dunsky, 1992; Barretto and Mathog, 1999; Guyomarc'h et al., 2012; Kim et al., 2016). There is no difference in the protrusion values of the eye from the inferior orbital margin in South Africans, and these values are similar to the reported values of a French sample (Guoyomarc'h et al., 2012), but greater than the values of a Korean sample (Kim et al., 2016). Unfortunately, variations noted in the protrusion values of the eyeball from the lateral orbital margin cannot only be ascribed to population differences, as all studies utilized different modalities, such as CT scans and patients, as well as methodologies, as noted in the study performed by Kim and colleagues (2016).

Variation in the protrusion values from the medial orbital margin of South Africans were sex-specific, as differences were observed between males only (substantial BF). South African females have comparable protrusion values from the medial orbital margin compared to Korean females (Kim et al., 2016). The eye projects further from the superior orbital margin in black South Africans compared to white South Africans (strong to very strong BF) and even further when compared to a French sample (decisive BF). Similar protrusion values were reported in Koreans (Kim et al., 2016) which were slightly greater than white South Africans.

© University of Pretoria

The palpebral fissure dimensions varied significantly with the published data (Supplementary Table 1). The height of the palpebral fissure of South Africans is smaller compared to most other population groups identified in the literature, with black South African females presenting with the smallest palpebral fissure heights. The greatest similarity was noted between white South African females and white European (Kunjur et al., 2006), Indian (Kunjur et al., 2006), American (Price et al., 2009) and Korean (Song et al., 2007) females. No difference was noted between South African males (Substantial BF) who showed weak similarity to Chinese (Kunjur et al., 2006) and White American (Price et al., 2009) males. Iranians have the greatest palpebral fissure height, which is approximately 5 mm greater compared to South Africans. Apart from possible inter-populational variations, the modality used could be accountable, at least partly, for the smaller palpebral fissure distances noted in this study. The current study is the only using CBCT scans, while the other studies used either photos or patients who could have been instructed to look at a certain point and open their eyes. Using CBCTs when assessing palpebral fissure dimensions could be considered an inherent limitation in retrospectively collected scans and therefore the results on the palpebral fissure dimensions should be interpreted with caution and should be confirmed using photos or participants.

Similar to the palpebral fissure heights, our population presented with shorter palpebral fissure widths compared to the literature. The greatest similarity was noted when compared to white Europeans (Kunjur et al., 2006) and Chinese (Kunjur et al., 2006) samples. Sex and population-specific similarities were also noted (Supplementary Table 1).

The effect of sexual dimorphism on the dimensions of the orbit, eye, palpebral fissure and the position of the eyes in the orbit was investigated by studying sexual dimorphism reported in existing literature (Supplementary Table 2). In general, the horizontal or breadth dimensions measured in this study were sexually dimorphic and were greater in males compared to their female counterparts. The ocular dimensions were only sexually dimorphic in the black South African population with females presenting with significantly smaller eyes compared to their male counterparts.

In general, the horizontal or breadth dimensions measured in this study were sexually dimorphic and were greater in males compared to their female counterparts. The ocular dimensions were only sexually dimorphic in the black South African population with females presenting with significantly smaller eyeballs compared to their male counterparts.

A trend in the sexually dimorphic dimensions of the orbital region was found following a thorough review of the existing literature (Supplementary table 2). Orbital height is often not influenced by sex (Dayal et al., 2008; Özer et al., 2017), while orbital breadth commonly differs between sexes (Özer et al., 2017; Attia et al., 2018; Kim et al., 2016; Weaver et al., 2010. Ji

© University of Pretoria

et al., 2010., Guyomarc'h et al., 2012; Khani et al., 2023; Shin et al., 2016; Dayal et al., 2008; Cappella et al., 2020). Orbital height tends to be greater in males, although some exceptions have been reported in the literature (Shin et al., 2016; Attia et al., 2018; Cappella et al., 2020).

In general, males have bigger eyeballs compared to females, although it is not always significant in all planes. Besides the significantly smaller eyeballs noted in black South African females, Australian (Rana et al., 2022) and Korean (Shin et al., 2016) females have significantly shorter ocular axial lengths and ocular widths than their male counterparts. Uniquely, white South Africans have similar ocular dimensions between sexes.

As sexual differences exist in the orbital breadth and ocular width it is expected that the distance from the medial and lateral orbital margins to the oculus anterius would be greater in males compared to females. The results of this study as well as the existing literature support this argument, as the eyeball often protrudes further from the medial and lateral orbital margins as seen in white South Africans, French (Guyomarc'h 2012) and Black Americans (Dunsky, 1992; Barretto and Mathog, 1999). This should be taken into consideration during manual facial reconstructions.

Asymmetry was noted in this study. White South African males presented with the greatest extent of asymmetry, with greater dimensions commonly observed on the left. Asymmetry was noted in the orbital breadth, palpebral fissure width and the distance between the lateral orbital margin and the oculus laterale and oculus anterius, respectively. A possible explanation could be that white males in whom the greatest dimensions of all sex-population groups were reported, could also be more inclined to demonstrate asymmetry. The longer duration of puberty in males in general and in this case white males, producing larger measurements, could render them more vulnerable to factors associated with asymmetry. According to the literature, facial asymmetry has been linked to facial masculinity (Gangestad and Thornhill, 2003; Schlager 2013b). Extremely masculine or feminine faces exhibit greater asymmetry (Gangestad and Thornhill, 2003), which could be the case in the white South African male sample.

Greater asymmetry was recorded in the palpebral fissure dimensions of Korean females, compared to their male counterparts (Song et al., 2007), while very little asymmetry was recorded in the ocular and orbital dimensions of Turkish males and females (Özer et al., 2016). Asymmetry in the orbital breadth and position of the eyeball in relation to the medial orbital wall were documented in a French sample, although no differentiation was made between males and females (Guyomarch et al., 2012). No asymmetry was found in the orbital dimensions of Chinese or Egyptian samples (Ji et al., 2010; Attia et al., 2018).

© University of Pretoria

5.1.2 Approximation of the eyeball dimensions and position

As discussed in section 5.1.1, the dimensions of the orbit, eyeball, palpebral fissure, and eyeball position vary across individuals. These variations should be considered when approximating the orbital region. This study proposes the use of normative ocular dimensions as established for South Africans during facial approximations. Notably, black South African females have significantly smaller eyeballs, necessitating the use of group-specific eyeball sizes. An eyeball with the following dimensions should be considered: 21.98 mm x 22.44 mm x 23.77 mm. For white South Africans and black South African males, a standard-sized eyeball (± 23.14 mm x 23.34 mm x 24.6 mm) can likely be used due to the absence of significant size differences between these groups. As the dimensions of the eyeball could be predicted with small SEE based on proportionality, it could be used as an alternative method to determine individual specific eyeball sizes for the use in facial approximations.

Based on the differences in the dimensions of the orbit and the protrusion values of the eyeball, guidelines were developed for the placement of the eyeball in relation to the orbital rim in the form of prediction equations. Two methods are proposed: the first method is based on linear regressions, while the second is based on orbital proportions (orbital height or orbital breadth) (Guyomarc'h et al., 2012).

Prediction equations were created for the entire South African sample, for each population group and sex as well as for each sex-population group. It can be noted that the SEE were greater when the prediction equations were derived for each sex-population group individually. This could be due to the smaller sample size per sex-population group, in which individual variation greatly influences the equations. This trend was also observed by Guyomarc'h and colleagues (2012). Smaller SEE values were reported for the prediction of the eyeball based on regression equations by Guyomarc'h and colleagues (2012). Very weak correlations were noted between the orbital dimensions and eyeball protrusion in this study. This could be due to the presence of "random noise" in the dataset not captured by the independent variable (predictor) (Warton et al., 2006; Hammer and Harper, 2024). Although low correlations were noted, the linear regression still fitted the average trend of the data points, but further studies with increased sample sizes are necessary to test the accuracy of these prediction equations.

Mala and Veleminska (2018) tested the two proposed methods for eyeball positioning as described by Guyomarc'h and colleagues (2012) and concluded that the prediction by proportionality method yielded more accurate prediction results, which corresponds with the findings of this study, while the SEE values were greater when tested on this Central European sample. The authors advise that the prediction of eyeball position should be performed considering the prediction by proportionality method.

© University of Pretoria

It is perhaps not surprising that the eyeball dimensions and position showed low variability and poor correlation with the orbital dimensions considering that the eye, regardless of the dimensions of the orbit, still needs to perform its optic function, i.e. produce a sharp retinal image of a distant object (Charman, 1995).

5.1.3 Approximation of the palpebral fissure

The two current methods used to approximate the eyelids include the extrusion and addition methods. The approximation of the eyelids using these techniques are very subjective, as it requires the forensic artist to manually adjust the eyelids (extrusion method) or orbicularis oculi muscles (addition method) to fit the skull structure of the unidentified person. These methods do not take population affinity or sex into account but rely on the artistic skills of the scientist to compensate for sex and population variation. As described in section 5.1.1, the palpebral fissure width varied significantly between South African males and females, although similar palpebral fissure heights were noted for all sex-population groups.

This study created novel guidelines, not only specific to South Africans, but the first to be created, for the approximation of the open eye based on the linear dimensions of the bony orbit and palpebral fissures for use in the manual (clay) or computerised (Virtual Sculpture method) facial approximations. Due to higher r, R^2 and lower SEE values with the prediction equations for palpebral fissure diameter, these equations may prove useful in the approximation of the eyelids of South African faces. A stronger correlation coefficient and coefficient of determination were noted in black South Africans as a group as well as black South African females, emphasising the interrelationship between the orbital breadth and palpebral fissure width in these groups.

Although normative dimensions for each sex-population group were established, the dimensions of the palpebral fissure could be estimated with greater accuracy based on the orbital rim dimensions of each individual, regardless of their sex or population affinity. From the two methods suggested, “prediction through regression” and “prediction by proportionality” the prediction by proportionality performed better as smaller SEE values were obtained for this method.

This is the first study to propose predictive equations aiming to determine the palpebral fissure dimensions for the approximation of the open eye.

5.1.4 Shape analysis: based on manually placed landmarks

The shape of the palpebral fissure displays greater variability between South African population groups compared to sex. The greatest variation between population groups could

© University of Pretoria

be attributed to the increased inner canthal distance noted in the black South African sample. Greater variability was observed within the South African female group. Besides the more lateral location of the endocanthions in black South Africans, it is also located more superficially in black females, resulting in a less anteriorly curved palpebral fissure. Variations in the curve of the palpebral fissures between population groups are not an uncommon finding and have been described by Rüdell (2012) in a European and Chinese sample. The exocanthion was located slightly lower in black females resulting in a slightly smaller slant (obliquity) of the palpebral fissure compared to white females. The slant of the palpebral fissure has been noted to vary between population groups (Hanada et al., 2001) and should be taken into consideration during facial approximations.

Slight differences were noted in the shape of the palpebral fissure between sexes of this South African sample. The greatest variation, influenced by sex, was a wider palpebral fissure noted in males compared to females. Greater shape variability was observed in the black South African sample. The palpebral fissure of black females appears more open, although no significant difference was noted in the palpebral fissure height in black South Africans. The more open palpebral fissures are due to the more medial position of the exocanthion, which corresponds with the narrower palpebral fissure width observed in back females. The exocanthion is also located higher, or superiorly, in black females resulting in an upward slant of the palpebral fissure compared to black males. Less variation in the shape of the palpebral fissure was noted in white South Africans, although significant variation was noted in palpebral fissure dimensions in this group. Differences in the palpebral fissure are size-driven in white South Africans, and shape-driven in black South Africans.

The literature has described the influence of population affinity on the shape of the orbital region, although only a limited number of studies have been published. The discriminatory ability based on the shape of the orbital margin has also been investigated. In 2013, Xing and co-workers analysed the shape of the orbital rim in European, African and Asian skulls using GMM (Xing et al., 2013). Two anatomical and 45 semi-landmarks were placed around the orbital margins of photographs taken from skulls. Variation in the shape of the orbital margins was apparent. The results showed that the superior orbital margin was less accurate in differentiating between the three population groups with classification accuracies ranging between 41 – 60%, while classification accuracy increased to 72.5 – 80% based on the shape of the inferior orbital margin. Although this study contributed valuable insights with regard to population variation in the shape of the orbital rim, sexes were pooled and the shape analysis was conducted on 2D photographs, with no ability to examine variation in the curves of the lateral and medial orbital walls.

© University of Pretoria

One year later Stull and colleagues aimed to estimate the ancestry of South Africans (white, black and coloured) based on the position of several cranial landmarks (Stull et al., 2014). Six bilateral landmarks were included around the orbital region. Three dimensional points were placed at the identified bony landmarks using a microscribe. The study concluded that a significant difference exists in the shape of the cranium between white and black South Africans, while the size of the cranium of coloured South Africans is similar to white South Africans, and the shape of the cranium of coloured South Africans is similar to black South Africans. The lollipop graphs presented in the publication indicated a change in the position of the dacryon and ectoconchion, which directly affects the depth of the curve of the medial and lateral orbital walls (Stull et al., 2014). Unfortunately, this study pooled male and female samples, which affects the accuracy of the results as sex has a significant influence on the shape of the skull and orbital region (Milella et al., 2021; Toneva et al., 2022; Ajanović et al., 2023).

The greatest variation observed in the shape of the orbital rim between black and white South African males was noted at the position of the supraconchion, which protrudes more in white males, and may be indicative of a more pronounced superciliary arch. The deepest point on the lateral orbital rim and frontomolare orbitale was located more posteriorly in white males, resulting in a more concave lateral orbital margin. Population variation noted between South African females was mainly visible at the position of the dacryon and ectoconchion, which were located more laterally in black South African females. The lateral orbital margin was however more concave in black compared to white South African females. Population affinity can be established, based on the shape variations of the orbital region of South Africans, with 75.25 % accuracy, although the accuracy increases, especially in females, with known sex.

The foremost difference in the shape of the orbital margin between sexes is the rounded orbital rim observed in females and a more rectangular orbit observed in males, which was also noted in the current study (Pretorius et al., 2006; Bigoni et al., 2010; Milella et al., 2021; Toneva et al., 2022). Geometric morphometric studies of the cranium and orbital region, investigating the effect of sex and population affinity, have been conducted in 2D based on photographs taken from skulls (Pretorius et al., 2006; Xing et al., 2013; Stull et al., 2014). In more recent years, most GMM studies have been conducted using 3D landmarks either placed on the skull using a Microscribe or by placing landmarks on 3D renderings based on CT or CBCT scans which can be used to assess variation in the curved medial and lateral orbital margins (Bejdová et al., 2018; Milella et al., 2021; Toneva et al., 2022; Ajanović et al., 2023; Prevost et al., 2023).

Besides a rounder orbital rim observed in black South African females, a posterolateral shift was noted in the landmarks located along the lateral orbital margin as compared to black

© University of Pretoria

South African males. Black and white South African females presented with shallower orbital margins, as an anterior movement of the supraconchion was noted in South African males, especially in white males compared to white females. The more anteriorly located supraconchion is indicative of a more protruding superciliary arch which is commonly noted in males and is often used as a sex indicator (Graw et al., 1999; Bejdová et al., 2018; Milella et al., 2021).

Classification of the orbital region in South Africans according to sex increased greatly when population group was taken into consideration, especially in white South Africans (84.40 %) for shape dimensions, and for linear dimensions in black South Africans (73.08 %). Sex classification accuracies vary significantly between population groups. The white South African sample had the highest cross-validated classification accuracy (84.40 %), followed by Czech (83.3 %), Bosnian (81.28 %), Central European (74.75 %), Greek (72.7 % and 72.4 %), Bulgarian (70.05 %) and black South African (61.86 %) samples (Bigoni et al., 2010; Gonzalez et al., 2011; Bejdová et al., 2018; Chovalopoulou and Bertsatos, 2018; Toneva et al., 2022; Ajanović et al., 2023). Although the effect of size or form as factors were not tested on the shape and the orbital region, it should be considered as the classification accuracy was noted to increase by using form rather than shape of the orbital region (Gonzalez et al., 2011; Bejdová et al., 2018; Chovalopoulou and Bertsatos, 2018; Ajanović et al., 2023).

As noted from the variations in linear and shape dimensions, it is of utmost importance to first classify sex and population affinity of an unknown person when approximating the eyeball and eyelids, as the size of the eyeball and the position of the eyeball within the bony orbit as well as the features of the palpebral fissure varies between groups. In the process of creating guidelines for the approximation of the eyeball and periorbital regions, accuracies of orbital dimensions to predict population affinity and sex were established that could be useful for biological profiling in the forensic anthropological context.

5.2 Part 2: Soft tissue prediction based on automatically placed landmarks

Statistical models were created to determine the soft tissue structure of the palpebral fissure or open eyes from the underlying bony tissue. Cross-validation testing was used to validate the accuracy of the prediction models. Although the prediction of the open eye (palpebral fissure) from the underlying skeleton in this study is novel, the GMM used were derived from that proposed by Schlager and colleagues (2013) for the nose and chin shape, Guyromarc'h and co-workers (2014) for various facial features and Ridel and associates (2018) for the nose shape in South Africans.

The GMM involved automatic landmarking since the automatic method proved to be less time-consuming, more objective and more accurate in the placement of craniometric and

© University of Pretoria

capulometric landmarks (Ridel et al., 2020a). The reproducibility of the automatically projected landmarks had fantastic repeatability, with mean dispersion errors consistently below 1.10 mm for craniometric and 0.67 mm for capulometric landmarks for both intra- and inter-observer errors. The influence of sex and population affinity on the shape of the orbital region and palpebral fissures were determined followed by the prediction of the soft tissue structure from the underlying bone.

The shape variation noted in the orbital region and palpebral fissures based on the automatic landmarking method corresponded with the results obtained based on the manually placed landmarks. However, the classification accuracy was greater for population affinity based on the automatic landmarking method, whereas the classification accuracy was greater for sex based on the manual landmarking method. These variations could be due to the accuracy and repeatability of the landmark placement which was noted to vary between the landmarking methods. The repeatability of the projected automatic landmarks was greater compared to the manual landmarking method. Less variation was noted between the methods with regard to the capulometric landmarks as similar results were obtained during the DFA.

The cross-validated results, based on the automatic landmark procedure, indicated that the soft tissue shape of the palpebral fissures could be predicted from the underlying bony tissue with a prediction error of 1.63 mm, which is lower than the reported 2.90 mm by Guyomarc'h and colleagues (2014) for the prediction of the palpebral fissure landmarks (endocanthion, exocanthion, palpebrale inferior and oculus anterius). Geometric deviations of 2.50 – 5.00 mm around the orbital region were reported by Shui and co-workers (2017), although the focus of this study was not on the orbital region only.

As noted using the manual landmarking method, population affinity had a greater, as well as significant influence on the shape of the orbital region and palpebral fissure compared to sex. Thus, adding population affinity as a factor in the prediction model, the soft tissue structure of the palpebral fissures could be predicted with greater accuracy (0.18 mm), while adding sex as a factor had a negative impact on the prediction errors, increasing it (0.99 mm). The effect of sexual dimorphism on the shape of the palpebral fissures was more profound in the white South African sample, resulting in 0.38 mm better average prediction errors compared to the black South African sample. By adding sex and population affinity as factors in the prediction of the soft tissue shape of the palpebral fissures, the prediction errors continued to increase. This could be due to the smaller sample size of each subgroup, or since only two hard-tissue templates were used (black and white South Africans, sex pooled) and one soft-tissue template (population and sexes pooled), explaining the improved results noted when only

© University of Pretoria

population affinity is taken into account. By increasing the sample size, this limitation can be addressed.

5.3 Applications, limitations and future recommendations

This study confirmed that population affinity and sex influence the dimensions and shape of the orbit, eyeballs, palpebral fissure as well as the position of the eyeball within the bony orbit. These findings emphasise the necessity for the use of population and sex-specific data for the facial approximation process of South Africans. Successful prediction equations (linear distances) and models (shape) could be created for the protrusion of the eyeball from the orbital rim and approximation of the open palpebral fissures of this South African sample, which was based on the presumed morphological relationship between the skeletal framework of the orbital region and the soft-tissue structure of the eyelids.

One of the most important aspects of forensic anthropology is to establish the biological profile (sex, population affinity, age and stature) of the deceased (İşcan and Steyn, 2013). Sex is usually one of the first factors to estimate before age and population affinity are determined (Kimmerle et al., 2008). The pelvis is preferred for sex estimation, but may not necessarily be present due to disarticulation, weather, or scavenger activity, leading to the recovery of fragmented or incomplete skeletal remains (L' Abbé 2005; İşcan and Steyn, 2013; Spies et al., 2018; Bejdová et al., 2018; Chovalopoulou and Bertsatos, 2018; Keyes et al., 2022). In such cases, the skull is used (Bejdová et al., 2018).

The dimensions of the orbital region have been used to estimate sex and population affinity in South Africans with varying degrees of classification accuracies (L' Abbé et al., 2013; Stull et al., 2014; Liebenberg et al., 2015; Small et al., 2018). Similar results were published based on the shape of the orbital region of South Africans (Pretorius et al., 2006; Xing et al., 2013; Rubin and deLeon, 2017; Small et al., 2018). This study improved on the existing literature by including males and females from two prominent population groups in South Africa, to comprehensively evaluate the effect of sex and population affinity on the dimensions and shape of the orbital region. This study further investigated the protrusion of the eyeball from the orbital margin as well as the position of the eyeball within the bony orbit for the use in facial approximations. As the landmarks were placed on CBCT scans, the gravitational effect on the soft tissue structures of the orbital region imitated the erect anatomical position as opposed to the use of computer tomography scanning (CT). CBCT scans have the additional advantage as it has a higher resolution and lower radiation dose compared to other modalities, e.g. CT scans (Swennen and Schutyser, 2006; Casselman et al., 2013; Dorfling, 2017).

The placement of landmarks in three dimensions further allowed the assessment of the curved lateral and medial orbital rims, which have been proved to vary between sex and population

© University of Pretoria

groups. It should be noted that sex can be estimated with greater accuracy based on the linear dimensions of the orbital region (80.10 %), while population affinity can be determined with greater accuracy based on the shape of the orbital region (81.07 %). Uniquely white South African females had similar orbital heights as compared to males of both populations, despite a shorter orbital breadth giving rise to a greater orbital index or a squarer-shaped orbit. These findings should be considered when establishing the biological profile of an unknown individual when incomplete or fragmented skeletal material is discovered.

A facial approximation should be created based on the biological profile created by the forensic anthropologist. However, during the reconstruction of the orbital region according to established guidelines, the same-sized eyeball is placed within the orbit, closer to the superolateral orbital margins (Wilkinson, 2002; Stephan and Davidson, 2009; İşcan and Steyn, 2013). According to this study, it should be taken into consideration that black South African females had significantly smaller eyeballs compared to their male counterparts and compared to white South African males and females. When the eyeball is placed within the orbit in black South Africans, it should protrude more in the vertical plane (from the superior and inferior orbital margins) when compared to white South Africans. The eyeball was also located deeper within the bony orbit of South African females, as they present with a less concave lateral orbital margin compared to their male counterparts. The prediction equations based on proportionality can be used with high accuracy to determine the placement and projection of the eyeball from the orbital rim in the anteroposterior, mediolateral and supero-inferior planes.

When reconstructing the palpebral fissures, current guidelines focus on the position of the medial and lateral canthi in relation to the bony orbit and to each other (İşcan and Steyn, 2013). It should be noted that South African females have significantly narrower palpebral fissure widths and upward-slanted fissures compared to South African males, especially in black South Africans, while neither sex nor population affinity influences the height of the palpebral fissures. The shape of the palpebral fissure, however, varies between South African females and black South African females presenting with a greater inner canthal distance and less slanted palpebral fissure. The significant shape variation noted in the black South African sample between sexes was due to the more superior position of the exocanthion in black females, and the wider palpebral fissure noted in black males.

Towards more objective facial approximations of South African faces, an automated computerised method to predict the facial features from the underlying bone is advocated. This study demonstrated that the palpebral fissure can be predicted successfully from the underlying bony tissue. In 2020, Ridel and colleagues (2020b) reported an accurate prediction of the soft-tissue structure of the nose of white and black South Africans based on the

© University of Pretoria

underlying bone. Variations in the shape of the menton and chin as well as the external acoustic meatus and ear of South Africans suggest the possibility of predicting the chin and ear from the underlying bone (Braun et al., 2023; Erasmus et al., 2023).

In order to determine the effect of age on the dimensions and shape of the orbit, eyeball and palpebral fissure, future studies could be designed to include a more homogenous sample with regard to age. Findings on age variations may further aid in establishing the biological profile of unidentified South Africans.

Knowledge of the normative dimensions of the orbit, eyeball, eyelid and palpebral fissure not only benefits forensic anthropologists, but could also be useful in a clinical setting for facial prosthesis, reconstructive surgery and the field of ophthalmology. For instance, the smaller axial ocular length noted in black South African females, might affect near sight and reading abilities in the young. Although a relationship in this group has not been described in the literature, it is well-known that variation in axial length affects visual acuity (Matsumura et al., 2019). Further, the wider interorbital distance noted in the black South African sample could impact the design of virtual reality apparatuses and could affect nearby focus in this group (Dodgson, 2004; Woldegiorgis et al., 2019). The normative values determined by this study can also be used to investigate and quantify the effect of trauma, pathology and defective growth on the STT values of the face as it is commonly used as exclusion criteria without further investigation.

© University of Pretoria

6. Chapter 6: Conclusion

This research study aimed to create guidelines for the approximation of the eyeball and periorbital regions of South Africans to produce more accurate and objective facial approximations in order assist in the identification of unknown individuals. This study is the first to derive prediction equations to determine the position of the eyeball in the orbit and the palpebral fissure dimensions. It is also the first to predict the open palpebral fissures from the underlying bony orbit of South Africans. Landmarks were placed on CBCT scans negating the effects of gravity on the supine position with the benefit of 3D landmarking on living individuals with intact anatomy. The guidelines based on the 2D and 3D dimensions as well as the automated computerised method were derived from highly repeatable landmarks and therefore should be applicable beyond this study.

Significant variation exists in the dimensions and shape of the bony orbit, eyeball and palpebral fissures which were in some cases sex or population specific. The orbital, eyeball and palpebral fissure dimensions varies significantly compared to other population groups as indicated by the BF. South Africans, with the exception of black South African females, often present with greater dimensions with regard to the orbit and eyeball when compared to other population groups, while the palpebral fissure dimensions seemed to be smaller. Sexual dimorphism was also investigated and variations noted. These variations warrant the creation of population and sex specific guidelines for the approximation of the eyeball and periorbital regions of South Africans.

Guidelines could successfully be created for the placement of the eyeball in relation to the orbital rim and the approximation of the open eyelids. The position of the eyeball can be predicted with high accuracy based on its proportionality with the bony orbit for the entire sample, without taking sex or population affinity into account. The palpebral fissure dimensions of South Africans can be estimated based on the orbital dimensions with high accuracy. Low SEE values were obtained for both predictive methods (proportionality or predictive equations). These guidelines will be useful for computerised or manual facial approximations and can be used successfully with no regard to population affinity and sex, but will take the morphology of each unidentified person into account.

The soft-tissue shape of the palpebral fissures could be accurately predicted from the underlying bony tissue. The effect of sex and population affinity was taken into account. Population affinity was identified as an important influencer of shape highlighting the population specific variation. Sex had less of an influence on the shape of the orbit and palpebral fissure within the entire sample. By including these factors in the prediction, it was

© University of Pretoria

noted that adding population affinity as factor improved the SEE values, while adding sex as factor negatively impacted the SEE values. The prediction results could be combined with the prediction of other facial features of South Africans to create an objective, time-saving automatic computerised facial approximation method.

The prediction models created for the approximation of the open eye (palpebral fissures) from the underlying bony tissue should be tested on larger samples and other groups in future studies. Future studies could also include a sample more representative of all age groups to study the effect of aging. The findings of this study could also be useful in a clinical setting, especially for facial reconstructive surgeries, facial prostheses and in the field of ophthalmology.

© University of Pretoria

References

Abdel Fatah, E.E., Shirley, N.R., Jantz, R.L., Mahfouz, M.R. 2014. Improving sex estimation from crania using a novel three-dimensional quantitative method. Journal of Forensic Sciences. 59(3):590-600. https://doi: 10.1111/1556-4029.12379.

Abdi, H. 2010. Partial least squares regression and projection on latent structure regression (PLS regression). Wiley Interdisciplinary Reviews: Computational Statistics. 2(1):97-106. https://doi: 10.1002/wics.51

Adams, D., Collyer, M., Kaliontzopoulou, A. 2020. Geometric morphometric analyses of 2D/3D landmark data. R package version 3.0.6. Available from: https://CRAN.R-project.org/package=geomorph

Adams, D.C., Rohlf, F.J., Slice, D.E. 2004. Geometric morphometrics: Ten years of progress following the 'revolution'. Italian Journal of Zoology. 71(1):5-16. https://doi.org/10.1080/11250000409356545

Ajanović, Z., Ajanović, U., Dervišević, L., Hot, H., Voljevica, A., Talović, E., Dervišević, E., Hašimbegović, S., Sarač-Hadžihalilović, A. 2023. A geometric morphometrics approach for sex estimation based on the orbital region of human skulls from Bosnian population. Scanning. e2223138. https://doi.org/10.1155/2023/2223138

Anastassov, G.E., Van Damme, P.A. 1996. Evaluation of the Anatomical position of the lateral canthal ligament: Clinical implications and guidelines. Journal of Craniofacial Surgery. 7(6):429-36. https://doi.org/10.1097/00001665-199611000-00008

Arnholt, A., Evans, B. 2017. BSDA: Basic statistics and data analysis. R package version 1.2. 0.

Attia, A.M., Ghoneim, M., Elkhamary, S.M. 2018. Sex discrimination from orbital aperture dimensions using computed tomography: Sample of Egyptian population. Journal of Forensic Radiology and Imaging. 14:32-38. https://doi.org/10.1016/j.jofri.2018.08.007

Aulsebrook, W., İşcan, M., Slabbert, J., Becker, P. 1995. Superimposition and reconstruction in forensic facial identification: A survey. Forensic Science International. 75(2):101-20. https://doi.org/10.1016/0379-0738(95)01770-4

Avelar, L.E.T., Cardoso, M.A., Bordoni, L.S., De Miranda Avelar, L., De Miranda Avelar, J.V. 2017. Aging and sexual differences of the human skull. Plastic and Reconstructive Surgery Global Open. 5(4):e1297. https://doi.or/10.1097/GOX.0000000000001297

© University of Pretoria

Beaini, T.L., Miamoto, P., Duailibi-Neto, E.F., Tedeschi-Oliveira, S.V., Chilvarquer, I., Melani, R.F.H. 2021. Facial soft tissue depth measurements in cone-beam computed tomography: A study of a Brazilian sample. Legal Medicine. 50:101866. https://doi.org/10.1016/j.legalmed.2021.101866

Baillie, L.J., Muirhead, J.C., Blyth, P., Niven, B.E., Dias, G.J. 2015. Position effect on facial soft tissue depths: a sonographic investigation, Journal of Forensic Science 61:S60– S70. https://doi.org/10.1111/1556-4029.12935

Barretto, R.L., Mathog, R.H. 1999. Orbital measurement in black and white populations. The Laryngoscope. 109(7):1051-4. https://doi.org/10.1097/00005537-199907000-00007.

Bejdová, Š., Dupej, J., Krajíček, V., Velemínská, J., Velemínský, P. 2018. Stability of upper face sexual dimorphism in central European populations (Czech Republic) during the modern age. International Journal of Legal Medicine. 132:321-330. https://doi.org/10.1007/s00414-017-1625-3.

Bekerman, I., Gottlieb, P., Vaiman, M. 2014. Variations in eyeball diameters of the healthy adults. Journal of Ophthalmology. 2014:503645. https://doi.org/10.1155/2014/503645

Bigoni, L., Velemínská, J., Brůžek, J. 2010. Three-dimensional geometric morphometric analysis of cranio-facial sexual dimorphism in a Central European sample of known sex. Homo. 61(1):16-32. https://doi.org/10.1016/j.jchb.2009.09.004.

Bogren, H.G., Franti, C.E., Wilmarth, S.S. 1986. Normal variations of the position of the eye in the orbit. Ophthalmology. 93(8):1072-7. https://doi.org/10.1016/s0161-6420(86)33618-2

Bookstein, F.L. 1991. Morphometric tools for landmark data: Geometry and Biology. United Kingdom: Cambridge University Press.

Bookstein, F.L. 1996. Biometrics, Biomathematics and the Morphometric synthesis. Bulletin of Mathematical Biology. 58(2):313. https://doi.org/10.1007/BF02458311.

Braun, S., Ridel, A.F., L'Abbé, E.N., Oettlé, A.C. 2023. Analysis of the hard-tissue menton shape variation in adult South Africans using cone-beam computed tomography (CBCT) scans. Forensic Imaging. 32:200532. https://doi.org/10.1016/j.fri.2023.200532

Brown, R., Douglas, J. 1975. Exophthalmometry of blacks. Annals of Internal Medicine. 83(6):835-7. https://doi.org/10.7326/0003-4819-83-6-835_2.

Bayat, M., Shariati, M., Rajaeirad, F., Yekaninejad, M.S., Momen-Heravi, F., Davoudmanesh, Z. 2018. Facial anthropometric norms of the young Iranian population. Journal of Maxillofacial and Oral Surgery. 17:150-157. https://doi.org/10.1007/s12663-016-0897-3

© University of Pretoria

Byers, SN. 2016. Introduction to Forensic Anthropology. 5th ed. New York: Taylor & Francis.

Cabungcal, J., Misslisch, H., Scherberger, H., Hepp, K., Hess, B. 2001. Effect of light sleep on three-dimensional eye position in static roll and pitch. Vision Research. 41(4):495-505. https://doi.org/10.1016/s0042-6989(00)00279-0.

Casselman, J.W., Gieraerts, K., Volders, D., Delanote, J., Mermuys, K., De Foer, B., Swennen, G. 2013. Cone beam CT: non-dental applications. Journal of the Belgian Society of Radiology. 96(6):333-353. https://doi.org/10.5334/jbr-btr.453.

Caple, J., Stephan, C.N. 2016. A standardized nomenclature for craniofacial and facial anthropometry. International Journal of Legal Medicine. 130(3):863-79. https://doi.org/10.1007/s00414-015-1292-1.

Cappella, A., Gibelli, D., Vitale, A., Zago, M., Dolci, C., Sforza, C., Cattaneo, C. 2020. Preliminary study on sexual dimorphism of metric traits of cranium and mandible in a modern Italian skeletal population and review of population literature. Legal Medicine. 44:101695. https://doi.org/10.1016/j.legalmed.2020.101695.

Cavanagh, D., Steyn, M. 2011. Facial reconstruction: Soft tissue thickness values for South African black females. Forensic Science International. 206(1-3):215.e1-e7. https://doi.org/10.1016/j.forsciint.2011.01.009.

Celebi, A.A., Kau, C.H., Ozaydin, B. 2017. Three-dimensional anthropometric evaluation of facial morphology. Journal of Craniofacial Surgery. 28(5):470-e474. https://doi.org/10.1097/SCS.0000000000003773.

Celebi, A.A., Kau, C.H., Femiano, F., Bucci, L., Perillo, L. 2018. A three-dimensional anthropometric evaluation of facial morphology. Journal of Craniofacial Surgery. 29(2):304-308. https://doi.org/10.1097/SCS.0000000000004110.

Chau, A., Fung, K., Pak, K., Yap, M. 2004. Is eye size related to orbit size in human subjects? Ophthalmic and Physiological Optics. 24(1):35-40. https://doi.org/10.1046/j.1475-1313.2003.00159.x.

Charman, W.N., 1995. Optics of the eye. *Handbook of optics*, *1*, pp.24-18.

Chovalopoulou, M.E., Bertsatos, A. 2018. Exploring the shape variation of the human cranium. A geometric morphometrics study on a modern Greek population sample. Geometric morphometrics. Trends in Biology, Paleobiology and Archaeology. 25-39.

© University of Pretoria

Claes, P. 2007. A robust statistical surface registration framework using implicit function representations-application in craniofacial reconstruction. Dissertation, (PhD Eng.). Katholieke Universiteit Leuven. Belgium.

Claes, P., Vandermeulen, D., De Greef, S., Willems, G., Suetens, P. 2006. Craniofacial reconstruction using a combined statistical model of face shape and soft tissue depths: methodology and validation. Forensic Science International. 159:S147-S158. https://doi.org/10.1016/j.forsciint.2006.02.035.

Claes, P., Vandermeulen, D., De Greef, S., Willems, G., Clement, J.G.. Suetens, P. 2010. Computerized craniofacial reconstruction: conceptual framework and review. Forensic Science International. 201(1-3):138-145. https://doi.org/10.1016/j.forsciint.2010.03.008.

Davanger, M. 1969. Principles and sources of error in exophthalmometry. A new exophthalmometer. Acta Ophthalmologica. 48(4):625-33. PMID: 5536709.

Davy-Jow, S. 2013. The devil is in the details: A synthesis of psychology of facial perception and its applications in forensic facial reconstruction. Science and Justice. 53(2):230-5. https://doi.org/10.1016/j.scijus.2013.01.004.

Dayal, M.R., Spocter, M.A., Bidmos, M.A. 2008. An assessment of sex using the skull of black South Africans by discriminant function analysis. Homo. 59(3):209-221. https://doi.org/10.1016/j.jchb.2007.01.001.

De Barros, F., Da Costa Serra, M., Kuhnen, B., Scarso Filho, J., Gonçalves, M., Fernandes C.M.S. 2021. Midsagittal and bilateral facial soft tissue thickness: a Cone-Beam Computed Tomography assessment of Brazilian living adults. Forensic Imaging. 25:200444.

De Greef, S., Claes, P., Vandermeulen, D., Mollemans, W., Suetens, P., Willems, G. 2006. Large-scale in-vivo Caucasian soft tissue thickness database for craniofacial reconstruction. Forensic Science. International. 159:S126–S146. https://doi.org/10.1016/j.forsciint.2006.02.034.

De Juan, E., Hurley, D.P., Sapira, J.D. 1980. Racial differences in normal values of proptosis. Archives of Internal Medicine. 140(9):1230-1. https://doi.org/10.1001/archinte.140.9.1230.

Dodgson, N.A. 2004. Variation and extrema of human interpupillary distance. Stereoscopic Displays and Virtual Reality Systems XI. 5291:36-46

Dorfling, H.F., Lockhat, Z., Pretorius, S., Steyn, M., Oettlé, A.C. 2018. Facial approximations: Characteristics of the eye in a South African sample. Forensic Science International. 286:46-53. https://doi.org/10.1016/j.forsciint.2018.02.029.

© University of Pretoria

Dorfling, H.F. 2017. Aspects of facial features in a South African sample as applicable for facial approximations. Dissertation, (MSc.). University of Pretoria. South Africa.

Dryden, I.L., Mardia, K.V. 2016. Statistical shape analysis: With applications in R. 2nd Ed. Chichester: John Wiley and Sons.

Dunsky, I. 1992. Normative data for Hertel exophthalmometry in a normal adult black population. Optometry & Vision Science. 69(7):562-4. https://doi.org/10.1097/00006324-199207000-00009.

Dayal, M.R., Spocter, M.A., Bidmos, M.A. 2008. An assessment of sex using the skull of black South Africans by discriminant function analysis. Homo. 59(3):209-221. https://doi.org/10.1016/j.jchb.2007.01.001.

Ellis, H.D., Shepherd, J.W., Davies, G.M. 1979. Identification of familiar and unfamiliar faces from internal and external features: Some implications for theories of face recognition. Perception. 8(4):431-9. https://doi.org/10.1068/p080431.

Erasmus, M.K., L'Abbé, E.N., Ridel, A.F. 2023. A geometric morphometric assessment of the hard tissue external auditory meatus and soft tissue ear of South Africans. Forensic Science International: Reports. 8:100331.

Farkas, L.G. 1994. Anthropometry of the head and face. 2nd Ed. Raven Press.

Farkas, L.G., Katic, M.J., Forrest, C.R. 2007. Comparison of craniofacial measurements of young adult African-American and North American white males and females. Annals of Plastic Surgery. 59(6):692-698. https://doi.org/10.1097/01.sap.0000258954.55068.b4.

Farrar, F. 1977. Skull to visage-forensics technique for facial restoration. Police Chief. 44(4):78-80.

Franklin, D., Freedman, L., Milne, N. 2005. Three-dimensional technology for linear morphological studies: a re-examination of cranial variation in four Southern African indigenous populations. Homo. 56(1):17-34. https://doi.org/10.1016/j.jchb.2004.07.004.

Franklin, D., O'Higgins, P., Oxnard, C.E., Dadour, I. 2007. Sexual dimorphism and population variation in the adult mandible: forensic applications of geometric morphometrics. Forensic Science, Medicine, and Pathology. 3:15-22. https://doi.org/10.1385/FSMP:3:1:15.

Franklin, D., Cardini, A., Flavel, A., Kuliukas, A. 2012. The application of traditional and geometric morphometric analyses for forensic quantification of sexual dimorphism: preliminary investigations in a Western Australian population. International Journal of Legal Medicine. 126:549-558. https://doi.org/10.1007/s00414-012-0684-8.

© University of Pretoria

Frowd, C.D., Skelton, F.C., Butt, N., Hassan, A., Fields, S., Hancock, P.J. 2011. Familiarity effects in the construction of facial-composite images using modern software systems. Ergonomics. 54(12):1147-58. https://doi.org/10.1080/00140139.2011.623328.

Gaia, B.F., Pinheiro, L.R., Umetsubo, O.S., Costa, F.F., Cavalcanti, M.G.P. 2013. Comparison of precision and accuracy of linear measurements performed by two different imaging software programs and obtained from 3D-CBCT images for Le Fort I osteotomy. Dentomaxillofacial Radiology. 42(5):20120178. https://doi.org/10.1259/dmfr.20120178.

Galdames, I.C.S., López, M.C., Matamala, D.a.Z., Rojas, F.J.P., Muñoz, S.R.T., Suazo, G., Cantín, L., Zavando, M., Perez, R., Torres, M. 2008. Comparisons in soft-tissue thicknesses on the human face in fresh and embalmed corpses using needle puncture method. International Journal Morphology. 26(1):165-9.

Gangestad, S.W., Thornhill, R. 2003. Facial masculinity and fluctuating asymmetry. Evolution and Human Behavior. 24(4):231-241. https://doi.org/10.1016/S1090-5138(03)00017-5

Gatliff, B., Taylor, K. 2001. Three-dimensional facial reconstruction on the skull. Forensic Art and Illustration. Boca Raton: CRC Press. 419-75.

Gatliff, B.P. 1984. Facial sculpture on the skull for identification. The American Journal of Forensic Medicine and Pathology. 5(4):327-32. https://doi.org/10.1097/00000433-198412000-00009.

Gatliff, B.P., Snow, C.C. 1979. From skull to visage. The Journal of Biocommunication. 6(2):27. PMID: 457651.

Gerasimov, M. 1971. Face finder, New York: CRC Press.

Goldnamer, W.W. 1923. The anatomy of the human eye and orbit. Chicargo: Professional Press.

Gonzalez, P.N., Bernal, V., Perez, S.I. 2011. Analysis of sexual dimorphism of craniofacial traits using geometric morphometric techniques. International Journal of Osteoarchaeology, 21(1):82-91. https://doi.org/ https://doi.org/10.1002/oa.1109

Goodall, C. 1991. Procrustes methods in the statistical analysis of shape. Journal of the Royal Statistical Society: Series B (Methodological). 53(2):285-321. https://doi.org/10.1111/j.2517-6161.1991.tb01825.x

Gower, J.C. 1975. Generalized Procrustes analysis. Psychometrika. 40(1):33-51. https://doi.org/10.1007/BF02291478

© University of Pretoria

Graw, M., Czarnetzki, A., Haffner, H.T. 1999. The form of the supraorbital margin as a criterion in identification of sex from the skull: investigations based on modern human skulls. American Journal of Physical Anthropology. 108(1):91-96. https://doi.org/10.1002/(SICI)1096-8644(199901)108:1<91::AID-AJPA5>3.0.CO;2-X

Green, H., Curnoe, D. 2009. Sexual dimorphism in Southeast Asian crania: a geometric morphometric approach. Homo. 60:517-534. https://doi.org/10.1016/j.jchb.2009.09.001.

Guleria, A., Krishan, K., Sharma, V., Kanchan, T. 2023. Methods of forensic facial reconstruction and human identification: historical background, significance, and limitations. The Science of Nature. 110:8. https://doi.org/10.1007/s00114-023-01838-9.

Gupta, S., Gupta, V., Vij, H., Vij, R., Tyagi, N. 2015. Forensic facial reconstruction: The final frontier. Journal of Clinical and Diagnostic Research. 9:ZE26-ZE28. https://doi.org/10.7860/JCDR/2015/14621.6568.

Guyomarc'h, P., Dutailly, B., Charton, J., Santos, F., Desbarats, P., Coqueugniot, H. 2014. Anthropological facial approximation in three dimensions (AFA3D): Computer-assisted estimation of the facial morphology using geometric morphometrics. Journal of Forensic Sciences. 59(6):1502-1516. https://doi.org/10.1111/1556-4029.12547.

Guyomarc'h, P., Dutailly, B., Couture, C., Coqueugniot, H. 2012. Anatomical placement of the human eyeball in the orbit - validation using CT scans of living adults and prediction for facial approximation. Journal of Forensic Sciences. 57(5):1271-5. https://doi.org/10.1111/j.1556-4029.2012.02075.x.

Haig, N.D. 1984. The effect of feature displacement on face recognition. Perception. 13(5):505-12. https://doi.org/10.1068/p130505.

Hammer, Ø., Harper, D. A.. Ryan, P. D. 2001. PAST: Paleontological statistics software package for education and data analysis. Palaeontologia electronica. 4, 9.

Hammer, Ø., Harper, D.A.T. 2024. Paleontological Data Analysis. 2nd ed. Elsevier.

Hanada, A.L., de Souza Jr, E.N., Moribe, I., Cruz, A.A.V. 2001. Comparison of palpebral fissure obliquity in three different racial groups. Ophthalmic Plastic and Reconstructive Surgery. 17(6):423-426. https://doi.org/10.1097/00002341-200111000-00007.

Harris, L.R., Goltz, H.C., Steinbach, M.J. 1993. The effect of gravity on the resting position of the cat's eye. Experimental Brain Research. 96(1):107-16. https://doi.org/10.1007/BF00230444.

© University of Pretoria

Haslwanter, T., Straumann, D., Hess, B., Henn, V. 1992. Static roll and pitch in the monkey: Shift and rotation of listing's plane. Vision research. 32(7):1341-8. https://doi.org/10.1016/0042-6989(92)90226-9.

Hernandez, H., 2021. Testing for normality: What is the best method. ForsChem Research Reports. 6:2021-05.

His, W. 1895. Anatomische Forschungen über Johann Sebastian Bach's Gebeine und Antlitz, nebst Bemerkungen über dessen Bilder. Abh MathPhysikal Kl KGL Sachs Ges Wiss. 22:379-420.

İşcan, M.Y., Steyn, M. 2013. The human skeleton in forensic medicine. Springfield, Illinois, USA: Charles C Thomas.

Jagesur, S. 2022. Variations in pelvic canal and skull dimensions in South Africans: possible relationships and implications. Dissertation, (PhD.). University of Pretoria. South Africa.

Janik, S.W., Wellens, A.R., Goldberg, M.L., Dell'osso, L.F. 1978. Eyes as the center of focus in the visual examination of human faces. Perceptual and motor skills. 47(3 Pt 1):857-8. https://doi/org/10.2466/pms.1978.47.3.857.

Ji, Y., Qian, Z., Dong, Y., Zhou, H., Fan, X. 2010. Quantitative morphometry of the orbit in Chinese adults based on a three-dimensional reconstruction method. Journal of Anatomy. 217(5):501-6. https://doi.org/10.1111/j.1469-7580.2010.01286.x.

Kaur, J., Yadav, S., Singh, Z. 2012. Orbital dimensions - a direct measurement study using dry skulls. Journal of Academia and Industrial Research. 1(6):293-5.

Kendall, D.G. 1984. Shape manifolds, procrustean metrics, and complex projective spaces. Bulletin of the London Mathematical Society. 16(2):81-121. https://doi.org/10.1112/blms/16.2.81

Keyes, C.A., Myburgh, J., Brits, D. 2022. Identifying forensically relevant urban scavengers in Johannesburg, South Africa. Science and Justice. 62(3):399-409. https://doi.org/10.1016/j.scijus.2022.04.007.

Khani, H., Fazelinejad, Z., Hanafi, M.G., Mahdianrad, A., Moghadam, A.R.E. 2023. Morphometric and volumetric evaluations of orbit using three-dimensional computed tomography in Southwestern Iranian population. Translational Research in Anatomy. 30:100233. https://doi.org/10.1016/j.tria.2023.100233

© University of Pretoria

Kim, S.R., Lee, K.M., Cho, J.H., Hwang, H.S. 2016. Three-dimensional prediction of the human eyeball and canthi for craniofacial reconstruction using cone-beam computed tomography. Forensic Science International. 261:164-e1. https://doi.org/10.1016/j.forsciint.2016.01.031.

Kimmerle, E. H., Ross, A., Slice, D. 2008. Sexual dimorphism in America: Geometric morphometric analysis of the craniofacial region. Journal of Forensic Sciences. 53:54-57. https://doi.org/10.1111/j.1556-4029.2007.00627.x.

Klingenberg, C.P., Mcintyre, G.S. 1998. Geometric morphometrics of developmental instability: Analyzing patterns of fluctuating asymmetry with Procrustes methods. Evolution. 52(5):1363-75. https://doi.org/10.1111/j.1558-5646.1998.tb02018.x.

Klingenberg, C.P., Barluenga, M., Meyer, A. 2002. Shape analysis of symmetric structures: Quantifying variation among individuals and asymmetry. Evolution. 56(10):1909-20. https://doi.org/10.1111/j.0014-3820.2002.tb00117.x.

Klingenberg, C.P., Leamy, L.J., Routman, E.J., Cheverud, J.M. 2001. Genetic architecture of mandible shape in mice: Effects of quantitative trait loci analyzed by geometric morphometrics. Genetics. 157(2):785-802. https://doi.org/10.1093/genetics/157.2.785.

Koo, T.K., Li, M.Y. 2016. A guideline for selecting and reporting intraclass correlation coefficients for reliability research. Journal of Chiropractic Medicine, 15:155-163. https://doi.org/10.1016/j.jcm.2017.10.001.

Kosalagood, P., Silkosessak, O.C., Pittayapat, P., Pisarnturakit, P., Pauwels, R., Jacobs, R. 2015. Linear measurement accuracy of eight cone beam computed tomography scanners. Clinical Implant Dentistry and Related Research. 17(6):1217-1227. https://doi.org/10.1111/cid.12221.

Krogman, W., İşcan, M. 1986. The human skeleton in forensic medicine. Springfield, Illinois, USA: Charles C Thomas.

Krüger, G.C., L'Abbé, E.N., Stull, K.E., Kenyhercz, M.W. 2015. Sexual dimorphism in cranial morphology among modern South Africans. International Journal of Legal Medicine. 129(4):869-75. https://doi.org/10.1007/s00414-015-1233-z.

Krüger, G.C., Liebenberg, L., Myburgh, J., Meyer, A., Oettlé, A.C., Botha, D., Brits, D.M., Kenyhercz, M.W., Stull, K.E., Sutherland, C., L'Abbé, E.N. 2018. Forensic anthropology and the biological profile in South Africa. In New Perspectives in Forensic Human Skeletal Identification (pp. 313-321). Academic Press.

© University of Pretoria

Kunjur, J., Sabesan, T., Ilankovan, V. 2006. Anthropometric analysis of eyebrows and eyelids: An inter-racial study. British Journal of Oral and Maxillofacial Surgery. 44(2):89-93. https://doi.org/10.1016/j.bjoms.2005.03.020.

L'Abbé, E., Loots, M., Meiring, J. 2005. The Pretoria Bone Collection: A modern South African skeletal sample. Homo. 56(2):197-205. https://doi.org/10.1016/j.jchb.2004.10.004

L'Abbé, E.N., Kenyhercz, M., Stull, K.E., Keough, N., Nawrocki, S., 2013. Application of Fordisc 3.0 to explore differences among crania of North American and South African blacks and whites. Journal of Forensic Sciences. 58(6):1579-1583. https://doi.org/10.1111/1556-4029.12198.

Langsrud, Ø. 2002. 50–50 Multivariate analysis of variance for collinear responses. Journal of the Royal Statistical Society: Series D. The Statistician. 51(3):305-17.

Langsrud, Ø., Mevik, B. 2012. Ffmanova: Fifty-fifty manova. Available from http://CRAN.R-project.org/package5ffmanova

Langsrud, Ø., J∅ Rgensen, K., Ofstad, R., Næs, T. 2007. Analyzing designed experiments with multiple responses. Journal of Applied Statistics. 34(10):1275-96.

Lee, W.J., Wilkinson, C.M., Hwang, H.S. 2012. An accuracy assessment of forensic computerized facial reconstruction employing cone-beam computed tomography from live subjects. Journal of Forensic Sciences. 57(2):318-327. https://doi.org/10.1111/j.1556-4029.2011.01971.x.

Liebenberg, L., Stull, K.E., L'Abbé, E.N., Botha, D. 2015. Evaluating the accuracy of cranial indices in ancestry estimation among South African groups. Journal of Forensic Sciences. 60(5):1277-1282. https://doi.org/10.1111/1556-4029.12770.

Liu, Y., Pan, H., Wang, J., Yao, Q., Lin, M., Ma, B. and Li, J. 2020. Ophthalmological features and treatments in five cases of Waardenburg syndrome. Experimental and Therapeutic Medicine. *20*(4):3072-3077. https://doi.org/10.3892/etm.2020.9035

Mahoney, G., Rynn, C. 2011. Facial reconstruction: New approaches. In Thali, M., Viner, M.D., Brogdon, B.G. (Eds.). Brogdon's Forensic Radiology. 2nd Ed. pp. 479–484. Boca Raton, FL: CRC Press.

Manhein, M.H., Listi, G.H., Barsley, R. E., Musselman, R., Barrow, N.E., Ubelaker, D.H. 2000. In vivo facial tissue depth measurements for children and adults, Journal of Forensic Science. 45:48–60. PMID: 10641919

Martens, H., Naes, T. 1992. Multivariate calibration. New York: John Wiley and Sons.

© University of Pretoria

Matsumura, S., Kuo, A.N., Saw, S.M. 2019. An Update of Eye Shape and Myopia. Eye and Contact Lens. 45(5):279–285. https://doi.org/10.1097/ICL.0000000000000571.

Mbonani, T.M., Hagg, A.C., L'Abbé, E.N., Oettlé, A.C., Ridel, A.F. 2023. Validation of the utilisation of automatic placement of anatomical and sliding landmarks on three-dimensional models for shape analysis of human pelves. Forensic Imaging, 33:p.200542. https://doi.org/10.1016/j.fri.2023.200542

Mevik, B.H., Cederkvist, H.R. 2004. Mean squared error of prediction (MSEP) estimates for principal component regression (PCR) and partial least squares regression (PLSR). Journal of Chemometrics. 18(9):422-9. https://doi.org/10.1002/cem.887

MeVisLab. https://www.mevislab.de, MeVis Medical Solutions AG, Germany, 2016.

Milella, M., Franklin, D., Belcastro, M.G., Cardini, A. 2021. Sexual differences in human cranial morphology: Is one sex more variable or one region more dimorphic? The Anatomical Record. 304(12):2789-2810. https://doi.org/10.1002/ar.24626.

Mires, A., Mahoney, G., Manheim, M., Barrows, E. 2003. Forensic facial reconstruction using Freeform software. Poster Presentation at the 9th Proceedings of the American Academy of Forensic Sciences. Chicargo, Illinois.

Mitteroecker, P. 2009. The developmental basis of variational modularity: Insights from quantitative genetics, morphometrics, and developmental biology. Evolutionary Biology. 36(4):377-85.

Mitteroecker, P., Gunz, P. 2009. Advances in geometric morphometrics. Evolutionary Biology 36(2):235-247.

Moore, K.L., Dalley, A.f., Agur, A.M. 2013. Clinically Oriented Anatomy. 7th Ed. Baltimore: Lippincott Williams and Wilkins.

Morey, R., Rounder, J., Jamil, T. 2015. Computation of Bayes Factors for Common Design. R Package Version 0.9. 12-2.

Munn, L., Stephan, C.N. 2018. Changes in face topography from supine-to-upright position—and soft tissue correction values for craniofacial identification. Forensic Science International. 289:40-50. https://doi.org/10.1016/j.forsciint.2018.05.016.

Musilová, B., Dupej, J., Velemínská, J., Chaumoitre, K., Bruzek, J. 2016. Exocranial surfaces for sex assessment of the human cranium. Forensic Science International. 269:70-77. https://doi.org/10.1016/j.forsciint.2016.11.006.

© University of Pretoria

Naini, F.B. 2011. Facial Aesthetics: Concepts and Clinical Diagnosis. United Kingdom: John Wiley and Sons.

Özer, C.M., Öz, I.I., Serifoglu, I., Büyükuysal, M.Ç., Barut, Ç. 2016. Evaluation of eyeball and orbit in relation to gender and age. Journal of Craniofacial Surgery. 27(8):e793-e800. https://doi.org/10.1097/SCS.0000000000003133.

Phillips, V., Smuts, N. 1996. Facial reconstruction: Utilization of computerized tomography to measure facial tissue thickness in a mixed racial population. Forensic Science International. 83(1):51-9. https://doi.org/10.1016/0379-0738(96)02010-5.

Pierrot-Deseilligny, C. 2009. Effect of gravity on vertical eye position. Annals of the New York Academy of Sciences. 1164(1):155-65. https://doi.org/10.1111/j.1749-6632.2009.03864.x.

Praig, J., Neave, R. 1997. Making faces. London: British Museum Press.

Pretorius, E., Steyn, M., Scholtz, Y. 2006. Investigation into the usability of geometric morphometric analysis in assessment of sexual dimorphism. American Journal of Physical Anthropology. 129(1):64-70. https://doi.org/10.1002/ajpa.20251.

Prevost, A., Muller, S., Lauwers, F., Heuzé, Y. 2023. Quantification of global orbital shape variation. Clinical Anatomy. 36(8):1066-1074. https://doi.org/10.1002/ca.24007.

Price, K.M., Gupta, P.K., Woodward, J.A., Stinnett, S.S., Murchison, A.P. 2009. Eyebrow and eyelid dimensions: an anthropometric analysis of African Americans and Caucasians. Plastic and Reconstructive Surgery. 124(2):615-623. https://doi.org/10.1097/PRS.0b013e3181addc98.

Rana, K., Juniat, V., Yong, W., Casson, R.J., Patel, S., Selva, D. 2023. Normative globe position values on orbital computed tomography in Australians. Canadian Journal of Ophthalmology. 58(5):461-464. https://doi.org/10.1016/j.jcjo.2022.05.004.

Reid, K.M., Martin, L.J., Heathfield, L.J. 2023. Understanding the burden of unidentified bodies: a systematic review. International Journal of Legal Medicine. 137(4):1193-1202. https://doi.org/10.1007/s00414-023-02968-5.

Rhee, S.C., Woo, K.-S., Kwon, B. 2012. Biometric study of eyelid shape and dimensions of different races with references to beauty. Aesthetic Plastic Surgery. 36(5):1236-45. https://doi.org/10.1007/s00266-012-9937-7.

Rhine, J. 1990. Coming to terms with facial reproduction. Journal of Forensic Science. 35(4):960-3. https://doi.org/10.1007/s00266-012-9937-7.

© University of Pretoria

Ridel, A. 2018. An automated computer-assisted approximation of the nose in South Africans from CBCT (Cone Beam Computed Tomography) scans. Dissertation, (PhD.). University of Pretoria. South Africa.

Ridel, A.F., Demeter, F., Liebenberg, J., L'abbé, E.N., Vandermeulen, D., Oettlé, A. 2018. Skeletal dimensions as predictors for the shape of the nose in a South African sample: A Cone-Beam Computed Tomography (CBCT) study. Forensic Science International. 289:18-26. https://doi.org/10.1016/j.forsciint.2018.05.011.

Ridel, A.F., Demeter, F., Galland, M., L'Abbé, E., Vandermeulen, D., Oettlé, A. 2020a. Automatic landmarking as a convenient prerequisite for geometric morphometrics. Validation on Cone Beam Computed Tomography (CBCT)-based shape analysis of the nasal complex. Forensic Science International. 306:110095. https://doi.org/10.1016/j.forsciint.2019.110095.

Ridel, A.F, Demeter, F, L'Abbé, E.N, Vandermeulen, D, Oettlé, A.C. 2020b. Nose approximation among South African groups from cone-beam computed tomography (CBCT) using a new computer-assisted method based on automatic landmarking. Forensic Science International. 313:110357. https://doi.org/10.1016/j.forsciint.2020.110357.

Rohlf, F.J., Slice, D. 1990. Extensions of the Procrustes method for the optimal superimposition of landmarks. Systematic Biology. 39(1):40-59. https://doi.org/10.2307/2992207.

Rohlf, F.J., Marcus, L.F. 1993. A revolution morphometrics. Trends in Ecology & Evolution. 8(4):129-32. https://doi.org/10.1016/0169-5347(93)90024-J.

Rohlf, F.J., Corti, M. 2000. Use of two-block partial least-squares to study covariation in shape. Systematic Biology. 49(4):740-53. https://doi.org/10.1080/106351500750049806.

Rosas, A., Bastir, M. 2002. Thin-plate spline analysis of allometry and sexual dimorphism in the human craniofacial complex. American Journal of Physical Anthropology: The Official Publication of the American Association of Physical Anthropologists, 117:236-245. https://doi.org/10.1002/ajpa.10023.

Rubin, K.M., DeLeon, V.B. 2017. Ancestral variation in orbital rim shape: a three-dimensional pilot study. Journal of Forensic Sciences, 62(6):1575-1581. https://doi.org/10.1111/1556-4029.13493.

Rüdell, A. 2012. Shape analysis of the palpebral fissure in humans. American Journal of Physical Anthropology. 147:256-256.

© University of Pretoria

Scarfe, W.C., Farman, A.G. 2008. What is Cone-Beam CT and How Does it Work? Dental Clinics of North America. 52:707–730. https://doi.org/10.1016/j.cden.2008.05.005.

Schlager, S. 2013a. Soft-tissue reconstruction of the human nose: Population differences and sexual dimorphism. Dissertation, (PhD.). Ludwigs University of Freiburg. Germany.

Schlager, S. 2013b. Morpho: Calculations and visualisations related to geometric morphometrics. R-package version 2.0. 3-1. Available from cran.r-project.org/web/packages/Morpho/index.html.

Schlager, S., Rüdell, A. 2015. Analysis of the human osseous nasal shape—population differences and sexual dimorphism. American Journal of Physical Anthropology. 157(4):571-81. https://doi.org/10.1002/ajpa.22749.

Scrucca, L. 2000. Assessing multivariate normality through interactive dynamic graphics. Quaderni di Statistica. 2:221-40.

See, M,S., Roberts, C., Nduka, C. 2008. Age- and gravity-related changes in facial morphology: 3-dimensional analysis of facial morphology in mother-daughter pairs. Journal of Oral and Maxillofacial Surgery. 66(7):1410–6. https://doi.org/ 10.1016/j.joms.2007.12.041.

Shakoane, G.P., Dussault, M.C., L'Abbé, E.N. 2021. Estimating sex among South African groups using the dentition. Forensic Science International: Reports 4:100233. https://doi.org/10. 5281/zenodo.5226935.

Shin, K.J., Gil, Y.C., Lee, S.H., Kim, J.N., Yoo, J.Y., Kim, S.H., Choi, H.G., Shin, H.J., Koh, K.S., Song, W.C. 2016. Assessment of normal eyeball protrusion using computed tomographic imaging and three-dimensional reconstruction in Korean adults. Seminars in Ophthalmology. 32(5):575-581. https://doi.org/10.3109/08820538.2015.1131837.

Shui, W., Zhou, M., Maddock, S., He, T., Wang, X., Deng, Q. 2017. A PCA-Based method for determining craniofacial relationship and sexual dimorphism of facial shapes. Computers in Biology and Medicine. 90:33-49. https://doi.org/10.1016/j.compbiomed.2017.08.023.

Slice, D.E. 2001. Landmark coordinates aligned by Procrustes analysis do not lie in Kendall's shape space. Systematic biology. 50(1):141-9. https://doi.org/10.1080/10635150119110.

Slice, D.E. 2007. Geometric morphometrics. Annual Review of Anthropology. 36:261-281. https://doi.org/10.1146/annurev.anthro.34.081804.120613

Small, C., Schepartz, L., Hemingway, J., Brits, D. 2018. Three-dimensionally derived interlandmark distances for sex estimation in intact and fragmentary crania. Forensic Science International. 287:127-135. https://doi.org/10.1016/j.forsciint.2018.02.012.

© University of Pretoria

Snow, C.C., Gatliff, B.P., Mcwilliams, K.R. 1970. Reconstruction of facial features from the skull: An evaluation of its usefulness in Forensic Anthropology. American Journal of Physical Anthropology. 33(2):221-7. https://doi.org/10.1002/ajpa.1330330207.

Song, W., Kim, S., Kim, S., Hu, K.-S., Kim, H., Koh, K. 2007. Asymmetry of the palpebral fissure and upper eyelid crease in Koreans. Journal of Plastic, Reconstructive and Aesthetic Surgery. 60(3):251-5. https://doi.org/10.1016/j.bjps.2006.04.027.

Spies, M.J., Finaughty, D.A., Gibbon, V.E., 2018. Forensic taphonomy: scavenger-induced scattering patterns in the temperate Southwestern Cape, South Africa—a first look. Forensic Science International. 290:29-35. https://doi.org/10.1016/j.forsciint.2018.06.015.

Spoor, C.F., Zonneveld, F.W., Macho, G.A. 1993. Linear measurements of cortical bone and dental enamel by Computed Tomography: Applications and problems. American Journal of Physical Anthropology. 91(4):469-84. https://doi.org/ 0.1002/ajpa.1330910405.

Stephan, C.N. 2002. Facial approximation: Globe projection guideline falsified by exophthalmometry literature. Journal of Forensic Science. 47(4):1-6. https://doi.org/10.1520/JFS15457

Stephan, C.N. 2003. Anthropological facial 'reconstruction' - recognizing the fallacies, 'unembracing' the errors, and realizing method limits. Science and Justice. 43(4):193-200. https://doi.org/10.1016/S1355-0306(03)71776-6.

Stephan, C.N., Davidson, P.L. 2008. The placement of the human eyeball and canthi in craniofacial identification. Journal of Forensic Sciences. 53(3):612-9. https://doi.org/10.1111/j.1556-4029.2008.00718.x.

Stephan, C.N., Huang, A.J., Davidson, P.L. 2009. Further evidence on the anatomical placement of the human eyeball for facial approximation and craniofacial superimposition. Journal of Forensic Sciences. 54(2):267-9. https://doi.org/10.1111/j.1556-4029.2008.00982.x.

Stephan, C.N., Preisler, R. 2018. In vivo facial soft tissue thicknesses of adult Australians. Forensic Science International. 282:220-e1. https://doi.org/10.1016/j.forsciint.2017.11.014.

Stephan, C.N., Caple, J.M., Guyomarc'h, P., Claes, P. 2019. An overview of the latest developments in facial imaging. Forensic Science Research. 4:10–28. https://doi.org/10.1080/20961790.2018.1519892.

Standring, S. 2016. Gray's anatomy. 41st Ed. Boston: Elsevier.

© University of Pretoria

Stull, K.E., Kenyhercz, M.W., L'Abbé, E.N. 2014. Ancestry estimation in South Africa using craniometrics and geometric morphometrics. Forensic Science International. 245:206-e1. https://doi.org/10.1016/j.forsciint.2014.10.021.

Suzuki, T. 1973. Reconstitution of a skull. International Criminal Police Review. 264:76-80.

Swennen, G.R., Schutyser, F. 2006. Three-dimensional cephalometry: spiral multi-slice vs cone-beam computed tomography. American Journal of Orthodontics and Dentofacial Orthopedics. 130(3):410-416. https://doi.org/10.1016/j.ajodo.2005.11.035.

Taylor, K.T. 2000. Forensic art and illustration. Bosa Roca, United States: CRC Press.

Taylor, R., Craig, P. 2005. The wisdom of bones: Facial approximation on the skull. In Computer-Graphic Facial Reconstruction. Boston: Elsevier Academic Press:34-56.

Tilotta, F.M., Glaunès, J.A., Richard, F.J., Rozenholc, Y. 2010. A local technique based on vectorized surfaces for craniofacial reconstruction. Forensic Science International. 200:50-59. https://doi.org/10.1016/j.forsciint.2010.03.029.

Toneva, D., Nikolova, S., Tasheva-Terzieva, E., Zlatareva, D., Lazarov, N. 2022. A geometric morphometric study on sexual dimorphism in viscerocranium. Biology. 11(9):1333. https:/doi.org/10.3390/biology11091333.

Turner, W.D., Brown, R.E.B., Kelliher, T.P., Tu, P.H., Taister, M.A., Miller, K.W.P. 2005. A novel method of automated skull registration for forensic facial approximation. Forensic Science International. 154(2-3):49-158. https://doi.org/10.1016/j.forsciint.2004.10.003.

Turner, W., Tu, P., Kelliher, T., Brown, R. 2006. Computer-aided forensics: facial reconstruction. Student Health Technology and Informatics. 119:550-555. PMID: 16404119.

Tyrrell, A.J., Chamberlain, A.T., Evison, M.P., Green, M.A. 1997. Forensic three-dimensional facial reconstruction: Historical review and contemporary developments. Journal of Forensic Science. 42(4):653-61. PMID: 9243827.

Ubelaker, D.H., Bubniak, E. and O'Donnell, G. 1992. Computer-assisted photographic superimposition. Journal of Forensic Sciences, 37(3):750-762.

Ubelaker, D.H. 2015. Craniofacial superimposition: historical review and current issues. Journal of Forensic Science. 60:1412–1419. https://doi.org/10.1111/1556-4029.12842.

Vandermeulen, D., Claes, P., Loeckx, D., De Greef, S., Willems, G., Suetens, P. 2006. Computerized craniofacial reconstruction using CT-derived implicit surface representations. Forensic Science International. 159:S164-S74. https://doi.org/10.1016/j.forsciint.2006.02.036.

© University of Pretoria

Vanezis, P., Vanezis, M., McCombe, G., Niblett, T. 2000. Facial reconstruction using 3-D computer graphics. Forensic Science International, 108(2):81-95. https://doi.org/10.1016/s0379-0738(99)00026-2.

Vanezis, M., Vanezis, P. 2000. Cranio-facial reconstruction in forensic identification—historical development and a review of current practice. Medicine, Science and the Law. 40(3):197-205. https://doi.org/10.1177/002580240004000303.

Verzé, L. 2009. History of facial reconstruction. Acta Biomed. 80(1):5-12. PMID: 19705614.

Warton, D.I., Wright, I.J., Falster, D.S, Westoby, M. 2006. Bivariate line-fitting methods for allometry. Biological Reviews. *81*(2):259-291. https://doi.org/10.1017/S1464793106007007.

Weaver, A.A., Loftis, K.L., Tan, J.C., Duma, S.M., Stitzel, J.D. 2010. CT based three-dimensional measurement of orbit and eye anthropometry. Investigative Ophthalmology and Visual Science. 51(10):4892-4897. https://doi.org/10.1167/iovs.10-5503.

Welcker, H. 1884. Der schädel rafaels und die rafael-portraits. Sendschreiben an geh. Rath dr. H. Schaaffhausen. . Archiv für Anthropologie. 15:417-40.

Wesoly, S., 2017. From syndromes to normal variation: a candidate gene study of interorbital distances. Dissertation, (MSc.). University of Pittsburgh. United States.

Whitnall, S. 1932. The anatomy of the human orbit and accessory organs of vision. 2nd Ed. London: Oxford University Press.

Wilkinson, C.M. 2002. In vivo facial tissue depth measurements for White British children. Journal of Forensic Science. 47(3):459–65. https://doi.org/10.1520/JFS15286J.

Wilkinson, C. 2003. Virtual sculpture as a method of computerized facial reconstruction. Proceedings of the 1st International Conference on Reconstruction of Soft Facial Parts. 17-8.

Wilkinson, C. 2004. Forensic facial reconstruction. New York: Cambridge University Press. https://doi.org/10.1002/oa.790

Wilkinson, C. 2005. Computerized forensic facial reconstruction: a review of current systems. Forensic Science, Medicine and Pathology. 1:173-177. https://doi.org/10.1385/FSMP:1:3:173.

Wilkinson, C. 2010. Facial reconstruction–anatomical art or artistic anatomy? Journal of Anatomy. 216(2):235-50. https://doi.org/10.1111/j.1469-7580.2009.01182.x.

Wilkinson, C., Rynn, C. 2012. Craniofacial identification. Cambridge: Cambridge University Press. https://doi.org/10.1017/CBO9781139049566

© University of Pretoria

Wilkinson, C., Rynn, C., Peters, H., Taister, M., Kau, C.H., Richmond, S. 2006. A blind accuracy assessment of computer-modeled forensic facial reconstruction using Computed Tomography data from live subjects. Forensic Science, Medicine, and Pathology. 2(3):179-87. https://doi.org/10.1007/s12024-006-0007-9.

Wilkinson, C.M., Mautner, S.A. 2003. Measurement of eyeball protrusion and its application in facial reconstruction. Journal of Forensic Science. 48(1):1-5. https://doi.org 10.1520/JFS2002053

Wold, S., Sjöström, M., Eriksson, L. 2001. Pls-regression: A basic tool of chemometrics. Chemometrics and Intelligent Laboratory Systems. 58(2):109-30. https://doi.org/10.1016/S0169-7439(01)00155-1.

Woldegiorgis, B.H., Lin, C.J., Liang, W.Z. 2019. Impact of parallax and interpupillary distance on size judgment performances of virtual objects in stereoscopic displays. Ergonomics 62:76–87. https://doi.org/10.1080/00140139.2018.1526328.

Wolff, E. 1977. Wolff's anatomy of the eye and orbit. London: Chapman & Hall Medical.

Xing, S., Gibbon, V., Clarke, R., Liu, W. 2013. Geometric morphometric analyses of orbit shape in Asian, African, and European human populations. Anthropological Science. 121(1):1-11. https://doi.org/10.1537/ase.120803.

Yoo, J.H., Lee, Y.H., Lee, H., Kim, J.W., Chang, M., Park, M., Baek, S. 2013. Correlation between orbital volume, body mass index, and eyeball position in healthy East Asians. Journal of Craniofacial Surgery. 24(3):822-5. https://doi.org/10.1097/SCS.0b013e3182802600.

Zelditch, M., Swiderski, D., Sheets, D., Fink, W. 2004. Geometric morphometrics for Biologists. San Diego: Elsevier Academic Press. https://doi.org/ 10.1016/B978-012778460-1/50007-7

Zollikofer, C.P., Ponce De León, M.S. 2002. Visualizing patterns of craniofacial shape variation in Homo Sapiens. Proceedings of the Royal Society of London. Series B: Biological Sciences. 269(1493):8011. https://doi.org/10.1098/rspb.2002.1960.

© University of Pretoria

Supplementary Table 1: Comparative analysis of data with existing literature

	This study							Bayes Factor
Linear distance / dimension	**Sex (sample size)**	**Mean ± SD**	**Author**	**Sex (sample size)**	**Population**	**Modality**	**Mean ± SD**	**Log 10 value***
Left Orbital height	Black South African Female (n = 45)	35.73 ± 2.98	Current study, 2024	F (n = 57)	White South African	CBCT	37.39 ± 2.27	1.123
			Ozer et al., 2016	F (n = 83)	Turkish	CT	36.97 ± 2.19	0.458
			Attia et al., 2018	F (n = 48)	Egyptian	CT	35.90 ± 2.80	-0.647
			Kim et al., 2016	F (n = 50)	Korean	CBCT	37.90 ± 2.00	2.421
			Weaver et al., 2010	F (n = 23)	White American	CT	31.75 ± 2.51	3.687
			Ji et al., 2010	F (n = 34)	Chinese	CT	33.22 ± 1.73	3.188
			Guyomarch et al., 2012	F (n = 171)	French	CT	35.40 ± 2.45	-0.652
			Khani et al., 2023	F (n = 51)	Iranian	CT	36.70 ± 1.80	-0.233
			Shin et al., 2016	F (n = 72)	Korean	CT	35.40 ± 2.00	-0.612
			Dayal et al., 2008	F (n = 60)	Black South African	Skulls	33.65 ± 2.25	2.161
			Cappella et al., 2020	F (n = 40)	Italian	Skulls	35.00 ± 2.00	-0.306
	White South African Female (n = 57)	37.39 ± 2.27	Current study, 2024	F (n = 45)	Black South African	CBCT	35.73 ± 2.98	1.123
			Ozer et al., 2016	F (n = 83)	Turkish	CT	36.97 ± 2.19	-0.499
			Attia et al., 2018	F (n = 48)	Egyptian	CT	35.90 ± 2.80	0.971
			Kim et al., 2016	F (n = 50)	Korean	CBCT	37.90 ± 2.00	-0.393
			Weaver et al., 2010	F (n = 23)	White American	CT	31.75 ± 2.51	8.707
			Ji et al., 2010	F (n = 34)	Chinese	CT	33.22 ± 1.73	12.850
			Guyomarch et al., 2012	F (n = 171)	French	CT	35.40 ± 2.45	5.296
			Khani et al., 2023	F (n = 51)	Iranian	CT	36.70 ± 1.80	0.297
			Shin et al., 2016	F (n = 72)	Korean	CT	35.40 ± 2.00	4.266
			Dayal et al., 2008	F (n = 60)	Black South African	Skulls	33.65 ± 2.25	11.827
			Cappella et al., 2020	F (n = 40)	Italian	Skulls	35.00 ± 2.00	4.558
	Black South African Males (n = 52)	37.64 ± 2.33	Current study, 2024	M (n = 52)	White South African	CBCT	38.15 ± 2.27	-0.436
			Ozer et al., 2016	M (n = 115)	Turkish	CT	37.77 ± 2.48	-0.725
			Attia et al., 2018	M (n = 44)	Egyptian	CT	36.90 ± 2.90	-0.312
			Kim et al., 2016	M (n = 50)	Korean	CBCT	38.10 ± 2.30	-0.485

© University of Pretoria

Left Orbital height (cont)	Black South African Males (n = 52)	37.64 ± 2.33	Weaver et al., 2010	M (n = 16)	White American	CT	32.44 ± 1.89	10.168
			Ji et al., 2010	M (n = 30)	Chinese	CT	33.35 ± 1.44	13.189
			Guyomarch et al., 2012	M (n = 204)	French	CT	35.80 ± 2.45	4.165
			Khani et al., 2023	M (n = 100)	Iranian	CT	37.80 ± 2.00	-0.702
			Shin et al., 2016	M (n = 102)	Korean	CT	35.60 ± 1.90	4.804
			Dayal et al., 2008	M (n = 60)	Black South African	Skulls	33.63 ± 2.00	13.341
			Cappella et al., 2020	M (n = 40)	Italian	Skulls	33.63 ± 2.00	5.141
	White South African Males (n = 52)	38.15 ± 2.27	Current study, 2024	M (n = 52)	Black South African	CBCT	37.64 ± 2.33	-0.436
			Ozer et al., 2016	M (n = 115)	Turkish	CT	37.77 ± 2.48	-0.558
			Attia et al., 2018	M (n = 44)	Egyptian	CT	36.90 ± 2.90	0.352
			Kim et al., 2016	M (n = 50)	Korean	CBCT	38.10 ± 2.30	-0.677
			Weaver et al., 2010	M (n = 16)	White American	CT	32.44 ± 1.89	11.801
			Ji et al., 2010	M (n = 30)	Chinese	CT	33.35 ± 1.44	15.787
			Guyomarch et al., 2012	M (n = 204)	French	CT	35.80 ± 2.45	7.423
			Khani et al., 2023	M (n = 100)	Iranian	CT	37.80 ± 2.00	-0.563
			Shin et al., 2016	M (n = 102)	Korean	CT	35.60 ± 1.90	7.893
			Dayal et al., 2008	M (n = 60)	Black South African	Skulls	33.63 ± 2.00	16.465
			Cappella et al., 2020	M (n = 40)	Italian	Skulls	33.63 ± 2.00	7.369
Left Orbital breadth	Black South African Female (n = 45)	40.10 ± 2.79	Current study, 2024	F (n = 57)	White South African	CBCT	40.58 ± 1.45	-0.465
			Ozer et al., 2016	F (n = 83)	Turkish	CT	33.27 ± 1.77	26.086
			Attia et al., 2018	F (n = 48)	Egyptian	CT	37.00 ± 3.60	3.204
			Kim et al., 2016	F (n = 50)	Korean	CBCT	35.90 ± 2.80	7.916
			Weaver et al., 2010	F (n = 23)	White American	CT	36.60 ± 1.71	4.704
			Ji et al., 2010	F (n = 34)	Chinese	CT	38.00 ± 2.25	1.822
			Guyomarch et al., 2012	F (n = 171)	French	CT	37.80 ± 1.98	4.437
			Khani et al., 2023	F (n = 51)	Iranian	CT	34.60 ± 1.60	16.701
			Shin et al., 2016	F (n = 72)	Korean	CT	44.50 ± 1.80	1.476
			Dayal et al., 2008	F (n = 60)	Black South African	Skulls	41.10 ± 1.75	0.173
			Cappella et al., 2020	F (n = 40)	Italian	Skulls	39.00 ± 2.00	2.253

© University of Pretoria

Left orbital breadth (cont)	White South African Female (n = 57)	40.58 ± 1.45	Current study, 2024	F (n = 57)	Black South African	CBCT	40.10 ± 2.79	-0.465
			Ozer et al., 2016	F (n = 83)	Turkish	CT	33.27 ± 1.77	52.670
			Attia et al., 2018	F (n = 48)	Egyptian	CT	37.00 ± 3.60	6.425
			Kim et al., 2016	F (n = 50)	Korean	CBCT	35.90 ± 2.80	15.198
			Weaver et al., 2010	F (n = 23)	White American	CT	36.60 ± 1.71	9.386
			Ji et al., 2010	F (n = 34)	Chinese	CT	38.00 ± 2.25	5.382
			Guyomarch et al., 2012	F (n = 171)	French	CT	37.80 ± 1.98	20.686
			Khani et al., 2023	F (n = 51)	Iranian	CT	34.60 ± 1.60	34.648
			Shin et al., 2016	F (n = 72)	Korean	CT	44.50 ± 1.80	2.020
			Dayal et al., 2008	F (n = 60)	Black South African	Skulls	41.10 ± 1.75	-0.108
			Cappella et al., 2020	F (n = 40)	Italian	Skulls	39.00 ± 2.00	7.291
	Black South African Males (n = 52)	42.30 ± 1.83	Current study, 2024	M (n = 52)	White South African	CBCT	42.74 ± 1.51	-0.338
			Ozer et al., 2016	M (n = 115)	Turkish	CT	34.17 ± 2.10	54.989
			Attia et al., 2018	M (n = 44)	Egyptian	CT	36.70 ± 4.10	10.053
			Kim et al., 2016	M (n = 50)	Korean	CBCT	42.10 ± 1.80	-0.620
			Weaver et al., 2010	M (n = 16)	White American	CT	37.42 ± 2.44	7.302
			Ji et al., 2010	M (n = 30)	Chinese	CT	40.02 ± 1.63	5.004
			Guyomarch et al., 2012	M (n = 204)	French	CT	39.50 ± 1.98	15.908
			Khani et al., 2023	M (n = 100)	Iranian	CT	35.00 ± 1.60	50.163
			Shin et al., 2016	M (n = 102)	Korean	CT	41.70 ± 1.90	8.207
			Dayal et al., 2008	M (n = 60)	Black South African	Skulls	42.62 ± 1.91	-0.538
			Cappella et al., 2020	M (n = 40)	Italian	Skulls	38.00 ± 2.00	9.455
	White South African Males (n = 52)	42.74 ± 1.51	Current study, 2024	M (n = 52)	Black South African	CBCT	42.30 ± 1.83	-0.338
			Ozer et al., 2016	M (n = 115)	Turkish	CT	34.17 ± 2.10	64.572
			Attia et al., 2018	M (n = 44)	Egyptian	CT	36.70 ± 4.10	11.828
			Kim et al., 2016	M (n = 50)	Korean	CBCT	42.10 ± 1.80	0.042
			Weaver et al., 2010	M (n = 16)	White American	CT	37.42 ± 2.44	8.755
			Ji et al., 2010	M (n = 30)	Chinese	CT	40.02 ± 1.63	7.913
			Guyomarch et al., 2012	M (n = 204)	French	CT	39.50 ± 1.98	26.203
			Khani et al., 2023	M (n = 100)	Iranian	CT	35.00 ± 1.60	60.195
			Shin et al., 2016	M (n = 102)	Korean	CT	41.70 ± 1.90	6.698
			Dayal et al., 2008	M (n = 60)	Black South African	Skulls	42.62 ± 1.91	-0.670

© University of Pretoria

			Cappella et al., 2020	M (n = 40)	Italian	Skulls	38.00 ± 2.00	12.883
Left Orbital Index	Black South African Females (n = 45)	89.14 ± 5.09	Current study, 2024	F (n = 57)	White South African	CBCT	92.23 ± 6.12	0.787
			Attia et al., 2018	F (n = 48)	Egyptian	CT	97.90 ± 10.60	3.950
			Khani et al., 2023	F (n = 51)	Iranian	CT	108.59 ± 6.03	27.186
	White South African Females (n = 57)	92.23 ± 6.12	Current study, 2024	F (n = 45)	Black South African	CBCT	89.14 ± 5.09	0.787
			Attia et al., 2018	F (n = 48)	Egyptian	CT	97.90 ± 10.60	1.332
			Khani et al., 2023	F (n = 51)	Iranian	CT	108.59 ± 6.03	22.433
	Black South African Males (n = 52)	89.04 ± 5.12	Current study, 2024	M (n = 52)	White South African	CBCT	89.72 ± 4.89	-0.591
			Attia et al., 2018	M (n = 44)	Egyptian	CT	101.40 ± 11.40	6.658
			Khani et al., 2023	M (n = 100)	Iranian	CT	108.25 ±7.38	37.557
	White South African Males (n = 52)	89.72 ± 4.89	Current study, 2024	M (n = 52)	Black South African	CBCT	89.04 ± 5.12	-0.591
			Attia et al., 2018	M (n = 44)	Egyptian	CT	101.40 ± 11.40	6.053
			Khani et al., 2023	M (n = 100)	Iranian	CT	108.25 ±7.38	36.906
Interorbital distance	Black South African Females (n = 45)	21.65 ± 2.68	Current study, 2024	F (n = 57)	White South African	CBCT	19.09 ± 2.35	3.880
			Ji et al., 2010	F (n = 34)	Chinese	CT	25.11 ± 2.25	5.644
			Attia et al., 2018	F (n = 48)	Egyptian	CT	24.50 ± 4.70	1.746
			Khani et al., 2023	F (n = 51)	Iranian	CT	21.80 ± 2.10	-0.650
			Weaver et al., 2010	F (n = 23)	White American	CT	25.11 ± 2.25	3.458
			Cappella et al., 2020	F (n = 40)	Italian	Skulls	23.00 ± 2.00	-0.555
	White South African Females (n = 57)	19.09 ± 2.35	Current study, 2024	F (n = 45)	Black South African	CBCT	21.65 ± 2.68	3.735
			Ji et al., 2010	F (n = 34)	Chinese	CT	25.11 ± 2.25	17.324
			Attia et al., 2018	F (n = 48)	Egyptian	CT	24.50 ± 4.70	7.967
			Khani et al., 2023	F (n = 51)	Iranian	CT	21.80 ± 2.10	6.203
			Weaver et al., 2010	F (n = 23)	White American	CT	25.11 ± 2.25	10.920
			Cappella et al., 2020	F (n = 40)	Italian	Skulls	23.00 ± 2.00	6.503
	Black South African Males (n = 52)	21.65 ± 2.68	Current study, 2024	M (n = 52)	White South African	CBCT	22.62 ± 2.80	3.735
			Ji et al., 2010	M (n = 30)	Chinese	CT	27.18 ± 2.67	7.623
			Attia et al., 2018	M (n = 44)	Egyptian	CT	27.40 ± 11.3	0.740
			Khani et al., 2023	M (n = 100)	Iranian	CT	23.10 ± 2.70	-0.533
			Weaver et al., 2010	M (n = 16)	White American	CT	27.18 ± 2.76	4.657
			Cappella et al., 2020	M (n = 40)	Italian	Skulls	22.00 ± 2.00	-0.547

© University of Pretoria

Interorbital distance (cont)	White South African Males (n = 52)	22.62 ± 2.80	Current study, 2024	M (n = 52)	Black South African	CBCT	21.65 ± 2.68	3.735
			Ji et al., 2010	M (n = 30)	Chinese	CT	27.18 ± 2.67	16.460
			Attia et al., 2018	M (n = 44)	Egyptian	CT	27.40 ± 11.3	2.542
			Khani et al., 2023	M (n = 100)	Iranian	CT	23.10 ± 2.70	8.165
			Weaver et al., 2010	M (n = 16)	White American	CT	27.18 ± 2.76	10.485
			Cappella et al., 2020	M (n = 40)	Italian	Skulls	22.00 ± 2.00	6.103
Bizygomatic breadth	Black South African Females (n = 45)	121.80 ± 7.87	Current study, 2024	F (n = 57)	White South African	CBCT	123.03 ± 4.97	-0.516
			Attia et al., 2018	F (n = 48)	Egyptian	CT	95.80 ± 4.90	29.858
			Farkas et al., 2007	F (n = 50)	African American	Patients	130.50 ± 4.50	6.404
			Farkas et al., 2007	F (n = 200)	North American white	Patients	130.00 ± 4.60	7.812
			Byat et al., 2018	F (n = 100)	Iranian	Patients	129.20 ± 4.18	2.838
			Dayal et al., 2008	F (n = 60)	Black South African	Patients	123.97 ± 5.03	-0.178
			Celebi et al., 2018	F (n = 60)	Egyptian	Patients	98.73 ± 6.45	26.303
			Celebi et al., 2018	F (n = 67)	Italian	Patients	98.29 ± 4.86	30.794
			Celebi et al., 2017	F (n = 68)	Colombian	Patients	136.18 ± 5.77	15.223
			Celebi et al., 2017	F (n = 48)	Mexican American	Patients	116.71 ± 4.88	1.874
	White South African Females (n = 57)	123.03 ± 4.97	Current study, 2024	F (n = 52)	Black South African	CBCT	121.80 ± 7.87	-0.516
			Attia et al., 2018	F (n = 48)	Egyptian	CT	95.80 ± 4.90	46.442
			Farkas et al., 2007	F (n = 50)	African American	Patients	130.50 ± 4.50	9.878
			Farkas et al., 2007	F (n = 200)	North American white	Patients	130.00 ± 4.60	15.355
			Byat et al., 2018	F (n = 100)	Iranian	Patients	129.20 ± 4.18	4.610
			Dayal et al., 2008	F (n = 60)	Black South African	Patients	123.97 ± 5.03	-0.504
			Celebi et al., 2018	F (n = 60)	Egyptian	Patients	98.73 ± 6.45	40.960
			Celebi et al., 2018	F (n = 67)	Italian	Patients	98.29 ± 4.86	51.000
			Celebi et al., 2017	F (n = 68)	Colombian	Patients	136.18 ± 5.77	23.120
			Celebi et al., 2017	F (n = 48)	Mexican American	Patients	116.71 ± 4.88	6.604
	Black South African Males (n = 52)	132.19 ± 7.21	Current study, 2024	M (n = 52)	White South African	CBCT	131.35 ± 4.33	-0.583
			Attia et al., 2018	M (n = 43)	Egyptian	CT	98.60 ± 4.10	43.957
			Farkas et al., 2007	M (n = 50)	African American	Patients	139.00 ± 5.30	4.550
			Farkas et al., 2007	M (n = 109)	North American white	Patients	139.10 ± 5.30	6.235
			Byat et al., 2018	M (n= 100)	Iranian	Patients	130.90 ± 4.43	-0.462
			Dayal et al., 2008	M (n = 60)	Black South African	Patients	130.60 ± 4.71	-0.338

© University of Pretoria

Bizygomatic breadth (cont)	Black South African Males (n = 52)	132.19 ± 7.21	Celebi et al., 2018	M (n = 60)	Egyptian	Patients	104.95 ± 7.31	34.489
			Celebi et al., 2018	M (n = 72)	Italian	Patients	105.57 ± 6.37	39.249
			Celebi et al., 2017	M (n = 63)	Colombian	Patients	142.67 ± 5.98	10.512
			Celebi et al., 2017	M (n = 44)	Mexican American	Patients	127.11 ± 6.97	1.602
	White South African Males (n = 52)	131.35 ± 4.33	Current study, 2024	M (n = 52)	Black South African	CBCT	132.19 ± 7.21	-0.583
			Attia et al., 2018	M (n = 43)	Egyptian	CT	98.60 ± 4.10	54.318
			Farkas et al., 2007	M (n = 50)	African American	Patients	139.00 ± 5.30	9.365
			Farkas et al., 2007	M (n = 109)	North American white	Patients	139.10 ± 5.30	15.043
			Byat et al., 2018	M (n= 100)	Iranian	Patients	130.90 ± 4.43	-0.665
			Dayal et al., 2008	M (n = 60)	Black South African	Patients	130.60 ± 4.71	-0.547
			Celebi et al., 2018	M (n = 60)	Egyptian	Patients	104.95 ± 7.31	41.167
			Celebi et al., 2018	M (n = 72)	Italian	Patients	105.57 ± 6.37	49.200
			Celebi et al., 2017	M (n = 63)	Colombian	Patients	142.67 ± 5.98	18.068
			Celebi et al., 2017	M (n = 44)	Mexican American	Patients	127.11 ± 6.97	1.604
Left ocular height	Black South African Females (n = 45)	23.77 ± 1.44	Current study, 2024	F (n = 57)	White South African	CBCT	24.60 ± 1.86	0.547
			Shin et al., 2016	F (n = 72)	Korean	CT	26.60 ± 1.80	12.784
	White South African Females (n = 57)	24.60 ± 1.86	Current study, 2024	F (n = 45)	Black South African	CBCT	23.77 ± 1.44	0.547
			Shin et al., 2016	F (n = 72)	Korean	CT	26.60 ± 1.80	6.037
Left ocular height	Black South African Males (n = 52)	23.88 ± 1.43	Current study, 2024	M (n = 52)	White South African	CBCT	25.23 ± 1.55	3.149
			Shin et al., 2016	M (n = 102)	Korean	CT	26.50 ± 1.80	14.656
	White South African Males (n = 52)	25.23 ± 1.55	Current study, 2024	M (n = 52)	Black South African	CBCT	23.88 ± 1.43	3.149
			Shin et al., 2016	M (n = 102)	Korean	CT	26.50 ± 1.80	3.193
Left Ocular breadth	Black South African Females (n = 45)	22.44 ± 1.60	Current study, 2024	F (n = 57)	White South African	CBCT	23.34 ± 1.47	0.934
			Shin et al., 2016	F (n = 72)	Korean	CT	25.70 ± 1.30	15.039
			Rana et al., 2022	F (n = 111)	Australian	MRI	25.20 ± 1.00	20.898
	White South African Females (n = 57)	23.34 ± 1.47	Current study, 2024	F (n = 45)	Black South African	CBCT	22.44 ± 1.60	0.934
			Shin et al., 2016	F (n = 72)	Korean	CT	25.70 ± 1.30	15.039
			Rana et al., 2022	F (n = 111)	Australian	MRI	25.20 ± 1.00	16.207

© University of Pretoria

Left Ocular breadth	Black South African Males (n = 52)	23.23 ± 1.20	Current study, 2024	M (n = 52)	White South African	CBCT	23.55 ± 1.39	-0.338
			Shin et al., 2016	M (n = 102)	Korean	CT	26.20 ± 1.30	23.509
			Rana et al., 2022	M (n = 90)	Australian	MRI	25.80 ± 1.00	24.179
	White South African Males (n = 52)	26.20 ± 1.30	Current study, 2024	M (n = 52)	Black South African	CBCT	23.23 ± 1.20	-0.338
			Shin et al., 2016	M (n = 102)	Korean	CT	26.20 ± 1.30	23.509
			Rana et al., 2022	M (n = 90)	Australian	MRI	25.80 ± 1.00	17.968
Left ocular / axial length	Black South African Females (n = 45)	21.98 ± 1.23	Current study, 2024	F (n = 57)	White South African	CBCT	23.14 ± 1.30	3.170
			Ozer et al., 2016	F (n = 83)	Turkish	CT	22.76 ± 6.38	-0.479
			Wilkinson and Mautner, 2003	F (n = 28)	UK	MRI	23.42 ± 1.41	2.793
			Rana et al., 2022	F (n = 111)	Australian	MRI	24.70 ± 0.95	24.001
			Shin et al., 2016	F (n = 72)	Korean	CT	26.10 ± 1.10	32.391
	White South African Females (n = 57)	21.98 ± 1.23	Current study, 2024	F (n = 45)	Black South African	CBCT	21.98 ± 1.23	3.170
			Ozer et al., 2016	F (n = 83)	Turkish	CT	22.76 ± 6.38	-0.680
			Wilkinson and Mautner, 2003	F (n = 28)	UK	MRI	23.42 ± 1.41	-0.476
			Rana et al., 2022	F (n = 111)	Australian	MRI	24.70 ± 0.95	10.522
			Shin et al., 2016	F (n = 72)	Korean	CT	26.10 ± 1.10	23.502
	Black South African Males (n = 52)	23.50 ± 1.22	Current study, 2024	M (n = 52)	White South African	CBCT	23.27 ± 1.17	-0.497
			Ozer et al., 2016	M (n = 115)	Turkish	CT	23.25 ± 0.88	-0.399
			Wilkinson and Mautner, 2003	M (n = 11)	UK	MRI	23.21 ± 1.76	-0.448
			Rana et al., 2022	M (n = 90)	Australian	MRI	25.20 ± 1.10	10.673
			Shin et al., 2016	M (n = 102)	Korean	CT	26.60 ± 1.10	29.028
	White South African Males (n = 52)	23.27 ± 1.17	Current study, 2024	M (n = 52)	Black South African	CBCT	23.50 ± 1.22	-0.497
			Ozer et al., 2016	M (n = 115)	Turkish	CT	23.25 ± 0.88	-0.744
			Wilkinson and Mautner, 2003	M (n = 11)	UK	MRI	23.21 ± 1.76	-0.492
			Rana et al., 2022	M (n = 90)	Australian	MRI	25.20 ± 1.10	14.163
			Shin et al., 2016	M (n = 102)	Korean	CT	26.60 ± 1.10	33.531
Left eye protrusion from LOM (dLOM - oa	Black South African Females (n = 45)	24.02 ± 2.26	Current study, 2024	F (n = 55)	White South African	CBCT	23.59 ± 1.61	-0.453
			Guyomarch et al., 2012	F (n = 171)	French	CT	17.60 ± 2.32	37.513
			Barretto and Mathog, 1999	F (n = 28)	Black American	Patients	17.27 ± 1.41	21.412
			Barretto and Mathog, 1999	F (n = 31)	White American	Patients	16.02 ± 2.23	21.214

© University of Pretoria

Left eye protrusion from LOM (dLOM –oa)	Black South African Fem (n=45)	24.02 ± 2.26	Dunsky, 1992	F (n = 170)	Black American	Patients	17.46 ± 2.64	36.921
			Kim et al., 2016	F (n = 50)	Korean	CBCT	16.40 ± 1.30	31.641
	White South African Females (n = 55)	23.59 ± 1.61	Current study, 2024	F (n = 45)	Black South African	CBCT	24.02 ± 2.26	-0.453
			Guyomarch et al., 2012	F (n = 171)	French	CT	17.60 ± 2.32	52.174
			Barretto and Mathog, 1999	F (n = 28)	Black American	Patients	17.27 ± 1.41	27.121
			Barretto and Mathog, 1999	F (n = 31)	White American	Patients	16.02 ± 2.23	24.819
			Dunsky, 1992	F (n = 170)	Black American	Patients	17.46 ± 2.64	49.906
			Kim et al., 2016	F (n = 50)	Korean	CBCT	16.40 ± 1.30	42.239
	Black South African Males (n = 49)	24.60 ± 1.91	Current study, 2024	M (n = 48)	White South African	CBCT	25.16 ± 1.81	-0.249
			Guyomarch et al., 2012	M (n = 204)	French	CT	18.70 ± 2.32	45.334
			Barretto and Mathog, 1999	M (n = 33)	Black American	Patients	18.23 ±2.19	19.162
			Barretto and Mathog, 1999	M (n = 34)	White American	Patients	17.01 ± 2.70	20.205
			Dunsky, 1992	M (n = 139)	Black American	Patients	18.20 ± 2.97	36.788
			Kim et al., 2016	M (n = 50)	Korean	CBCT	17.10 ± 1.30	37.088
	White South African Males (n = 48)	25.16 ± 1.81	Current study, 2024	M (n = 49)	Black South African	CBCT	24.60 ± 1.91	-0.249
			Guyomarch et al., 2012	M (n = 204)	French	CT	18.70 ± 2.32	53.298
			Barretto and Mathog, 1999	M (n = 33)	Black American	Patients	18.23 ±2.19	21.438
			Barretto and Mathog, 1999	M (n = 34)	White American	Patients	17.01 ± 2.70	22.128
			Dunsky, 1992	M (n = 139)	Black American	Patients	18.20 ± 2.97	42.157
			Kim et al., 2016	M (n = 50)	Korean	CBCT	17.10 ± 1.30	40.445
Left eye protrusion from IOM	Black South African Females (n = 45)	20.51 ± 2.90	Current study, 2024	F (n = 55)	White South African	CBCT	20.13 ± 1.80	-0.561
			Guyomarch et al., 2012	F (n = 171)	French	CT	19.70 ± 1.72	-0.109
			Kim et al., 2016	F (n = 50)	Korean	CBCT	16.70 ± 1.70	8.675
	White South African Females (n = 55)	20.13 ± 1.80	Current study, 2024	F (n = 45)	Black South African	CBCT	20.51 ± 2.90	-0.561
			Guyomarch et al., 2012	F (n = 171)	French	CT	19.70 ± 1.72	-0.290
			Kim et al., 2016	F (n = 50)	Korean	CBCT	16.70 ± 1.70	13.829
	Black South African Males (n = 49)	19.70 ± 1.99	Current study, 2024	M (n = 48)	White South African	CBCT	20.42 ± 1.75	0.013
			Guyomarch et al., 2012	M (n = 204)	French	CT	19.90 ± 1.72	-0.682
			Kim et al., 2016	M (n = 50)	Korean	CBCT	16.90 ± 1.40	9.531

© University of Pretoria

left eye protrusion from IOM	White South African Males (n = 48)	20.42 ± 1.75	Current study, 2024	M (n = 49)	Black South African	CBCT	19.70 ± 1.99	0.013
			Guyomarch et al., 2012	M (n = 204)	French	CT	19.90 ± 1.72	-0.074
			Kim et al., 2016	M (n = 50)	Korean	CBCT	16.90 ± 1.40	15.445
Left eye protrusion from MOM	Black South African Females (n = 45)	23.35 ± 2.47	Current study, 2024	F (n = 55)	White South African	CBCT	22.81 ± 1.67	-0.373
			Guyomarch et al., 2012	F (n = 171)	French	CT	21.70 ± 1.81	2.678
			Kim et al., 2016	F (n = 50)	Korean	CBCT	22.30 ± 1.40	0.524
	White South African Females (n = 55)	22.81 ± 1.67	Current study, 2024	F (n = 45)	Black South African	CBCT	23.35 ± 2.47	-0.373
			Guyomarch et al., 2012	F (n = 171)	French	CT	21.70 ± 1.81	2.687
			Kim et al., 2016	F (n = 50)	Korean	CBCT	22.30 ± 1.40	-0.128
MOM - oa	Black South African Males (n = 49)	23.20 ± 1.97	Current study, 2024	M (n = 48)	White South African	CBCT	24.33 ± 1.71	1.037
			Guyomarch et al., 2012	M (n = 204)	French	CT	22.80 ± 1.81	-0.430
			Kim et al., 2016	M (n = 50)	Korean	CBCT	23.50 ± 1.70	-0.547
	White South African Males (n = 48)	24.33 ± 1.71	Current study, 2024	M (n = 49)	Black South African	CBCT	23.20 ± 1.97	1.037
			Guyomarch et al., 2012	M (n = 204)	French	CT	22.80 ± 1.81	5.117
			Kim et al., 2016	M (n = 50)	Korean	CBCT	23.50 ± 1.70	0.428
Left eye protrusion from SOM	Black South African Females (n = 45)	21.31 ± 2.74	Current study, 2024	F (n = 55)	White South African	CBCT	19.59 ± 2.06	1.606
			Guyomarch et al., 2012	F (n = 171)	French	CT	15.70 ± 1.91	25.229
			Kim et al., 2016	F (n = 50)	Korean	CBCT	20.70 ± 1.80	-0.358
	White South African Females (n = 55)	19.59 ± 2.06	Current study, 2024	F (n = 45)	Black South African	CBCT	21.31 ± 2.74	1.606
			Guyomarch et al., 2012	F (n = 171)	French	CT	15.70 ± 1.91	23.745
			Kim et al., 2016	F (n = 50)	Korean	CBCT	20.70 ± 1.80	0.986
	Black South African Males (n = 49)	20.84 ± 2.04	Current study, 2024	M (n = 48)	White South African	CBCT	19.65 ± 1.85	1.028
			Guyomarch et al., 2012	M (n = 204)	French	CT	16.00 ± 1.91	33.508
			Kim et al., 2016	M (n = 50)	Korean	CBCT	20.50 ± 1.50	-0.503
	White South African Males (n = 48)	19.65 ± 1.85	Current study, 2024	M (n = 49)	Black South African	CBCT	20.84 ± 2.04	1.028
			Guyomarch et al., 2012	M (n = 204)	French	CT	16.00 ± 1.91	23.859
			Kim et al., 2016	M (n = 50)	Korean	CBCT	20.50 ± 1.50	0.504
Left palpebral fissure height	Black South African Females (n = 33)	8.86 ± 1.23	Current study, 2024	F (n = 57)	White South African	CBCT	9.72 ± 1.88	0.632
			Kunjur et al., 2006	F (n = 13)	White Europeans	Photos	9.80 ± 1.20	0.436
			Kunjur et al., 2006	F (n = 13)	Indians	Photos	10.20 ± 1.20	1.340
			Kunjur et al., 2006	F (n = 13)	Chinese	Photos	10.60 ± 0.90	3.575

© University of Pretoria

Left Palpebral fissure height (cont)	Black South African Females (n = 33)	8.86 ± 1.23	Barretto and Mathog, 1999	F (n = 28)	Black Americans	Patients	10.56 ± 1.58	2.944
			Barretto and Mathog, 1999	F (n = 31)	White Americans	Patients	10.65 ± 1.21	4.795
			Farkas et al., 2007	F (n = 50)	Black Americans	Patients	10.40 ± 1.20	4.696
			Farkas et al., 2007	F (n = 200)	White Americans	Patients	10.90 ± 1.20	13.253
			Byat et al., 2018	F (n = 100)	Iranian	Patients	14.96 ± 6.86	11.099
			Price et al., 2009	F (n = 30)	Black American	Photos	9.50 ± 1.40	0.077
			Price et al., 2009	F (n = 24)	White American	Photos	10.30 ± 1.00	3.226
			Song et al., 2007	F (n = 321)	Korean	Photos	10.00 ± 1.70	3.911
	White South African Females (n = 57)	9.72 ± 1.88	Current study, 2024	F (n = 33)	Black South African	CBCT	8.86 ± 1.23	0.632
			Kunjur et al., 2006	F (n = 13)	White Europeans	Photos	9.80 ± 1.20	-0.514
			Kunjur et al., 2006	F (n = 13)	Indians	Photos	10.20 ± 1.20	-0.290
			Kunjur et al., 2006	F (n = 13)	Chinese	Photos	10.60 ± 0.90	0.547
			Barretto and Mathog, 1999	F (n = 28)	Black Americans	Patients	10.56 ± 1.58	0.241
			Barretto and Mathog, 1999	F (n = 31)	White Americans	Patients	10.65 ± 1.21	0.825
			Farkas et al., 2007	F (n = 50)	Black Americans	Patients	10.40 ± 1.20	0.288
			Farkas et al., 2007	F (n = 200)	White Americans	Patients	10.90 ± 1.20	3.178
			Byat et al., 2018	F (n = 100)	Iranian	Patients	14.96 ± 6.86	8.428
			Price et al., 2009	F (n = 30)	Black American	Photos	9.50 ± 1.40	-0.559
			Price et al., 2009	F (n = 24)	White American	Photos	10.30 ± 1.00	-0.007
			Song et al., 2007	F (n = 321)	Korean	Photos	10.00 ± 1.70	-0.583
	Black South African Males (n = 52)	8.95 ± 1.15	Current study, 2024	M (n = 52)	White South African	CBCT	8.99 ± 1.33	-0.678
			Kunjur et al., 2006	M (n = 13)	White Europeans	Photos	10.20 ± 1.60	0.678
			Kunjur et al., 2006	M (n = 13)	Indians	Photos	10.50 ± 0.70	5.223
			Kunjur et al., 2006	M (n = 13)	Chinese	Photos	9.50 ± 1.40	-0.221
			Barretto and Mathog, 1999	M (n = 33)	Black Americans	Patients	9.84 ± 1.61	0.769
			Barretto and Mathog, 1999	M (n = 34)	White Americans	Patients	10.25 ± 1.21	3.641
			Farkas et al., 2007	M (n = 50)	Black Americans	Patients	10.00 ± 1.10	3.329
			Farkas et al., 2007	M (n = 109)	White Americans	Patients	10.80 ± 0.90	15.953
			Byat et al., 2018	M (n = 100)	Iranian	Patients	14.01 ± 4.08	19.214
			Price et al., 2009	M (n = 26)	Black American	Photos	9.80 ± 1.70	0.359
			Price et al., 2009	M (n = 32)	White American	Photos	9.40 ± 1.30	-0.147
			Song et al., 2007	M (n = 273)	Korean	Photos	9.90 ± 1.60	4.335

© University of Pretoria

Left palpebral fissure height (cont)	White South African Males (n = 52)	8.99 ± 1.33	Current study, 2024	M (n = 52)	Black South African	CBCT	8.95 ± 1.15	-0.678
			Kunjur et al., 2006	M (n = 13)	White Europeans	Photos	10.20 ± 1.60	0.563
			Kunjur et al., 2006	M (n = 13)	Indians	Photos	10.50 ± 0.70	4.405
			Kunjur et al., 2006	M (n = 13)	Chinese	Photos	9.50 ± 1.40	-0.274
			Barretto and Mathog, 1999	M (n = 33)	Black Americans	Patients	9.84 ± 1.61	0.553
			Barretto and Mathog, 1999	M (n = 34)	White Americans	Patients	10.25 ± 1.21	2.990
			Farkas et al., 2007	M (n = 50)	Black Americans	Patients	10.00 ± 1.10	2.532
			Farkas et al., 2007	M (n = 109)	White Americans	Patients	10.80 ± 0.90	12.572
			Byat et al., 2018	M (n = 100)	Iranian	Patients	14.01 ± 4.08	18.332
			Price et al., 2009	M (n = 26)	Black American	Photos	9.80 ± 1.70	0.220
			Price et al., 2009	M (n = 32)	White American	Photos	9.40 ± 1.30	-0.269
			Song et al., 2007	M (n = 273)	Korean	Photos	9.90 ± 1.60	3.006
Left palpebral fissure width	Black South African Females (n = 45)	26.87 ± 3.43	Current study, 2024	F (n = 57)	White South African	CBCT	25.90 ± 1.62	-0.099
			Kunjur et al., 2006	F (n = 13)	White Europeans	Photos	26.50 ± 2.20	-0.475
			Kunjur et al., 2006	F (n = 13)	Indians	Photos	28.20 ± 2.10	-0.013
			Kunjur et al., 2006	F (n = 13)	Chinese	Photos	26.80 ± 2.30	-0.511
			Barretto and Mathog, 1999	F (n = 28)	Black Americans	Patients	31.46 ± 2.20	6.714
			Barretto and Mathog, 1999	F (n = 31)	White Americans	Patients	29.40 ± 2.46	1.844
			Farkas et al., 2007	F (n = 50)	Black Americans	Patients	32.20 ± 2.00	11.396
			Farkas et al., 2007	F (n = 200)	White Americans	Patients	30.70 ± 1.20	9.265
			Amini et al., 2014	F (n = 50)	Iranian	Patients	31.00 ± 1.70	7.807
			Byat et al., 2018	F (n = 100)	Iranian	Patients	28.93 ± 4.28	1.106
			Celebi et al., 2017	F (n = 68)	Colombian	Patients	29.56 ± 2.12	3.296
			Celebi et al., 2017	F (n = 48)	Mexican American	Patients	29.70 ± 1.79	3.591
			Celebi et al., 2018	F (n = 67)	Italian	Patients	30.39 ± 2.06	5.866
			Celebi et al., 2018	F (n = 60)	Egyptian	Patients	29.47 ± 2.10	2.950
			Song et al., 2007	F (n = 321)	Korean	Photos	27.60 ± 3.50	-0.415
			Price et al., 2009	F (n = 30)	Black American	Photos	27.00 ± 1.40	-0.605
			Price et al., 2009	F (n = 24)	White American	Photos	27.20 ± 1.80	-0.539

© University of Pretoria

Left palpebral fissure width (cont)	White South African Females (n = 57)	25.90 ± 1.62	Current study, 2024	F (n = 45)	Black South African	CBCT	26.87 ± 3.43	-0.099
			Kunjur et al., 2006	F (n = 13)	White Europeans	Photos	26.50 ± 2.20	-0.371
			Kunjur et al., 2006	F (n = 13)	Indians	Photos	28.20 ± 2.10	1.783
			Kunjur et al., 2006	F (n = 13)	Chinese	Photos	26.80 ± 2.30	-0.211
			Barretto and Mathog, 1999	F (n = 28)	Black Americans	Patients	31.46 ± 2.20	16.350
			Barretto and Mathog, 1999	F (n = 31)	White Americans	Patients	29.40 ± 2.46	7.405
			Farkas et al., 2007	F (n = 50)	Black Americans	Patients	32.20 ± 2.00	29.859
			Farkas et al., 2007	F (n = 200)	White Americans	Patients	30.70 ± 1.20	53.074
			Amini et al., 2014	F (n = 50)	Iranian	Patients	31.00 ± 1.70	26.121
			Byat et al., 2018	F (n = 100)	Iranian	Patients	28.93 ± 4.28	6.566
			Celebi et al., 2017	F (n = 68)	Colombian	Patients	29.56 ± 2.12	16.651
			Celebi et al., 2017	F (n = 48)	Mexican American	Patients	29.70 ± 1.79	16.564
			Celebi et al., 2018	F (n = 67)	Italian	Patients	30.39 ± 2.06	22.792
			Celebi et al., 2018	F (n = 60)	Egyptian	Patients	29.47 ± 2.10	14.937
			Song et al., 2007	F (n = 321)	Korean	Photos	27.60 ± 3.50	5.987
			Price et al., 2009	F (n = 30)	Black American	Photos	27.00 ± 1.40	1.348
	Black South African Males (n = 52)	28.22 ± 2.10	Price et al., 2009	F (n = 24)	White American	Photos	27.20 ± 1.80	1.077
			Current study, 2024	M (n = 52)	White South African	CBCT	27.16 ± 2.14	0.554
			Kunjur et al., 2006	M (n = 13)	White Europeans	Photos	27.60 ± 1.90	-0.334
			Kunjur et al., 2006	M (n = 13)	Indians	Photos	30.30 ± 1.70	1.823
			Kunjur et al., 2006	M (n = 13)	Chinese	Photos	28.80 ± 2.10	-0.380
			Barretto and Mathog, 1999	M (n = 33)	Black Americans	Patients	32.34 ± 2.31	9.544
			Barretto and Mathog, 1999	M (n = 34)	White Americans	Patients	29.51 ± 2.19	0.724
			Farkas et al., 2007	M (n = 50)	Black Americans	Patients	32.90 ± 1.60	19.269
			Farkas et al., 2007	M (n = 109)	White Americans	Patients	31.30 ± 1.20	14.995
			Amini et al., 2014	M (n = 50)	Iranian	Patients	31.60 ± 1.90	10.529
			Byat et al., 2018	M (n = 100)	Iranian	Patients	28.93 ± 4.73	-0.414
			Celebi et al., 2017	M (n = 63)	Colombian	Patients	31.54 ± 1.79	11.923
			Celebi et al., 2017	M (n = 44)	Mexican American	Patients	30.89 ± 2.17	5.641
			Celebi et al., 2018	M (n = 72)	Italian	Patients	30.37 ± 1.56	6.179
			Celebi et al., 2018	M (n = 60)	Egyptian	Patients	30.33 ± 2.24	4.076
			Song et al., 2007	M (n = 273)	Korean	Photos	29.00 ± 3.00	0.251

© University of Pretoria

Left palpebral fissure width (cont)	Black South African Males (n = 52)	28.22 ± 2.10	Price et al., 2009	M (n = 26)	Black American	Photos	27.50 ± 1.40	-0.012
			Price et al., 2009	M (n = 32)	White American	Photos	26.70 ± 1.70	1.747
	White South African Males (n = 52)	27.16 ± 2.14	Current study, 2024	M (n = 52)	Black South African	CBCT	28.22 ± 2.10	0.554
			Kunjur et al., 2006	M (n = 13)	White Europeans	Photos	27.60 ± 1.90	-0.426
			Kunjur et al., 2006	M (n = 13)	Indians	Photos	30.30 ± 1.70	4.401
			Kunjur et al., 2006	M (n = 13)	Chinese	Photos	28.80 ± 2.10	0.555
			Barretto and Mathog, 1999	M (n = 33)	Black Americans	Patients	32.34 ± 2.31	13.496
			Barretto and Mathog, 1999	M (n = 34)	White Americans	Patients	29.51 ± 2.19	3.551
			Farkas et al., 2007	M (n = 50)	Black Americans	Patients	32.90 ± 1.60	24.684
			Farkas et al., 2007	M (n = 109)	White Americans	Patients	31.30 ± 1.20	23.444
			Amini et al., 2014	M (n = 50)	Iranian	Patients	31.60 ± 1.90	15.923
			Byat et al., 2018	M (n = 100)	Iranian	Patients	28.93 ± 4.73	1.216
			Celebi et al., 2017	M (n = 63)	Colombian	Patients	31.54 ± 1.79	18.071
			Celebi et al., 2017	M (n = 44)	Mexican American	Patients	30.89 ± 2.17	10.182
			Celebi et al., 2018	M (n = 72)	Italian	Patients	30.37 ± 1.56	12.569
			Celebi et al., 2018	M (n = 60)	Egyptian	Patients	30.33 ± 2.24	8.912
			Song et al., 2007	M (n = 273)	Korean	Photos	29.00 ± 3.00	4.728
			Price et al., 2009	M (n = 26)	Black American	Photos	27.50 ± 1.40	-0.476
			Price et al., 2009	M (n = 32)	White American	Photos	26.70 ± 1.70	-0.409

* Note: The Bayes Factor was interpreted based on Jeffreys' (1961) scale of the base 10 logarithmic Bayes Factor (logBF). The logBF provides evidence for the alternative hypothesis which posits variation between normative population means. The colours of the LogBF values can be interpreted as:

	< -2	Decisive evidence that there is no difference between population means
	-2 < BF <-1,5	Very strong evidence that there is no difference between population means
	-1,5 < BF < -1	Strong evidence that there is no difference between population means
	-1 < BF < -0,5	Substantial evidence that there is no difference between population means
	-0,5 < BF < 0	Weak evidence that there is no difference between population means
	0 < BF < 0,5	Weak evidence that there is a difference between population means
	0,5 < BF < 1	Substantial evidence that there is a difference between population means
	1 < BF < 1,5	Strong evidence that there is a difference between population means
	1,5 < BF <2	Very strong evidence that there is a difference between population means

© University of Pretoria

Supplementary Table 2. Sexual dimorphism in linear dimensions of the orbital region

Study	Population	n	Modality	Female	Male	p-value
Left orbital height						
Current study, 2024	Black South Africans	97	CBCT	35.73 ± 2.98	37.64 ± 2.33	**0.00**
	White South Africans	109	CBCT	37.39 ± 2.27	38.15 ± 2.27	0.40
Ozer et al., 2017	Turkish	198	CT	36.97 ± 2.19	37.77 ± 2.48	**0.02**
Attia et al., 2018	Egyptian	92	CT	35.90 ± 2.8	36.9 ± 2.9	0.11
Kim et al., 2016	Korean	100	CBCT	37.90 ± 2.0	38.10 ± 2.30	0.55
Weaver et al., 2010	American	32	CT	31.75 ± 2.51	32.44 ± 1.89	0.41
Ji et al., 2010	Chinese	64	CT	33.22 ± 1.73	33.35 ± 1.44	0.74
Guyomarch et al., 2012	French	375	CT	35.40 ± 2.45	35.80 ± 2.45	0.08
Khani et al., 2023	Iranian	151	CT	36.70 ± 1.80	37.80 ± 2.00	>0.05
Shin et al., 2016	Korean	174	CT	35.40 ± 2.00	35.60 ± 1.90	>0.05
Dayal et al., 2008	Black South Africans	120	Skulls	33.65 ± 2.25	33.63 ± 2.00	**0.01**
Capella et al., 2020	Italians	80	Skulls	35.00 ± 2.00	35.00 ± 2.00	0.145
Left orbital breadth						
Current study, 2024	Black South Africans	97	CBCT	40.10 ± 2.79	42.30 ± 1.83	**0.00**
	White South Africans	109	CBCT	40.58 ± 1.45	42.74 ± 1.51	**0.00**
Ozer et al., 2017	Turkish	198	CT	33.27 ± 1.77	34.17 ± 2.10	**<0.001**
Attia et al., 2018	Egyptian	92	CT	37.00 ± 3.60	36.70 ± 4.10	0.74
Kim et al., 2016	Korean	100	CBCT	35.90 ± 2.80	42.10 ± 1.80	**0.00**
Weaver et al., 2010	American	32	CT	36.60 ± 1.71	37.42 ± 2.44	0.22
Ji et al., 2010	Chinese	64	CT	38.00 ± 2.25	40.02 ± 1.63	**<0.001**
Guyomarch et al., 2012	French	375	CT	37.80 ± 1.98	39.5 ± 1.98	**0.00**
Khani et al., 2023	Iranian	151	CT	34.60 ± 1.60	35.00 ± 1.60	>0.05
Shin et al., 2016	Korean	174	CT	44.50 ± 1.80	41.70 ± 1.90	**<0.05**
Dayal et al., 2008	Black South Africans	120	Skulls	41.10 ± 1.75	42.62 ± 1.91	**0.00**
Capella et al., 2020	Italians	80	Skulls	39.00 ± 2.00	38.00 ± 2.00	**0.005**
Left orbital index						
Current study, 2024	Black South Africans	97	CBCT	89.14 ± 5.09	89.04 ± 5.12	0.89
	White South Africans	109	CBCT	92.23 ± 6.12	89.72 ± 4.89	**0.00**
Attia et al., 2018	Egyptian	92	CT	97.90 ± 10.60	101.40 ± 11.40	0.13
Khani et al., 2023	Iranian	151	CT	108.59 ± 6.03	108.25 ±7.38	>0.05
Interorbital distance						
Current study, 2024	Black South Africans	97	CBCT	21.65 ± 2.68	22.62 ± 2.80	0.21
	White South Africans	109	CBCT	19.09 ± 2.35	20.11 ± 2.34	0.17
Ji et al., 2010	Chinese	64	CT	25.11 ± 2.25	27.18 ± 2.67	**0.00**
Attia et al., 2018	Egyptian	92	CT	24.50 ± 4.70	27.40 ± 11.3	0.11
Khani et al., 2023	Iranian	151	CT	21.80 ± 2.10	23.10 ± 2.70	>0.05
Weaver et al., 2010	American	32	CT	25.11 ± 2.25	27.18 ± 2.76	**0.00**
Capella et al., 2020	Italians	80	Skulls	23.00 ± 2.00	22.00 ± 2.00	**0.04**

© University of Pretoria

Supplementary Table 2 continuation						
Bizygomatic breadth						
Current study, 2024	Black South Africans	97	CBCT	121.80 ± 7.87	132.19 ± 7.21	**0.00**
	White South Africans	109	CBCT	123.03 ± 4.97	131.35 ± 4.33	**0.00**
Attia et al., 2018	Egyptian	92	CT	95.80 ± 4.90	98.60 ± 4.10	**0.00**
Farkas et al., 2007	African American	100	Patients	130.50 ± 4.50	139.00 ± 5.30	**0.00**
	North American white	309	Patients	130.00 ± 4.60	139.10 ± 5.30	**0.00**
Byat et al., 2018	Iranian	200	Patients	129.20 ± 4.18	130.90 ± 4.43	0.07
Dayal et al., 2008	Black South Africans	120	Skulls	123.97 ± 5.03	130.60 ± 4.71	**0.00**
Celebi et al., 2007	Egyptian	120	Patients	98.73 ± 6.45	104.95 ± 7.31	**<0.001**
	Italian	139	Patients	98.29 ± 4.86	105.57 ± 6.37	**<0.001**
	Colombian	131	Patients	136.18 ± 5.77	142.67 ± 5.98	>0.05
	Mexican American	92	Patients	116.71 ± 4.88	127.11 ± 6.97	**<0.001**
Eyeball protrusion (dLOM – oa)						
Current study, 2024	Black South Africans	94	CBCT	24.02 ± 2.26	24.60 ± 1.91	0.46
	White South Africans	103	CBCT	23.59 ± 1.61	25.16 ± 1.81	**0.00**
Guyomarch et al., 2012	French	375	CT	17.60 ± 2.32	18.70 ± 2.32	**0.00**
Barretto and Mathog, 1999	Black Americans	61	Patients	17.27 ± 1.41	18.23 ±2.19	**0.05**
	White Americans	65	Patients	16.02 ± 2.23	17.01 ± 2.70	0.11
Dunskey., 1992	Black Americans	309	Patients	17.46 ± 2.64	18.20 ± 2.97	**<0.02**
Kim et al., 2016	Korean	100	CBCT	16.40 ± 1.30	17.10 ± 1.30	0.665
Eyeball protrusion from SOM						
Current study, 2024	Black South Africans	94	CBCT	21.31 ± 2.74	20.84 ± 2.04	0.72
	White South Africans	103	CBCT	19.59 ± 2.06	19.65 ± 1.85	0.99
Guyomarch et al., 2012	French	375	CT	15.70 ± 1.91	16.00 ± 1.91	0.29
Kim et al., 2016	Korean	100	CBCT	20.70 ± 1.80	20.50 ± 1.50	0.67
Eyeball protrusion from IOM						
Current study, 2024	Black South Africans	94	CBCT	20.51 ± 2.90	19.70 ± 1.99	0.26
	White South Africans	103	CBCT	20.13 ± 1.80	20.42 ± 1.75	0.99
Guyomarch et al., 2012	French	375	CT	19.70 ± 1.72	19.90 ± 1.72	0.20
Kim et al., 2016	Korean	100	CBCT	16.70 ± 1.70	16.90 ± 1.40	0.58
Eyeball protrusion from MOM						
Current study, 2024	Black South Africans	94	CBCT	23.35 ± 2.47	23.20 ± 1.97	0.73
	White South Africans	103	CBCT	22.81 ± 1.67	24.33 ± 1.71	**0.00**
Guyomarch et al., 2012	French	375	CT	21.70 ± 1.81	22.80 ± 1.81	**0.00**
Kim et al., 2016	Korean	100	CBCT	22.30 ± 1.40	23.50 ± 1.70	0.06
Left ocular height						
Current study, 2024	Black South Africans	97	CBCT	23.77 ± 1.44	23.88 ± 1.43	**0.05**
	White South Africans	103	CBCT	24.60 ± 1.86	25.23 ± 1.55	0.64
Shin et al., 2016	Korean	174	CT	26.60 ± 1.80	26.50 ± 1.80	>0.05

© University of Pretoria

Supplementary Table 2 continuation						
Left ocular breadth						
Current study, 2024	Black South Africans	97	CBCT	22.44 ± 1.60	23.23 ± 1.20	**0.01**
	White South Africans	103	CBCT	23.34 ± 1.47	23.55 ± 1.39	0.64
Rana et al., 2022	Australian	201	MRI	25.70 ± 1.30	26.20 ± 1.30	**0.01**
Shin et al., 2016	Korean	174	CT	25.20 ± 1.00	25.80 ± 1.00	**<0.05**
Left Ocular axial length						
Current study, 2024	Black South Africans	97	CBCT	21.98 ± 1.23	23.50 ± 1.22	**0.00**
	White South Africans	103	CBCT	23.14 ± 1.30	23.27 ± 1.17	0.76
Ozer et al., 2016	Turkish	198	CT	22.76 ± 6.38	23.25 ± 0.88	**0.00**
Wilkinson and Mautner, 2003	UK	39	MRI	23.42 ± 1.41	23.21 ± 1.76	0.61
Rana et al., 2022	Australian	201	MRI	24.70 ± 0.95	25.20 ± 1.10	**<0.01**
Shin et al., 2016	Korean	174	CT	26.10 ± 1.10	26.60 ± 1.10	**<0.05**
Left palpebral fissure height						
Current study, 2024	Black South Africans	85	CBCT	8.86 ± 1.23	8.95 ± 1.15	0.85
	White South Africans	109	CBCT	9.72 ± 1.88	8.99 ± 1.33	0.68
Kunjur et al., 2006	White Europeans	26	Photos	9.80 ± 1.20	10.20 ± 1.60	0.48
	Indians	26	Photos	10.20 ± 1.20	10.50 ± 0.70	0.44
	Chinese	26	Photos	10.60 ± 0.90	9.50 ± 1.40	**0.03**
Barretto and Mathog, 1999	Black Americans	61	Patients	10.56 ± 1.58	9.84 ± 1.61	0.08
	White Americans	65	Patients	10.65 ± 1.21	10.25 ± 1.21	0.19
Farkas et al., 2007	Black Americans	100	Patients	10.40 ± 1.20	10.00 ± 1.10	0.09
	White Americans	309	Patients	10.90 ± 1.20	10.80 ± 0.90	0.41
Byat et al., 2018	Iranian	200	Patients	14.96 ± 6.86	14.01 ± 4.08	0.384
Price et al., 2009	Black Americans	56	Photos	9.50 ± 1.40	9.80 ± 1.70	>0.05
	White Americans	56	Photos	10.30 ± 1.00	9.40 ± 1.30	>0.05
Song et al., 2007	Korean	594	Photos	10.00 ± 1.70	9.90 ± 1.60	**<0.01**
Left palpebral fissure width						
Current study, 2024	Black South Africans	97	CBCT	26.87 ± 3.43	28.22 ± 2.10	**0.02**
	White South Africans	109	CBCT	25.90 ± 1.62	27.16 ± 2.14	**0.03**
Celebi et al., 2007	Mexican American	92	Patients	29.70 ± 1.79	30.89 ± 2.17	**<0.01**
	Italian	139	Patients	30.39 ± 2.06	30.37 ± 1.56	>0.05
	Egyptian	120	Patients	29.47 ± 2.10	30.33 ± 2.24	**<0.05**
	Colombian	131	Patients	29.56 ± 2.12	31.54 ± 1.79	**<0.001**
Price et al., 2009	Black Americans	56	Photos	27.00 ± 1.40	27.50 ± 1.40	>0.05
	White Americans	56	Photos	27.20 ± 1.80	26.70 ± 1.70	>0.05
Song et al., 2007	Korean	594	Photos	27.60 ± 3.50	29.00 ± 3.00	**<0.01**
Amini et al.,	Persian	100	Patients	31.00 ± 1.70	31.60 ± 1.90	>0.05
Barretto and Mathog, 1999	Black American	61	Patients	31.46 ± 2.20	32.34 ± 2.31	0.13
	White American	65	Patients	29.40 ± 2.46	29.51 ± 2.19	0.85
Byat et al., 2018	Iranian	200	Patients	28.93 ± 4.28	28.93 ± 4.28	0.94
A two-way t-test was conducted based on the sample size, mean and standard deviation to statistically determine the variation between sex groups when not stated in the literature.						

© University of Pretoria

Supplementary Table 3. Eigenvalues and PC scores for shape analysis data on manually placed landmarks

Eigenvalues and PC scores of the complete SA sample indicating the effect of population affinity on the position of the 14 landmarks on the orbital rim

	Comp1	Comp2	Comp3	Comp4	Comp5	Comp6	Comp7	Comp8	Comp9	Comp10	Comp11	Comp12
Eigenvalues	0.001	0.001	0.000	0.000	0.000	0.000	0.000	0.000	0.000	0.000	0.000	0.000
Proportion of Variance	0.206	0.139	0.098	0.080	0.076	0.068	0.058	0.037	0.032	0.029	0.025	0.023

Eigenvalues and PC scores of the complete SA sample indicating the effect of population affinity on the position of the 8 landmarks on the palpebral fissures

	Comp1	Comp2	Comp3	Comp4	Comp5	Comp6	Comp7	Comp8	Comp9	Comp10	Comp11	Comp12
Eigenvalues	0.001	0.000	0.000	0.000	0.000	0.000	0.000	0.000	0.000	0.000	0.000	0.000
Proportion of Variance	0.274	0.165	0.131	0.075	0.070	0.061	0.053	0.038	0.028	0.023	0.019	0.015

Eigenvalues and PC scores of SA males indicating the effect of population affinity on the position of the 14 landmarks on the orbital rim

	Comp1	Comp2	Comp3	Comp4	Comp5	Comp6	Comp7	Comp8	Comp9	Comp10	Comp11	Comp12
Eigenvalues	0.001	0.000	0.000	0.000	0.000	0.000	0.000	0.000	0.000	0.000	0.000	0.000
Proportion of Variance	0.233	0.138	0.118	0.072	0.059	0.056	0.043	0.041	0.032	0.028	0.025	0.023

Eigenvalues and PC scores of SA males indicating the effect of population affinity on the position of the 8 landmarks on the palpebral fissures

	Comp1	Comp2	Comp3	Comp4	Comp5	Comp6	Comp7	Comp8	Comp9	Comp10	Comp11	Comp12
Eigenvalues	0.001	0.000	0.000	0.000	0.000	0.000	0.000	0.000	0.000	0.000	0.000	0.000
Proportion of Variance	0.274	0.165	0.131	0.075	0.070	0.061	0.053	0.038	0.028	0.023	0.019	0.015

© University of Pretoria

Eigenvalues and PC scores of SA females indicating the effect of population affinity on the position of the 14 landmarks on the orbital rim

	Comp1	Comp2	Comp3	Comp4	Comp5	Comp6	Comp7	Comp8	Comp9	Comp10	Comp11	Comp12
Eigenvalues	0.001	0.001	0.000	0.000	0.000	0.000	0.000	0.000	0.000	0.000	0.000	0.000
Proportion of Variance	0.232	0.185	0.117	0.088	0.059	0.052	0.048	0.031	0.030	0.024	0.022	0.016

Eigenvalues and PC scores of SA females indicating the effect of population affinity on the position of the 8 landmarks on the palpebral fissures

	Comp1	Comp2	Comp3	Comp4	Comp5	Comp6	Comp7	Comp8	Comp9	Comp10	Comp11	Comp12
Eigenvalues	0.001	0.000	0.000	0.000	0.000	0.000	0.000	0.000	0.000	0.000	0.000	0.000
Proportion of Variance	0.307	0.171	0.111	0.082	0.068	0.054	0.045	0.037	0.026	0.024	0.017	0.015

Eigenvalues and PC scores of the complete SA sample indicating the effect of sex on the position of the 14 landmarks on the orbital rim

	Comp1	Comp2	Comp3	Comp4	Comp5	Comp6	Comp7	Comp8	Comp9	Comp10	Comp11	Comp12
Eigenvalues	0.001	0.001	0.000	0.000	0.000	0.000	0.000	0.000	0.000	0.000	0.000	0.000
Proportion of Variance	0.206	0.139	0.098	0.080	0.076	0.068	0.058	0.037	0.032	0.029	0.025	0.023

Eigenvalues and PC scores of the complete SA sample indicating the effect of sex on the position of the 8 landmarks on the palpebral fissures

	Comp1	Comp2	Comp3	Comp4	Comp5	Comp6	Comp7	Comp8	Comp9	Comp10	Comp11	Comp12
Eigenvalues	0.001	0.000	0.000	0.000	0.000	0.000	0.000	0.000	0.000	0.000	0.000	0.000
Proportion of Variance	0.270	0.172	0.125	0.082	0.075	0.065	0.046	0.036	0.031	0.022	0.020	0.015

© University of Pretoria

Eigenvalues and PC scores of white SA indicating the effect of sex on the position of the 14 landmarks on the orbital rim

	Comp1	Comp2	Comp3	Comp4	Comp5	Comp6	Comp7	Comp8	Comp9	Comp10	Comp11	Comp12
Eigenvalues	0.001	0.000	0.000	0.000	0.000	0.000	0.000	0.000	0.000	0.000	0.000	0.000
Proportion of Variance	0.195	0.143	0.118	0.102	0.088	0.061	0.046	0.036	0.034	0.029	0.022	0.017

Eigenvalues and PC scores of white SA indicating the effect of sex on the position of the 8 landmarks on the palpebral fissures

	Comp1	Comp2	Comp3	Comp4	Comp5	Comp6	Comp7	Comp8	Comp9	Comp10	Comp11	Comp12
Eigenvalues	0.001	0.000	0.000	0.000	0.000	0.000	0.000	0.000	0.000	0.000	0.000	0.000
Proportion of Variance	0.278	0.167	0.118	0.076	0.071	0.062	0.058	0.042	0.028	0.021	0.020	0.015

Eigenvalues and PC scores of black SA indicating the effect of sex on the position of the 14 landmarks on the orbital rim

	Comp1	Comp2	Comp3	Comp4	Comp5	Comp6	Comp7	Comp8	Comp9	Comp10	Comp11	Comp12
Eigenvalues	0.001	0.001	0.000	0.000	0.000	0.000	0.000	0.000	0.000	0.000	0.000	0.000
Proportion of Variance	0.200	0.163	0.100	0.087	0.074	0.059	0.051	0.040	0.037	0.029	0.024	0.023

Eigenvalues and PC scores of black SA indicating the effect of sex on the position of the 8 landmarks on the palpebral fissures

	Comp1	Comp2	Comp3	Comp4	Comp5	Comp6	Comp7	Comp8	Comp9	Comp10	Comp11	Comp12
Eigenvalues	0.001	0.000	0.000	0.000	0.000	0.000	0.000	0.000	0.000	0.000	0.000	0.000
Proportion of Variance	0.273	0.183	0.129	0.085	0.065	0.058	0.049	0.032	0.031	0.023	0.019	0.014

© University of Pretoria

Annexure A: Ethics approval from UP

UNIVERSITEIT VAN PRETORIA
UNIVERSITY OF PRETORIA
YUNIBESITHI YA PRETORIA

Faculty of Health Sciences

Institution: The Research Ethics Committee, Faculty Health Sciences, University of Pretoria complies with ICH-GCP guidelines and has US Federal wide Assurance.
- FWA 00002567, Approved on 19 March 2002 and Expires: 18 March 2027
- IORG #: IORG0001762 OMB No. 0990-0279 Approved to expire on 31 October and Expires: 03/30/2026.

Faculty of Health Sciences **Research Ethics Committee**

11 April 2024

Approval Certificate
Annual Renewal

Dear Mrs S van der Walt,

Ethics Reference No.: 323/2020 – Line 4
Title: Creating guidelines for the approximation of the eye and periorbital regions of South Africans using Cone Beam Computed Tomography

The **Annual Renewal** as supported by documents received between 2024-03-12 and 2024-04-10 for your research, was approved by the Faculty of Health Sciences Research Ethics Committee on 2024-04-10 as resolved by its quorate meeting.

Please note the following about your ethics approval:

- Renewal of ethics approval is valid for 1 year, subsequent annual renewal will become due on 2025-04-11.
- The Research Ethics Committee (REC) must monitor your research continuously. To this end, you must submit as may be applicable for your kind of research:
  a) annual reports;
  b) reports requested *ad hoc* by the REC;
  c) all visitation and audit reports by a regulatory body (e.g. the HPCSA, FDA, SAHPRA) within 10 days of receiving one;
  d) all routine monitoring reports compiled by the Clinical Research Associate or Site Manager within 10 days of receiving one.
- The REC may select your research study for an audit or a site visitation by the REC.
- The REC may require that you make amendments and take corrective actions.
- The REC may suspend or withdraw approval.
- Please remember to use your protocol number (323/2020) on any documents or correspondence with the Research Ethics Committee regarding your research.

Ethics approval is subject to the following:

- The ethics approval is conditional on the research being conducted as stipulated by the details of all documents submitted to the Committee. In the event that a further need arises to change who the investigators are, the methods or any other aspect, such changes must be submitted as an Amendment for approval by the Committee.

We wish you the best with your research.

Yours sincerely

On behalf of the FHS REC, Dr R Sommers
MBChB, MMed (Int), MPharmMed, PhD
***Deputy Chairperson** of the Faculty of Health Sciences Research Ethics Committee, University of Pretoria*

The Faculty of Health Sciences Research Ethics Committee complies with the SA National Act 61 of 2003 as it pertains to health research and the United States Code of Federal Regulations Title 46 and 46. This committee abides by the ethical norms and principles for research, established by the Declaration of Helsinki, the South African Medical Research Council Guidelines as well as the Guidelines for Ethical Research: Principles Structures and Processes, Second Edition 2015 (Department of Health).

Research Ethics Committee
Room 4-60, Level 4, Tswaloyale Building
University of Pretoria, Pretoria Eng 0002
Gauteng 0031, South Africa
Tel: +27 (0)12 356 3084
E-mail: [illegible]@up.ac.za
www.up.ac.za

Fakulteit Gesondheidswetenskappe
Lefapha la Disaense tša Maphelo

© University of Pretoria

Annexure B: Permission to collect scans from Cintocare

Permission to access Records / Files / Data base at Life Groenkloof Hospital

TO: Dr Sarel Botha
Head of Department

Life Groenkloof Hospital
Hospital

FROM: Soné van der Walt
Investigator

University of Pretoria

Re: Permission to do research at Life Groenkloof Hospital

TITLE OF STUDY: Creating guidelines for the approximation of the eye and periorbital regions of South Africans using Cone Beam Computed Tomography scans.

This request is lodged with you in terms of the requirements of the Promotion of Access to Information Act. No. 2 of 2000.

I am a student at the Department of Anatomy at the University of Pretoria. I am working with Prof AC Oettlé (SMU), Prof E L'Abbé (UP) and Dr A Ridel. I herewith request permission on behalf of all of us to conduct a study on the above topic on the hospital / clinic grounds. This study involves access to patient records. This study involves clinical research.

The researchers request access to the following information: clinical files, record books and data bases (**CBCT**, CT, MRI and Proface scans).

We intend to publish the findings of the study in a professional journal and/ or to present them at professional meetings like symposia, congresses, or other meetings of such a nature.

We intend to protect the personal identity of the patients by assigning each individual a random code number.

We undertake not to proceed with the study until we have received approval from the Faculty of Health Sciences Research Ethics Committee, University of Pretoria.

Yours sincerely,

Signature of the Principal Investigator

Permission to do the research study at this hospital / clinic and to access the information as requested, is hereby approved.

Title and name of Chief Executive Officer: Dr. S Botha

Name of hospital / clinic: Life Groenkloof Hospital

Signature: _____ Date: 24/6/2020

Dr. Sarel Botha
Official Stamp
Maxillofacial & Oral Surgeon
MBChB (Pret) dChD (Pret) Dip Odont (Pret) MBA (Regent)
MChD (MFOS) (Pret) FCMFOS (SA) FIBCOMFS FIFHNOS
Tel: 012 346 6032 Fax: 012 346 7549 Cell: 084 799 1111
Practice Number: 0557846

© University of Pretoria

Annexure C: Ethical approval from SMU

Sefako Makgatho Health Sciences University
Research & Postgraduate Studies Directorate
Sefako Makgatho University Research Ethics Committee
(SMUREC)

Molotlegi Street, Ga-Rankuwa 0208
Tel: (012) 521 5617/3698 | fax: (012) 521 3749
Email: lorato.phiri@smu.ac.za
P.O. Box 163 Medunsa 0204

Prof AC Oettlé
Department of Anatomy
P.O Box 232

Dear Prof AC Oettlé

RE: PROF AC OETTLÉ– ETHICS NO.: 183/2016: ADDITIONAL SAMPLE

SMUREC **NOTED** a letter dated 18 September 2017 requesting to incorporate additional scans from the Dental Radiology department affiliated to Sefako Makgatho Health Sciences University (SMU).

SMUREC **NOTED** that the researcher had received approval for the proposal from the University of Pretoria Ethics Committee.

Study Title:	Development of guidelines for facial approximations in the South African context
Researcher:	Dr F Demeter, Prof AC Oettlé
Coordinator:	Prof AC Oettlé, Mrs S vander Walt, Prof D Vandermeulen, Ms A Ridel, Ms F Dorfling, J Liebenberg, Z Lockhar and Prof M Steyn
Degree/Type	Self-initiated post-doctoral research project
University:	University of Pretoria, Faculty of Health Sciences, Department of Anatomy
Ethics Reference No.:	301/2016

SMUREC **NOTED** and **GRANTED** the researcher permission to conduct the study at SMU.

Yours Sincerely,

PROF C BAKER
DEPUTY CHAIRPERSON SMUREC

05 October 2017

SEFAKO MAKGATHO
HEALTH SCIENCES UNIVERSITY
SMU Research Ethics Committee
Chairperson
Date: 05/10/2017

© University of Pretoria

Annexure D: Normality results for shape analysis

Results of normality tests on manual landmark placement within sex-population groups from craniometric and capulometric landmarks.

The Q-Q plots of Mahalanobis distances expected in perfectly normal distributed data versus those calculated from the sample indicated that the orbital and palpebral fissure shape in females (Figure 1 c, d) had a greater deviation from the norm compared to their male counterparts (Figure 1 a, b), although the data followed a normal distribution.

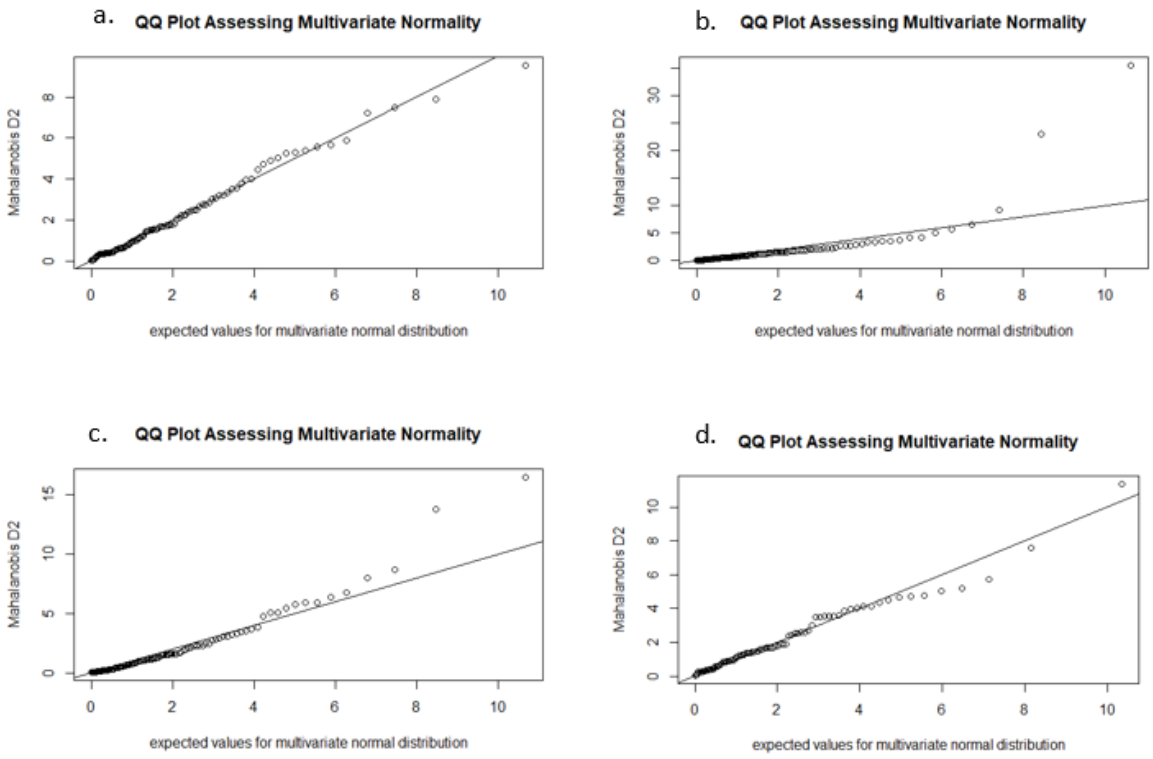

Figure 1. Q-Q-plots of the residuals of the linear model a) hard-tissue shape against population within males, b) soft-tissue shape against population within males, c) hard-tissue shape against population within females, d) soft-tissue shape against population within males

The influence of sex within population groups was also determined. Figure 2 illustrates the distribution of these datasets. Q-Q plots comparing Mahalanobis distances expected in ideally normally distributed data with those calculated from the sample revealed similar deviations from the norm for the orbital and palpebral fissure shape in white and black South Africans.

© University of Pretoria

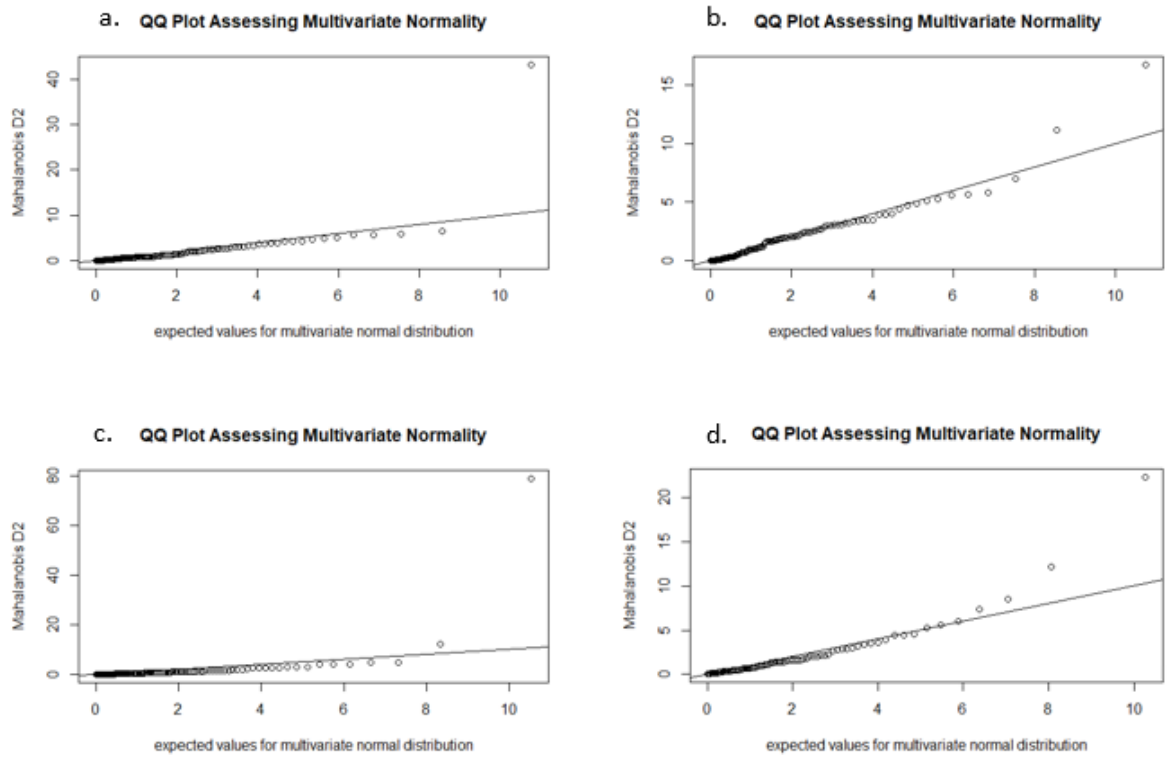

Figure 2. Q-Q-plots of the residuals of the linear model a) hard-tissue shape against sex within white South Africans, b) soft-tissue shape against sex within white South Africans, c) hard-tissue shape against sex within black South Africans, d) soft-tissue shape against sex within black South Africans

Results of normality tests on automatic landmark projections within sex-population groups from craniometric and capulometric landmarks.

The effect of population affinity within sex groups was also investigated. Figure 3 indicates the distribution of these data sets. The Q-Q plots of Mahalanobis distances expected in perfectly normal distributed data versus those calculated from the sample, indicated that the orbital and palpebral fissure shape in males (Figure 3 a, b) had a greater deviation from the normality, and were positively skewed, while the orbital and palpebral fissure shape of females (Figure 3 c, d) showed less deviation with possible outliers in the palpebral fissure shape.

© University of Pretoria

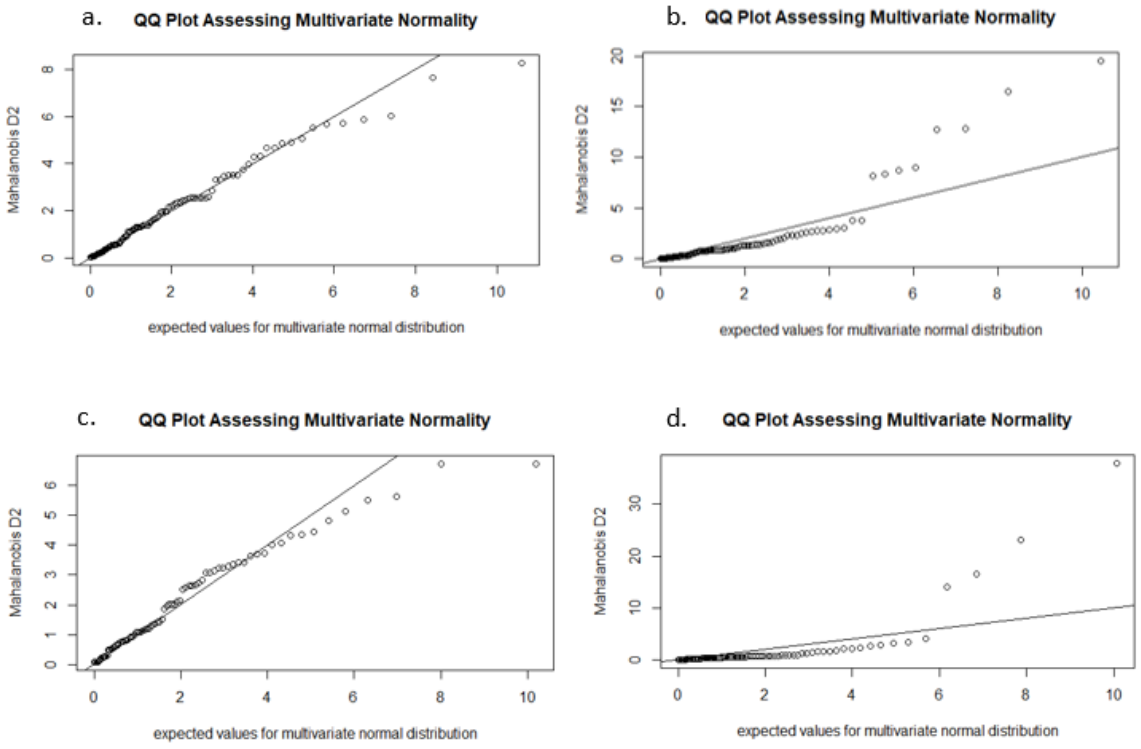

Figure 3. Q-Q-plots of the residuals of the linear model a) hard-tissue shape against population within males, b) soft-tissue shape against population within males, c) hard-tissue shape against population within females, d) soft-tissue shape against population within females

The influence of sex within population groups was determined (Figure 4). Q-Q plots comparing Mahalanobis distances expected in ideally normally distributed data with those calculated from the sample showed similar deviations for soft-tissue shape, while the hard-tissue shape had a relatively normal distribution in both South African groups.

© University of Pretoria

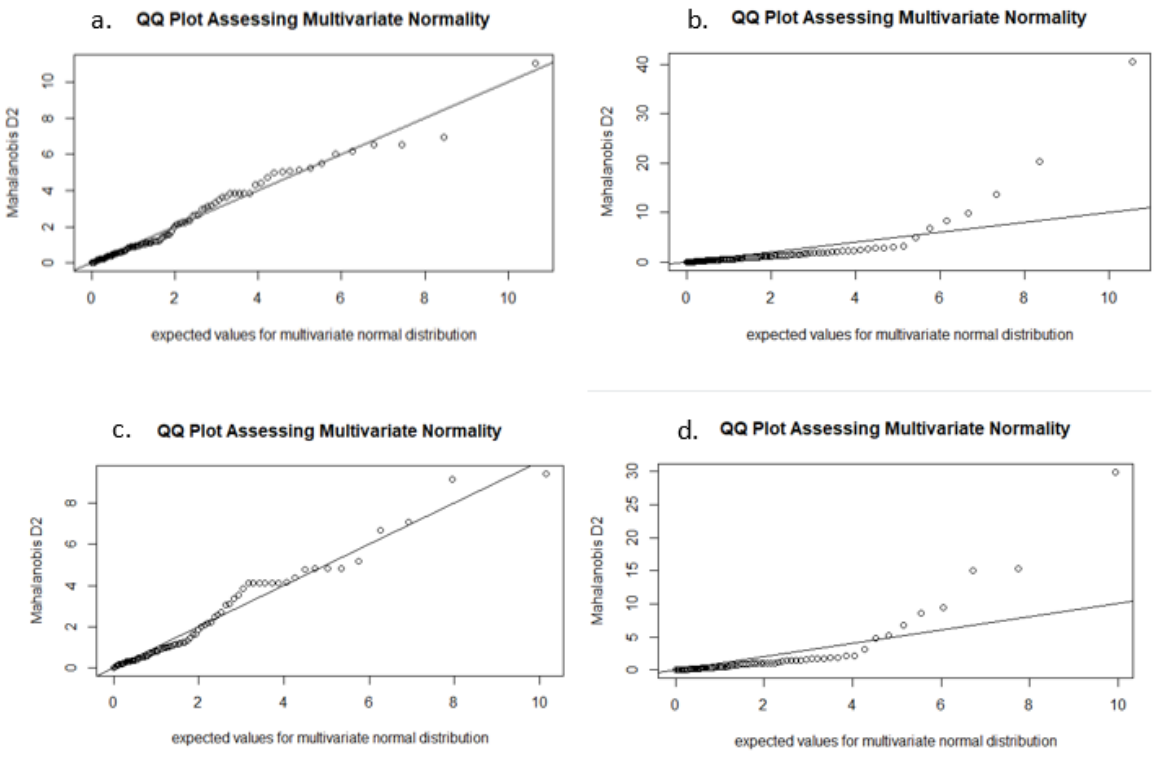

Figure 4. Q-Q-plots of the residuals of the linear model a) hard-tissue shape against sex within white South Africans, b) soft-tissue shape against sex within white South Africans, c) hard-tissue shape against sex within black South Africans, d) soft-tissue shape against sex within black South Africans.

© University of Pretoria

Annexure E: Dimensions of the orbital and periorbital regions for the use in forensic facial approximations of South Africans

(Anatomical Society of Southern Africa, April 2022 presentation; BioantTalks: Applications of 3D Technology to Unidentified and Missing Persons Cases, July 2022; Sefako Makgatho Health Sciences University research day, August 2022)

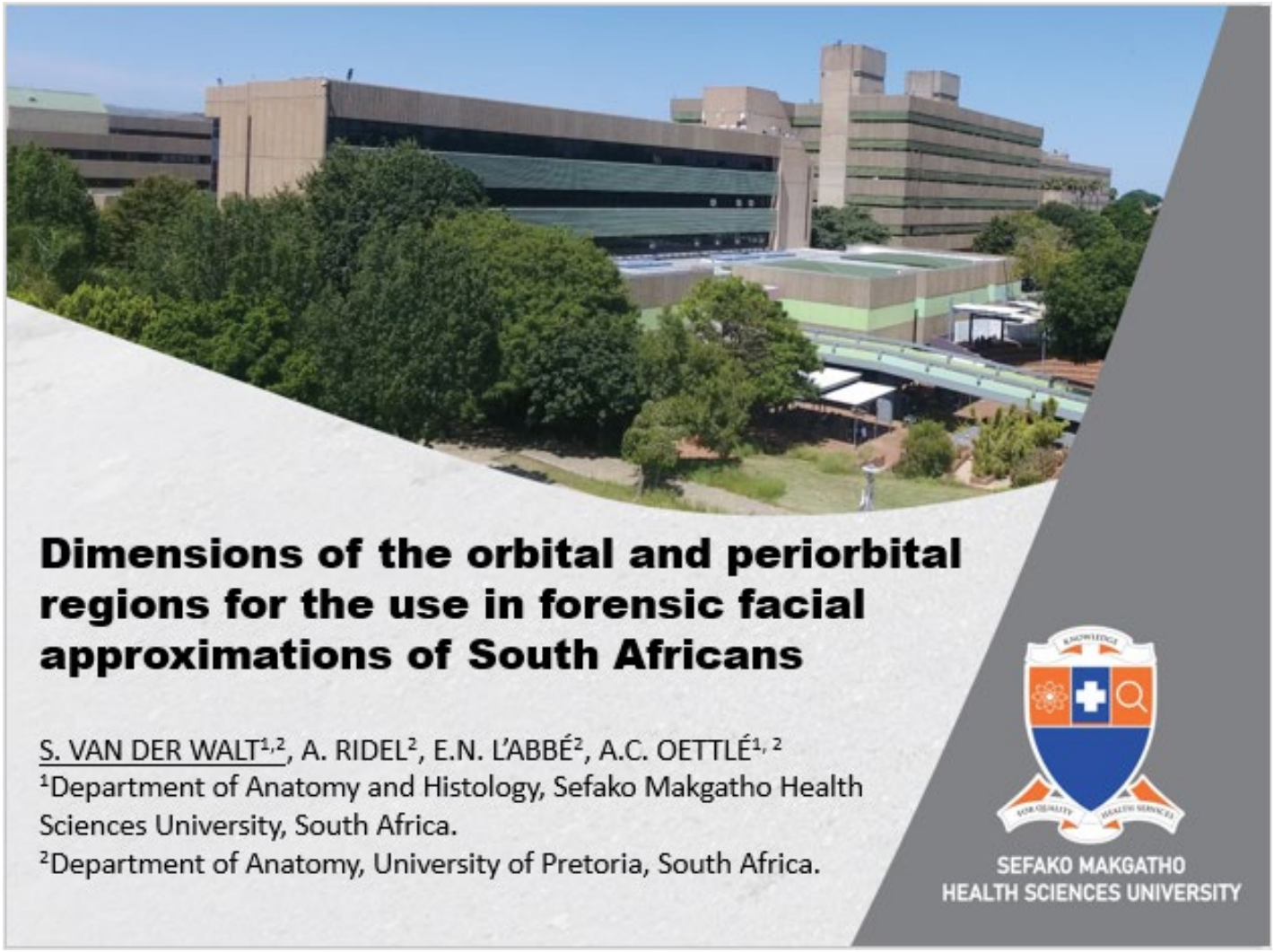

© University of Pretoria

Introduction

- Latest crime statistics: 9.2% increase in murders and 3.5 % in attempted murders[1]
- Identification of the deceased not always be possible[2]
  - Migrants
  - Illegal immigrants
- Identification methods used[2]
  - DNA analysis
  - Dental record comparisons
  - Craniofacial superimposition
  - Facial approximation

Traditional methods:
Comparative information required

KNOWLEDGE FOR QUALITY HEALTH SERVICES

Introduction

- Facial approximation/reconstruction: construction of a face over a skull
- Published to public to provide a potential identification
- Eyes are more likely than other facial features to lead to recognition[3-5]
- The first structure to consider when building a face[6]

KNOWLEDGE FOR QUALITY HEALTH SERVICES

© University of Pretoria

Literature review

- SAPS reconstruction: Virtual Sculpture method
- Based on Manchester/Combined Method
  - Facial muscles
  - Soft tissue thickness values (STT) based on North Americans
  - Skull robusticity
- STT vary among population groups
- Substantial variation in periorbital region[7-14]
- Effect of gravity[16]

Aim

To determine the dimensions of the orbit and periorbital structures and the variations observed among South African population groups to assist in facial approximations

© University of Pretoria

Objectives

1. Calculate absolute distances from the manual placement of landmarks on the 3D or 2D surfaces to determine
   - Dimensions of the bony orbit
   - Dimensions of the palpebral fissure
   - Size of the eyeball
   - Position of the eye in relation to the orbital rim
2. Evaluate weather sex and ancestry has an effect on these linear distances

KNOWLEDGE FOR QUALITY HEALTH SERVICES

Materials

- Ethical clearance nr: UP: 323/2020
- 206 CBCT scans were collected from
  - Life Groenkloof Hospital (Cintocare)
  - Oral and Dental Hospital at UP
  - Oral Health Centre at SMU

	Black females	White females	Black males	White males
n	45	57	52	52

- Data collection was performed using the MeVisLab © v.3.0.2 software
- Inclusion criteria: adults only, with open eyes
- Exclusion criteria: children, pathological and traumatic effects

KNOWLEDGE FOR QUALITY HEALTH SERVICES

© University of Pretoria

Methods

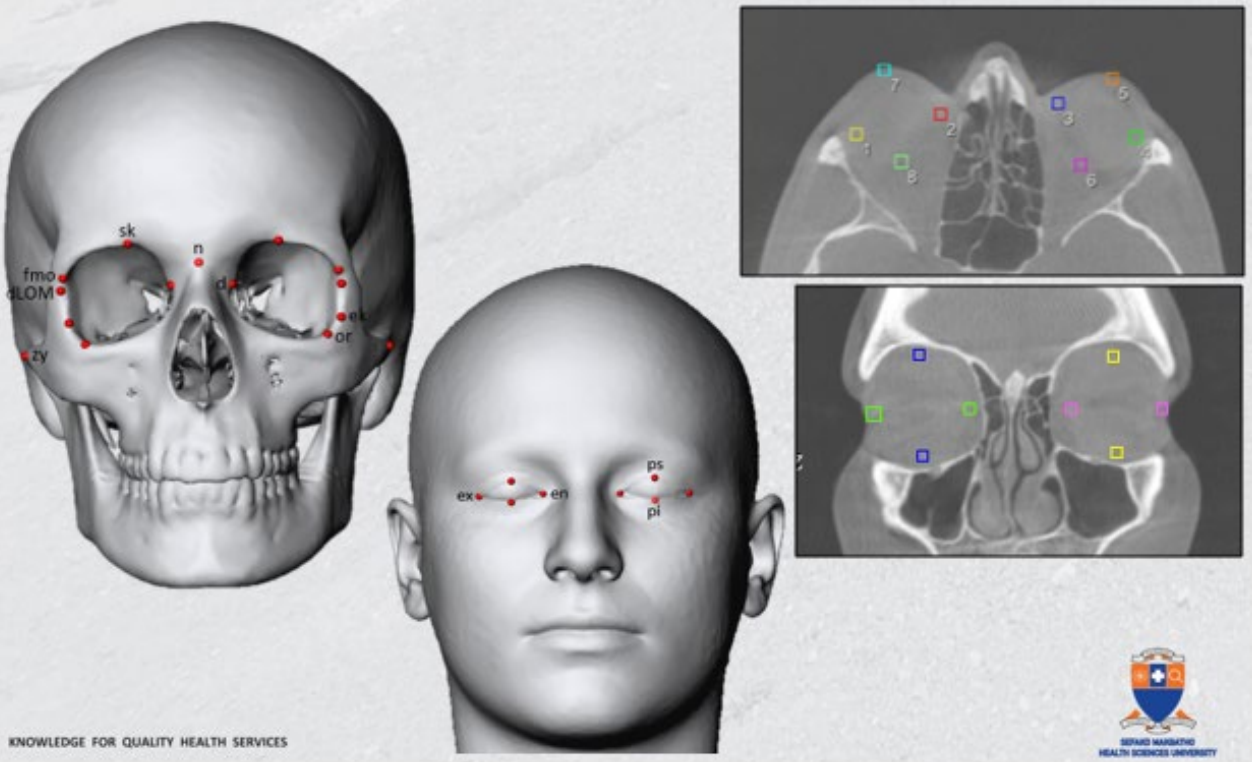

KNOWLEDGE FOR QUALITY HEALTH SERVICES

Results: observer error and laterality

- Intra-observer error: 1.41 ± 1.17
- Inter-observer error: 0.64 ±1.02

Asymmetry within sex groups:

Parameter	South African black females	South African white females	South African black males	South African white males
Orbital breadth	0.939	0.704	0.510	0.039
MOM to oculus mediale	0.007	0.391	0.732	0.081
LOM to oculus laterale	0.706	0.001	0.736	0.037
LOM to oculus anterius	0.625	0.124	0.142	0.005
Palpebral fissure width	0.451	0.391	0.428	0.013

- Asymmetry were also reported by Özer and colleagues (2016) in the orbital diameters of a Turkish population

KNOWLEDGE FOR QUALITY HEALTH SERVICES

© University of Pretoria

Results: orbital dimensions

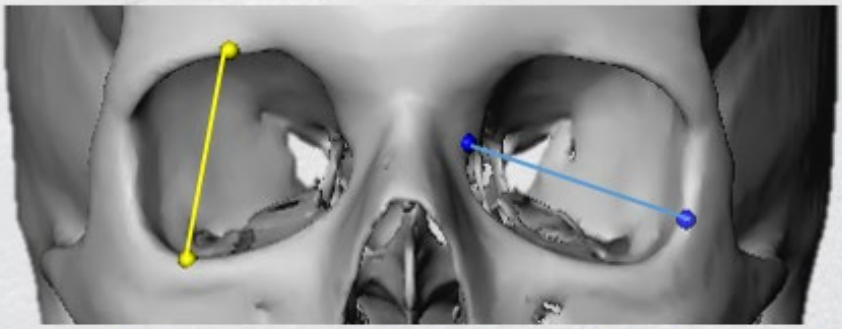

Measurement (mm)	South African black females (n=45)	South African white females (n=57)	South African black males (n=52)	South African white males (n=52)
Orbital height (L)	35.73[a] ± 2.98	37.39[a] ± 2.27	37.64[a] ± 2.33	38.15[a] ± 2.27
Orbital height (R)	35.91[a] ± 2.94	37.76[a] ± 2.15	37.60[a] ± 2.76	38.10[a] ± 2.52
Orbital breadth (L)	40.10[a] ± 2.79	40.58[b] ± 1.46	42.30[a,b] ± 1.83	42.74[a,b] ± 1.51
Orbital breadth (R)	40.14[d] ± 2.63	40.70[b] ± 1.81	42.55[d,b] ± 2.02	43.49 [d,b] ± 2.10
Orbital index: OH/OB *100 (L)	89.173[a] ±5.09	92.23 [a,b] ± 6.12	89.04 [b] ± 5.12	89.30[b] ± 4.89
Orbital index: OH/OB *100 (R)	89.53[a] ± 5.80	92.88[a,b] ± 5.50	88.40[b] ± 5.75	87.72[b] ± 5.88

Discussion: orbital dimensions

Study:	Pop	n	Modality	Orbital height	Orbital breadth
Current study 2022	South African	206	CBCT	BF(L): 35.73 ± 2.98 BF(R): 35.91 ± 2.94 BM(L): 37.64 ± 2.33 BM(R): 37.60 ± 2.76 WF(L): 37.39 ± 2.27 WF(R): 37.76 ± 2.15 WM(L): 38.15 ± 2.27 WM(R):38.10 ± 2.52	BF(L): 40.10 ± 2.79 BF(R): 40.14 ± 2.63 BM(L): 42.30 ± 1.83 BM(R): 42.55 ± 2.02 WF(L): 40.58 ± 1.46 WF(R):40.70 ± 1.81 WM(L): 42.74± 1.51 WM(R):43.49 ± 2.10
Kim et al (2016)	Korean	100	CBCT	Male: 38.1 ± 2.3 Female: 37.9 ± 2.0	Male: 42.1 ± 1.8 Female: 40.3 ± 1.7
Bekerman (2014)	Israeli	250	CT	L: 42.55 ± 2.5 R: 41.08 ± 2.4	L: 35.86 ± 2.2 R: 35.33 ± 2.2
Guyomarc'h et al (2012)	French	900	CT	L: 35.6 ± 2.45 R: 35.7 ± 2.45	L: 38.7 ± 1.83 R: 39.2 ± 1.93
Weaver et al (2010)	American	39	CT	Male: 32.44 ± 1.89 Female:31.75±2.51	Male: 37.42 ± 2.44 Female: 36.6 ±1.71

© University of Pretoria

Results: eyelid dimensions

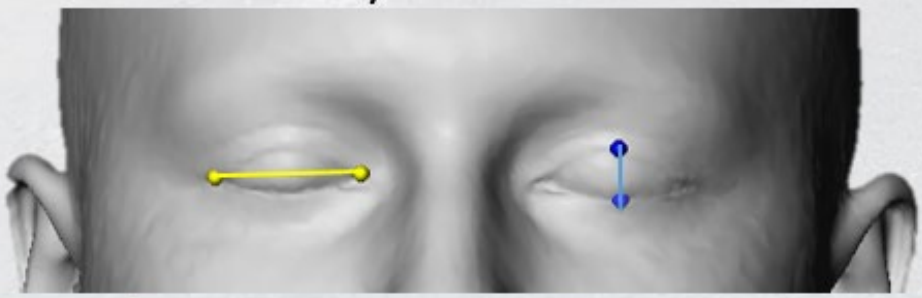

	Sex-Population groups			
Measurement (mm)	South African black females	South African white females	South African black males	South African white males
n	45	57	52	52
Width of palpebral fissure (L)	26.87[a] ± 3.43	25.90[b] ± 1.62	28.22[a,b] ± 2.10	27.16[b] ± 2.14
Width of palpebral fissure (R)	26.89[a] ± 3.58	26.18[e] ± 1.75	27.86[e] ± 2.45	28.22[a,e] ± 2.11
n	33	57	52	52
Height of palpebral fissure (L)	9.27 ± 1.61	8.86[e] ± 1.23	9.72[e] ± 1.88	8.95 ± 1.15
Height of palpebral fissure (R)	8.99 ± 1.33	8.88 ± 1.10	9.54 ± 1.80	8.83 ± 1.21

KNOWLEDGE FOR QUALITY HEALTH SERVICES

Discussion: eyelid dimensions

Study:	Population	n	Modality	Eyelid width	Eyelid height
Current study 2022	South African	206	CBCT	BF(L): 26.87 ± 3.43 BF(R): 26.89 ± 3.58 BM(L): 28.22 ± 2.10 BM(R): 27.86 ± 2.45 WF(L): 25.90 ± 1.62 WF(R): 26.18 ± 1.75 WM(L): 27.16 ± 2.14 WM(R):28.22 ± 2.11	BF(L): 9.27 ± 1.61 BF(R): 8.99 ± 1.33 BM(L): 9.72 ± 1.88 BM(R): 8.83 ± 1.21 WF(L): 8.86 ± 1.23 WF(R): 8.88 ± 1.10 WM(L):8.95 ± 1.15 WM(R):8.83± 1.21
Chong et al 2021	Chinese females	188	Photos	20-29: 27.88 ± 1.61 50-65: 25.21 ± 1.51	20-29: 9.96 ± 0.98 50-56: 8.09 ± 1.18
Ibraheem et al 2016	Nigerian	1020	Patients	L: 31.9 ± 3.2 R: 32.1 ± 3.2	L: 8.3 ± 1.7 R: 8.3 ± 1.6
Price et al 2009	American	164	Photos	BM: 27.5 ± 1.4 BF: 27.0 ± 1.4 WM: 26.7 ± 1.7 WF: 27.2 ± 1.8	BM: 9.8 ± 1.7 BF: 9.5 ± 1.4 WM: 9.4 ± 1.3 WF: 10.3 ± 1.0

KNOWLEDGE FOR QUALITY HEALTH SERVICES

© University of Pretoria

Results: ocular dimensions

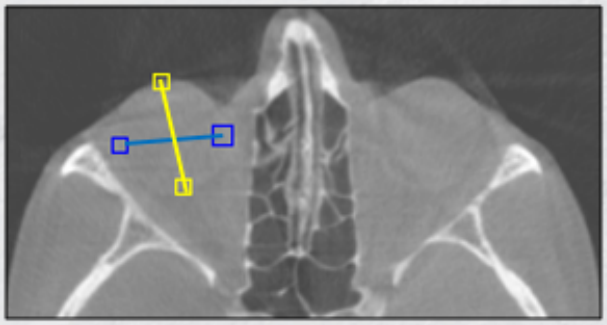

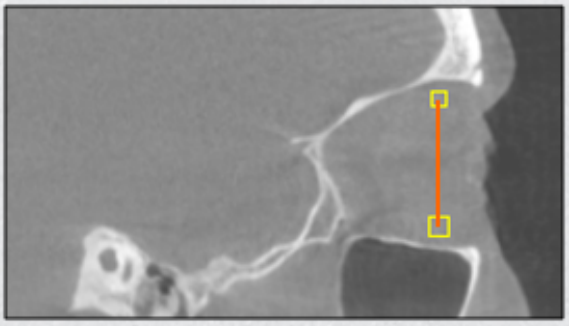

	Sex-Population groups			
Measurement (mm)	South African black females (n=45)	South African white females (n=57)	South African black males (n=52)	South African white males (n=52)
Eyeball width (L)	22.30[a] ± 1.78	23.23[a] ± 1.38	23.57[a] ± 1.64	23.72[a] ± 1.63
Eyeball width (R)	22.70[a] ± 1.68	23.10 ± 1.50	23.54[a] ± 1.64	23.60[a] ± 1.74
Eyeball height (L)	23.78[a] ± 1.51	23.92[b] ± 1.46	24.69[a] ± 1.95	25.31[a,b] ± 1.69
Eyeball height (R)	23.85[a] ± 1.70	23.89[b] ± 1.43	23.95[c] ± 2.08	25.43[a,b,c] ± 1.65
Anterior-posterior diameter (L)	21.87[a] ± 1.33	23.50[a] ± 1.32	23.09[a] ± 1.45	23.25[a] ± 1.32
Anterior-posterior diameter (R)	22.10[d] ± 1.46	23.23[d] ± 1.30	23.44[d] ± 1.36	23.39[d] ± 1.38

Discussion: ocular dimensions

Study:	Pop	n	Modality	Eyeball width	Eyeball height	Ant-Post
Current study 2022	South African	206	CBCT	BF(L): 22.30 ± 1.78 BF(R): 22.70 ± 1.68 BM(L):23.57±1.64 BM(R):23.54±1.64 WF(L):23.23 ± 1.38 WF(R):23.10±1.50 WM(L):23.72±1.63 WM(R):23.60±1.74	BF(L):23.75±1.51 BF(R):23.85±1.70 BM(L):24.69±1.95 BM(R):23.95±2.08 WF(L):23.92±1.46 WF(R):23.89±1.43 WM(L):25.31±1.69 WM(R):25.43±1.65	BF(L):21.87±1.33 BF(R):22.10±1.46 BM(L):23.09±1.45 BM(R):23.44±1.36 WF(L):23.50±1.32 WF(R):23.23±1.30 WM(L):23.25±1.32 WM(R):23.39±1.38
Dorfling et al 2018	South African Blacks	36 30 30	Cadavers CT CBCT	25.2 ± 1.42 24.1 ± 0.73 25.4±0.38	23.6±0.75 23.1 ± 0.75 24.1±0.64	n/a 23.2 ± 1.07 25.1±0.55
Bekerman 2014	Israeli	250	CT	R: 24.156 ± 1.9 L: 24.324 ± 1.9	R: 23.799 ± 1.6 L: 23.752 ± 1.7	R: 24.477 ± 1.8 L: 24.893 ± 2.2
Wilkinson et al 2003	European	39	MRI			WF: 23.21± 1.76 WM:23.42±1.42

KNOWLEDGE FOR QUALITY HEALTH SERVICES

© University of Pretoria

Results: position of the eyeball

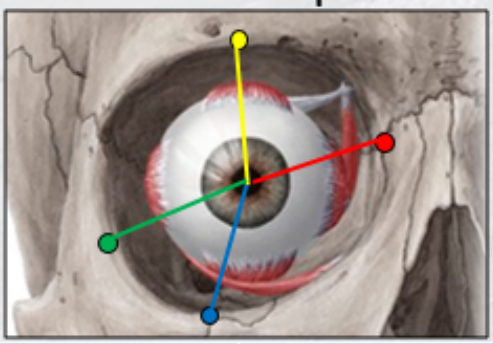

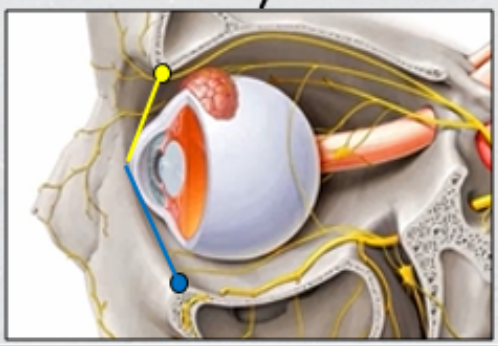

https://www.kenhub.com/en/library/anatomy/eye-anatomy

Measurement (mm)	South African Sex-Population groups			
	Black females (n=45)	White females (n=57)	Black males (n=52)	White males (n=52)
SOM-oculus anterius (L)	20.37 ± 2.51	19.79 ± 2.11	20.91 ± 1.98	19.82 ± 2.06
SOM-oculus anterius (R)	20.49 ± 2.58	19.81[b] ± 2.28	21.09[b] ± 2.02	19.81 ± 2.29
IOM-oculus anterius (L)	19.44[a] ± 1.98	20.20 ± 1.87	19.74 ± 2.01	20.44[a] ± 1.95
IOM-oculus anterius (R)	18.95[a] ± 2.10	20.25[a, b] ± 2.28	19.05[b] ± 2.01	20.08[a] ± 2.13
MOM-oculus anterius (L)	22.67[a] ± 2.36	22.88[b] ± 1.84	23.31[c] ± 2.07	24.48[a,b,c] ± 1.90
MOM-oculus anterius (R)	22.97[a] ± 2.17	22.76[b] ± 2.32	23.01 ± 2.03	23.88[a,b] ± 2.14
LOM-oculus anterius	23.52 ± 1.58	22.95[b] ± 2.29	24.20[b] ± 1.78	23.84 ± 1.94
LOM-oculus anterius	23.78[a] ± 2.34	23.55[b] ± 1.89	24.80[b] ± 2.06	24.85[a,b] ± 1.79

Discussion: position of the eyeball

Study:	Population	n	Modality	Females	Males
Current study 2022	South African	206	CBCT	SOM-oa (L): 19.79-20.37 SOM-oa (R): 19.81–20.49 IOM-oa (L): 19.44–20.20 IOM -oa (R): 18.95–20.25	SOM-oa (L): 19.82-20.91 SOM-oa (R): 19.81–21.09 IOM-oa (L): 19.74–20.44 IOM -oa (R): 19.05–20.08
				LOM-oa (L): 22.95–23.52 LOM-oa (R): 23.55-23.78 MOM-oa (L):22.67-22.88 MOM-oa(R): 22.76-22.97	LOM-oa (L): 23.84-24.20 LOM-oa (R): 24.80-24.85 MOM-oa (L):23.31-24.48 MOM-oa(R): 23.01-23.88
Goldberg et al (1999)	American	79	MRI	Oculus ant – orbital roof: 19.96 ± 1.6 Oculus ant – orbital floor: 19.2 ± 1.5	
Guyomarc'h et al 2012	French	900	CT	SOM-oa(L): 16.0 SOM-oa(R): 15.7 IOM-oa (L): 19.2 IOM – oa (R): 20.3	SOM-oa(L): 15.9 SOM-oa(R): 15.7 IOM-oa (L): 19.8 IOM – oa (R): 20.0
				LOM-oa (L): 16.7 LOM-oa (R): 16.8 MOM-oa (L): 22.8 MOM-oa(R): 23.2	LOM-oa (L): 16.4 LOM-oa (R): 16.6 MOM-oa (L): 22.3 MOM-oa(R): 23.6

© University of Pretoria

Conclusion

- Variations have been noted among South African sex-population groups
- Black females presented with the smallest orbits, eyes and palpebral fissure width
- White males presented with the largest dimensions which corresponds to more robust features
- Differences between South Africans and Americans have been emphasized

References

1. Staff writer, 18 February 2022. The Crimes that are getting worse in South Africa, viewed 4 April 2022, https://businesstech.co.za/news/government/560270/the-crimes-that-are-getting-worse-in-south-africa/

2. Dorfling, H.F., Lockhat, Z., Pretorius, S., Steyn, M., Oettlé, A.C. 2018. Facial approximations: Characteristics of the eye in a South African sample. Forensic Science International. 286:46-53.

3. Janik, S.W., Wellens, A.R., Goldberg, M.L., Dell'osso, L.F. 1978. Eyes as the center of focus in the visual examination of human faces. Perceptual and motor skills. 47(3 Pt 1):857-8.

4. Ellis, H.D., Shepherd, J.W., Davies, G.M. 1979. Identification of familiar and unfamiliar faces from internal and external features: Some implications for theories of face recognition. Perception. 8(4):431-9.

5. Haig, N.D. 1984. The effect of feature displacement on face recognition. Perception. 13(5):505-12.

6. Wilkinson, C. 2003. Forensic facial reconstruction. New York: Cambridge University Press.

7. Kunjur, J., Sabesan, T., Ilankovan, V. 2006. Anthropometric analysis of eyebrows and eyelids: An inter-racial study. British Journal of Oral and Maxillofacial Surgery. 44(2):89-93.

8. Özer, C.M., Öz, I.I., Serifoglu, I., Büyükuysal, M.Ç., Barut, Ç. 2016. Evaluation of eyeball and orbit in relation to gender and age. Journal of Craniofacial Surgery. 27(8):e793-e800.

9. Kim, S.R., Lee, K.M., Cho, J.H. and Hwang, H.S., 2016. Three-dimensional prediction of the human eyeball and canthi for craniofacial reconstruction using cone-beam computed tomography. *Forensic Science International*, *261*, pp.164-e1.

10. Bekerman, I., Gottlieb, P., Vaiman, M. 2014. Variations in eyeball diameters of the healthy adults. Journal of Ophthalmology. 2014:503645.

11. Guyomarc'h, P., Dutailly, B., Couture, C., Coqueugniot, H. 2012. Anatomical placement of the human eyeball in the orbit - validation using CT scans of living adults and prediction for facial approximation. Journal of Forensic Sciences. 57(5):1271-5.

12. Weaver, A.A., Loftis, K.L., Tan, J.C., Duma, S.M. and Stitzel, J.D., 2010. CT based three-dimensional measurement of orbit and eye anthropometry. *Investigative ophthalmology & visual science*, *51*(10), pp.4892-4897.

13. Chong, Y., Li, J., Liu, X., Wang, X., Huang, J., Yu, N. and Long, X., 2021. Three-dimensional anthropometric analysis of eyelid aging among Chinese women. *Journal of Plastic, Reconstructive & Aesthetic Surgery*, *74*(1), pp.135-142.

14. Ibraheem, W.A., Ibraheem, A.B. and Bekibele, C.O., 2014. Exophthalmometric value and palpebral fissure dimension in an African population. *African Journal of Medical and Health Sciences/Jul-Dec*, *13*(2).

15. Price, K.M., Gupta, P.K., Woodward, J.A., Stinnett, S.S. and Murchison, A.P., 2009. Eyebrow and eyelid dimensions: an anthropometric analysis of African Americans and Caucasians. *Plastic and reconstructive surgery*, *124*(2), pp.615-623.

16. Wilkinson, C.M., Mautner, S.A. 2003. Measurement of eyeball protrusion and its application in facial reconstruction. Journal of Forensic Science. 48(1):1-5.

17. Md, R.G., Ba, A.R. and Md, J.H., 1999. Relationship of the eye to the bony orbit, with clinical correlations. *Australian and New Zealand Journal of Ophthalmology*, *27*(6), pp.399-403.

© University of Pretoria

Annexure F: Dimensions of the orbital region for biological profiling in a South African sample

(XXVIII International Symposium of Morphological Sciences , August 2023; Sefako Makgatho Health Sciences University Research Day, August 2023)

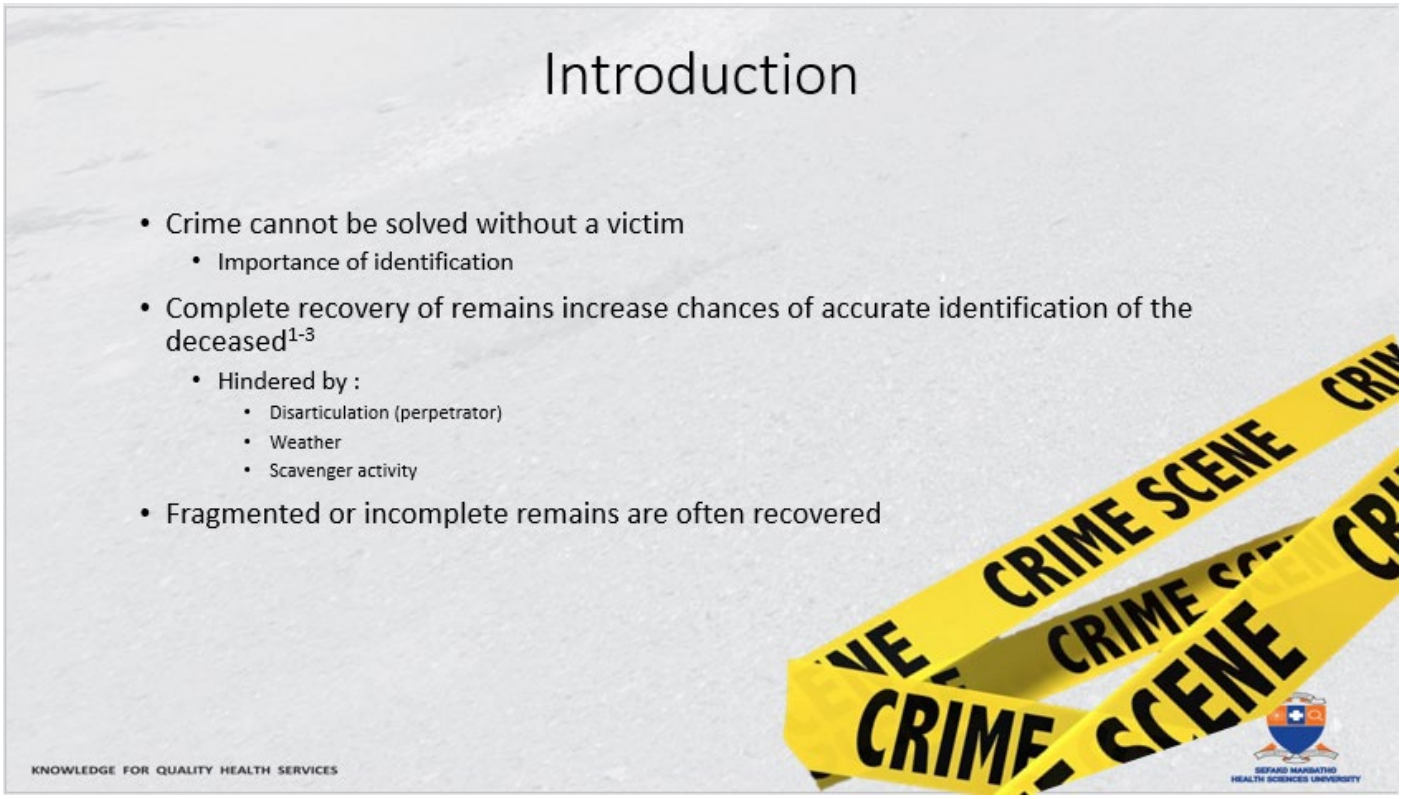

© University of Pretoria

Literature review

- Osteometric variables of the cranium is useful
  - predicting population affinity[4,5]
  - sex estimation[6-9]
- Cranium not always discovered intact
  - components have been scrutinized for their role in biological profiling
- Based on linear interlandmark distances on South Africans:
  - Sex estimation of white South African orbits: 71% accuracy[9]
  - Population affinity in black and white South African crania: 67.3 – 74.2% vs 80-91% vs 84-88% [6-8]

Literature review

- Discriminative ability of linear measurements is well known
  - FORDISC 3: uses any combination of standard measurements for ancestry and sex estimations[6]
- Geometric morphometrics conveys information about shape
  - enhances discriminatory power of classification [10,11]
- Shape analysis on the orbits have been performed on:
  - 2D photographs [10,12]
  - 3D digitised points using a MicroScribe [9,11]
  - 3D points using CT scans [13]

© University of Pretoria

Aim

To determine the discriminatory ability of the orbital dimensions for the estimation of sex and population affinity in South Africans for forensic purposes

Materials

- Ethical clearance nr: UP: 323/2020
- 206 CBCT scans were collected from public and private hospitals

	Black females	White females	Black males	White males
n	45	57	52	52

- Data collection was performed using the MeVisLab © v.3.0.2 software

KNOWLEDGE FOR QUALITY HEALTH SERVICES

© University of Pretoria

Methods: linear distances

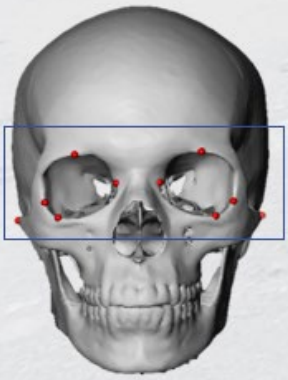

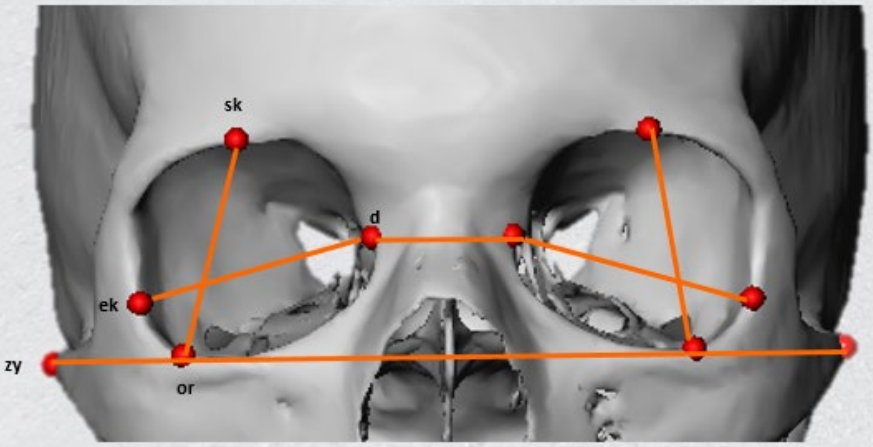

Key:
sk: supraconchion
or: orbitale
d: dacryon
ek: ectoconchion
zy: zygion

$$Distance = \sqrt{(x_2 - x_1)^2 + (y_2 - y_1)^2 + (z_2 - z_1)^2}$$

KNOWLEDGE FOR QUALITY HEALTH SERVICES

Methods: shape analysis

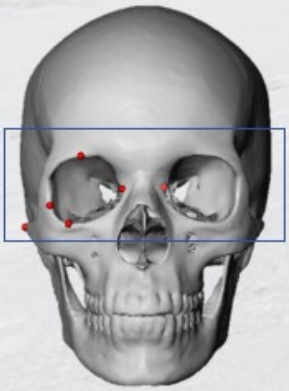

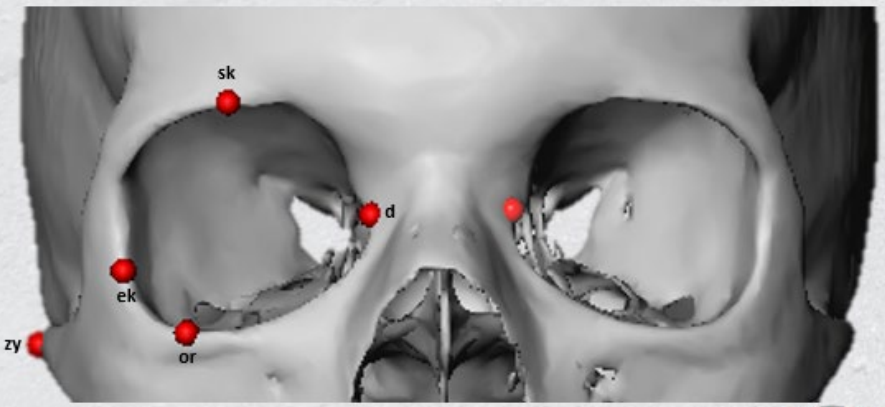

Key:
sk: supraconchion
or: orbitale
d: dacryon
ek: ectoconchion
zy: zygion

KNOWLEDGE FOR QUALITY HEALTH SERVICES

© University of Pretoria

Results: linear dimensions

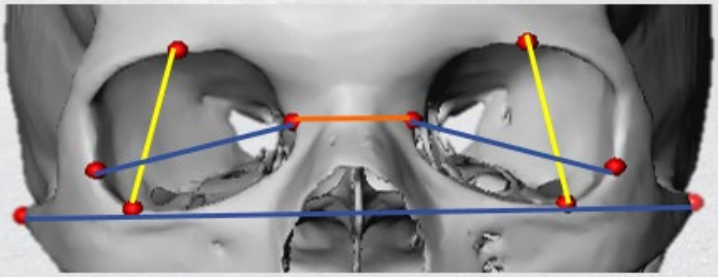

Measurement (mm)	South African black females (n=45)	South African white females (n=57)	South African black males (n=52)	South African white males (n=52)
Orbital height (L)	35.73 ± 2.98	37.39 ± 2.27	37.64 ± 2.33	38.15 ± 2.27
Orbital height (R)	35.91 ± 2.94	37.76 ± 2.15	37.60 ± 2.76	38.10 ± 2.52
Orbital breadth (L)	40.10 ± 2.79	40.58 ± 1.46	42.30 ± 1.83	42.74 ± 1.51
Orbital breadth (R)	40.14 ± 2.63	40.70 ± 1.81	42.55 ± 2.02	43.49 ± 2.10
Interorbital distance	21.65 ± 2.68	19.08 ± 2.35	22.62 ± 2.80	20.11 ± 2.34
Bizygomatic breadth	121.80 ± 7.87	123.03 ± 4.97	132.19 ± 7.21	131.35 ± 4.33

KNOWLEDGE F

Results: discriminant ability

			Sex determination with known population		Population determination with known sex	
Dimensions	Sex	Population	White SA	Black SA	Males	Females
OH (L&R)	58.74	56.8	66.34	51.92	61.86	62.39
OB (L&R)	73.3	52.91	50.5	59.62	68.04	79.82
IOD & ZB	79.61	69.42	73.53	66.35	75.26	82.57
OB & ZB	78.16	54.85	50.98	57.69	74.23	83.49
All	80.1	75.24	78.43	73.08	77.32	84.4

KNOWLEDGE FOR QUALITY HEALTH SERVICES

© University of Pretoria

Results: shape analysis

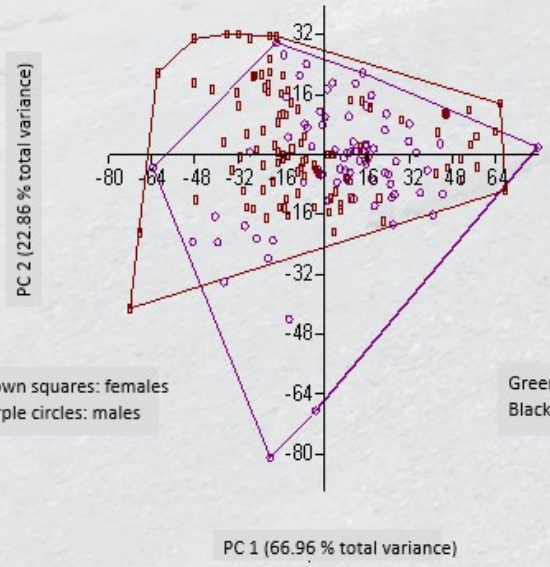

Brown squares: females
Purple circles: males

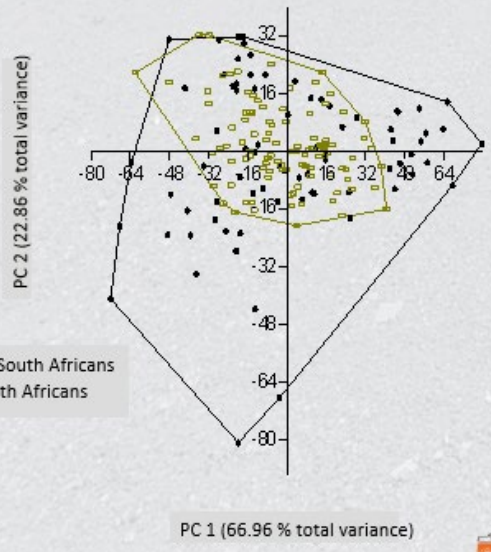

Green squares: White South Africans
Black circles: Black South Africans

KNOWLEDGE FOR QUALITY HEALTH SERVICES

The shape analysis were conducted based on projected landmark data

Results: shape analysis

Shape deformations indicating the shape variations in the orbital rim between male and female South Africans

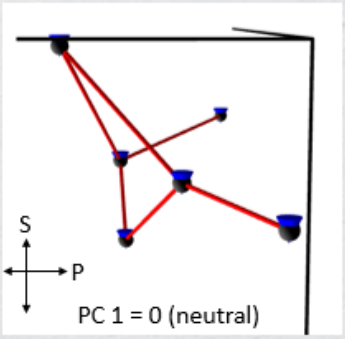

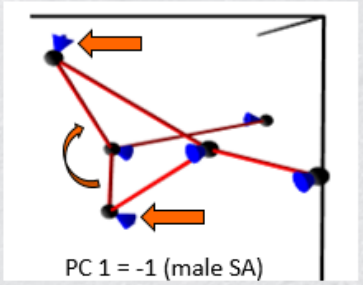

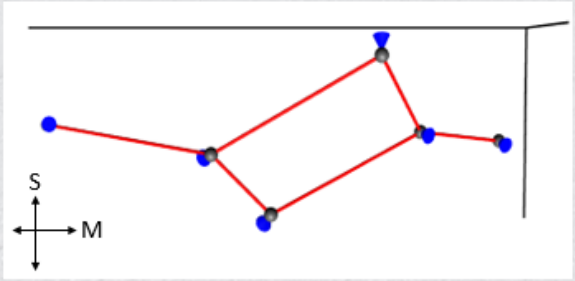

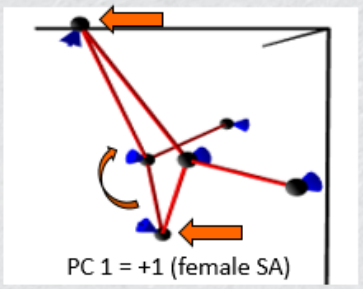

Medial view of orbit

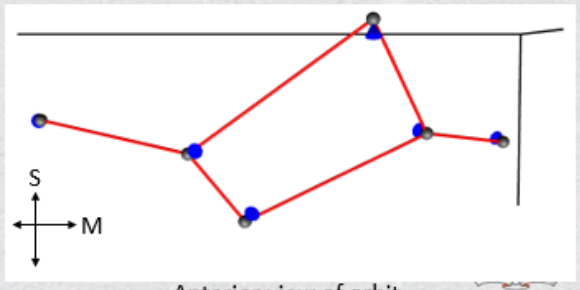

Anterior view of orbit

KNOWLEDGE FOR QUALITY HEALTH SERVICES

© University of Pretoria

Results: Shape analysis

Shape deformations indicating the shape variations in the orbital rim between white and black South Africans

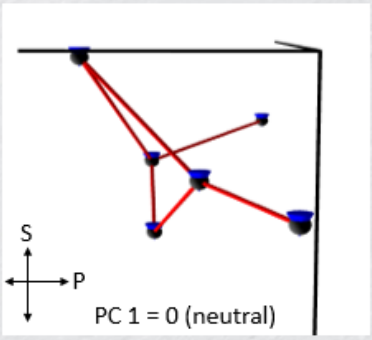

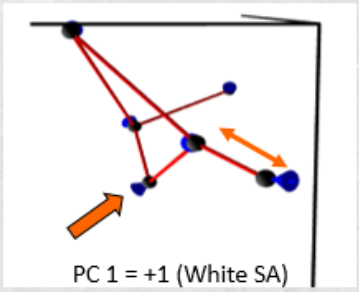

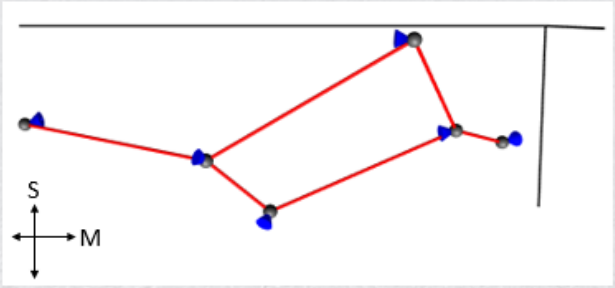

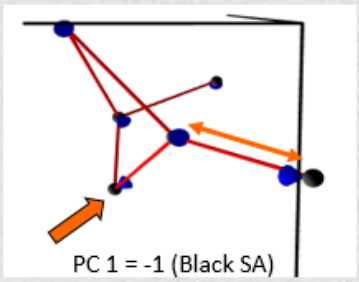

Medial view of orbit

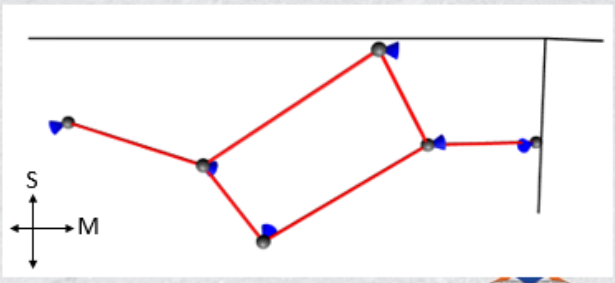

Anterior view of orbit

KNOWLEDGE FOR QUALITY HEALTH SERVICES

Results: Shape analysis

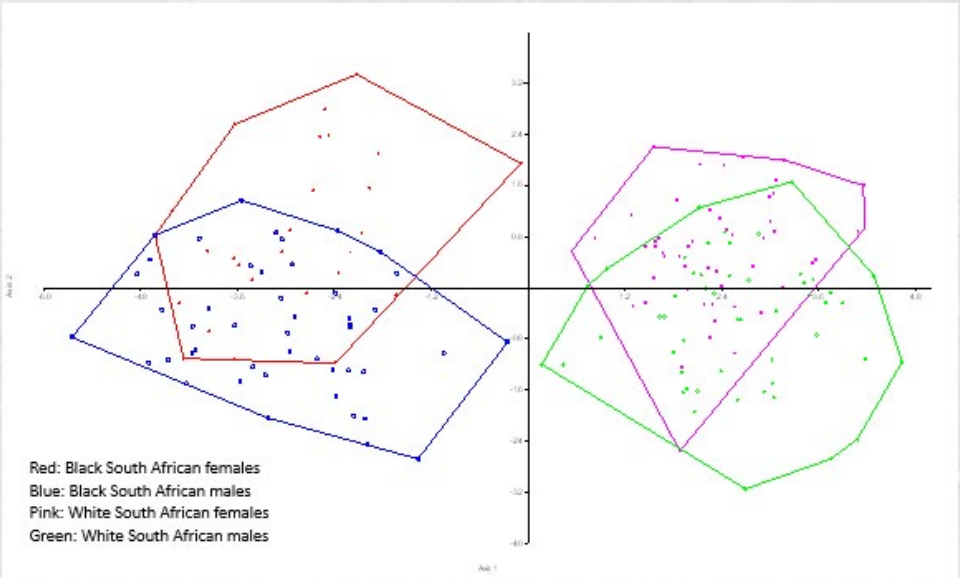

KNOWLEDGE FOR QUALITY HEALTH SERVICES

© University of Pretoria

Results: discriminant ability

Shape of the orbital rim	DFA
Sex	84.32%
Sex*White South Africans	93.20%
Sex*Black South Africans	86.59%
Population affinity	98.91%
Population affinity*males	100%
Population affinity*females	100%

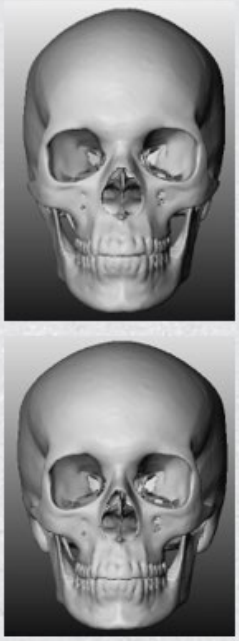

Discussion

- Orbital breadth is sexually dimorphic, as noted in Americans [14], Koreans [15] Turkish [16] and South Africans
- Interorbital distance varies between population groups and sexes [9,17]
- Wider interorbital distance noted in black South Africans, similar to black Americans [11]
- Linear dimensions can be used to estimate sex and predict population affinity, but with less accuracy compared to shape analysis

© University of Pretoria

Discussion

Study	Sample	Modality	Landmark nr	Accuracy
Sex estimation				
Pretorius et al., 2006	Black SA	2D photographs	10	73.3 – 80%
Small et al., 2018	White SA	3D landmarks	45	71.8%
Vd Walt et al., 2023	Black and white SA	3D landmarks	6	98.91 %
Population affinity				
Xing et al., 2013	Africans, Europeans and Asians	2D photographs	45	53.8 – 75.6 %
Rubin and deLeon, 2017	Africans, Europeans and Asians	3D landmarks	Every 1mm	Not calculated
Vd Walt., 2023	Black and white SA	3D landmarks	6	84.32 – 100%

Conclusion

- Linear dimensions may be useful in estimation of sex and population affinity
  - Should be combined with other cranial dimension
- Based on shape of the orbital rim:
  - Curve along the lateral orbital margin are useful in estimation of sex, while the positions of the supraconchion, orbitale and dacryons are useful in the prediction of population affinity
- Population affinity can be predicted with 98.91% accuracy
- Sex estimation with 100% accuracy

© University of Pretoria

References

Available on request

1. L'Abbé EN. A case of commingled remains from rural South Africa. Forensic science international. 2005 Jul 16;151(2-3):201-6.
2. Spies MJ, Finaughty DA, Gibbon VE. Forensic taphonomy: scavenger-induced scattering patterns in the temperate South-western Cape, South Africa—a first look. Forensic science international. 2018 Sep 1;290:29-35.
3. Keyes CA, Myburgh J, Brits D. Identifying forensically relevant urban scavengers in Johannesburg, South Africa. Science & Justice. 2022 May 1;62(3):399-409.Jagesur, S. 2022. Variations in pelvic canal and skull dimensions in South Africans considering possible relationships and implications. Dissertation, (PhD Health Sciences). University of Pretoria.
4. Green, H. and Curnoe, D. (2009). "Sexual dimorphism in southeast Asian crania: a geometric morphometric approach." *HOMO Journal of Comparative Human Biology* 60(6): 517-534.
5. Işcan, M.Y. and Steyn, M. (2013). "The human skeleton in forensic medicine". *Third Edition. Charles C Thomas Pub Ltd.*
6. L'Abbé, E.N., Kenyhercz, M.W., Stull, K.E., Keough, N., Nawrocki, N. (2013). "Application of Fordisc 3.0 to explore differences among crania of North American and South African black South Africans and whites." *Journal of Forensic Science* 58(6):1579-83
7. Stull, K.E., Kenyhercz, M.W., L'Abbé, E.N. (2014). "Ancestry estimation in South Africa using craniometrics and geometric morphometrics." *Forensic Science International* 245: 206.e1-206.e7.
8. Liebenberg, L., Stull, K.E., L'Abbé, E.N., Botha, D. (2015). "Evaluating the accuracy of cranial indices in ancestry estimation among South African groups." *Journal of Forensic Sciences* 60(5): 1277-1282
9. Small C, Schepartz L, Hemingway J, Brits D. Three-dimensionally derived interlandmark distances for sex estimation in intact and fragmentary crania. Forensic science international. 2018 Jun 1;287:127-35.
10. Xing, S., Gibbon, V., Clarke, R. & Liu, W. 2013. Geometric morphometric analyses of orbit shape in Asian, African, and European human populations. *Anthropological Science,* 121, 1-11.
11. Rubin, K. M. & DeLeon, V. B. 2017. Ancestral variation in orbital rim shape: a three-dimensional pilot study. *Journal of forensic sciences,* 62, 1575-1581.
12. Pretorius E, Steyn M, Scholtz Y. Investigation into the usability of geometric morphometric analysis in assessment of sexual dimorphism. American Journal of Physical Anthropology: The Official Publication of the American Association of Physical Anthropologists. 2006 Jan;129(1):64-70.
13. Prevost, A., Muller, S., Lauwers, F. & Heuzé, Y. Quantification of Global Orbital Shape Variation. *Clinical Anatomy*.
14. Weaver, A. A., Loftis, K. L., Tan, J. C., Duma, S. M. & Stitzel, J. D. 2010. CT based three-dimensional measurement of orbit and eye anthropometry. *Investigative ophthalmology & visual science,* 51, 4892-4897.
15. Kim, S.-R., Lee, K.-M., Chow, J.-H. & Wang, H.-S. 2016. Three-dimensional prediction of the human eyeball and canthi for craniofacial reconstruction using cone-beam computed tomography. *Forensic science international,* 261, 164. e1-164. e8.
16. Özer, C. M., Öz, I. I., Serifoglu, I., Büyükuysal, M. Ç. & Barut, Ç. 2016. Evaluation of eyeball and orbit in relation to gender and age. *Journal of Craniofacial Surgery,* 27, e793-e800.
17. Ji, Y., Qian, Z., Dong, Y., Zhou, H. & Fan, X. 2010. Quantitative morphometry of the orbit in Chinese adults based on a three-dimensional reconstruction method. *Journal of anatomy,* 217, 501-506.

© University of Pretoria